

Chairman:	Prof. Dr Ken Haenen, UHasselt
Promoter:	Prof. Dr Wouter Maes, UHasselt
Copromoters:	Prof. Dr Dirk Vanderzande, UHasselt Dr Laurence Lutsen, IMO-IMOMEC
Members of the jury:	Prof. Dr Peter Adriaensens, UHasselt Prof. Dr Tanja Junkers, UHasselt Prof. Dr Guy Koeckelberghs, KULeuven Dr Sébastien Clément, Université de Montpellier



# TABLE OF CONTENTS

## **Chapter 1: Introduction**

1.1: General introduction	2
1.2: Conjugated polymers	3
1.3: Polythiophenes	6
1.4: Controlled polymerization of conjugated polymers	10
1.4.1: Introduction	10
1.4.2: Controlled polymerization of 3-alkylthiophenes	14
1.4.3: Synthesis of all-conjugated block copolymers	16
1.5: Organic photovoltaics	19
1.6: Thesis outline	24
1.7: References	26

## **Chapter 2: Conjugated ionic (co)polythiophene-based cathode interlayers for bulk heterojunction organic solar cells**

2.1: Introduction	35
2.2: Results and discussion	38
2.2.1: Polymer synthesis	38
2.2.2: Polymer characterization	44
2.2.3: Photovoltaic properties	47
2.3: Conclusions	52
2.4: References	54
2.5: Supporting information	58
2.5.1: Reagents and instrumentation	58
2.5.2: Photovoltaic device fabrication and characterization	60
2.5.3: Monomer synthesis	61

## Table of contents

---

2.5.4: Polymer synthesis	61
2.5.4.1: Homopolymer synthesis	61
2.5.4.2: Random copolymer synthesis	63
2.5.4.3: Block copolymer synthesis	65
2.5.4.4: Functionalization with <i>N</i> -methylimidazole	67
2.5.4.5: Counteranion exchange	69
2.5.5: <sup>1</sup> H NMR spectra of the polymers	72
2.5.6: Cyclic voltammetry	78
2.5.7: Thermal analysis	79
2.5.8: References	80

## **Chapter 3: Synthesis of highly fluorescent all-conjugated alternating donor-acceptor (block) copolymers via Kumada catalyst-transfer condensation polymerization**

3.1: Introduction	83
3.2: Results and discussion	85
3.2.1: Monomer synthesis	85
3.2.2: Alternating copolymer synthesis	87
3.2.3: Block copolymer synthesis	91
3.2.4: Thermal, electrochemical and optical characterization	95
3.3: Conclusions	101
3.4: References	103
3.5: Supporting information	107
3.5.1: Reagents and instrumentation	107
3.5.2: Monomer synthesis	109
3.5.3: Alternating copolymer synthesis	112
3.5.4: Block copolymer synthesis	114
3.5.5: <sup>1</sup> H NMR spectra	116

3.5.6: Polymerization plots	122
3.5.7: MALDI-TOF measurements	124
3.5.8: Study of the block copolymer purity	125
3.5.9: Thermal analysis	128
3.5.10: Polymer fluorescence	129
3.5.11: Paper chromatography	129
3.5.12: References	130

**Chapter 4: Synthesis of all-conjugated alternating thiophene-thieno[3,4-*b*]pyrazine (block) copolymers via Kumada catalyst-transfer condensation polymerization**

4.1: Introduction	133
4.2: Results and discussion	135
4.2.1: Monomer synthesis	135
4.2.2: Polymer synthesis and characterization	138
4.3: Conclusions	144
4.4: References	145
4.5: Supporting information	148
4.5.1: Reagents and instrumentation	148
4.5.2: Monomer synthesis	149
4.5.3: Polymer synthesis	151
4.5.4: <sup>1</sup> H NMR spectra	154
4.5.5: Polymer solutions	162
4.5.6: References	162

**Chapter 5: The introduction of branching in a low bandgap alternating cyclopentadithiophene-quinoxaline copolymer**

5.1: Introduction	165
5.2: Results and discussion	167
5.2.1: Monomer synthesis	167
5.2.2: Polymer synthesis and characterization	169
5.2.3: Photovoltaic properties	175
5.3: Conclusions	177
5.4: References	178
5.5: Supporting information	182
5.5.1: Reagents and instrumentation	182
5.5.2: Photovoltaic device fabrication and characterization	183
5.5.3: Monomer synthesis	184
5.5.4: Polymer synthesis	185
5.5.5: <sup>1</sup> H NMR spectra	187
5.5.6: References	190

**Chapter 6: Summary and outlook**

6.1: Summary	191
6.2: Outlook	194
6.3: Nederlandse samenvatting	195

<b>List of publications</b>	199
-----------------------------	-----

<b>Dankwoord</b>	201
------------------	-----

---

# Chapter 1

## Introduction

---



## 1.1 GENERAL INTRODUCTION

Since the initial discovery of Shirakawa, Heeger and MacDiarmid in 1977 that polyacetylene shows high conductivities after doping with halides,<sup>[1]</sup> researchers worldwide started searching actively for new technological applications in which the physical properties of plastics could be combined with the electronic properties of semiconductors. Throughout the years, different classes of conjugated polymers were synthesized and investigated in several organic electronic applications, such as light-emitting diodes, transistors, photovoltaics, (bio)sensors, ...<sup>[2]</sup> One of the most studied conjugated polymers is poly(3-hexylthiophene) (P3HT), which for instance served as an important workhorse material to gain fundamental insights into the working principles of organic photovoltaics.<sup>[3,4]</sup> Nowadays, P3HT is outperformed by another class of conjugated polymers, the low bandgap donor-acceptor (D-A) alternating copolymers, which allow a more optimal harvesting of the solar spectrum.<sup>[5,6]</sup> These D-A or push-pull copolymers are generally synthesized by transition metal catalyzed polycondensation reactions, whereof the Stille and Suzuki polymerizations are the most popular.<sup>[7-9]</sup> These polymerizations follow a step-growth mechanism, meaning that high molar mass polymers can only be obtained at high conversions after long reaction times. As a result, rather poor control over the polymer molar mass, dispersity and end groups is achieved. On the other hand, controlled chain-growth transition metal catalyzed polycondensations allow precise control over the above-mentioned polymer characteristics and high molar mass polymers can already be obtained after short reaction times. On top of that, they enable the synthesis of all-conjugated block copolymers and other advanced polymer architectures via one-pot polymerizations. Such materials can give rise to

interesting morphological structures and enhanced light absorption, beneficial for their use in organic solar cells.<sup>[10-16]</sup>

Although many pathways have already been explored and good devices have been realized, most of these results were obtained by using linear conjugated polymers. More advanced conjugated polymer architectures – like block copolymers, star and hyperbranched polymers – have rarely been investigated, mainly due to synthetic challenges. These materials are nowadays usually obtained by performing multistep procedures and/or using click chemistry. All-conjugated polymers with advanced macromolecular architectures synthesized via one-pot synthesis protocols are, however, very appealing target molecules for applications in organic electronics since conjugation in two or three dimensions could lead to several advantages, such as isotropic charge transport, enhanced dielectric constants and better solubilities.<sup>[10,17,18]</sup> This research domain has barely been explored, but could pave the way toward new possibilities.

## **1.2 CONJUGATED POLYMERS**

The large majority of consumer polymers are non-conjugated polymers, such as polyethylene, polypropylene, polystyrene, ... . These polymers are in general characterized by a good mechanical strength, a light weight and a good flexibility. On the other hand, conjugated polymers consist of non-saturated or aromatic segments that are in conjugation with one another. In fact, conjugated polymers can be simply represented as chains that exist of alternating single and double (or triple) bonds (Figure 1). This gives rise to a system of  $sp^2$ -hybridized (or  $sp$ -hybridized) atoms with overlapping  $p_z$ -orbitals, in which the  $n$ -electrons are delocalized across the system.

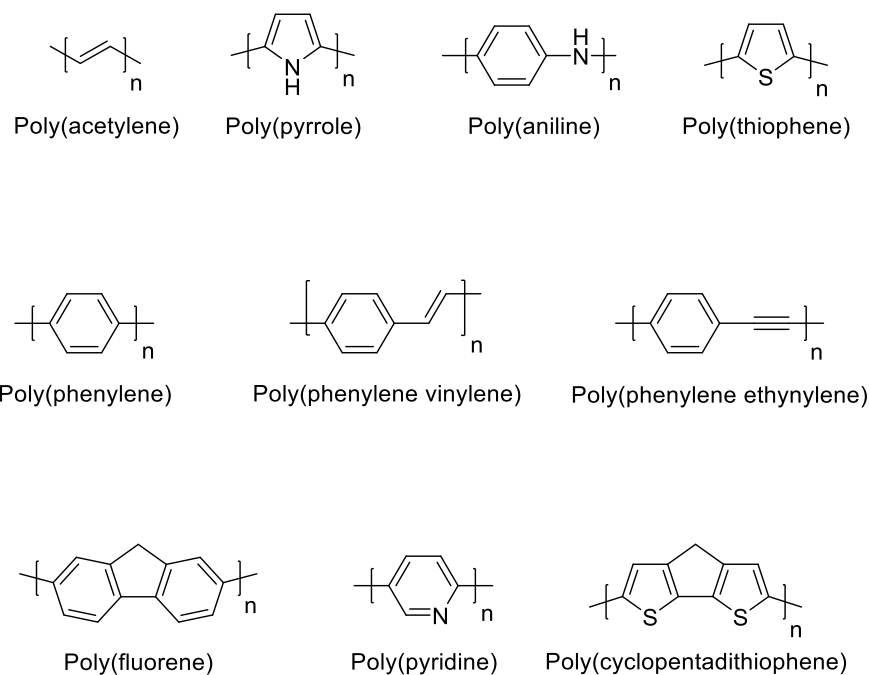


**Figure 1:** Examples of conjugated polymers.

This conjugation leads to a rise in the HOMO (highest occupied molecular orbital) energy level and a lowering of the LUMO (lowest unoccupied molecular orbital) energy level. Due to this, a smaller bandgap ( $E_g$ : the energy difference between the HOMO and LUMO) is obtained for conjugated polymers, leading to absorption bands in the visible and even the near-infrared (NIR) region (Figure 2). Besides this, the conjugation also influences the electronic properties by enabling the electrons to cross this smaller  $E_g$  barrier and thereby giving conjugated polymers a semi-conducting behavior.

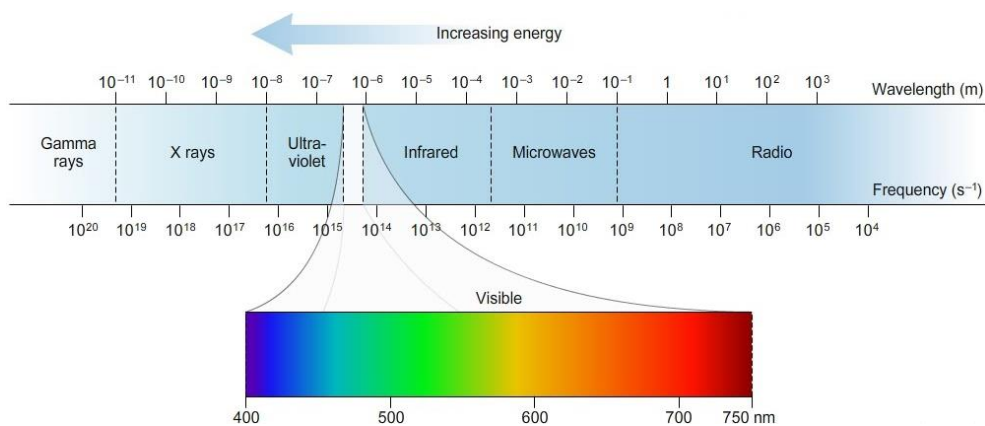


**Figure 2:** The electromagnetic spectrum.

The conjugation, and hence the optical and electronic properties, of the polymers is dependent on several factors. First of all, the aromaticity of the monomers plays an important role. The larger the aromatic resonance energy in the cyclic building blocks of the conjugated polymer, the stronger the localization of the  $\pi$ -system within the boundaries of the monomer, which leads to a diminished delocalization along the contour length of the conjugated polymer and thus to a larger bandgap. A second aspect is the planarity of the conjugated polymer. If the planarity is disrupted by twists due to steric hindrance, the overlap between the  $p_z$ -orbitals decreases and the polymer is less conjugated. Besides this, also the substituents on the polymers can have a strong influence on the alignment of the HOMO-LUMO energy levels and the bandgap. In case of conjugation with an electron-donating group, both the HOMO and LUMO level of the polymer rise, but the influence on the HOMO level is higher, thereby reducing the bandgap. This is also the case for conjugation with an electron-accepting group, whereby both the HOMO and LUMO level of the polymer decrease, but the lowering of the LUMO happens to a higher extent. Since all of the above factors exert their influence on the optoelectronic

properties of conjugated polymers, these should be taken into account when considering for which application the polymers will be used.

### 1.3 POLYTHIOPHENES

One of the most studied conjugated polymers are the polythiophenes. These show a good conjugation ( $\lambda_{\text{max}} \sim 435\text{--}450\text{ nm}$ ) and the possibility to adopt a semi-crystalline stacked structure, leading to some interesting characteristics such as a high mobility of charge carriers. As a consequence, these polymers have already been used in several applications, such as organic field-effect transistors (oFETs),<sup>[19]</sup> organic light-emitting diodes (oLEDs),<sup>[20]</sup> and organic photovoltaics (OPVs).<sup>[3,4,21]</sup>

At the very beginning, unsubstituted polythiophenes were synthesized by means of electrochemical or oxidative polymerizations. These polymerizations gave rise to insoluble polythiophenes (Figure 3a) with a reasonable charge carrier mobility.<sup>[22,23]</sup>

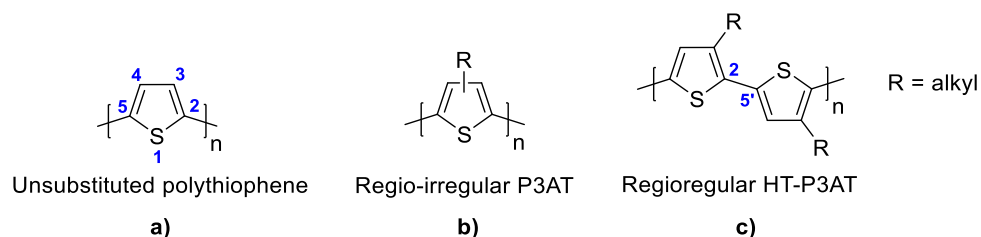


**Figure 3:** Structures of different polythiophenes.

In the late 1980s, alkyl chains were introduced on the 3-position of the thiophene monomer to obtain soluble polythiophenes. This resulted in an asymmetric monomer, due to which the electrochemical and oxidative polymerizations produced regio-irregular poly(3-alkylthiophenes) (P3ATs) (Figure 3b). This regio-

irregularity can be ascribed to the fact that three different couplings between the monomer units can take place: head-to-tail (HT) coupling, head-to-head (HH) coupling and tail-to-tail (TT) coupling (Figure 4). The occurrence of TT couplings gives rise to twists in the polymer chains due to steric hindrance, leading to a diminished  $\pi$ -conjugation.<sup>[24]</sup>

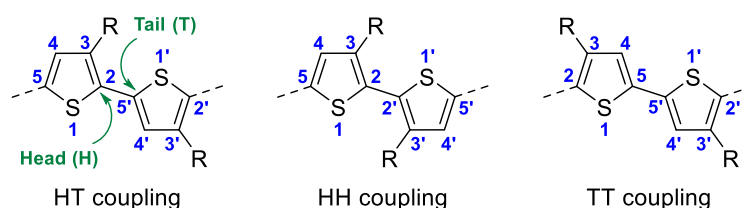


**Figure 4:** Different couplings between 3-alkylthiophenes.

In order to obtain polythiophenes with a strong  $\pi$ -conjugation, a synthesis strategy for regioregular HT-P3ATs (Figure 3c) was explored in the 1990s. The first synthesis procedure that was reported, is the so-called McCullough method. In this case, the monomer was obtained in a regioselective way (i.e. only one isomer was formed) by consecutive treatment of the precursor monomer 2-bromo-3-alkylthiophene with lithium diisopropylamide (LDA) and  $\text{MgBr}_2 \cdot \text{Et}_2\text{O}$  (Scheme 1a), whereupon  $\text{Ni}(\text{dppp})\text{Cl}_2$  was added to start the polymerization.<sup>[25]</sup> Soon afterwards, also Rieke reported a synthesis procedure to obtain HT-P3ATs. In this method, reactive Rieke zinc ( $\text{Zn}^*$ ) is added to the precursor monomer 2,5-dibromo-3-alkylthiophene, resulting into the formation of two isomeric monomers **A** and **B** (Scheme 1b). The regioselectivity is in this case obtained by adding  $\text{Ni}(\text{dppe})\text{Cl}_2$  as the catalyst, which ensures that only isomer **A** is consumed during the polymerization (*vide infra*; Figure 5).<sup>[26,27]</sup>



To summarize, there are two different approaches for the synthesis of regioregular HT-P3ATs. The first approach is based on the regioselective conversion of the precursor monomer into the monomer (Scheme 1a and 2b), resulting in only one isomer that is polymerized with Ni(dppp)Cl<sub>2</sub>. In the second approach, two isomeric monomer species are obtained, whereof only one (isomer **A** or **C**) is consumed during the polymerization (Scheme 1b and 2a). In this case, the regioselectivity is achieved by choosing the right catalyst (Ni(dppe)Cl<sub>2</sub> or Ni(dppp)Cl<sub>2</sub>) for the polymerization. These Ni catalysts make sure that no HH couplings can be formed, since the steric hindrance around the Ni core is too big in this case (Figure 5). As a consequence, only isomer **A** or **C** can participate in the polymerization process which, besides the formation of one TT coupling (in the first step), consists of a sequence of HT couplings (for all next steps).<sup>[29]</sup> This is further explained in section 1.4.2, where the polymerization mechanism of all the above methods is elucidated in more detail.

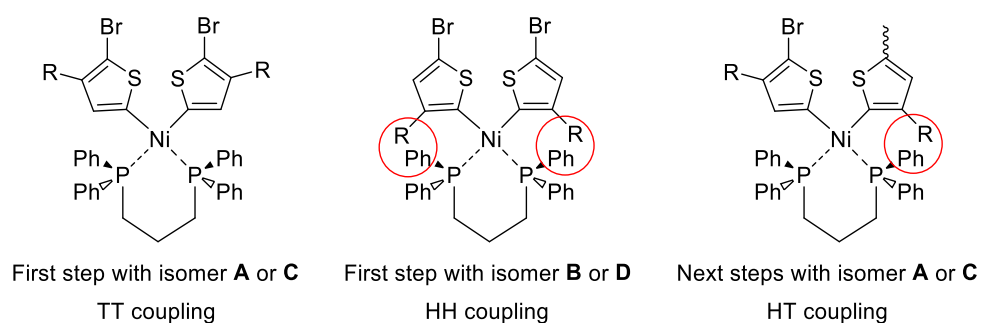
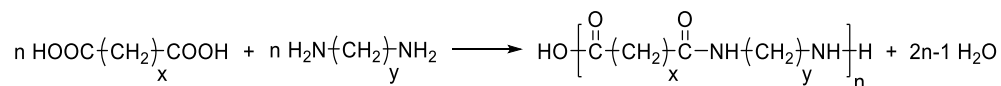


**Figure 5:** Steric hindrance (red circles) around the Ni core for the different possible couplings.

## 1.4 CONTROLLED POLYMERIZATION OF CONJUGATED POLYMERS

### 1.4.1 Introduction

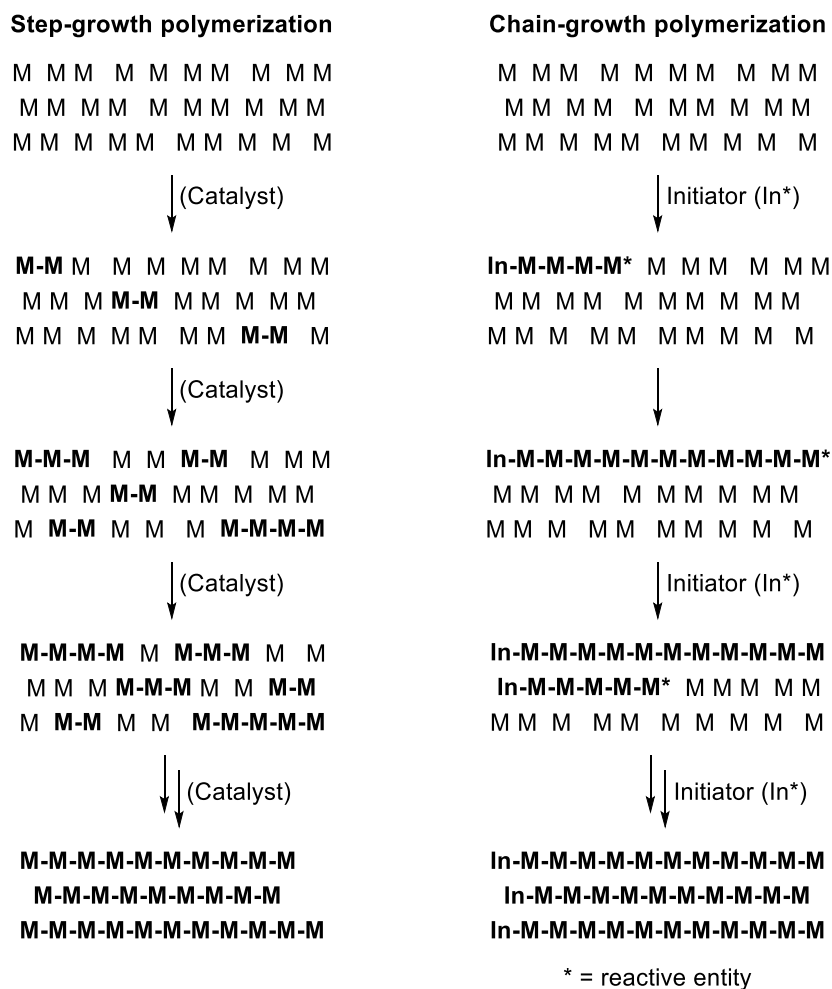
Polymers can be synthesized via different polymerization reactions. A first important polymerization type are the polycondensations, whereof an example is displayed in Scheme 3.



**Scheme 3:** Example of a polycondensation.

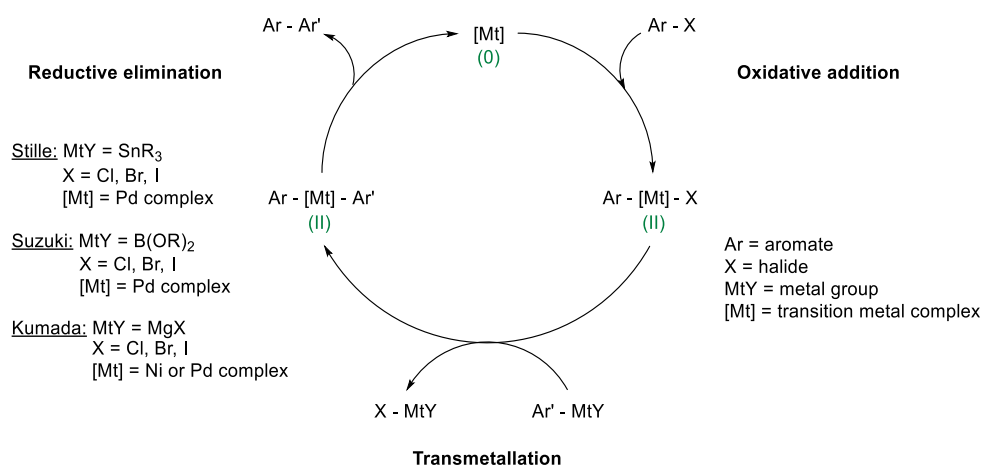
Polycondensations are often associated with a step-growth polymerization, but this does not mean that these two can be considered equal. Polycondensations refer to the structure and composition of the formed polymers, whereas step-growth and chain-growth polymerizations are linked with the polymerization mechanism. The difference between a step-growth and chain-growth polymerization for the synthesis of classical, non-conjugated polymers is illustrated in Scheme 4. During step-growth polymerizations, a few monomers will initially react with each other and form dimers. These dimers will then react further to form trimers, tetramers or some bigger oligomers. In this way, the reaction mixture still contains monomer and also quite some oligomers (2, 3, 4, 5, 6, ... repeating units) after a certain amount of time. In order to obtain polymers with a high molar mass, two oligomers with a large number of repeating units will have to couple with each other. This means that in case of step-growth polymerizations high molar masses can only be obtained at high conversions. On the other hand,

chain-growth polymerizations require the use of an initiator, which is built in at the beginning of every polymer chain. This initiator ( $\text{In}^*$ ) first reacts with a monomer unit, thereby activating the monomer ( $\text{In-M}^*$ ). This activated species then reacts with another monomer unit to form a reactive dimer ( $\text{In-M-M}^*$ ), which on its turn can react with another monomer to form a reactive trimer ( $\text{In-M-M-M}^*$ ), and so on. As a consequence, high molar mass polymers can already be obtained at rather low conversions.



**Scheme 4:** Mechanism of step-growth and chain-growth polymerizations.

For the synthesis of conjugated polymers, polycondensations are often applied. Several organic reactions can be used for these polycondensations, including transition metal-catalyzed coupling reactions. The general mechanism of these coupling reactions consists of three consecutive steps and is displayed in Scheme 5. The first step is an oxidative addition, whereby the transition metal complex ( $[Mt]$ ) is inserted in the C-X bond of an aromatic halide (Ar-X). Afterwards, a transmetallation takes place with the metal group ( $-MtY$ ) of another aromatic molecule (Ar'-MtY). As a third step a reductive elimination occurs, resulting into the formation of a C-C bond between the two aromatic systems. In this way, the coupled product (Ar-Ar') is obtained.<sup>[24]</sup>



**Scheme 5:** General mechanism of transition metal-catalyzed coupling reactions.

In a polycondensation reaction as depicted in Scheme 5, the transition metal catalyst is not consumed, since it is retrieved each time two aromatic systems are coupled. This polymerization follows a step-growth mechanism. There is, however, a method to convert this step-growth mechanism into a chain-growth mechanism. This is achieved if the transition metal catalyst remains associated to the growing entity after reductive elimination, thereby ensuring that the growing entity

remains active and can keep on undergoing consecutive cycles of oxidative additions, transmetallations and reductive eliminations, resulting into a chain-growth behavior. In addition, this chain-growth mechanism can also take place in a controlled way, provided that no termination or transfer reactions occur. The controlled character of a polymerization can be investigated by taking quenches at different time intervals during a polymerization experiment, and then plotting the molar mass ( $M_n$ ) versus conversion ( $p$ ) and  $\ln([M]_0/[M])$  versus time ( $t$ ). If the  $\ln([M]_0/[M])$  versus  $t$  plot gives a linear relationship, it means that no termination reactions occur (if initiation only happens at the start of the polymerization) and transmetallation is the rate-determining step (Figure 6a). If the  $M_n$  versus  $p$  plot gives a linear relationship, it means that no transfer reactions take place (Figure 6b). [31-33]

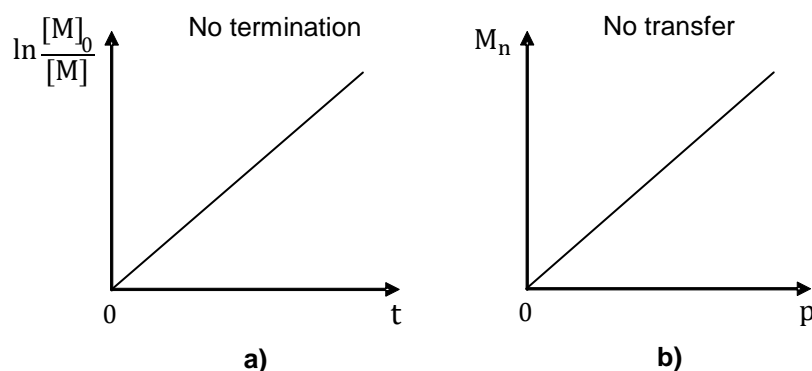
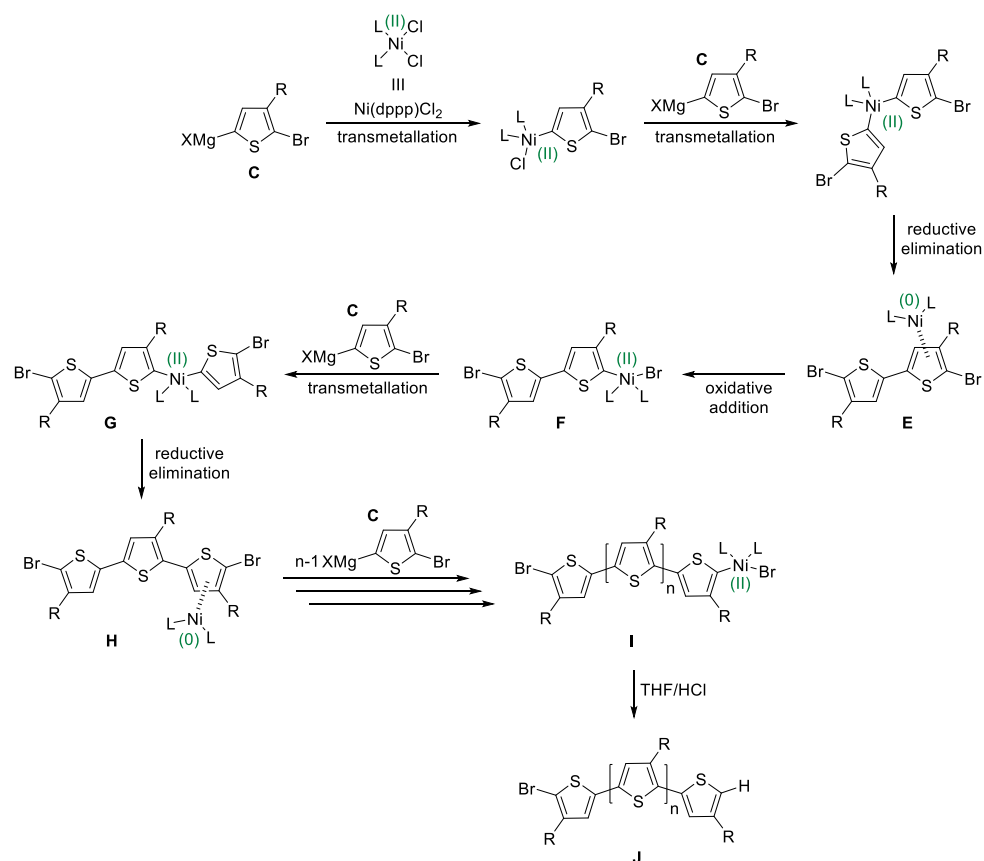


**Figure 6:** Plots for a controlled polymerization.

Such controlled chain-growth polymerizations offer several advantages. First of all, they allow a precise control over the polymer molar mass, dispersity and end groups. On top of that, they enable the synthesis of all-conjugated block copolymers and other advanced structures via one-pot polymerizations.

### 1.4.2 Controlled polymerization of 3-alkylthiophenes

In 2004, the groups of Yokozawa<sup>[31]</sup> and McCullough<sup>[34]</sup> reported that the Ni-catalyzed polymerization of 3-alkylthiophenes via the GRIM method follows a controlled chain-growth mechanism. The mechanism is depicted in Scheme 6.



**Scheme 6:** Controlled polymerization of 3-alkylthiophenes.

The first step in the polymerization process consists of two consecutive transmetallations of  $\text{Ni(dppp)Cl}_2$  with two monomer units (**C**), followed by a reductive elimination. This results in the formation of a Ni(0) moiety and a TT dimer (**E**), whereby the Ni(0) moiety remains associated to the dimer. This association is crucial to obtain the controlled chain-growth mechanism, since it

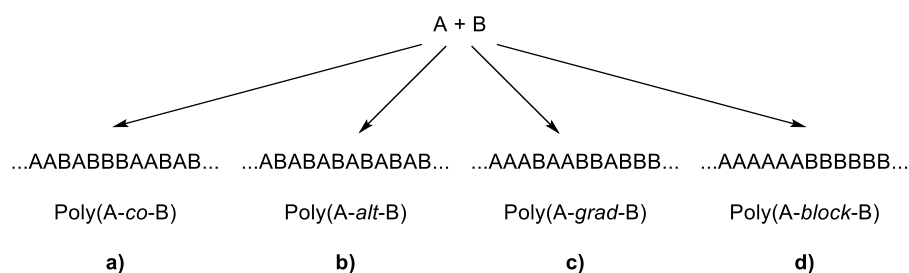
ensures that every initiated polymer chain remains active for further growth. On top of that, this association enables the Ni(0) moiety to undergo a fast oxidative addition into a terminal C-Br bond of the TT dimer (**F**). This process, whereby the Ni moiety remains associated to the polymer chain and is transferred to the end of the polymer chain, is called 'ring walking'. Then, a new transmetalation with another monomer unit (**C**) takes place, this time resulting into a HT coupling (**G**). Afterwards, the Ni(0) moiety is again obtained after a reductive elimination (**H**), whereupon the whole process can start all over again. This process of sequential oxidative additions, transmetalations and reductive eliminations keeps on reoccurring until all monomer (**C**) is consumed, finally resulting into a P3AT that, apart from the first TT coupling, only contains HT couplings (**I**). In a final step, the polymerization is quenched with a THF/HCl mixture in order to replace all terminal Ni moieties of the polymer chains with a hydrogen. This leads to polymer chains with one bromine end group and one hydrogen end group (**J**).<sup>[30]</sup> If the formed polymer only consists of polymer chains with Br/H end groups, it confirms the controlled chain-growth mechanism since the occurrence of termination or transfer reactions also leads to polymer chains with Br/Br or H/H end groups.<sup>[35]</sup>

Due to the fact that the cross-coupling reactions of Scheme 6 are of the Kumada-type and that the 'ring walking' of the catalyst over the polymer chains is very important to obtain the controlled chain-growth mechanism, this type of polymerization was named Kumada catalyst-transfer condensation polymerization (KCTCP). This polymerization method has also been used for the synthesis of poly(alkoxythiophene)s,<sup>[36,37]</sup> poly(selenophene)s,<sup>[38,39]</sup> poly(tellurophene)s,<sup>[40]</sup> poly(pyrrole)s,<sup>[41]</sup> poly(cyclopentadithiophene)s,<sup>[33]</sup> poly(thiazole)s,<sup>[42]</sup> poly(dithienosilole)s,<sup>[13]</sup> poly(thienothiophene)s,<sup>[43]</sup> poly(phenylene)s,<sup>[44,45]</sup>

poly(fluorene)s,<sup>[46,47]</sup> poly(pyridine)s,<sup>[48,49]</sup> poly(thienopyrazine)s,<sup>[50]</sup> and poly(benzotriazole)s.<sup>[51]</sup> In all cases polymers were obtained, but the amount of control differed for several reasons. Nevertheless, the KCTCP method still holds a lot of advantages and should be explored further for the synthesis of conjugated polymers with advanced architectures, mainly in view of their application in organic electronics.

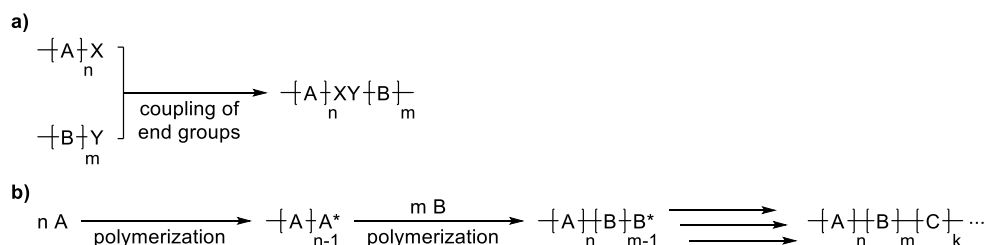
### 1.4.3 Synthesis of all-conjugated block copolymers

In most cases, polymers are built up from one single monomer unit, resulting into homopolymers. On the other hand, copolymers consist of two (or more) different monomer units. These copolymers can be divided into four different classes. First of all, there are the random or statistical copolymers, in which the different monomers are randomly distributed among the polymer chain (Scheme 7a). A second class are the alternating copolymers, whereby the different monomers are built in alternatingly among the polymer chain (Scheme 7b). A third class are the gradient copolymers. In this case, the copolymer composition undergoes a gradual transition from monomer A to monomer B (Scheme 7c). Finally, there are also block copolymers, which are built up from two (or more) blocks of different homopolymers (Scheme 7d).



**Scheme 7:** Different copolymer classes.

Block copolymers can be synthesized in two different ways. A first approach is the modular method, whereby the block copolymers are obtained in two steps. In this case, the different blocks are synthesized individually with specific functional end groups, whereafter these blocks are coupled to each other in a second step by performing a reaction between the functional end groups of the different blocks (Scheme 8a). Besides this, there is also the sequential method, in which block copolymers can be obtained by sequentially adding the different monomers in a one-pot procedure (Scheme 8b).



**Scheme 8:** Synthesis of block copolymers via a) the modular and b) the sequential method.

The synthesis of all-conjugated block copolymers is most often performed via the sequential method. Since this method requires the use of a controlled chain-growth polymerization, KCTCP is a suitable candidate. In addition, the polymerization conditions of the different blocks should be compatible due to the one-pot procedure. As a consequence, the first block copolymers that were synthesized via this method by KCTCP were composed of the same aromatic moieties (mainly thiophenes) with different side chains (Figure 7).<sup>[11,34,47,52-55]</sup> Some of these block copolymers (**a**,<sup>[11]</sup> **c**,<sup>[55]</sup> and **d**<sup>[53]</sup>) showed microphase separation of the two blocks, which leads to some interesting nanostructures that can be of interest for OPV applications.<sup>[56]</sup>

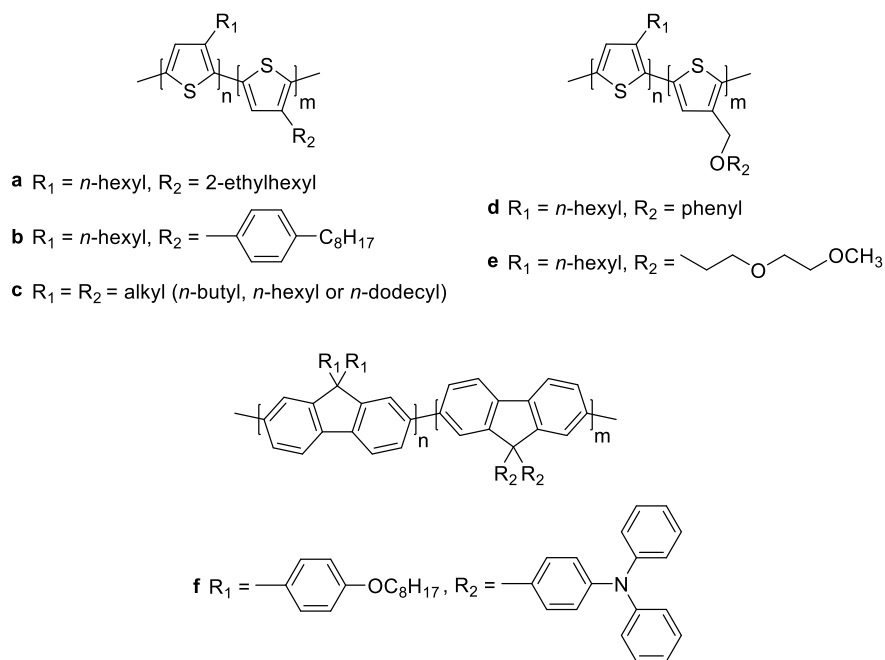


**Figure 7:** All-conjugated block copolymers composed of the same type of aromatic moieties.

Due to the prerequisite of compatible polymerization conditions, some block copolymers with different aromatic moieties were synthesized by KCTCP, but their scope remained rather limited (Figure 8).<sup>[13,33,41,47,57,58]</sup> On top of that, the order of monomer addition appeared to play an important role. In a lot of cases, it was only feasible to create block copolymers if the less electron rich monomer was polymerized first. This was attributed to the higher affinity of the Ni catalyst for the more electron rich monomer, causing a very slow or no initiation at all of the more electron poor monomer in case the latter was added secondly.<sup>[57]</sup>

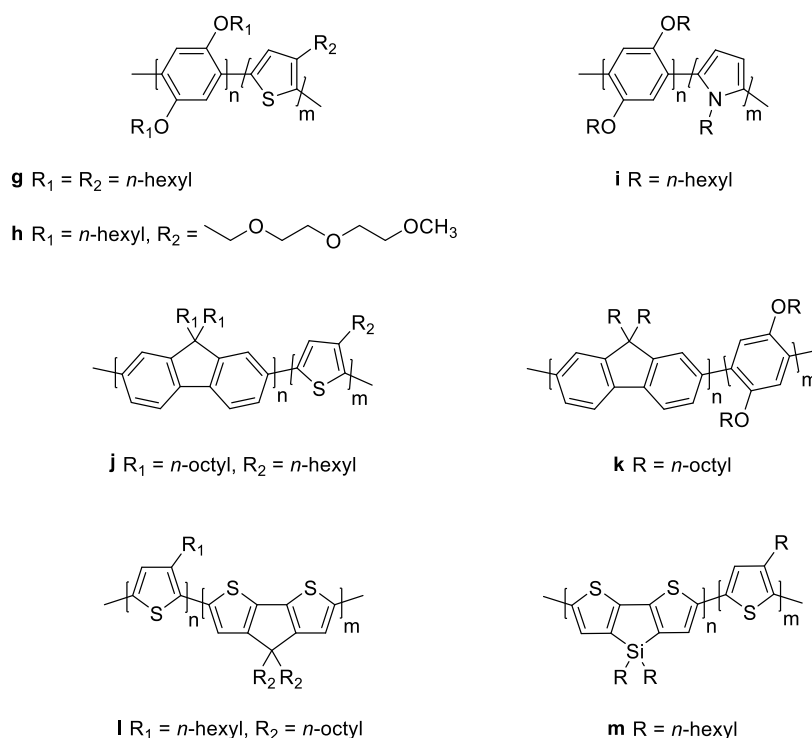


**Figure 8:** All-conjugated block copolymers composed of different aromatic moieties.

## 1.5 ORGANIC PHOTOVOLTAICS

Over the past decades, organic photovoltaics have seen an increasing interest as an alternative renewable energy source, directly harvesting electricity from the sun, in particular because they show some additional appealing features such as flexibility, semi-transparency and low-cost (high-throughput) large area production.<sup>[5,6,59]</sup> The standard device architecture of an organic solar cell is depicted in Figure 9. In general, such an OPV device consists of a photoactive layer, which contains both an electron donor (mostly a conjugated polymer) and an electron acceptor (commonly a fullerene derivative), sandwiched between two

electrodes. Typically, a transparent layer of indium-tin-oxide (ITO) is used as the anode, while aluminum is used as the cathode. Furthermore, interfacial layers are added between the photoactive layer and the electrodes to improve charge transport and collection.<sup>[60]</sup>

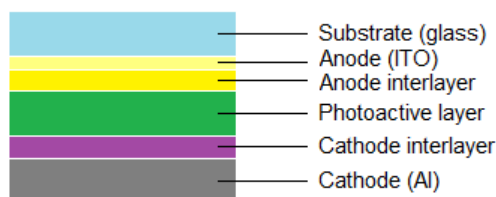


**Figure 9:** Standard device architecture of an organic solar cell.

The basic working principle of a (fullerene-based) organic solar cell is illustrated in Figure 10. When solar light strikes the photoactive layer of an OPV device, photons are absorbed by the photoactive donor material. This absorption excites electrons ( $e^-$ ) from the HOMO to the LUMO level of the donor, thereby leaving a hole ( $h^+$ ) behind. In this way, electron-hole pairs or excitons are formed, which are bound to each other via Coulombic interactions (step 1). In order to create free charges, these excitons first have to diffuse to the donor-acceptor interface (step 2). At this interface, the driving force provided by the offset between the HOMO and LUMO levels of the donor and acceptor leads to the dissociation of excitons into free charges (step 3). Afterwards, the electrons are transported by the acceptor material to the cathode, while the holes are transported through the donor material to the anode, thereby generating an electric current (step 4). Since the excitons show a very low lifetime before they recombine, they can only travel distances of  $\sim 5-10$  nm.<sup>[61]</sup> This means that only excitons that are created within 5-10 nm of the donor-acceptor interface can generate free charges. To overcome this problem, the bulk heterojunction (BHJ) concept was introduced,<sup>[62]</sup> whereby

the interfacial area between the electron donor and acceptor was increased substantially by intimately mixing them. Nowadays, all OPV devices that provide high efficiencies are based on this BHJ concept, wherein the morphology of the photoactive layer plays a key role.<sup>[5]</sup>

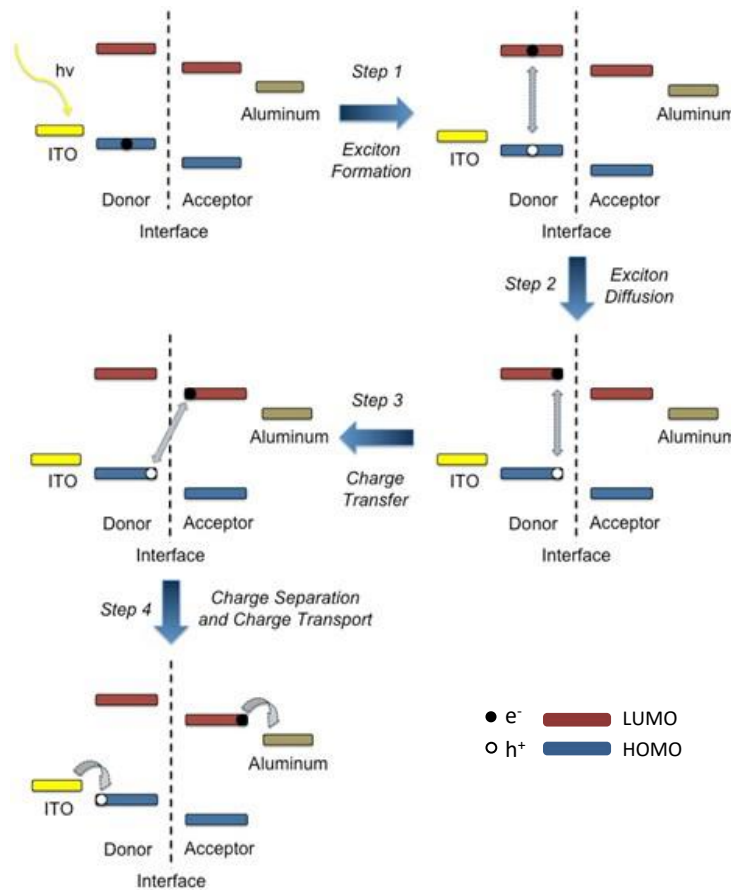


**Figure 10:** General mechanism of photoconversion in a (fullerene-based) organic solar cell.

For the evaluation of the solar cell performance, OPV devices are illuminated under standard test conditions, i.e. at 25 °C and an irradiation of 1000 W/m<sup>2</sup> with an air mass 1.5 (AM 1.5G) global spectrum, which corresponds to the solar irradiation with the sun at 45° above the horizon. This typically leads to current density-

voltage ( $J$ - $V$ ) curves as depicted in Figure 11, from which several parameters can be deduced.

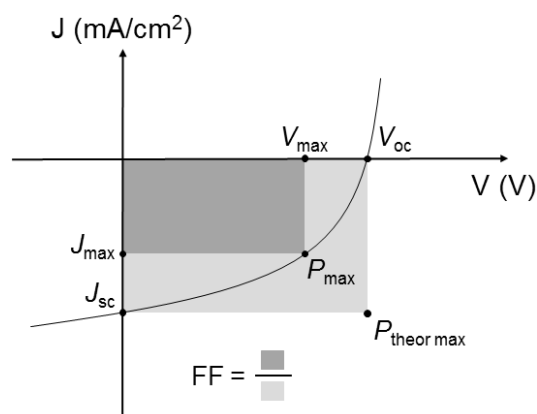


**Figure 11:**  $J$ - $V$  curve of a solar cell under illumination.

A first one is the short-circuit current density ( $J_{sc}$ ), which is the maximum current that a device can produce under illumination when applying a 0 V bias. Since this current is related to the amount of excitons that are created and separated into free charges which can be collected at the electrodes, it is largely dependent on the overlap of the absorption spectrum of the organic material and the emission spectrum of the sun. To increase this overlap, low bandgap alternating donor-acceptor copolymers were developed as the preferential donor materials, leading to extended absorption profiles. Additionally, the  $J_{sc}$  is also governed by the amount of charge recombination, the photoactive layer thickness and the charge collection efficiency. A second parameter is the open-circuit voltage ( $V_{oc}$ ), which is the maximum voltage that can be obtained when no current is flowing through the device. This voltage is related to the energy difference between the HOMO level of the donor and the LUMO level of the acceptor.<sup>[63]</sup> The theoretical maximum power output ( $P_{theor\ max}$ ) of a solar cell can then be calculated by taking the product of  $J_{sc}$  and  $V_{oc}$  (light gray rectangle in Figure 11). Under device operation, the

actual maximum power output ( $P_{max}$ ) can be determined by the product of the current ( $J_{max}$ ) and voltage ( $V_{max}$ ) at the maximum power point (dark gray rectangle in Figure 11). Another useful parameter, the fill factor (FF), can then be calculated by comparing the solar cell's actual maximum power output to its theoretical maximum power output:

$$FF = \frac{P_{max}}{P_{theor\ max}} = \frac{J_{max}V_{max}}{J_{sc}V_{oc}} \quad (1)$$

This fill factor gives an indication about the charge collection efficiency at the electrodes, thereby illustrating the connectivity of the pathways between the electrodes. With all of this knowledge, the solar cell performance can finally be determined by the ratio of the maximum power output of the solar cell ( $P_{max}$ ) to the total power input of photon irradiation ( $P_{in}$ ), which is expressed as the power conversion efficiency (PCE or  $\eta$ ):

$$PCE (\eta) = \frac{P_{max}}{P_{in}} = \frac{J_{sc}V_{oc}FF}{P_{in}} \quad (2)$$

Since the efficiency and stability of organic solar cells still need further improvement to give viable applications, a lot of different approaches have already been explored to boost these characteristics. Through the introduction of the bulk heterojunction concept, the development of low bandgap organic semiconductors to enhance the solar spectrum coverage, and the use of optimized device architectures, the efficiency of OPV devices could be elevated considerably to values currently exceeding 12%.<sup>[64-67]</sup> Even though most research activities have been oriented on the development of novel photoactive layer materials with appropriate optoelectronic properties, the introduction of interlayer materials has become an important approach to further enhance the device efficiency.<sup>[60,68-72]</sup> A variety of materials have been investigated as interlayer materials for organic solar cells.<sup>[60]</sup> Poly(3,4-ethylenedioxythiophene):poly(styrene sulfonate)

(PEDOT:PSS) is typically used as the anode interlayer to assist hole extraction from the photoactive layer. On the other hand, conjugated polyelectrolytes (CPEs) have been shown to be an interesting class of possible cathode interlayer materials, leading to PCE improvements of more than 20% compared to reference devices.<sup>[60,73–78]</sup>

## 1.6 THESIS OUTLINE

To become viable for commercialization, organic solar cells still need to improve in terms of production cost, efficiency and stability. Since the efficiency can be boosted by incorporating conjugated polyelectrolytes as cathode interlayers, a first part of this work describes the synthesis and application of ionic copolythiophenes as interlayers in OPV devices. The efficiency is also influenced by the molar mass and dispersity of the donor material, so it would be interesting if these parameters could be controlled. That is why in a second part of this work, the controlled synthesis of low bandgap alternating donor-acceptor copolymers was pursued via KCTCP. Another important factor governing the efficiency and stability of organic solar cells is the morphology of the photoactive layer. Hence, the synthesis of all-conjugated block copolymers or hyperbranched polymers was also explored. As such, the general goal of this doctoral thesis was to synthesize and characterize ionic (co)polythiophenes and all-conjugated copolymers with advanced architectures via transition-metal catalyzed polymerization procedures and to explore their possible applications in organic electronics.

In **Chapter 2**, a large series of random and block copolythiophene derivatives is synthesized in a controlled way via KCTCP, upon which they are turned ionic via post-polymerization reactions. As a consequence, the resulting conjugated

polyelectrolytes are soluble in more environmentally friendly solvents (such as methanol), facilitating their processing as cathode interlayer materials for organic solar cells. These materials were also applied in BHJ OPV devices, utilizing PCDTBT:PC<sub>71</sub>BM as the photoactive layer, resulting into an average efficiency increase of ~15%.

**Chapter 3** highlights the synthesis and characterization of an alternating thiophene-pyridine copolymer via KCTCP of the corresponding donor-acceptor monomer. Furthermore, also an all-conjugated block copolymer, containing P3HT as the first block and the alternating copolymer structure as the second block, was obtained in a one-pot procedure. These materials showed some interesting fluorescence features as well.

The same method was used in **Chapter 4** to obtain another alternating donor-acceptor (block) copolymer with a smaller bandgap. Therefore, a stronger acceptor unit was chosen, namely thieno[3,4-*b*]pyrazine. The obtained block copolymer showed an interesting absorption profile extending into the near-infrared (NIR) region.

In **Chapter 5**, a benzo[1,2-*b*:3,4-*b'*:5,6-*b''*]trithiophene core was synthesized and added in a small amount to the Stille polymerization of PCPDT-*alt*-Qx to introduce some branching in this low bandgap donor-acceptor copolymer. The obtained branched copolymer was evaluated as a donor material in an OPV device with PC<sub>71</sub>BM as the acceptor and compared with the linear copolymer.

Finally, in **Chapter 6** a general summary of the work is presented and an outlook is provided.

## 1.7 REFERENCES

- [1] Shirakawa, H.; Louis, E. J.; MacDiarmid, A. G.; Chiang, C. K.; Heeger, A. *J. J. Chem. Soc. Chem. Commun.* **1977**, 578–580.
- [2] Skotheim, T. A.; Reynolds, J. *Conjugated Polymers: Theory, Synthesis, Properties, and Characterization [Handbook of Conducting Polymers, Third Edition]*; CRC Press, 2006.
- [3] Dang, M. T.; Hirsch, L.; Wantz, G. *Adv. Mater.* **2011**, *23*, 3597–3602.
- [4] Marrocchi, A.; Lanari, D.; Facchetti, A.; Vaccaro, L. *Energy Environ. Sci.* **2012**, *5*, 8457–8474.
- [5] Lu, L.; Zheng, T.; Wu, Q.; Schneider, A. M.; Zhao, D.; Yu, L. *Chem. Rev.* **2015**, *115*, 12666–12731.
- [6] Mazzio, K. A.; Luscombe, C. K. *Chem. Soc. Rev.* **2015**, *44*, 78–90.
- [7] Xu, S.; Kim, E. H.; Wei, A.; Negishi, E. *Sci. Technol. Adv. Mater.* **2014**, *15*, 044201–044223.
- [8] Bao, Z.; Chan, W. K.; Yu, L. *J. Am. Chem. Soc.* **1995**, *117*, 12426–12435.
- [9] Suzuki, A. *J. Organomet. Chem.* **1999**, *576*, 147–168.
- [10] Roncali, J.; Leriche, P.; Cravino, A. *Adv. Mater.* **2007**, *19*, 2045–2060.
- [11] Zhang, Y.; Tajima, K.; Hirota, K.; Hashimoto, K. *J. Am. Chem. Soc.* **2008**, *130*, 7812–7813.
- [12] Topham, P. D.; Parnell, A. J.; Hiorns, R. C. *J. Polym. Sci. Part B Polym. Phys.* **2011**, *49*, 1131–1156.
- [13] Boon, F.; Hergué, N.; Deshayes, G.; Moerman, D.; Desbief, S.; De Winter, J.; Gerbaux, P.; Geerts, Y. H.; Lazzaroni, R.; Dubois, P. *Polym. Chem.* **2013**, *4*, 4303–4307.
- [14] Lee, Y.; Gomez, E. D. *Macromolecules* **2015**, *48*, 7385–7395.

- 
- [15] Wang, J.; Higashihara, T. *Polym. Chem.* **2013**, *4*, 5518–5526.
- [16] Qiu, Y.; Fortney, A.; Tsai, C.-H.; Baker, M. A.; Gil, R. R.; Kowalewski, T.; Noonan, K. J. T. *ACS Macro Lett.* **2016**, *5*, 332–336.
- [17] Mangold, H. S.; Richter, T. V.; Link, S.; Würfel, U.; Ludwigs, S. *J. Phys. Chem. B* **2012**, *116*, 154–159.
- [18] Guo, M.; Hayakawa, T.; Kakimoto, M.; Goodson, T. *J. Phys. Chem. B* **2011**, *115*, 13419–13432.
- [19] Sirringhaus, H.; Tessler, N.; Friend, R. H. *Science* **1998**, *280*, 1741–1744.
- [20] Andersson, M. R.; Thomas, O.; Mammo, W.; Svensson, M.; Theander, M.; Inganäs, O. *J. Mater. Chem.* **1999**, *9*, 1933–1940.
- [21] Li, G.; Shrotriya, V.; Huang, J.; Yao, Y.; Moriarty, T.; Emery, K.; Yang, Y. *Nat. Mater.* **2005**, *4*, 864–868.
- [22] Lin, J. W.-P.; Dudek, L. P. *J. Polym. Sci. Polym. Chem. Ed.* **1980**, *18*, 2869–2873.
- [23] Yamamoto, T.; Sanechika, K.; Yamamoto, A. *J. Polym. Sci. Polym. Lett. Ed.* **1980**, *18*, 9–12.
- [24] Osaka, I.; McCullough, R. D. *Acc. Chem. Res.* **2008**, *41*, 1202–1214.
- [25] McCullough, R. D.; Lowe, R. D.; Jayaraman, M.; Anderson, D. L. *J. Org. Chem.* **1993**, *58*, 904–912.
- [26] Chen, T.-A.; Rieke, R. D. *J. Am. Chem. Soc.* **1992**, *114*, 10087–10088.
- [27] Chen, T.-A.; Wu, X.; Rieke, R. D. *J. Am. Chem. Soc.* **1995**, *117*, 233–244.
- [28] Loewe, R. S.; Khersonsky, S. M.; McCullough, R. D. *Adv. Mater.* **1999**, *11*, 250–253.
- [29] Loewe, R. S.; Ewbank, P. C.; Liu, J.; Zhai, L.; McCullough, R. D. *Macromolecules* **2001**, *34*, 4324–4333.
- [30] Miyakoshi, R.; Yokoyama, A.; Yokozawa, T. *J. Am. Chem. Soc.* **2005**, *127*,

- 17542–17547.
- [31] Yokoyama, A.; Miyakoshi, R.; Yokozawa, T. *Macromolecules* **2004**, *37*, 1169–1171.
- [32] Qiu, J.; Charleux, B.; Matyjaszewski, K. *Polimery* **2001**, *46*, 453–460.
- [33] Willot, P.; Govaerts, S.; Koeckelberghs, G. *Macromolecules* **2013**, *46*, 8888–8895.
- [34] Iovu, M. C.; Sheina, E. E.; Gil, R. R.; McCullough, R. D. *Macromolecules* **2005**, *38*, 8649–8656.
- [35] Liu, J.; Loewe, R. S.; McCullough, R. D. *Macromolecules* **1999**, *32*, 5777–5785.
- [36] Koeckelberghs, G.; Vangheluwe, M.; Samyn, C.; Persoons, A.; Verbiest, T. *Macromolecules* **2005**, *38*, 5554–5559.
- [37] Sheina, E. E.; Khersonsky, S. M.; Jones, E. G.; McCullough, R. D. *Chem. Mater.* **2005**, *17*, 3317–3319.
- [38] Hollinger, J.; Jahnke, A. A.; Coombs, N.; Seferos, D. S. *J. Am. Chem. Soc.* **2010**, *132*, 8546–8547.
- [39] Palermo, E. F.; McNeil, A. J. *Macromolecules* **2012**, *45*, 5948–5955.
- [40] Ye, S.; Steube, M.; Carrera, E. I.; Seferos, D. S. *Macromolecules* **2016**, *49*, 1704–1711.
- [41] Yokoyama, A.; Kato, A.; Miyakoshi, R.; Yokozawa, T. *Macromolecules* **2008**, *41*, 7271–7273.
- [42] Pammer, F.; Jäger, J.; Rudolf, B.; Sun, Y. *Macromolecules* **2014**, *47*, 5904–5912.
- [43] Willot, P.; Koeckelberghs, G. *Macromolecules* **2014**, *47*, 8548–8555.
- [44] Miyakoshi, R.; Shimono, K.; Yokoyama, A.; Yokozawa, T. *J. Am. Chem. Soc.* **2006**, *128*, 16012–16013.

- 
- [45] Ohshimizu, K.; Takahashi, A.; Higashihara, T.; Ueda, M. *J. Polym. Sci. Part A Polym. Chem.* **2011**, *49*, 2709–2714.
- [46] Verswyvel, M.; Verstappen, P.; De Cremer, L.; Verbiest, T.; Koeckelberghs, G. *J. Polym. Sci. Part A Polym. Chem.* **2011**, *49*, 5339–5349.
- [47] Sui, A.; Shi, X.; Wu, S.; Tian, H.; Geng, Y.; Wang, F. *Macromolecules* **2012**, *45*, 5436–5443.
- [48] Nanashima, Y.; Yokoyama, A.; Yokozawa, T. *Macromolecules* **2012**, *45*, 2609–2613.
- [49] Nanashima, Y.; Shibata, R.; Miyakoshi, R.; Yokoyama, A.; Yokozawa, T. *J. Polym. Sci. Part A Polym. Chem.* **2012**, *50*, 3628–3640.
- [50] Wen, L.; Duck, B. C.; Dastoor, P. C.; Rasmussen, S. C. *Macromolecules* **2008**, *41*, 4576–4578.
- [51] Bridges, C. R.; McCormick, T. M.; Gibson, G. L.; Hollinger, J.; Seferos, D. *S. J. Am. Chem. Soc.* **2013**, *135*, 13212–13219.
- [52] Ouhib, F.; Hiorns, R. C.; de Bettignies, R.; Bailly, S.; Desbrières, J.; Dagron-Lartigau, C. *Thin Solid Films* **2008**, *516*, 7199–7204.
- [53] Ohshimizu, K.; Ueda, M. *Macromolecules* **2008**, *41*, 5289–5294.
- [54] Yokozawa, T.; Adachi, I.; Miyakoshi, R.; Yokoyama, A. *High Perform. Polym.* **2007**, *19*, 684–699.
- [55] Ge, J.; He, M.; Qiu, F.; Yang, Y. *Macromolecules* **2010**, *43*, 6422–6428.
- [56] Yang, X.; Loos, J.; Veenstra, S. C.; Verhees, W. J. H.; Wienk, M. M.; Kroon, J. M.; Michels, M. A. J.; Janssen, R. A. J. *Nano Lett.* **2005**, *5*, 579–583.
- [57] Miyakoshi, R.; Yokoyama, A.; Yokozawa, T. *Chem. Lett.* **2008**, *37*, 1022–1023.
- [58] Javier, A. E.; Varshney, S. R.; McCullough, R. D. *Macromolecules* **2010**, *43*, 3233–3237.

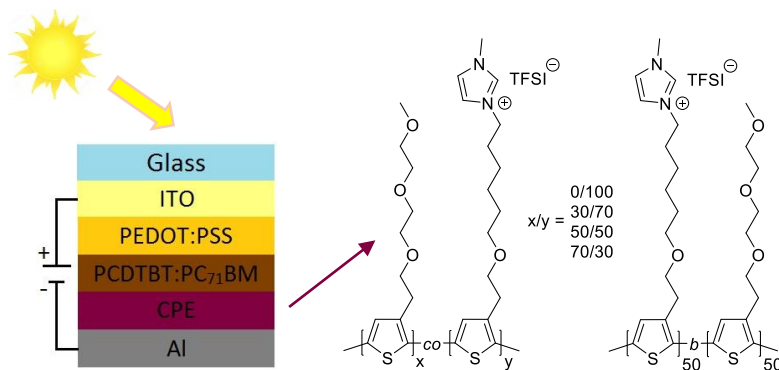
- [59] Cao, W.; Xue, J. *Energy Environ. Sci.* **2014**, *7*, 2123–2144.
- [60] Houston, J. E.; Richeter, S.; Clément, S.; Evans, R. C. *Polym. Int.* **2017**, DOI: 10.1002/pi.5397.
- [61] Scharber, M. C.; Sariciftci, N. S. *Prog. Polym. Sci.* **2013**, *38*, 1929–1940.
- [62] Yu, G.; Gao, J.; Hummelen, J. C.; Wudl, F.; Heeger, A. J. *Science* **1995**, *270*, 1789–1791.
- [63] Scharber, M. C.; Mühlbacher, D.; Koppe, M.; Denk, P.; Waldauf, C.; Heeger, A. J.; Brabec, C. J. *Adv. Mater.* **2006**, *18*, 789–794.
- [64] Li, S.; Ye, L.; Zhao, W.; Zhang, S.; Mukherjee, S.; Ade, H.; Hou, J. *Adv. Mater.* **2016**, *28*, 9423–9429.
- [65] Hu, H.; Jiang, K.; Yang, G.; Liu, J.; Li, Z.; Lin, H.; Liu, Y.; Zhao, J.; Zhang, J.; Huang, F.; Qu, Y.; Ma, W.; Yan, H. *J. Am. Chem. Soc.* **2015**, *137*, 14149–14157.
- [66] He, Z.; Zhong, C.; Su, S.; Xu, M.; Wu, H.; Cao, Y. *Nat. Photonics* **2012**, *6*, 591–595.
- [67] Liu, Y.; Zhao, J.; Li, Z.; Mu, C.; Ma, W.; Hu, H.; Jiang, K.; Lin, H.; Ade, H.; Yan, H. *Nat. Commun.* **2014**, *5*, 5293.
- [68] Sun, Z.; Xiao, K.; Keum, J. K.; Yu, X.; Hong, K.; Browning, J.; Ivanov, I. N.; Chen, J.; Alonzo, J.; Li, D.; Sumpter, B. G.; Payzant, E. A.; Rouleau, C. M.; Geohegan, D. B. *Adv. Mater.* **2011**, *23*, 5529–5535.
- [69] Seo, J. H.; Gutacker, A.; Sun, Y.; Wu, H.; Huang, F.; Cao, Y.; Scherf, U.; Heeger, A. J.; Bazan, G. C. *J. Am. Chem. Soc.* **2011**, *133*, 8416–8419.
- [70] Ju, H.; Kesting, K. M.; Zhang, W.; Pan, X.; Wang, C.-H.; Yang, Y.-W.; Ginger, D. S.; Zhu, J. *ACS Appl. Mater. Interfaces* **2016**, *8*, 2125–2131.
- [71] Gao, M.; Subbiah, J.; Geraghty, P. B.; Chen, M.; Purushothaman, B.; Chen, X.; Qin, T.; Vak, D.; Scholes, F. H.; Watkins, S. E.; Skidmore, M.; Wilson,

- G. J.; Holmes, A. B.; Jones, D. J.; Wong, W. W. H. *Chem. Mater.* **2016**, *28*, 3481–3487.
- [72] Li, C.-Z.; Chueh, C.-C.; Yip, H.-L.; O'Malley, K. M.; Chen, W.-C.; Jen, A. K.-Y. *J. Mater. Chem.* **2012**, *22*, 8574–8578.
- [73] Oh, S.-H.; Na, S.-I.; Jo, J.; Lim, B.; Vak, D.; Kim, D.-Y. *Adv. Funct. Mater.* **2010**, *20*, 1977–1983.
- [74] Chang, Y.-M.; Zhu, R.; Richard, E.; Chen, C.-C.; Li, G.; Yang, Y. *Adv. Funct. Mater.* **2012**, *22*, 3284–3289.
- [75] Chevrier, M.; Houston, J. E.; Kesters, J.; Van den Brande, N.; Terry, A. E.; Richeter, S.; Mehdi, A.; Coulembier, O.; Dubois, P.; Lazzaroni, R.; Van Mele, B.; Maes, W.; Evans, R. C.; Clément, S. *J. Mater. Chem. A* **2015**, *3*, 23905–23916.
- [76] Liu, H.; Hu, L.; Wu, F.; Chen, L.; Chen, Y. *ACS Appl. Mater. Interfaces* **2016**, *8*, 9821–9828.
- [77] Kesters, J.; Govaerts, S.; Pirotte, G.; Drijkoningen, J.; Chevrier, M.; Van den Brande, N.; Liu, X.; Fahlman, M.; Van Mele, B.; Lutsen, L.; Vanderzande, D.; Manca, J.; Clément, S.; Von Hauff, E.; Maes, W. *ACS Appl. Mater. Interfaces* **2016**, *8*, 6309–6314.
- [78] Kesters, J.; Ghoo, T.; Penxten, H.; Drijkoningen, J.; Vangerven, T.; Lyons, D. M.; Verreet, B.; Aernouts, T.; Lutsen, L.; Vanderzande, D.; Manca, J.; Maes, W. *Adv. Energy Mater.* **2013**, *3*, 1180–1185.



# Chapter 2

## Conjugated ionic (co)polythiophene-based cathode interlayers for bulk heterojunction organic solar cells



S. Govaerts, J. Kesters, M. Defour, B. Van Mele, H. Penxten, S. Neupane, F. U. Renner, L. Lutsen, D. Vanderzande and W. Maes, manuscript submitted.

## **ABSTRACT**

The incorporation of conjugated polyelectrolytes as cathode interlayers in organic photovoltaics has been proven to be an effective way to boost the device efficiency. Nevertheless, more detailed investigations of the structure-property relationships of these interlayer materials, in particular related to the film deposition behavior, can provide further insights into their mode of action. With this aim, a series of ionic (co)polythiophenes is successfully synthesized via Kumada catalyst-transfer condensation polymerization and subsequent introduction of ionic moieties on the polymer side chains. Both the topology (i.e. homopolymers, random and block copolymers) and the amount of ionic groups are systematically varied. The polymers are fully characterized and then applied as cathode interlayers in polymer solar cells based on PCDTBT:PC<sub>71</sub>BM, affording an average efficiency increase of ~15%. The structural screening on one hand indicates that the efficiency gain is a rather general phenomenon for this material class. On the other hand, the best photovoltaic responses are observed for the conjugated polyelectrolytes with a higher triethylene glycol side chain ratio and the block copolymer structure performs slightly better as compared to the random copolymer with the same (50/50) monomer ratio. Based on these findings, the field can move on to a more rational development of novel interfacial materials and thereby push the device efficiency even further.

## 2.1 INTRODUCTION

Over the past decade, organic photovoltaics (OPVs) have shown a growing potential as an alternative renewable energy source, in particular because of some additional appealing features such as flexibility, semi-transparency, improved low-light performance, and low-cost (high-throughput) large area production.<sup>[1-3]</sup> The introduction of the bulk heterojunction (BHJ) concept, in which the photoactive layer consists of electron donating and accepting materials intimately mixed at the nanoscale, the development of push-pull type low bandgap organic semiconductors to enhance the solar spectrum coverage, and the use of optimized device architectures have been key developments to elevate the power conversion efficiency (PCE) of OPV devices to values currently exceeding 12%.<sup>[4-8]</sup> Even though most research activities have been oriented on the development of novel active layer materials with appropriate optoelectronic properties, the introduction of interlayer materials has become a widely accepted approach to further enhance the device efficiency.<sup>[9-17]</sup> One class of interlayer materials of particular interest are conjugated polyelectrolytes (CPEs). They can be processed from eco-friendly, orthogonal solvents, thereby preventing re-dissolution of the underlying layer during device fabrication. The incorporation of such CPEs has led to PCE improvements of more than 20% compared to reference devices, which can mainly be attributed to the formation of interfacial dipoles, influencing the work function of the adjacent electrode.<sup>[10,18-23]</sup> This improves the energy level alignment between the photoactive layer and the cathode (in standard device stacks), resulting in an enhanced charge collection and a reduced charge recombination.

Several CPE materials have already been studied as cathode interlayers. The conjugated polymer backbone has not been explored much further than polyfluorene and polythiophene derivatives and most variation has been introduced in the ionic moieties.<sup>[12]</sup> Previous work in our group focused on imidazolium-functionalized polythiophenes, outperforming the ammonium-functionalized counterparts.<sup>[11]</sup> More recently, impedance spectroscopy measurements revealed that the dielectric permittivity, induced by the ionic functionalities, is an important parameter to improve charge collection.<sup>[23]</sup> The exact CPE structure also influences other aspects. An ionic random (50/50) copolythiophene with triethylene glycol and imidazolium-functionalized side chains (**P3**; Figure 1) for instance demonstrated superior performance in comparison to a fully imidazolium-functionalized homopolymer, resulting from an improved affinity with the photoactive layer beneath due to the presence of the non-ionic side chains.<sup>[23]</sup> For inverted OPV devices incorporating the CPE at the bottom side, Chen *et al.* demonstrated that more smooth and homogeneous photoactive layer deposition could be obtained by increasing the amount of polar groups in polyfluorene-based CPEs.<sup>[22]</sup>

In this context, a series of polythiophene CPEs with TFSI (bis(trifluoromethane)sulfonimide) counteranions was synthesized by Kumada catalyst-transfer condensation polymerization (KCTCP), subsequent substitution of the bromide-functionalized side chains, and final exchange of the Br counteranions. Due to the controlled chain-growth character of this type of polymerization, different polymer topologies (homopolymers, random and block copolymers) were obtained with a high control over the molar mass, dispersity and end groups in a relatively straightforward way via one-pot procedures. The

ratio of the ionic groups present in the random copolymers was systematically varied and a block copolymer was prepared as well for comparison. The synthesized materials were then evaluated as cathode interlayer materials in standard BHJ OPV devices based on PCDTBT:PC<sub>71</sub>BM to further explore the effect of structural changes on the overall device performance.

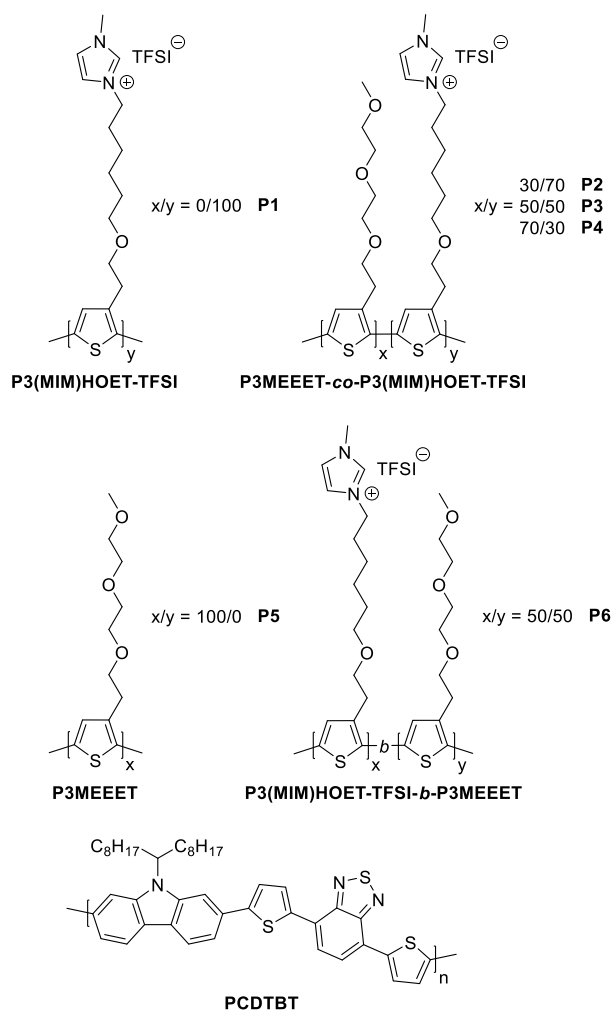


**Figure 1:** Overview of the synthesized polymers and the used donor material.

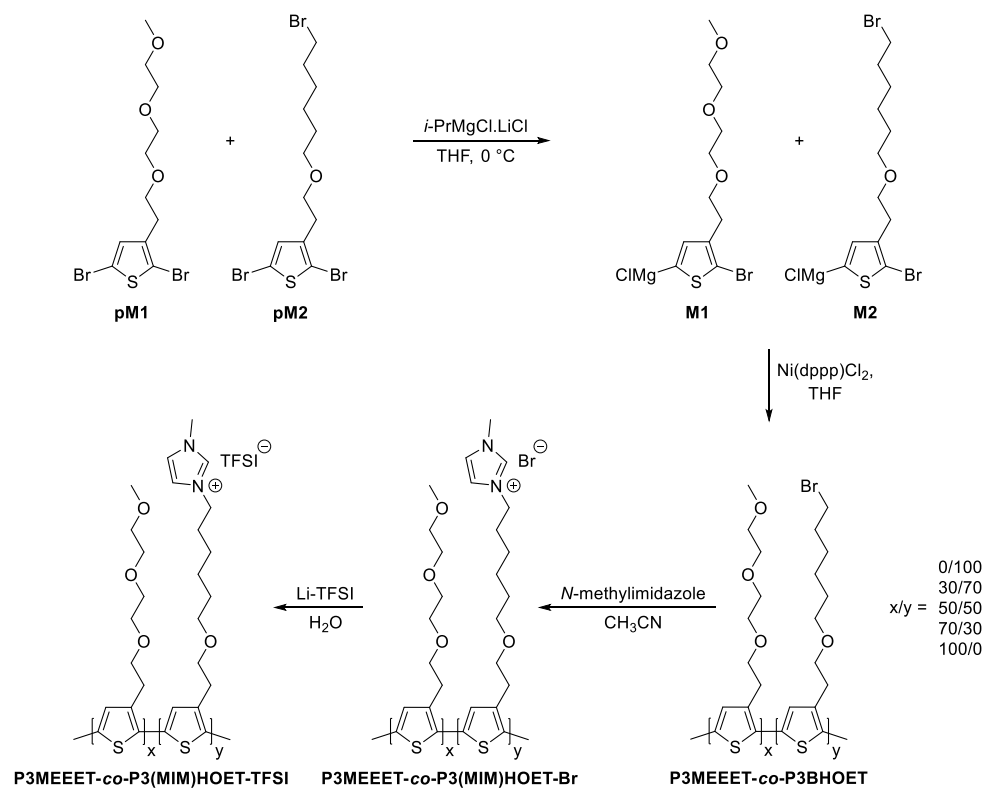
## 2.2 RESULTS AND DISCUSSION

### 2.2.1 Polymer synthesis

From previous work, the **P3MEEET-co-P3(MIM)HOET-TFSI** (50/50) random copolymer (**P3**; Figure 1) was identified as the CPE material affording best OPV device efficiencies for various photoactive layer blend combinations.<sup>[23–25]</sup> This material was hence used as the starting point to create further structural variation. A series of random copolymers with monomer ratios varying from 0/100, 30/70, 50/50, 70/30 to 100/0 was targeted. For the synthesis of these random copolymers, the two different precursor monomers were first prepared, i.e. 2,5-dibromo-3-[2'-(2'-(2'-methoxyethoxy)ethoxy)ethyl]thiophene (**pM1**) and 2,5-dibromo-3-[2'-(6'-bromohexyloxy)ethyl]thiophene (**pM2**) (Scheme 1).<sup>[26]</sup> These precursor monomers were then activated via a Grignard metathesis (GRIM) reaction. This was done prior to the polymerization by combining **pM1** and **pM2** in the respective ratio in dry THF, whereby a monomer concentration of 0.1 M was maintained, and adding 1.0 equivalents of *i*-PrMgCl.LiCl to this mixture at 0 °C. After stirring for 1 h, the active monomers **M1** and **M2** (and their isomers with MgCl on the 2-position) were obtained.<sup>1</sup> After the GRIM reaction, the resulting reaction mixture was transferred to a flask with the Ni(dppp)Cl<sub>2</sub> catalyst in dry THF (monomer concentration = 0.075 M) to start the polymerization (Scheme 1). Due to the controlled character of the KCTCP, the amount of Ni-catalyst could be adjusted for each individual polymerization to always end up with a number-average molar mass ( $M_n$ ) of ~25 000 g/mol.

---

<sup>1</sup> Since these isomers are not able to participate in the polymerization reaction, they are not displayed in Scheme 1.



**Scheme 1:** Synthesis of the ionic (co)polythiophenes via KCTCP and two post-polymerization reactions.

To optimize the polymerization conditions and to be able to use a uniform polymerization method for the synthesis of all ionic (co)polythiophenes, the polymerization conditions for the two homopolymers, **P3BHOET** (poly{3-[2'-(6'-bromohexyloxy)ethyl]thiophene-2,5-diyl};  $x/y = 0/100$ ) and **P3MEEET** (poly{3-[2'-(2'-(2'-methoxyethoxy)ethoxy)ethyl]thiophene-2,5-diyl};  $x/y = 100/0$ ) were investigated first. In a first polymerization test, **M2** was polymerized at RT and aliquots of the polymerization mixture were taken after 30 minutes, 1 hour, 5 hours, and 21 hours, and quenched with a MeOH/HCl mixture. These aliquots were then analyzed by gel permeation chromatography (GPC) and the results are shown in Figure 2a. From the GPC profiles it can be seen that a shoulder arises

after 30 minutes, with a molar mass that is about two times the molar mass of the main peak, resulting in a rise in dispersity ( $\mathcal{D}$ ) from 1.14 to 1.34. The appearance of this shoulder can be explained by the occurrence of disproportionation, whereby two polymer chains are coupled to each other.<sup>[27]</sup> To evaluate whether this is also the case for the polymerization of **P3MEEET**, **M1** was also polymerized at RT and aliquots were taken after 30 minutes, 1 hour and 2 hours. The resulting GPC profiles (Figure 2b) once again show a shoulder arising after 30 minutes, leading to a rise in dispersity from 1.31 to 1.50.

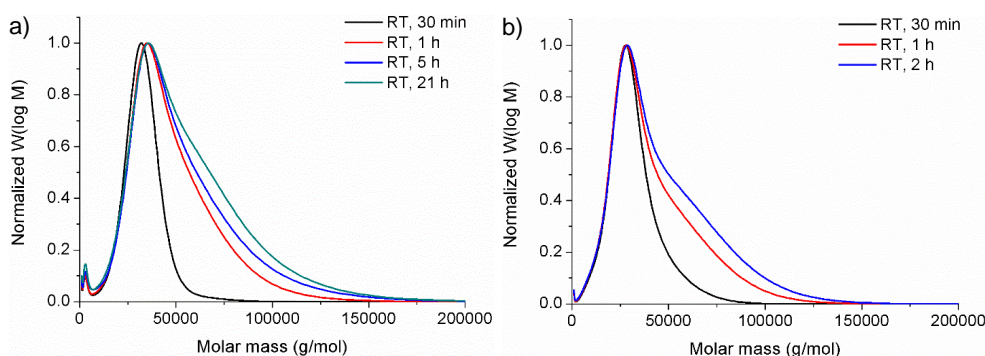


**Figure 2:** GPC profiles of the polymerization tests at RT of a) **M2** and b) **M1**.

The above results indicated that a polymerization time of 30 minutes is optimal to obtain the desired molar mass and to avoid undesired termination reactions. Due to these findings, all polymerizations described in Scheme 1 were performed at RT and stopped after 30 minutes by quenching with a MeOH/HCl mixture. Afterwards, the (co)polymers were purified by Soxhlet extractions with MeOH, acetone (for **P3BHOET** (0/100), **P3MEEET-co-P3BHOET** (30/70) and **P3MEEET-co-P3BHOET** (50/50)), hexanes, and chloroform, respectively. For the polymers with a higher **P3MEEET** content, it was not possible to use acetone for the Soxhlet extraction since these polymers readily dissolve in acetone. After final precipitation in MeOH, the **P3MEEET-co-P3BHOET** random copolymers

were obtained as purple solids. The resulting molar masses and dispersities are listed in Table 1. The built-in ratios of the respective monomers were confirmed in the  $^1\text{H}$  NMR spectra of the polymers (Figures S3–S6, Supporting Information).

**Table 1:** GPC data of the synthesized polymers.

Polymer (x/y)	$M_n \times 10^4$ (g/mol)	$\bar{D}$
<b>P3BHOET</b> (0/100)	1.7	1.18
<b>P3MEEET-co-P3BHOET</b> (30/70)	2.4	1.23
<b>P3MEEET-co-P3BHOET</b> (50/50)	2.8	1.16
<b>P3BHOET-b-P3MEEET</b> (50/50)	2.9	1.34
<b>P3MEEET-co-P3BHOET</b> (70/30)	2.6	1.17
<b>P3MEEET</b> (100/0)	1.9	1.30

After obtaining the random copolymers, two post-polymerization reactions were performed to obtain the desired ionic (co)polythiophenes (Scheme 1). In the first reaction, the bromide groups at the end of the alkyl chains were replaced by *N*-methylimidazolium moieties. This was done *via* reaction with a large excess of *N*-methylimidazole in acetonitrile under microwave irradiation for 4 hours at 100 °C. The resulting ionic **P3MEEET-co-P3(MIM)HOET-Br** (co)polymers were then precipitated in Et<sub>2</sub>O and purified by Soxhlet extractions in Et<sub>2</sub>O and MeOH (dissolving the polymers), respectively, to remove the excess of *N*-methylimidazole.

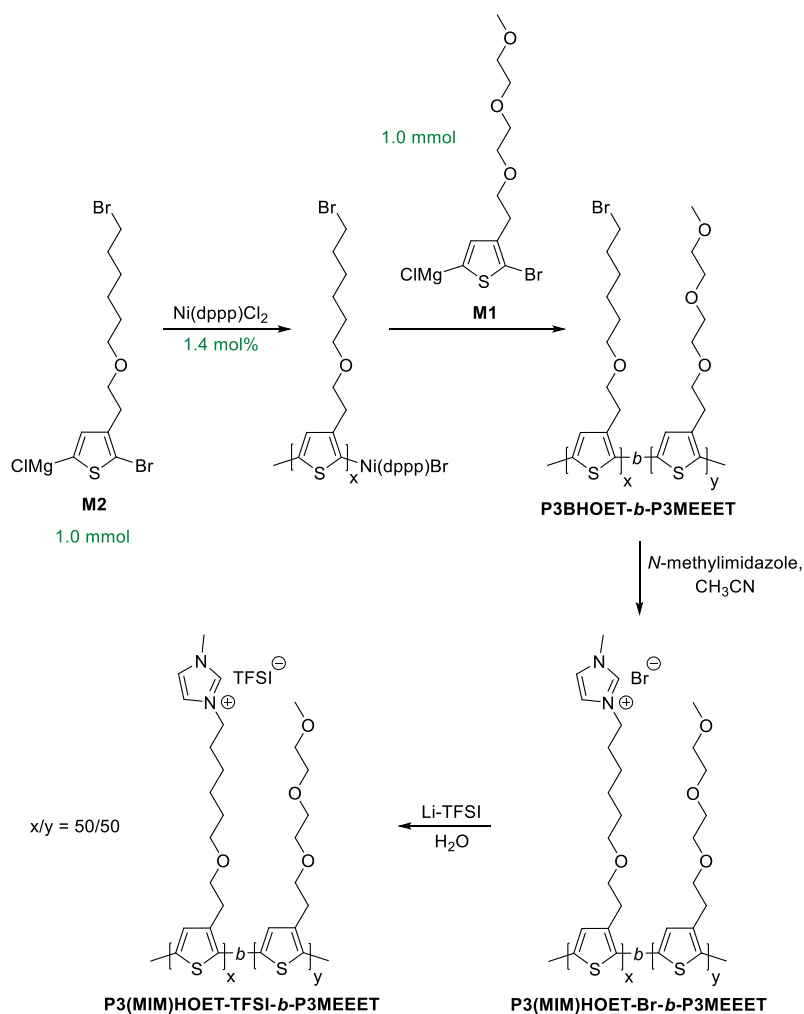
It was already shown before that ionic (co)polymers with bromide counteranions are strongly hygroscopic and as such not ideal for device incorporation.<sup>[23,26,28]</sup> Therefore, the bromide counteranions were replaced by more hydrophobic TFSI counteranions in a final step. This was performed by dissolving the **P3MEEET-co-P3(MIM)HOET-Br** (co)polymers in water, followed by a dropwise addition of a Li-TFSI solution in water (Scheme 1). After a few hours, the resulting precipitates were filtered off over a cellulose membrane, washed with water and dried under

vacuum. In this way, the desired ionic **P3MEEET-co-P3(MIM)HOET-TFSI** (co)polymers were finally obtained.

Since the solar cell performance among others depends on the morphology of the interlayer material on top of the photoactive layer and block copolymers are known for their peculiar self-assembly properties,<sup>[28-30]</sup> a block copolythiophene was synthesized as well from the same two monomer units in a 50/50 ratio (Scheme 2). This was done by first polymerizing the **P3BHOET** block by adding one equivalent of *i*-PrMgCl.LiCl to **pM2** at 0 °C, resulting in the active monomer **M2** (and its isomer) after 1 h, and then adding this reaction mixture to 1.4 mol% of Ni(dppp)Cl<sub>2</sub> at RT.<sup>2</sup> After a polymerization time of 15 minutes, a small fraction of the polymerization mixture was quenched with a MeOH/HCl mixture, affording the **P3BHOET** reference homopolymer. To the rest of the polymerization mixture, the *in situ* prepared reaction mixture containing active monomer **M1** was added to create the **P3MEEET** second block.<sup>2</sup> The polymerization of the second block was allowed to further proceed for 30 minutes at RT, before being quenched with a MeOH/HCl mixture. The resulting block copolymer was then purified by Soxhlet extractions with MeOH, hexanes, and chloroform, respectively, finally yielding the **P3BHOET-*b*-P3MEEET** block copolymer.

---

<sup>2</sup> Again both isomers (with MgCl on the 2-position) of the active monomers **M1** and **M2** are not displayed in Scheme 2, since they do not participate in the polymerization reaction.



**Scheme 2:** Synthesis of the ionic **P3(MIM)HOET-TFSI-*b*-P3MEEET** block copolymer.

To verify the block copolymer formation, both the **P3BHOET** homopolymer sample and the **P3BHOET-*b*-P3MEEET** block copolymer were analyzed by GPC. From the resulting GPC profiles, it can be observed that there is a clear shift to higher  $M_n$  values for the block copolymer in comparison to the homopolymer (Figure 3). The **P3BHOET** homopolymer showed an  $M_n$  of 10 000 g/mol and a  $\mathcal{D}$  of 1.38, while the **P3BHOET-*b*-P3MEEET** block copolymer has an  $M_n$  of 15 000

g/mol and a  $\mathcal{D}$  of 1.42 (before Soxhlet extraction). After Soxhlet extraction, the block copolymer showed an  $M_n$  of 29 000 g/mol and a  $\mathcal{D}$  of 1.34 (Table 1), nicely corresponding to the expectations and specifically targeted to be in range with the random copolymers described above. By using 1.4 mol% of Ni(dppp)Cl<sub>2</sub>, an  $M_n$  of ~26 000 g/mol (~50 monomer units of 289 g/mol for the **P3BHOET** block and ~50 monomer units of 228 g/mol for the **P3MEEET** block) was foreseen for the **P3BHOET-*b*-P3MEEET** block copolymer (taking into account a monomer loss of ~25% due to the non-selective GRIM reaction).

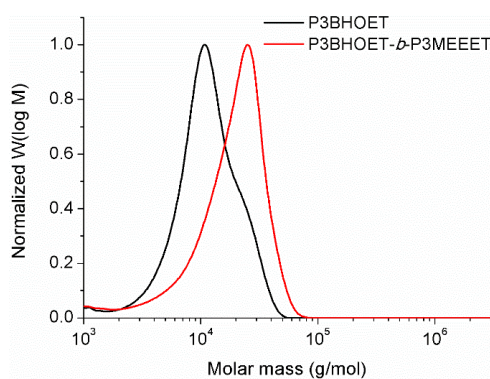


**Figure 3:** GPC profiles for the **P3BHOET** homopolymer (quench) and the **P3BHOET-*b*-P3MEEET** block copolymer (before Soxhlet extraction).

Finally, the obtained block copolymer was made ionic, following a similar procedure as described above, resulting into the ionic **P3(MIM)HOET-TFSI-*b*-P3MEEET** block copolymer (Scheme 2). An overview of the final synthesized ionic copolythiophenes is given in Figure 1. For the sake of clarity, the polymers are denoted as **P1–P6**, which will be used further on.

### 2.2.2 Polymer characterization

The optical properties of the synthesized polymers were investigated by UV-vis absorption spectroscopy. Because of the different amounts of incorporated ionic

groups, the polymers showed varying solubility characteristics and different solvents had to be used. From the spectra in Figure 4, it is clear that all polymers show about the same absorption profile, with a wavelength at maximal absorbance ( $\lambda_{\text{max}}$ ) located between 438 and 446 nm.

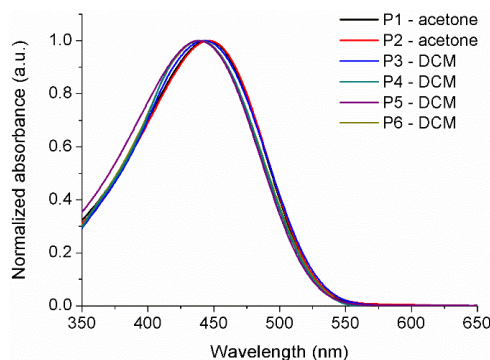


**Figure 4:** UV-vis absorption spectra in solution for the synthesized ionic polythiophenes **P1–P6**.

The electrochemical properties of the novel materials were analyzed by cyclic voltammetry (Table S1 and Figure S17, Supporting Information). Detailed comparison of the obtained oxidation and reduction onsets and resulting HOMO-LUMO values is, however, complicated by the different solubility characteristics, impeding analysis of the full polymer series in one single solvent or in film.

The thermal stability of all polymers was studied by thermogravimetric analysis (TGA), showing strong similarities for all polymers and no significant mass loss up to 325–350 °C (Figure S18, Supporting Information). Further detailed thermal analysis was performed by rapid heat-cool calorimetry (RHC) measurements (Figure 5; Table S2–S3 and Figure S19, Supporting Information). From these data, it is clear that the **P1** ionic homopolymer shows a relatively low glass transition temperature ( $T_g$ ) and a low melting enthalpy ( $\Delta H$ ) after the first heating cycle. This melting behavior is, however, no longer observed when the polymer is

reheated (second heating at 500 K/min) after a preceding cooling step at a relatively low cooling rate (20 K/min), implying that this cooling rate is too high to allow the development of a crystalline phase. On the other hand, the fully TEGylated (TEG = triethylene glycol) **P5** homopolymer shows a clear melting behavior after the first as well as the second heating cycle. The crystallinity of the random copolymers **P2–P4** and the block copolymer **P6** depends on the relative content of the two constituent monomers. By decreasing the content of **P3(MIM)HOET-TFSI**, which clearly has a lower  $\Delta H$  than **P3MEEET**, the melting enthalpy (and therefore the crystallinity) of the random copolymers increases. This is confirmed when the  $\Delta H$  values of **P2–P4** and **P6** are estimated based upon the relative content of the two monomers and the  $\Delta H$  values of the homopolymers **P1** and **P5** after the first heating cycle (Table S2, Supporting Information). The melting temperatures ( $T_m$ ) and  $\Delta H$  values after the second heating cycle are consistently lower than after the first heating cycle (Tables S2 and S3, Supporting Information) which could be explained by the continued development of stable crystals during casting or at room temperature. Another important observation is that the 50/50 random copolymer **P3** and the 50/50 block copolymer **P6** show very different heating profiles. The block copolymer shows a very broad melting behavior with two different peaks, while the random copolymer shows just one distinct melting peak located in between those of the two homopolymers **P1** and **P5** (Figure 5a). This difference further confirms the formation of a block copolymer.

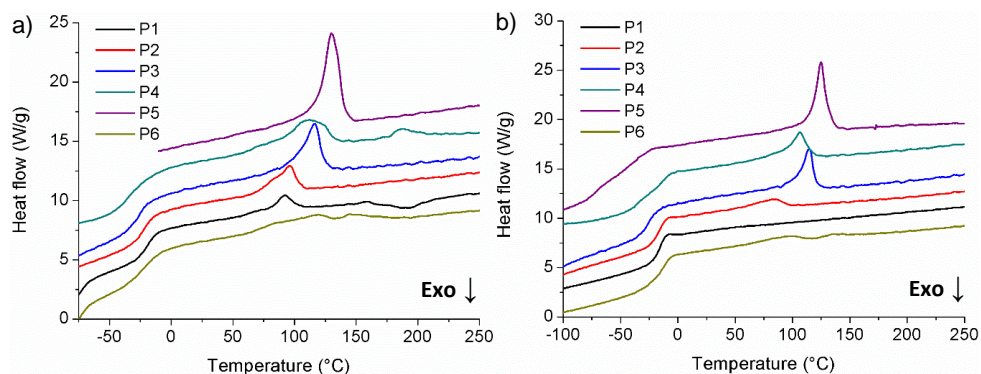


**Figure 5:** RHC heating profiles of the synthesized polymers **P1–P6**, obtained after a) a first heating cycle at 500 K/min, and b) a second heating cycle at 500 K/min (after preceding cooling at 20 K/min). The curves are shifted vertically for clarity.

### 2.2.3 Photovoltaic properties

The incorporation of CPE interlayers in OPV devices has already been proven to be a successful strategy to boost the performance. In past work, we briefly demonstrated how the chemical structure of polythiophene-based CPE materials can influence the deposition behavior on top of different donor:acceptor blends.<sup>[23]</sup> To gain further insights into the film formation properties, the newly synthesized CPE materials were incorporated in BHJ polymer solar cells with a standard device architecture consisting of glass/ITO/PEDOT:PSS/PCDTBT:PC<sub>71</sub>BM/interlayer/Al (the PCTDBT structure is depicted in Figure 1). The photoactive layer was prepared according to a literature recipe<sup>[31]</sup> with a total concentration of 20 mg/mL in *ortho*-dichlorobenzene (*o*DCB) and a 1:4 polymer:PC<sub>71</sub>BM ratio. The CPEs were deposited on top of the active layer from methanol solutions with varying concentrations. The device results are summarized in Table 2 and Figure 6a. Polymer **P5** was excluded from the series because of its insoluble nature in the chosen solvent. As can be observed, the reference device employing calcium

instead of a CPE exhibits an average PCE of 4.10%, with a top efficiency of 4.34%. Similar to previous studies on PCDTBT:PC<sub>71</sub>BM devices containing CPE interlayers,<sup>[11,23]</sup> all photovoltaic parameters (open-circuit voltage ( $V_{oc}$ ), short-circuit current density ( $J_{sc}$ ), fill factor (FF), and PCE) were enhanced, resulting in an average PCE increase of 15–17%. As such, the top performing device incorporating a CPE (**P4**) demonstrated, on average, a  $V_{oc}$  of 0.88 V (vs. 0.84 V), a  $J_{sc}$  of 9.02 mA/cm<sup>2</sup> (vs. 8.71 mA/cm<sup>2</sup>) and a FF of 62% (vs. 56%), resulting in an average PCE of 4.92% (vs. 4.10%). The increase in  $J_{sc}$  for all interlayer containing devices was also confirmed by extracting the currents from external quantum efficiency (EQE) measurements on average-performing devices (Figure 6b), with  $J_{EQE}$  values of 8.00, 8.81, 8.57, 8.44, 8.87, and 8.51 mA/cm<sup>2</sup> for the devices employing Ca, **P1**, **P2**, **P3**, **P4**, and **P6**, respectively (with corresponding  $J_{sc}$  values of 8.14, 8.79, 8.78, 8.77, 8.86, and 8.62 mA/cm<sup>2</sup>, respectively).

**Table 2:** Photovoltaic parameters of BHJ polymer solar cells (PCDTBT:PC<sub>71</sub>BM) with and without CPE cathode interlayers.

Entry	Cathode interlayer	Conc. (mg/mL)	$V_{oc}$ (V)	$J_{sc}$ (mA/cm <sup>2</sup> )	FF	Avg. $\eta$ (%) <sup>a</sup>	Best $\eta$ (%)
1	Ca	/	0.84 ± 0.01	8.71 ± 0.30	0.56 ± 0.03	4.10 ± 0.14	4.34
2	<b>P1</b>	0.25	0.85 ± 0.02	8.41 ± 0.35	0.60 ± 0.02	4.29 ± 0.32	4.65
3	<b>P1</b>	0.5	0.87 ± 0.02	8.90 ± 0.38	0.58 ± 0.03	4.49 ± 0.26	4.93
4	<b>P1</b>	1	0.88 ± 0.00	9.01 ± 0.39	0.59 ± 0.01	4.68 ± 0.23	4.86
5	<b>P1</b>	1.5	0.86 ± 0.02	9.09 ± 0.40	0.61 ± 0.01	4.77 ± 0.29	5.11
6	<b>P2</b>	0.25	0.87 ± 0.02	8.92 ± 0.33	0.61 ± 0.01	4.73 ± 0.19	5.04
7	<b>P2</b>	0.5	0.88 ± 0.00	8.86 ± 0.39	0.61 ± 0.01	4.76 ± 0.20	5.07
8	<b>P2</b>	1	0.87 ± 0.02	8.94 ± 0.28	0.60 ± 0.01	4.67 ± 0.26	4.91

Conjugated ionic (co)polythiophene-based cathode interlayers

9	<b>P2</b>	1.5	0.87 ± 0.02	9.04 ± 0.34	0.61 ± 0.01	4.80 ± 0.19	4.98
10	<b>P3</b>	0.25	0.84 ± 0.00	8.35 ± 0.19	0.62 ± 0.01	4.35 ± 0.01	4.38
11	<b>P3</b>	0.5	0.86 ± 0.02	8.76 ± 0.31	0.61 ± 0.01	4.60 ± 0.19	4.83
12	<b>P3</b>	1	0.87 ± 0.00	8.86 ± 0.21	0.61 ± 0.01	4.70 ± 0.15	4.81
13	<b>P3</b>	1.5	0.87 ± 0.02	8.56 ± 0.55	0.61 ± 0.01	4.54 ± 0.35	4.96
14	<b>P4</b>	0.25	0.86 ± 0.02	8.32 ± 0.33	0.63 ± 0.02	4.51 ± 0.23	4.80
15	<b>P4</b>	0.5	0.85 ± 0.02	8.35 ± 0.30	0.61 ± 0.01	4.33 ± 0.22	4.64
16	<b>P4</b>	1	0.88 ± 0.00	9.02 ± 0.29	0.62 ± 0.01	4.92 ± 0.17	5.11
17	<b>P4</b>	1.5	0.88 ± 0.00	8.98 ± 0.22	0.61 ± 0.00	4.82 ± 0.14	5.05
18	<b>P6</b>	0.25	0.88 ± 0.00	9.23 ± 0.40	0.60 ± 0.01	4.87 ± 0.16	5.06
19	<b>P6</b>	0.5	0.88 ± 0.00	9.21 ± 0.35	0.60 ± 0.02	4.86 ± 0.17	5.14
20	<b>P6</b>	1	0.88 ± 0.00	9.39 ± 0.36	0.59 ± 0.01	4.84 ± 0.10	4.95

<sup>a</sup> Average PCE over 8–16 devices.

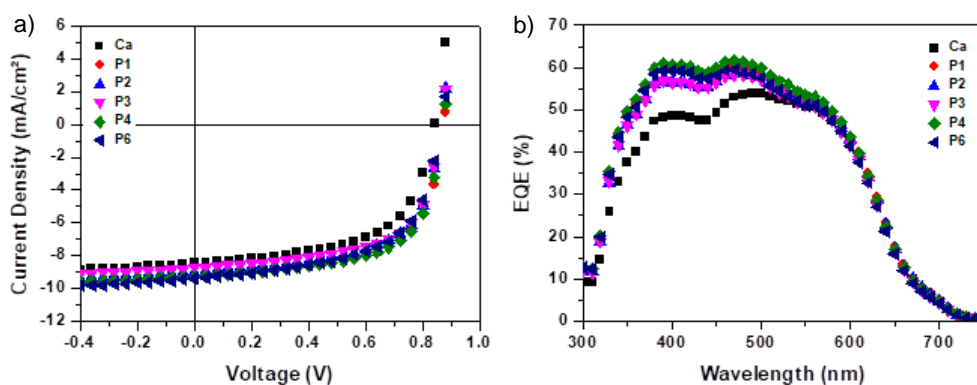


**Figure 6:** a) *J*-*V* curves under illumination for average performing PCDTBT:PC<sub>71</sub>BM BHJ photovoltaic devices with and without CPE cathode interlayers. b) EQE spectra of average performing devices bearing Ca and CPE interlayers **P1–P6**.

To investigate the interlayer deposition behavior in more detail, atomic force microscopy (AFM) imaging was performed on samples containing the CPE materials deposited on top of the PCDTBT:PC<sub>71</sub>BM active layer (Figure 7; the entry numbers from Table 2 were added for convenience). Similar to previous observations,<sup>[11,23]</sup> the polythiophene-based CPE interlayers never afford a completely covered layer, and the deposition patterns strongly vary depending on the CPE concentration (in methanol). Firstly, increasing the ratio of TEG-to-ionic side chains in the respective CPE materials results in an improved compatibility for deposition onto the photoactive layer blend, most profoundly observable for the samples with CPEs deposited from a concentration of 0.25 mg/mL. Moreover, especially for **P3** and **P4**, the lower device performances for the lower concentrations can be related to too narrowly distributed CPE domains (entries 10, 14 and 15), whereas slightly larger and interconnected domains appear to give rise to more elevated performances (entries 4, 5, 16 and 17). Furthermore, alteration of the chemical structure from the random copolymer **P3** to the block copolymer **P6**, with an identical TEG-to-ionic side chain ratio, also influences the photovoltaic parameters. Solar cells employing the **P6** interlayer demonstrated slightly superior performances across the entire concentration range in comparison to **P3**, mostly originating from an elevated  $J_{SC}$  (from an average of 8.65 to 9.28 mA/cm<sup>2</sup>), finally resulting into PCEs exceeding 5%. AFM imaging, however, did not reveal noteworthy differences between the deposition behavior of these two CPE interlayers.

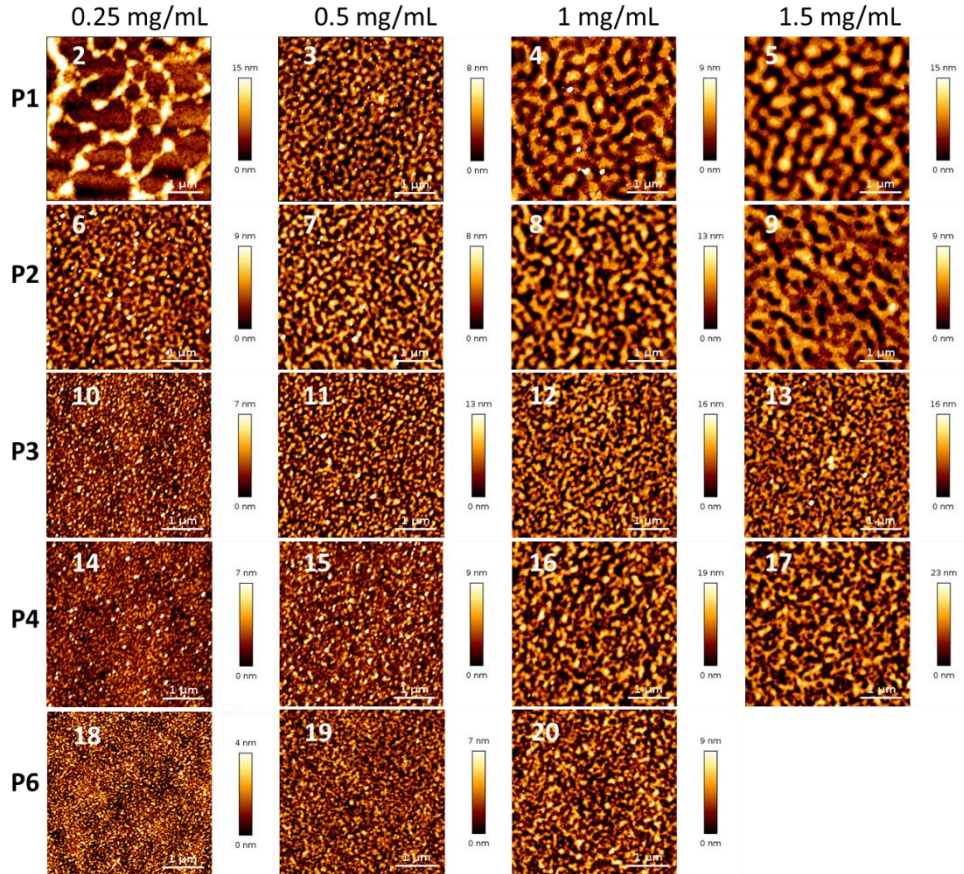


**Figure 7:** Atomic force microscopy images ( $4 \times 4 \mu\text{m}$ ) of CPE materials **P1–P4** and **P6** deposited from various concentrations in methanol on top of the PCDTBT:PC<sub>71</sub>BM active layer. The image numbers refer to the entries in Table 2.

In previous work, we demonstrated that the polythiophene-based CPE interlayers form a capacitive double layer due to the presence of the ionic moieties, thereby enhancing the dielectric constant and charge carrier dissociation of the overall solar cell.<sup>[23]</sup> As a complementary technique, the charge dissociation probability ( $P$ ), determined by the correlation between the photocurrent  $J_{\text{ph}}$  and the effective voltage  $V_{\text{eff}}$ , can provide further insights into the exciton dissociation.<sup>[32]</sup> Herein,  $J_{\text{ph}}$  can be defined as  $J_{\text{L}} - J_{\text{D}}$ , in which  $J_{\text{L}}$  and  $J_{\text{D}}$  are the current densities under

light and dark conditions, respectively, and  $V_{\text{eff}}$  can be defined as  $V_0 - V$ , where  $V_0$  is the voltage at which  $J_{\text{ph}} = 0$  and  $V$  is the applied bias. As such, the saturation current  $J_{\text{sat}}$  was determined to be 9.26, 9.56, 9.15, 9.88, 9.93 and 9.29 mA/cm<sup>2</sup> for the reference device and the solar cells containing **P1**, **P2**, **P3**, **P4** and **P6**, respectively (Figure 8). From these values,  $P$  could be estimated by  $J_{\text{ph}}/J_{\text{sat}}$  to be 89.7, 94.4, 98.6, 91.1, 91.7 and 95.5%, respectively, under short-circuit conditions, confirming that the CPE bearing devices show an elevated exciton dissociation rate and an enhanced charge collection efficiency in comparison to the reference device.

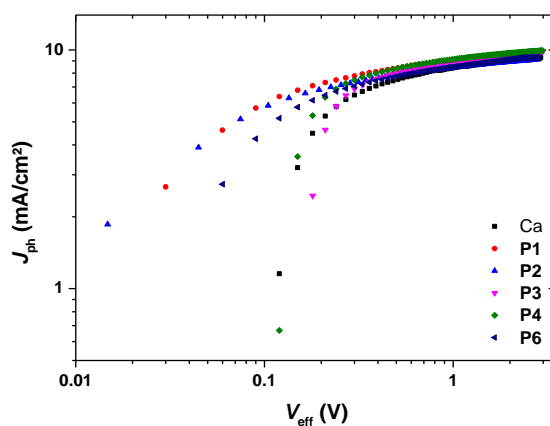


**Figure 8:** Photocurrent of PCDTBT:PC<sub>71</sub>BM photovoltaic devices with and without CPE cathode interlayers as a function of the effective voltage.

## 2.3 CONCLUSIONS

A series of **P3MEEET-co-P3(MIM)HOET-TFSI** random copolymers with different ratios of the ionic side chains (30/50/70%; **P2-P4**), the homopolymer counterparts **P1** and **P5**, and the 50/50 ionic block copolymer analogue **P6** were successfully synthesized via Kumada catalyst-transfer condensation

polymerization and subsequent introduction of the ionic moieties and counteranion exchange. Because of the high degree of control that can be achieved in such a polymerization, all copolymers were obtained in the desired monomer ratios and with the targeted molar masses of  $\sim 25\,000$  g/mol. All materials demonstrated similar absorption characteristics in solution. On the other hand, the polymer crystallinity clearly increased upon decreasing the amount of ionic groups.

The ionic (co)polythiophenes were then applied as cathode interlayer materials in BHJ photovoltaic devices based on PCDTBT:PC<sub>71</sub>BM. All photovoltaic parameters ( $V_{OC}$ ,  $J_{SC}$ , FF) improved throughout the complete series in comparison to a reference device employing Ca, pointing to the generality of the efficiency gain (on average 15–17%) for this interlayer class, regardless of the structural details. The elevated  $J_{SC}$  was confirmed by determining the charge dissociation probabilities of all devices. These measurements revealed an increase in  $P$ , and hence the exciton dissociation rate and charge collection efficiency, for all CPE bearing devices. AFM analysis of the final device stacks showed that the polythiophene-based CPE interlayers never afford a completely covered photoactive layer and that the deposition patterns strongly vary with the CPE concentration. The AFM images also illustrated that an improved compatibility for deposition onto the photoactive layer is obtained by increasing the ratio of triethylene glycol-to-ionic side chains. These results confirm our hypothesis that the presence of ionic groups induces the formation of interfacial dipoles, improving the charge collection, while at the same time reducing the affinity of the interlayer material for the photoactive layer, and that the increase in PCE is dependent on the interplay of these two phenomena.<sup>[23]</sup> An interesting observation is that the

50/50 block copolymer (slightly) outperforms the 50/50 random copolymer, which previously afforded record efficiencies.<sup>[23–25]</sup> Since it is known that control of the morphology is crucial for device performance and that block copolymers can self-assemble into nanostructured morphologies, it seems worthwhile to further explore this route.

## 2.4 REFERENCES

- [1] Cao, W.; Xue, J. *Energy Environ. Sci.* **2014**, *7*, 2123–2144.
- [2] Mazziro, K. A.; Luscombe, C. K. *Chem. Soc. Rev.* **2015**, *44*, 78–90.
- [3] Wang, K.; Liu, C.; Meng, T.; Yi, C.; Gong, X. *Chem. Soc. Rev.* **2016**, *45*, 2937–2975.
- [4] Li, S.; Ye, L.; Zhao, W.; Zhang, S.; Mukherjee, S.; Ade, H.; Hou, J. *Adv. Mater.* **2016**, *28*, 9423–9429.
- [5] Yang, Y.; Zhang, Z.-G.; Bin, H.; Chen, S.; Gao, L.; Xue, L.; Yang, C.; Li, Y. *J. Am. Chem. Soc.* **2016**, *138*, 15011–15018.
- [6] Hu, H.; Jiang, K.; Yang, G.; Liu, J.; Li, Z.; Lin, H.; Liu, Y.; Zhao, J.; Zhang, J.; Huang, F.; Qu, Y.; Ma, W.; Yan, H. *J. Am. Chem. Soc.* **2015**, *137*, 14149–14157.
- [7] Liu, Y.; Zhao, J.; Li, Z.; Mu, C.; Ma, W.; Hu, H.; Jiang, K.; Lin, H.; Ade, H.; Yan, H. *Nat. Commun.* **2014**, *5*, 5293.
- [8] He, Z.; Zhong, C.; Su, S.; Xu, M.; Wu, H.; Cao, Y. *Nat. Photonics* **2012**, *6*, 591–595.
- [9] Sun, Z.; Xiao, K.; Keum, J. K.; Yu, X.; Hong, K.; Browning, J.; Ivanov, I. N.; Chen, J.; Alonzo, J.; Li, D.; Sumpter, B. G.; Payzant, E. A.; Rouleau, C. M.; Geohegan, D. B. *Adv. Mater.* **2011**, *23*, 5529–5535.

- [10] Seo, J. H.; Gutacker, A.; Sun, Y.; Wu, H.; Huang, F.; Cao, Y.; Scherf, U.; Heeger, A. J.; Bazan, G. C. *J. Am. Chem. Soc.* **2011**, *133*, 8416–8419.
- [11] Kesters, J.; Ghoo, T.; Penxten, H.; Drijkoningen, J.; Vangerven, T.; Lyons, D. M.; Verreet, B.; Aernouts, T.; Lutsen, L.; Vanderzande, D.; Manca, J.; Maes, W. *Adv. Energy Mater.* **2013**, *3*, 1180–1185.
- [12] Houston, J. E.; Richeter, S.; Clément, S.; Evans, R. C. *Polym. Int.* **2017**, DOI: 10.1002/pi.5397.
- [13] Reese, M. O.; White, M. S.; Rumbles, G.; Ginley, D. S.; Shaheen, S. E. *Appl. Phys. Lett.* **2008**, *92*, 53307.
- [14] Ju, H.; Knesting, K. M.; Zhang, W.; Pan, X.; Wang, C.-H.; Yang, Y.-W.; Ginger, D. S.; Zhu, J. *ACS Appl. Mater. Interfaces* **2016**, *8*, 2125–2131.
- [15] Gao, M.; Subbiah, J.; Geraghty, P. B.; Chen, M.; Purushothaman, B.; Chen, X.; Qin, T.; Vak, D.; Scholes, F. H.; Watkins, S. E.; Skidmore, M.; Wilson, G. J.; Holmes, A. B.; Jones, D. J.; Wong, W. W. H. *Chem. Mater.* **2016**, *28*, 3481–3487.
- [16] Li, G.; Chu, C.-W.; Shrotriya, V.; Huang, J.; Yang, Y. *Appl. Phys. Lett.* **2006**, *88*, 253503.
- [17] Li, C.-Z.; Chueh, C.-C.; Yip, H.-L.; O'Malley, K. M.; Chen, W.-C.; Jen, A. K.-Y. *J. Mater. Chem.* **2012**, *22*, 8574–8578.
- [18] Oh, S.-H.; Na, S.-I.; Jo, J.; Lim, B.; Vak, D.; Kim, D.-Y. *Adv. Funct. Mater.* **2010**, *20*, 1977–1983.
- [19] Choi, H.; Park, J. S.; Jeong, E.; Kim, G.-H.; Lee, B. R.; Kim, S. O.; Song, M. H.; Woo, H. Y.; Kim, J. Y. *Adv. Mater.* **2011**, *23*, 2759–2763.
- [20] Chang, Y.-M.; Zhu, R.; Richard, E.; Chen, C.-C.; Li, G.; Yang, Y. *Adv. Funct. Mater.* **2012**, *22*, 3284–3289.

- [21] Chevrier, M.; Houston, J. E.; Kesters, J.; Van den Brande, N.; Terry, A. E.; Richeter, S.; Mehdi, A.; Coulembier, O.; Dubois, P.; Lazzaroni, R.; Van Mele, B.; Maes, W.; Evans, R. C.; Clément, S. *J. Mater. Chem. A* **2015**, *3*, 23905–23916.
- [22] Liu, H.; Hu, L.; Wu, F.; Chen, L.; Chen, Y. *ACS Appl. Mater. Interfaces* **2016**, *8*, 9821–9828.
- [23] Kesters, J.; Govaerts, S.; Pirotte, G.; Drijkoningen, J.; Chevrier, M.; Van den Brande, N.; Liu, X.; Fahlman, M.; Van Mele, B.; Lutsen, L.; Vanderzande, D.; Manca, J.; Clément, S.; Von Hauff, E.; Maes, W. *ACS Appl. Mater. Interfaces* **2016**, *8*, 6309–6314.
- [24] Pirotte, G.; Kesters, J.; Verstappen, P.; Govaerts, S.; Manca, J.; Lutsen, L.; Vanderzande, D.; Maes, W. *ChemSusChem* **2015**, *8*, 3228–3233.
- [25] Vanormelingen, W.; Kesters, J.; Verstappen, P.; Drijkoningen, J.; Kudrjasova, J.; Koudjina, S.; Liégeois, V.; Champagne, B.; Manca, J.; Lutsen, L.; Vanderzande, D.; Maes, W. *J. Mater. Chem. A* **2014**, *2*, 7535–7545.
- [26] Ghoo, T.; Brassinne, J.; Fustin, C.-A.; Gohy, J.-F.; Defour, M.; Van den Brande, N.; Van Mele, B.; Lutsen, L.; Vanderzande, D. J.; Maes, W. *Polymer* **2013**, *54*, 6293–6304.
- [27] Miyakoshi, R.; Yokoyama, A.; Yokozawa, T. *Macromol. Rapid Commun.* **2004**, *25*, 1663–1666.
- [28] Thomas, A.; Houston, J. E.; Van den Brande, N.; De Winter, J.; Chevrier, M.; Heenan, R. K.; Terry, A. E.; Richeter, S.; Mehdi, A.; Van Mele, B.; Dubois, P.; Lazzaroni, R.; Gerbaux, P.; Evans, R. C.; Clément, S. *Polym. Chem.* **2014**, *5*, 3352–3362.

- [29] Scherf, U.; Gutacker, A.; Koenen, N. *Acc. Chem. Res.* **2008**, *41*, 1086–1097.
- [30] Ghoo, T.; Van den Brande, N.; Defour, M.; Brassinne, J.; Fustin, C.-A.; Gohy, J.-F.; Hoepfener, S.; Schubert, U. S.; Vanormelingen, W.; Lutsen, L.; Vanderzande, D. J.; Van Mele, B.; Maes, W. *Eur. Polym. J.* **2014**, *53*, 206–214.
- [31] Park, S. H.; Roy, A.; Beaupré, S.; Cho, S.; Coates, N.; Moon, J. S.; Moses, D.; Leclerc, M.; Lee, K.; Heeger, A. J. *Nat. Photonics* **2009**, *3*, 297–303.
- [32] Zhang, G.; Yang, G.; Yan, H.; Kim, J.-H.; Ade, H.; Wu, W.; Xu, X.; Duan, Y.; Peng, Q. *Adv. Mater.* **2017**, *29*, 1606054.

## 2.5 SUPPORTING INFORMATION

### 2.5.1 Reagents and instrumentation

All reagents and chemicals were obtained from commercial sources and used without further purification. THF was dried using a solvent purification system (MBraun MB-SPS 800). Microwave synthesis was performed using a CEM Discover SP synthesis platform.  $^1\text{H}$  NMR chemical shifts ( $\delta$ , in ppm) were determined relative to the residual  $^1\text{H}$  signal of  $\text{CHCl}_3$  (7.26 ppm) or DMSO (2.50 ppm). Analysis of the molar masses and molar mass distributions of the polymer samples was performed on a Tosoh EcoSEC System, comprising of an autosampler, a PSS guard column SDV (50 x 7.5 mm) followed by three PSS SDV analytical linear XL columns (5  $\mu\text{m}$ , 300 x 7.5 mm), and a UV detector, using THF as the eluent at 40 °C with a flow rate of 1.0 mL/min. The SEC system was calibrated using linear narrow polystyrene standards ranging from 474 to  $7.5 \times 10^6$  g/mol ( $K = 14.1 \times 10^{-5}$  dL/g and  $\alpha = 0.70$ ). Background corrected UV-Vis absorption spectra were recorded on a Cary 5000 UV-Vis-NIR spectrophotometer from Agilent using a band width of 2 nm, full slit height and a scan speed of 600 nm/min. Electrochemical experiments were performed with an Eco Chemie Autolab PGSTAT30 potentiostat (Metrohm) using a three-electrode-one-compartment microcell set-up with a platinum wire working electrode, a platinum wire auxiliary electrode, a  $\text{Ag}/\text{AgNO}_3$  reference electrode (silver wire in 0.01 M  $\text{AgNO}_3$ ) and 0.1 M  $\text{NBu}_4\text{PF}_6$  in an anhydrous solvent (acetonitrile or dichloromethane) as the electrolyte. A constant flow of argon allows degassing and blanketing of the electrolyte before and during analysis. For solid state voltammetry, a solution of the polymer sample in chloroform was applied as a film on the working electrode. For solution state voltammetry, the polymer sample was dissolved in the appropriate electrolyte

solution. Cyclic voltammograms were recorded at a scan rate of 100 mV/s. HOMO and LUMO energy levels were determined from the onset of the oxidation and reduction voltammograms, respectively. The onset potential was defined as the intersection of the linear extrapolation of the onset slope of the respective peak and the baseline. Voltammograms are not background corrected and onset potential values are mean values of several experiments (typically scans 3, 4, and 5). The system was calibrated against ferrocene/ferrocenium (Fc/Fc<sup>+</sup>). For the conversion of V to eV, the onset potentials of the first oxidation/reduction peaks were used and referenced to Fc/Fc<sup>+</sup>, which has an ionization potential of -4.98 eV vs. vacuum. This correction factor is based on a value of 0.31 eV for Fc/Fc<sup>+</sup> vs. a saturated calomel electrode (SCE)<sup>[1]</sup> and a value of 4.68 eV for SCE vs. vacuum:<sup>[2]</sup>

$$E_{\text{HOMO}} (\text{eV}) = -4.98 - E_{\text{onset, ox}}^{\text{Ag/AgNO}_3} (\text{V}) + E_{\text{onset, Fc/Fc}^+}^{\text{Ag/AgNO}_3} (\text{V})$$

$$E_{\text{LUMO}} (\text{eV}) = -4.98 - E_{\text{onset, red}}^{\text{Ag/AgNO}_3} (\text{V}) + E_{\text{onset, Fc/Fc}^+}^{\text{Ag/AgNO}_3} (\text{V})$$

For the solution state measurements, the LUMO energy levels were calculated as the difference between the HOMO energy levels and the optical bandgaps. The optical bandgap was estimated from the absorption spectrum by introducing the wavelength at the intersection of the tangent line to the low energy side of the spectrum and the x-axis in the equation  $E_g (\text{eV}) = 1240/\text{wavelength (nm)}$ . The accuracy of measuring redox potentials by CV is about 0.01–0.02 V. Reproducibility can be less because the potentials do depend on concentration and temperature. Rapid heat-cool calorimetry (RHC) experiments were performed on a prototype RHC of TA Instruments, equipped with liquid nitrogen cooling and specifically designed for operation at high scanning rates. RHC measurements were performed at 500 K/min (after cooling at 20 K/min) using aluminum crucibles

filled with samples of 200–250  $\mu\text{g}$ , using helium (10 mL/min) as a purge gas. TGA experiments were performed at 10 K/min in platinum crucibles on a TA Instruments Q5000 TGA using nitrogen (50 mL/min) as purge gas.

### **2.5.2 Photovoltaic device fabrication and characterization**

*Device fabrication:* Bulk heterojunction polymer solar cells were fabricated using the standard architecture glass/ITO/PEDOT:PSS/PCDTBT:PC<sub>71</sub>BM/X/Al, with X = Ca or CPE. Prior to device construction, the prepatterned indium tin oxide (ITO, Kintec, 100 nm, 20 Ohm/sq) containing glass substrates were thoroughly cleaned using soap, demineralized water, acetone, isopropanol and a UV/O<sub>3</sub> treatment. Consequently, a thin layer of PEDOT:PSS [poly(3,4-ethylenedioxythiophene):poly(styrenesulfonic acid), Heraeus Clevios] was deposited by spin-coating with a thickness of  $\sim 30$  nm, followed by an annealing step at 130 °C for 15 mins to remove residual water. Further processing was carried out under nitrogen atmosphere in a glovebox ( $\text{O}_2/\text{H}_2\text{O} < 0.1$  ppm). The active layer blend solution of PCDTBT:PC<sub>71</sub>BM was spin-coated on top of PEDOT:PSS at a total concentration of 20 mg/mL in *ortho*-dichlorobenzene (*o*DCB) with a polymer:fullerene ratio of 1:4. For the CPE containing devices, the various interlayer materials were spin-coated on top of the active layer from methanol with varying concentrations (0.25, 0.5, 1, and 1.5 mg/mL). Finally, the devices were finished off with Ca/Al ( $\sim 30/80$  nm) in the case of the reference device, or solely Al ( $\sim 80$  nm) for the devices containing CPE cathode interlayers. In this way an active area of  $\sim 3$  mm<sup>2</sup> was obtained.

*Device characterization:* The *J-V* curves under illumination and dark conditions as well as the charge dissociation probability data for the polymer solar cells were obtained using a Newport class A solar simulator (model 91195A) calibrated with

a silicon solar cell to give an AM 1.5G spectrum. EQE measurements were performed with a Newport Apex illuminator (100 W Xenon lamp, 6257) as the light source, a Newport Cornerstone 130° monochromator and a Stanford SR830 lock-in amplifier for the current measurements. A silicon FDS100-CAL photodiode was employed as a reference cell. AFM experiments were performed with a JPK NanoWizard 3 AFM (JPK Instruments AG, Berlin, Germany) using AC mode in air. Silicon ACTA-50 tips from AppNano with cantilever length ~125 μm, spring constant ~40 N/m and resonance frequency ~300 kHz were used. The scan angle, set point height, gain values and scan rate were adjusted according to the calibration of the AFM tip.

### 2.5.3 Monomer synthesis

2,5-Dibromo-3-[2'-(2'-(2'-methoxyethoxy)ethoxy)ethyl]thiophene (**pM1**) and 2,5-dibromo-3-[2'-(6'-bromohexyloxy)ethyl]thiophene (**pM2**) were synthesized according to a literature procedure.<sup>[3]</sup> Prior to their use in the polymerizations, **pM1** and **pM2** were dried overnight under vacuum using P<sub>2</sub>O<sub>5</sub>.

### 2.5.4 Polymer synthesis

#### 2.5.4.1 Homopolymer synthesis

#### **P3MEEET – poly{3-[2'-(2'-(2'-methoxyethoxy)ethoxy)ethyl]thiophene-2,5-diyl}**

2,5-Dibromo-3-[2'-(2'-(2'-methoxyethoxy)ethoxy)ethyl]thiophene (**pM1**) (0.388 g, 1.00 mmol) was loaded in a flame-dried three-neck flask and brought under Ar atmosphere, after which dry THF (10 mL) was added via cannula. *i*-PrMgCl.LiCl (0.769 mL, 1.00 mmol; 1.3 M in THF) was added dropwise to this solution at 0 °C to start the GRIM reaction. After stirring for 1 h at 0 °C, this mixture was cannulated to another flame-dried three-neck flask containing Ni(dppp)Cl<sub>2</sub> (4.07

mg, 7.50  $\mu\text{mol}$ ; 0.75 mol%) and dry THF (3 mL), at RT and under Ar atmosphere. The polymerization was stopped after 30 min by quenching with a MeOH/HCl mixture (1 mL; 1 M). Then, the polymerization mixture was precipitated in methanol, whereafter the precipitate was filtered over a Soxhlet thimble and subsequently purified by means of Soxhlet extractions with methanol, hexanes and chloroform (dissolving the polymer), respectively. The solvent was evaporated under reduced pressure, after which the polymer was redissolved in a minimum amount of chloroform and again precipitated in methanol. The precipitate was filtered off over a PTFE membrane (47 mm/0.45  $\mu\text{m}$ ) and dried overnight under vacuum, affording **P3MEEET** as a dark purple solid (42 mg, 18%).  $^1\text{H}$  NMR (400 MHz,  $\text{CDCl}_3$ ):  $\delta$  = 7.07 (s, 1H), 3.77 (t,  $J$  = 7.0 Hz, 2H), 3.69–3.63 (m, 6H), 3.55–3.51 (m, 2H), 3.35 (s, 3H), 3.11 (t,  $J$  = 6.9 Hz, 2H); GPC (THF, PS standards):  $M_n$  =  $1.9 \times 10^4$  g/mol,  $M_w$  =  $2.4 \times 10^4$  g/mol,  $D$  = 1.30.

**P3BHOET – poly{3-[2'-(6'-bromohexyloxy)ethyl]thiophene-2,5-diyl}**

2,5-Dibromo-3-[2'-(6'-bromohexyloxy)ethyl]thiophene (**PM2**) (0.898 g, 2.00 mmol) was loaded in a flame-dried three-neck flask and brought under Ar atmosphere, after which dry THF (20 mL) was added via cannula. *i*-PrMgCl.LiCl (1.54 mL, 2.00 mmol; 1.3 M in THF) was added dropwise to this solution at 0 °C to start the GRIM reaction. After stirring for 1 h at 0 °C, this mixture was cannulated to another flame-dried three-neck flask containing Ni(dppp)Cl<sub>2</sub> (10.3 mg, 19.0  $\mu\text{mol}$ ; 0.95 mol%) and dry THF (7 mL), at RT and under Ar atmosphere. The polymerization was stopped after 30 min by quenching with a MeOH/HCl mixture (2 mL; 1 M). Then, the polymerization mixture was precipitated in methanol, whereafter the precipitate was filtered over a Soxhlet thimble and subsequently purified by means of Soxhlet extractions with methanol, acetone,

hexanes and chloroform (dissolving the polymer), respectively. The solvent was evaporated under reduced pressure, after which the polymer was redissolved in a minimum amount of chloroform and again precipitated in methanol. The precipitate was filtered off over a PTFE membrane (47 mm/0.45  $\mu\text{m}$ ) and dried overnight under vacuum, affording **P3BHOET** as a dark purple solid (224 mg, 39%).  $^1\text{H}$  NMR (400 MHz,  $\text{CDCl}_3$ ):  $\delta$  = 7.09 (s, 1H), 3.71 (t,  $J$  = 6.9 Hz, 2H), 3.49 (t,  $J$  = 6.5 Hz, 2H), 3.38 (t,  $J$  = 6.8 Hz, 2H), 3.09 (t,  $J$  = 6.7 Hz, 2H), 1.88–1.80 (m, 2H), 1.66–1.60 (m, 2H), 1.49–1.36 (m, 4H); GPC (THF, PS standards):  $M_n$  =  $1.7 \times 10^4$  g/mol,  $M_w$  =  $2.0 \times 10^4$  g/mol,  $D$  = 1.18.

#### 2.5.4.2 Random copolymer synthesis

##### **P3MEEET-co-P3BHOET (30/70) – poly{3-[2'-(2'-(2'-methoxyethoxy)ethoxy)ethyl]thiophene-2,5-diyl}-co-poly{3-[2'-(6'-bromohexyloxy)ethyl]thiophene-2,5-diyl} (30/70)**

2,5-Dibromo-3-[2'-(2'-(2'-methoxyethoxy)ethoxy)ethyl]thiophene (**PM1**) (0.233 g, 0.600 mmol) and 2,5-dibromo-3-[2'-(6'-bromohexyloxy)ethyl]thiophene (**PM2**) (0.629 g, 1.40 mmol) were loaded in a flame-dried three-neck flask and brought under Ar atmosphere, after which dry THF (20 mL) was added via cannula. *i*-PrMgCl.LiCl (1.54 mL, 2.00 mmol; 1.3 M in THF) was added dropwise to this solution at 0 °C to start the GRIM reaction. After stirring for 1 h at 0 °C, this mixture was cannulated to another flame-dried three-neck flask containing Ni(dppp)Cl<sub>2</sub> (9.21 mg, 17.0  $\mu\text{mol}$ ; 0.85 mol%) and dry THF (7 mL), at RT and under Ar atmosphere. The polymerization was stopped after 30 min by quenching with a MeOH/HCl mixture (2 mL; 1 M). Then, the polymerization mixture was precipitated in methanol, whereafter the precipitate was filtered over a Soxhlet thimble and subsequently purified by means of Soxhlet extractions with methanol,

acetone, hexanes and chloroform (dissolving the polymer), respectively. The solvent was evaporated under reduced pressure, after which the polymer was redissolved in a minimum amount of chloroform and again precipitated in methanol. The precipitate was filtered off over a PTFE membrane (47 mm/0.45  $\mu\text{m}$ ) and dried overnight under vacuum, affording **P3MEEET-co-P3BHOET (30/70)** as a dark purple solid (205 mg, 38%).  $^1\text{H}$  NMR (400 MHz,  $\text{CDCl}_3$ ):  $\delta$  = 7.10–7.06 (m, 1H), 3.80–3.60 (m, 3.8H), 3.55–3.51 (m, 0.6H), 3.49 (t,  $J$  = 6.4 Hz, 1.4H), 3.40–3.35 (m, 2.3H), 3.15–3.04 (m, 2H), 1.88–1.80 (m, 1.4H), 1.66–1.60 (m, 1.4H), 1.49–1.36 (m, 2.8H); GPC (THF, PS standards):  $M_n$  =  $2.4 \times 10^4$  g/mol,  $M_w$  =  $3.0 \times 10^4$  g/mol,  $D$  = 1.23.

#### **P3MEEET-co-P3BHOET (50/50)**

Similar to the polymerization procedure of **P3MEEET-co-P3BHOET (30/70)**, **pM1** (0.582 g, 1.50 mmol) and **pM2** (0.674 g, 1.50 mmol) were added together and dissolved in dry THF (30 mL). *i*-PrMgCl.LiCl (2.31 mL, 3.00 mmol; 1.3 M in THF) was added dropwise and the polymerization was started by cannulating this mixture to a flask containing Ni(dppp)Cl<sub>2</sub> (9.76 mg, 18.0  $\mu\text{mol}$ ; 0.60 mol%) and dry THF (10 mL). **P3MEEET-co-P3BHOET (50/50)** was obtained as a dark purple solid (162 mg, 21%).  $^1\text{H}$  NMR (400 MHz,  $\text{CDCl}_3$ ):  $\delta$  = 7.10–7.06 (m, 2H), 3.80–3.60 (m, 10H), 3.55–3.51 (m, 2H), 3.49 (t,  $J$  = 6.5 Hz, 2H), 3.40–3.35 (m, 5H), 3.15–3.04 (m, 4H), 1.88–1.80 (m, 2H), 1.66–1.60 (m, 2H), 1.49–1.36 (m, 4H); GPC (THF, PS standards):  $M_n$  =  $2.8 \times 10^4$  g/mol,  $M_w$  =  $3.3 \times 10^4$  g/mol,  $D$  = 1.16.

### **P3MEEET-co-P3BHOET (70/30)**

Similar to the polymerization procedure of **P3MEEET-co-P3BHOET (30/70)**, **pM1** (0.543 g, 1.40 mmol) and **pM2** (0.269 g, 0.600 mmol) were added together and dissolved in dry THF (20 mL). *i*-PrMgCl.LiCl (1.54 mL, 2.00 mmol; 1.3 M in THF) was added dropwise and the polymerization was started by cannulating this mixture to a flask containing Ni(dppp)Cl<sub>2</sub> (8.67 mg, 16.0 μmol; 0.80 mol%) and dry THF (7 mL). In this case, no acetone was used during the Soxhlet purification process. **P3MEEET-co-P3BHOET (70/30)** was obtained as a dark purple solid (143 mg, 29%). <sup>1</sup>H NMR (400 MHz, CDCl<sub>3</sub>): δ = 7.10–7.06 (m, 1H), 3.80–3.60 (m, 6.2H), 3.55–3.51 (m, 1.4H), 3.49 (t, *J* = 6.4 Hz, 0.6H), 3.40–3.35 (m, 2.7H), 3.15–3.04 (m, 2H), 1.88–1.80 (m, 0.6H), 1.66–1.60 (m, 0.6H), 1.49–1.36 (m, 1.2H); GPC (THF, PS standards): *M*<sub>n</sub> = 2.6 × 10<sup>4</sup> g/mol, *M*<sub>w</sub> = 3.1 × 10<sup>4</sup> g/mol, *D* = 1.17.

#### **2.5.4.3 Block copolymer synthesis**

##### **P3BHOET-*b*-P3MEEET (50/50) – poly{3-[2'-(6'-bromohexyloxy)ethyl]thiophene-2,5-diyl}-*block*-poly{3-[2'-(2'-(2'-methoxyethoxy)ethoxy)ethyl]thiophene-2,5-diyl} (50/50)**

2,5-Dibromo-3-[2'-(6'-bromohexyloxy)ethyl]thiophene (**pM2**) (0.449 g, 1.00 mmol) was loaded in a flame-dried three-neck flask and brought under Ar atmosphere. Then, dry THF (10 mL) was added via cannula, after which the solution was cooled down to 0 °C. *i*-PrMgCl.LiCl (0.769 mL, 1.00 mmol; 1.30 M in THF) was added dropwise to this solution to start the first Grignard metathesis reaction (GRIM 1). Meanwhile, 2,5-dibromo-3-[2'-(2'-(2'-methoxyethoxy)ethoxy)ethyl]thiophene (**pM1**) (0.388 g, 1.00 mmol) was also loaded in a flame-dried three-neck flask, brought under Ar atmosphere and

dissolved in dry THF (10 mL). 15 Min after the start of GRIM 1, *i*-PrMgCl·LiCl (0.769 mL, 1.00 mmol; 1.30 M in THF) was added dropwise to this solution at 0 °C to start the second Grignard metathesis reaction (GRIM 2). Both GRIM reactions were stirred for 1 h at 0 °C. After GRIM 1, the **M2** mixture was cannulated to another flame-dried three-neck flask containing Ni(dppp)Cl<sub>2</sub> (5.15 mg, 9.50 μmol; 0.95 mol%) and dry THF (3 mL), at RT and under Ar atmosphere. This polymerization mixture was then stirred for 15 min at RT, whereafter a small amount of it (1 mL) was quenched with a MeOH/HCl mixture (0.1 mL; 1 M), while to the rest of the mixture the **M1** mixture of GRIM 2 was added at RT. The block copolymerization was stopped after 30 min by quenching with a MeOH/HCl mixture (2 mL; 1 M). The block copolymer was precipitated in methanol, filtered over a Soxhlet thimble and subsequently purified by means of Soxhlet extractions with methanol, hexanes and chloroform (dissolving the polymer), respectively. The solvent was evaporated under reduced pressure, after which the block copolymer was redissolved in a minimum amount of chloroform and again precipitated in methanol. The precipitate was filtered off over a PTFE membrane (47 mm/0.45 μm) and dried overnight under vacuum, affording the **P3BHOET-*b*-P3MEEET (50/50)** block copolymer (100 mg, 19%). <sup>1</sup>H NMR (400 MHz, CDCl<sub>3</sub>): δ = 7.09 (s, 1H), 7.07 (s, 1H), 3.80–3.60 (m, 10H), 3.55–3.51 (m, 2H), 3.49 (t, *J* = 6.5 Hz, 2H), 3.40–3.35 (m, 5H), 3.15–3.04 (m, 4H), 1.88–1.80 (m, 2H), 1.66–1.60 (m, 2H), 1.49–1.36 (m, 4H); GPC (THF, PS standards): *M*<sub>n</sub> = 2.9 × 10<sup>4</sup> g/mol, *M*<sub>w</sub> = 3.9 × 10<sup>4</sup> g/mol, *D* = 1.34.

#### 2.5.4.4 Functionalization with *N*-methylimidazole

##### **P3(MIM)HOET-Br – poly{3-[2'-(6'-(1''-methylimidazolium-3''-yl)hexyloxy)ethyl]thiophene-2,5-diyl} bromide**

**P3BHOET** (0.200 g) was weighed in a 10 mL microwave vial and suspended in acetonitrile (2 mL), after which *N*-methylimidazole (3 mL) was added. Then, the vial was filled with Ar and closed, where after the reaction mixture was heated in the microwave at 100 °C for 4 h (with a maximum power of 200 W and a maximum pressure of 250 psi). After cooling down, the reaction mixture was precipitated into Et<sub>2</sub>O and filtered off over a Soxhlet thimble. The polymer was then purified by means of Soxhlet extractions with Et<sub>2</sub>O and MeOH (dissolving the polymer), respectively. The solvent was evaporated under reduced pressure and the polymer was redissolved in a minimum amount of MeOH, after which it was again precipitated into Et<sub>2</sub>O. Finally, the polymer was filtered off over a cellulose membrane (47 mm/0.45 μm) and dried overnight under vacuum, affording **P3(MIM)HOET-Br** as a dark purple solid (232 mg, 90%). <sup>1</sup>H NMR (400 MHz, DMSO-*d*<sub>6</sub>): δ = 9.28 (s, 1H), 7.81 (s, 1H), 7.74 (s, 1H), 7.30 (s, 1H), 4.16 (t, *J* = 6.9 Hz, 2H), 3.85 (s, 3H), 3.68 (br, 2H), 3.43 (br, 2H), 3.02 (br, 2H), 1.81–1.71 (m, 2H), 1.56–1.46 (m, 2H), 1.37–1.19 (m, 4H).

##### **P3MEEET-co-P3(MIM)HOET-Br (30/70) – poly{3-[2'-(2'-(2'-methoxyethoxy)ethoxy)ethyl]-thiophene-2,5-diyl}-co-poly{3-[2'-(6'-(1''-methylimidazolium-3''-yl)hexyloxy)ethyl]thiophene-2,5-diyl} bromide (30/70)**

Similar to the functionalization procedure of **P3(MIM)HOET-Br**. 150 mg of **P3MEEET-co-P3BHOET (30/70)**, suspended in 2 mL acetonitrile and 3 mL *N*-methylimidazole, was placed in the microwave at 100 °C for 4 h. **P3MEEET-co-**

**P3(MIM)HOET-Br (30/70)** was obtained as a dark purple solid (153 mg, 84%). <sup>1</sup>H NMR (400 MHz, DMSO-*d*<sub>6</sub>): δ = 9.21 (br, 0.7H), 7.76 (s, 0.7H), 7.71 (s, 0.7H), 7.35–7.23 (m, 1H), 4.14 (br, 1.4H), 3.84 (s, 2.1H), 3.76–3.37 (m, 5.8H), 3.18 (s, 0.9H), 3.01 (br, 2H), 1.81–1.71 (m, 1.4H), 1.56–1.46 (m, 1.4H), 1.37–1.19 (m, 2.8H).

**P3MEEET-co-P3(MIM)HOET-Br (50/50)**

Similar to the functionalization procedure of **P3(MIM)HOET-Br**. 100 mg of **P3MEEET-co-P3BHOET (50/50)**, suspended in 2 mL acetonitrile and 3 mL *N*-methylimidazole, was placed in the microwave at 100 °C for 4 h. **P3MEEET-co-P3(MIM)HOET-Br (50/50)** was obtained as a dark purple solid (101 mg, 87%). <sup>1</sup>H NMR (400 MHz, DMSO-*d*<sub>6</sub>): δ = 9.17 (br, 1H), 7.75 (s, 1H), 7.71 (s, 1H), 7.35–7.23 (m, 2H), 4.13 (br, 2H), 3.84 (s, 3H), 3.76–3.37 (m, 14H), 3.19 (s, 3H), 3.02 (br, 4H), 1.81–1.71 (m, 2H), 1.56–1.46 (m, 2H), 1.37–1.19 (m, 4H).

**P3MEEET-co-P3(MIM)HOET-Br (70/30)**

Similar to the functionalization procedure of **P3(MIM)HOET-Br**. 100 mg of **P3MEEET-co-P3BHOET (70/30)**, suspended in 2 mL acetonitrile and 3 mL *N*-methylimidazole, was placed in the microwave at 100 °C for 4 h. **P3MEEET-co-P3(MIM)HOET-Br (70/30)** was obtained as a dark purple solid (83 mg, 75%). <sup>1</sup>H NMR (400 MHz, DMSO-*d*<sub>6</sub>): δ = 9.10 (br, 0.3H), 7.73 (s, 0.3H), 7.68 (s, 0.3H), 7.35–7.23 (m, 1H), 4.11 (br, 0.6H), 3.82 (s, 0.9H), 3.76–3.37 (m, 8.2H), 3.19 (s, 2.1H), 3.02 (br, 2H), 1.81–1.71 (m, 0.6H), 1.56–1.46 (m, 0.6H), 1.37–1.19 (m, 1.2H).

**P3(MIM)HOET-Br-*b*-P3MEEET (50/50) – poly{3-[2'-(6'-(1''-methylimidazolium-3''-yl)hexyloxy)ethyl]thiophene-2,5-diyl}-*block*-poly{3-[2'-(2'-(2'-methoxyethoxy)ethoxy)ethyl]thiophene-2,5-diyl} bromide (50/50)**

Similar to the functionalization procedure of **P3(MIM)HOET-Br**. 60 mg of **P3BHOET-*b*-P3MEEET (50/50)**, suspended in 2 mL acetonitrile and 3 mL *N*-methylimidazole, was placed in the microwave at 100 °C for 4 h. **P3(MIM)HOET-Br-*b*-P3MEEET (50/50)** was obtained as a dark purple solid (54 mg, 77%). <sup>1</sup>H NMR (400 MHz, DMSO-*d*<sub>6</sub>): δ = 9.29 (br, 1H), 7.81 (s, 1H), 7.74 (s, 1H), 7.35–7.23 (m, 2H), 4.15 (br, 2H), 3.85 (s, 3H), 3.76–3.37 (m, 14H), 3.19 (s, 3H), 3.02 (br, 4H), 1.81–1.71 (m, 2H), 1.56–1.46 (m, 2H), 1.37–1.19 (m, 4H).

#### 2.5.4.5 Counteranion exchange

**P3(MIM)HOET-TFSI – poly{3-[2'-(6'-(1''-methylimidazolium-3''-yl)hexyloxy)ethyl]thiophene-2,5-diyl} bis(trifluoromethane)sulfonimide**

A solution of Li-TFSI (0.503 g, 1.75 mmol) in distilled water (2 mL) was added drop wise to a solution of **P3(MIM)HOET-Br** (130 mg, 0.350 mmol) in distilled water (25 mL). Immediately, a precipitate was formed and the mixture was stirred for another 6 h at RT. The resulting polymer was filtered off over a cellulose membrane (47 mm/0.45 μm) and dried overnight under vacuum, affording **P3(MIM)HOET-TFSI** as a sticky dark purple solid (176 mg, 88%). <sup>1</sup>H NMR (400 MHz, DMSO-*d*<sub>6</sub>): δ = 9.09 (s, 1H), 7.70 (s, 1H), 7.67 (s, 1H), 7.26 (s, 1H), 4.11 (t, *J* = 7.3 Hz, 2H), 3.82 (s, 3H), 3.66 (br, 2H), 3.42 (br, 2H), 3.01 (br, 2H), 1.81–1.71 (m, 2H), 1.56–1.46 (m, 2H), 1.37–1.19 (m, 4H).

**P3MEEET-co-P3(MIM)HOET-TFSI (30/70) - poly{3-[2'-(2'-(2'-methoxyethoxy)ethoxy)ethyl]thiophene-2,5-diyl}-co-poly{3-[2'-(6'-(1''-methylimidazolium-3''-yl)hexyloxy)ethyl]thiophene-2,5-diyl} bis(trifluoromethane)sulfonimide (30/70)**

Similar to the counteranion exchange procedure for **P3(MIM)HOET-TFSI**. A solution of Li-TFSI (0.438 g, 1.52 mmol) in distilled water (2 mL) was added drop wise to a solution of **P3MEEET-co-P3(MIM)HOET-Br (30/70)** (100 mg, 0.305 mmol) in distilled water (20 mL). **P3MEEET-co-P3(MIM)HOET-TFSI (30/70)** was obtained as a sticky dark purple solid (78 mg, 55%). <sup>1</sup>H NMR (400 MHz, DMSO-*d*<sub>6</sub>): δ = 9.07 (s, 0.7H), 7.70 (s, 0.7H), 7.67 (s, 0.7H), 7.35–7.23 (m, 1H), 4.10 (t, *J* = 7.3 Hz, 1.4H), 3.82 (s, 2.1H), 3.76–3.37 (m, 5.8H), 3.18 (s, 0.9H), 3.01 (br, 2H), 1.81–1.71 (m, 1.4H), 1.56–1.46 (m, 1.4H), 1.37–1.19 (m, 2.8H).

**P3MEEET-co-P3(MIM)HOET-TFSI (50/50)**

Similar to the counteranion exchange procedure for **P3(MIM)HOET-TFSI**. A solution of Li-TFSI (0.478 g, 1.67 mmol) in distilled water (2 mL) was added drop wise to a solution of **P3MEEET-co-P3(MIM)HOET-Br (50/50)** (100 mg, 0.333 mmol) in distilled water (20 mL). **P3MEEET-co-P3(MIM)HOET-TFSI (50/50)** was obtained as a sticky dark purple solid (112 mg, 84%). <sup>1</sup>H NMR (400 MHz, DMSO-*d*<sub>6</sub>): δ = 9.06 (s, 1H), 7.71 (s, 1H), 7.67 (s, 1H), 7.35–7.23 (m, 2H), 4.11 (t, *J* = 7.1 Hz, 2H), 3.82 (s, 3H), 3.76–3.37 (m, 14H), 3.18 (s, 3H), 3.02 (br, 4H), 1.81–1.71 (m, 2H), 1.56–1.46 (m, 2H), 1.37–1.19 (m, 4H).

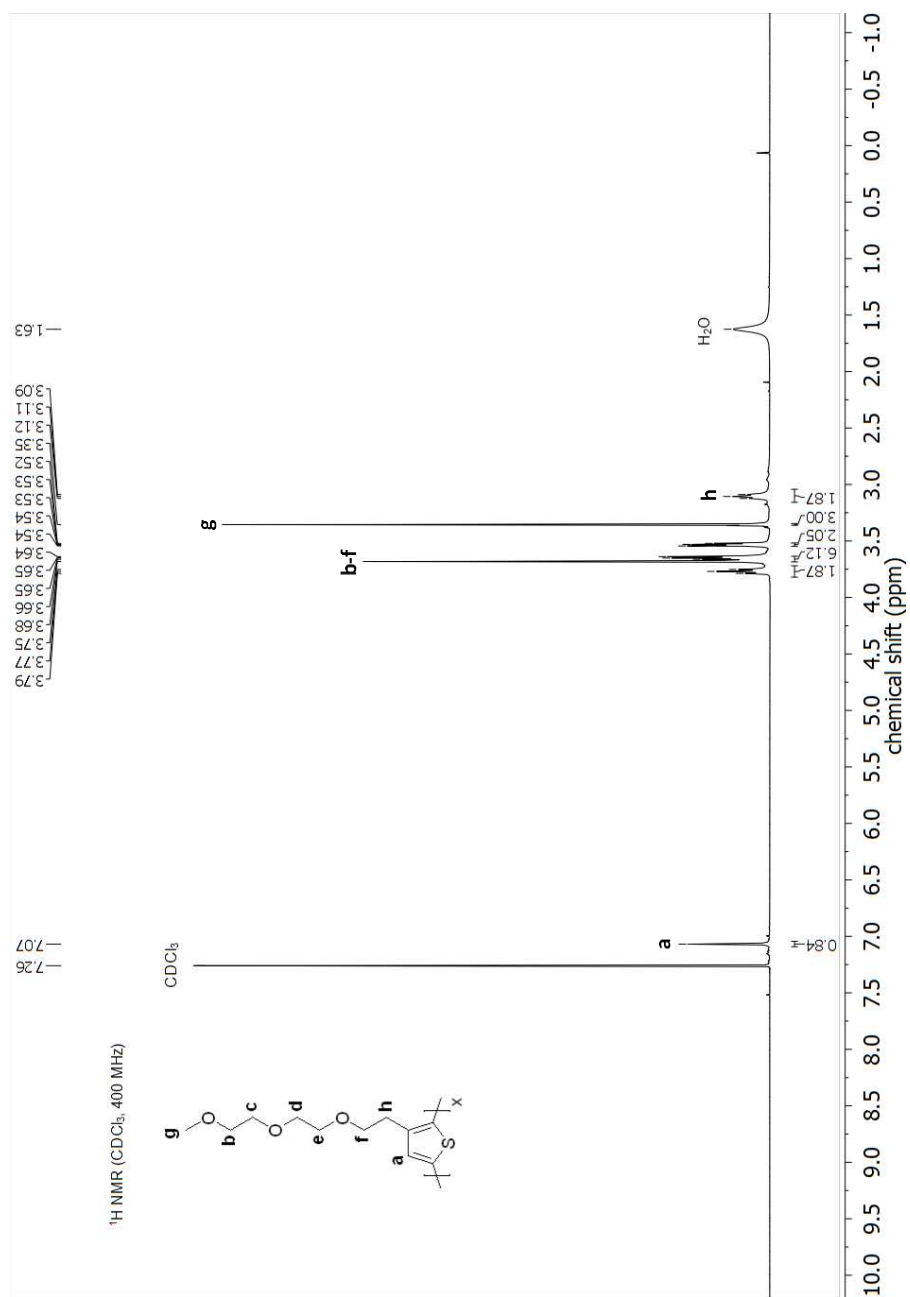
**P3MEEET-co-P3(MIM)HOET-TFSI (70/30)**

Similar to the counteranion exchange procedure for **P3(MIM)HOET-TFSI**. A solution of Li-TFSI (0.371 g, 1.29 mmol) in distilled water (2 mL) was added drop wise to a solution of **P3MEEET-co-P3(MIM)HOET-Br (70/30)** (70 mg, 0.258

mmol) in distilled water (15 mL). **P3MEEET-co-P3(MIM)HOET-TFSI (70/30)** was obtained as a sticky dark purple solid (58 mg, 68%). <sup>1</sup>H NMR (400 MHz, DMSO-*d*<sub>6</sub>): δ = 9.07 (s, 0.3H), 7.71 (s, 0.3H), 7.67 (s, 0.3H), 7.35–7.23 (m, 1H), 4.11 (t, *J* = 7.2 Hz, 0.6H), 3.82 (s, 0.9H), 3.76–3.37 (m, 8.2H), 3.19 (s, 2.1H), 3.02 (br, 2H), 1.81–1.71 (m, 0.6H), 1.56–1.46 (m, 0.6H), 1.37–1.19 (m, 1.2H).

**P3(MIM)HOET-TFSI-*b*-P3MEEET (50/50) - poly{3-[2'-(6'-(1'-methylimidazolium-3''-yl)hexyloxy)ethyl]thiophene-2,5-diyl}-*block*-poly{3-[2'-(2'-(2'-methoxyethoxy)ethoxy)ethyl]thiophene-2,5-diyl} bis(trifluoromethane)sulfonimide (50/50)**

Similar to the counteranion exchange procedure for **P3(MIM)HOET-TFSI**. A solution of Li-TFSI (0.191 g, 0.667 mmol) in distilled water (2 mL) was added drop wise to a solution of **P3(MIM)HOET-Br-*b*-P3MEEET (50/50)** (40 mg, 0.133 mmol) in distilled water (8 mL). **P3(MIM)HOET-TFSI-*b*-P3MEEET (50/50)** was obtained as a sticky dark purple solid (28 mg, 53%). <sup>1</sup>H NMR (400 MHz, DMSO-*d*<sub>6</sub>): δ = 9.07 (s, 1H), 7.69 (s, 1H), 7.66 (s, 1H), 7.29 (s, 1H), 7.26 (s, 1H), 4.10 (t, *J* = 7.3 Hz, 2H), 3.82 (s, 3H), 3.76–3.37 (m, 14H), 3.19 (s, 3H), 3.01 (br, 4H), 1.81–1.71 (m, 2H), 1.56–1.46 (m, 2H), 1.37–1.19 (m, 4H).

2.5.5  $^1\text{H}$  NMR spectra of the polymersFigure S1:  $^1\text{H}$  NMR spectrum of P3MEEET (P5).

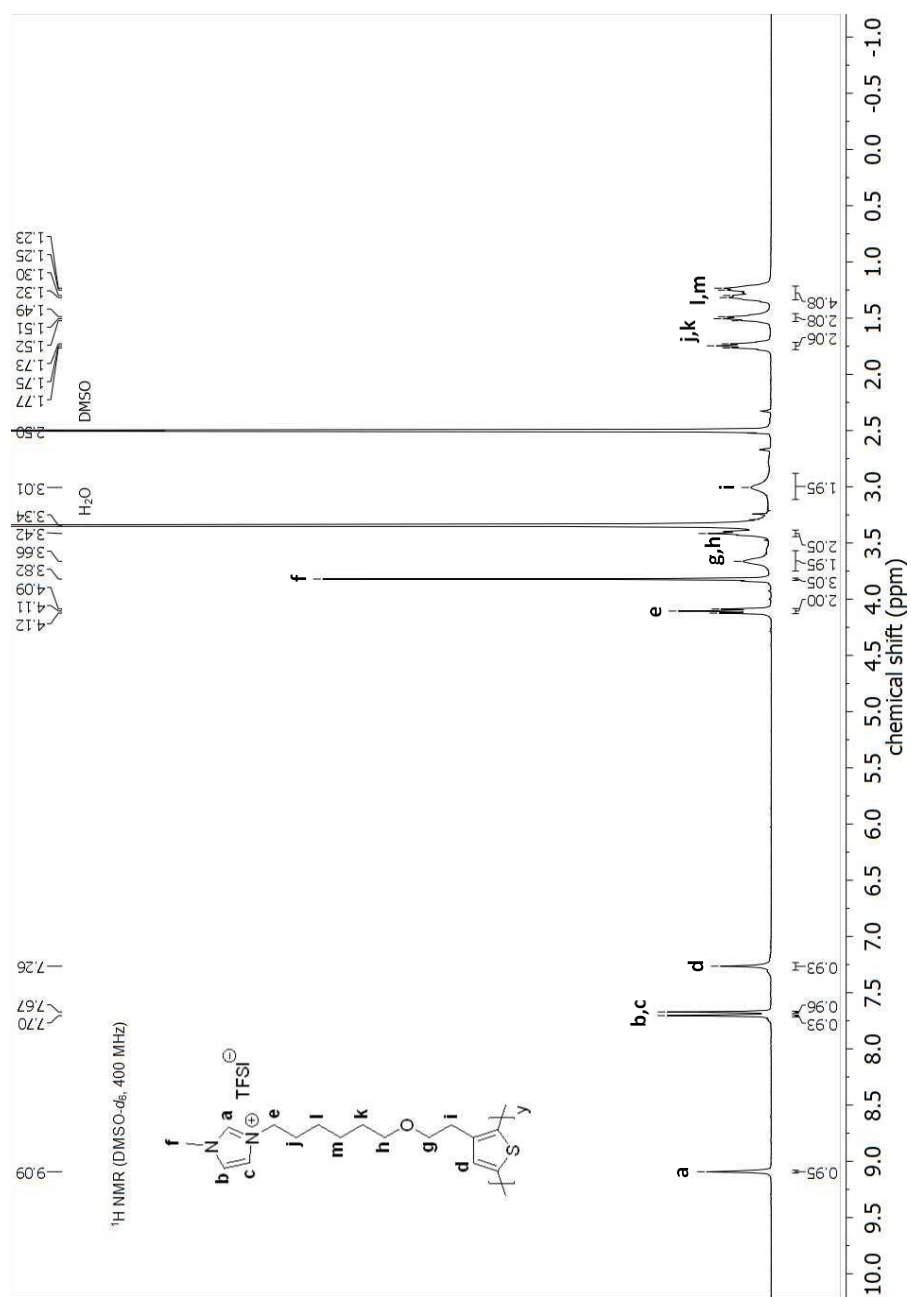


**Figure S2:** <sup>1</sup>H NMR spectrum of **P3(MIM)HOET-TFSI (P1)**.

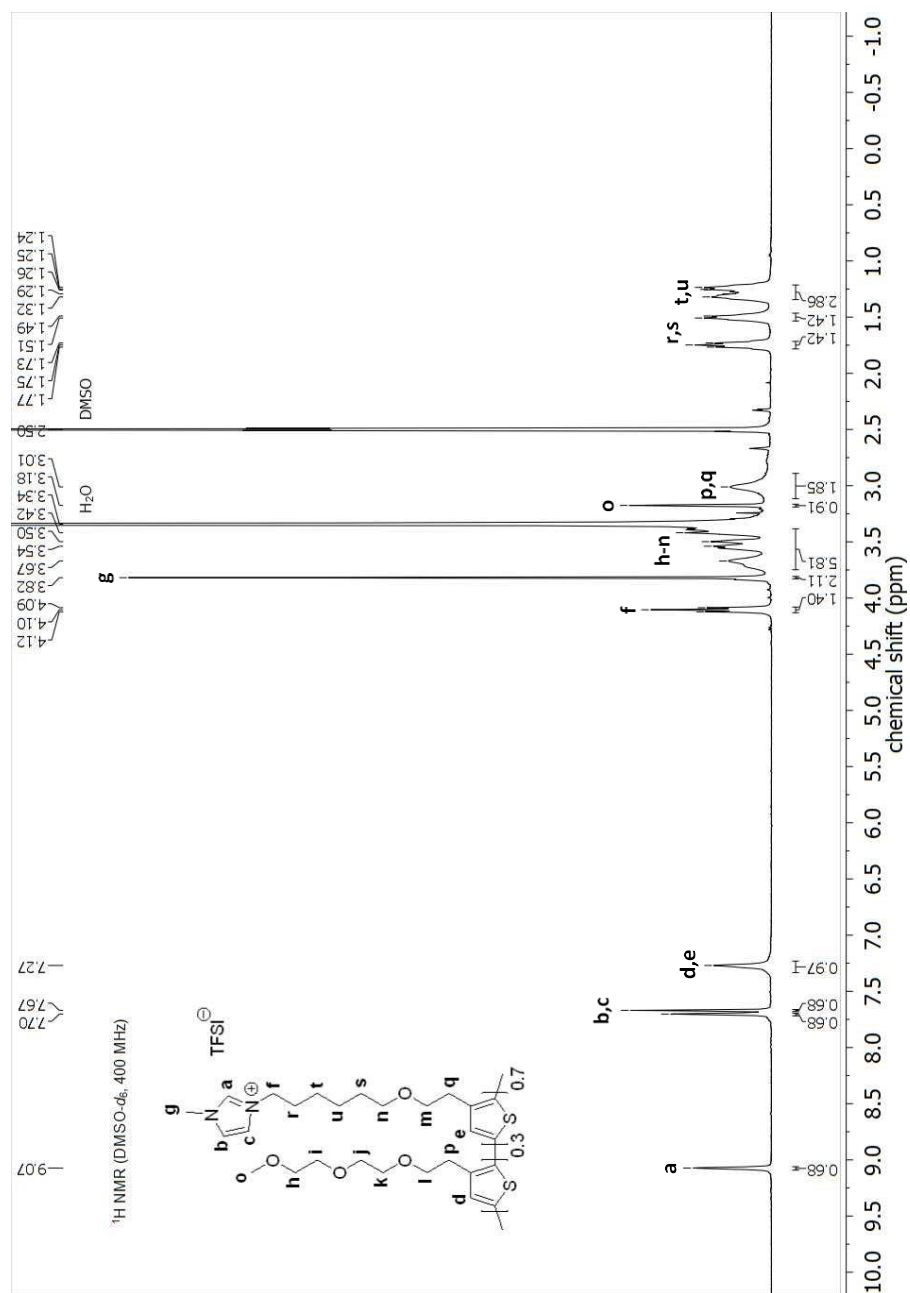


**Figure S3:** <sup>1</sup>H NMR spectrum of P3MEEET-co-P3(MIM)HOET-TFSI (30/70) (P2).



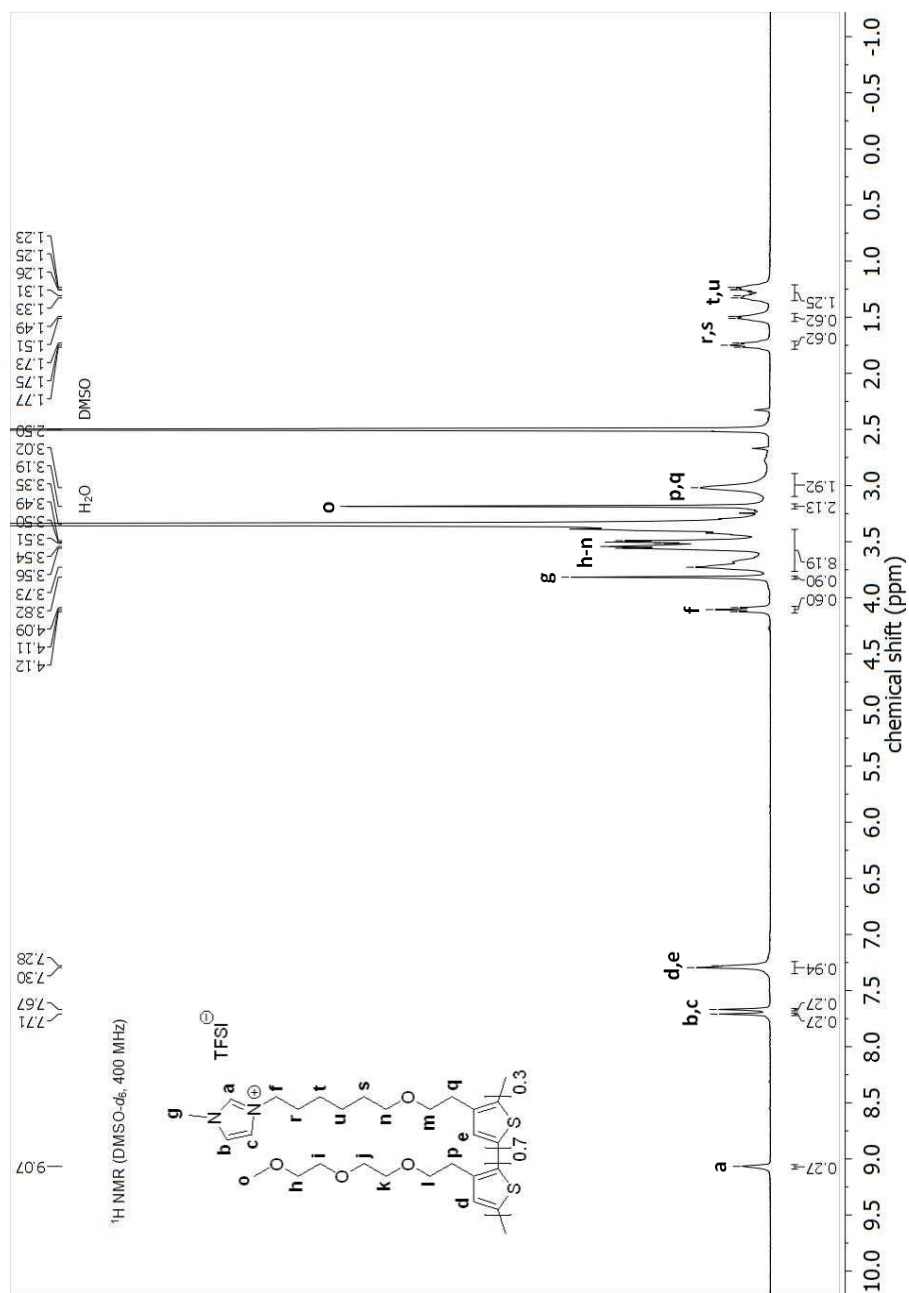


**Figure S5:** <sup>1</sup>H NMR spectrum of P3MEEET-co-P3(MIM)HOET-TFSI (70/30) (P4).

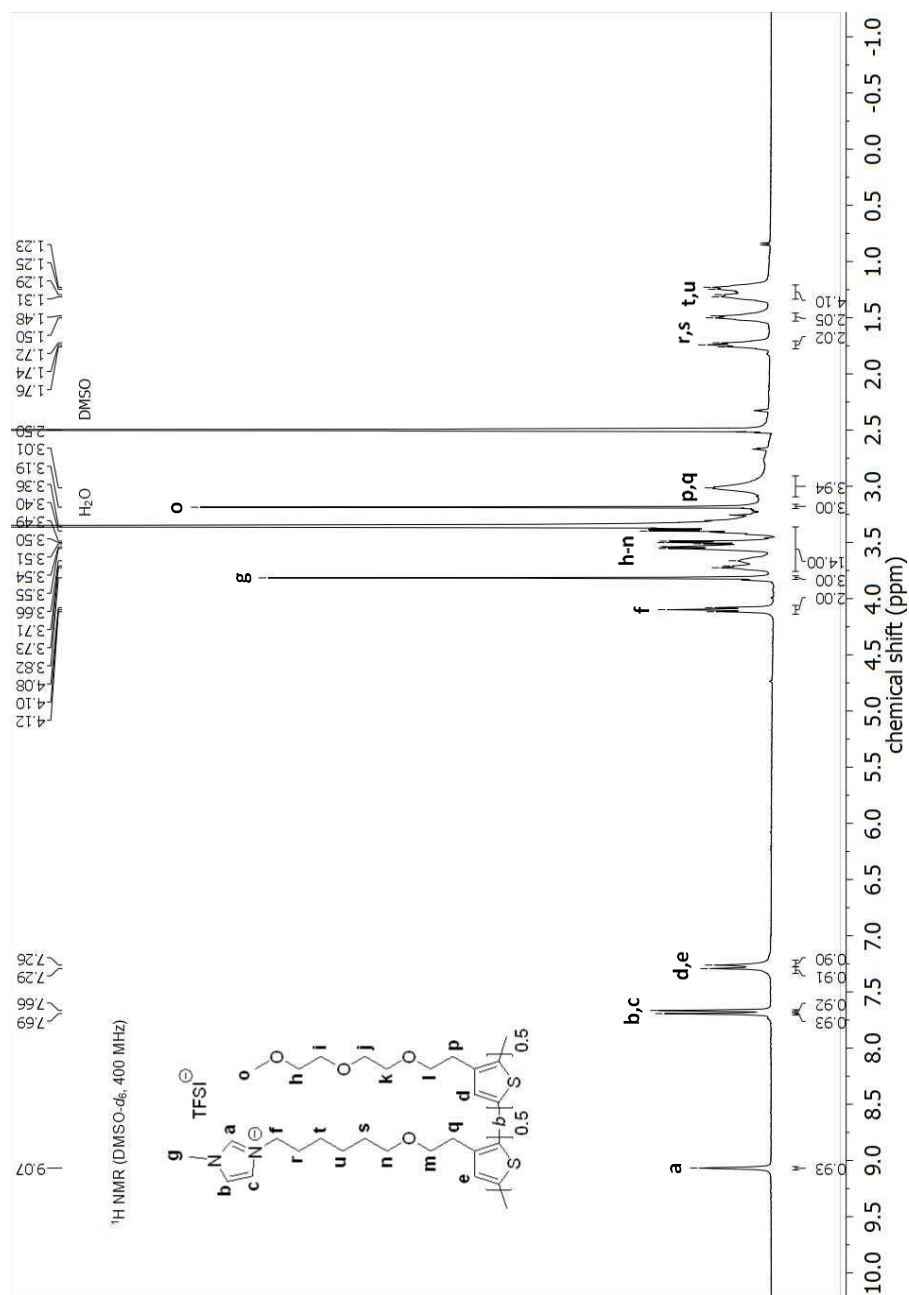


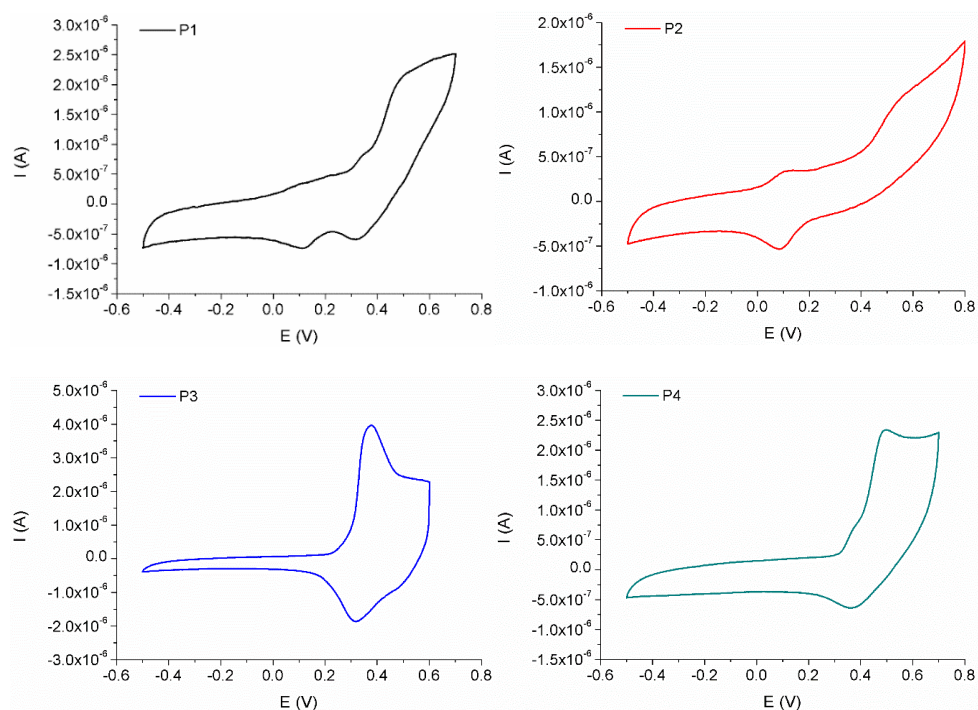
**Figure S6:** <sup>1</sup>H NMR spectrum of P3(MIM)HOET-TFSI-b-P3MEEET (50/50) (P6).

## 2.5.6 Cyclic voltammetry

**Table S1:** Electrochemical properties of the synthesized polymers **P1–P6**.

Polymer	$E_{\text{onset, ox}}$ (V) <sup>a</sup>	HOMO (eV)	$E_{\text{g, opt}}$ (eV) <sup>b</sup>	LUMO (eV) <sup>c</sup>
<b>P1</b>	0.37	-5.26	2.36	-2.90
<b>P2</b>	0.44	-5.34	2.35	-2.99
<b>P3</b>	0.29	-5.07	2.34	-2.73
<b>P4</b>	0.39	-5.18	2.36	-2.82
<b>P5<sup>d</sup></b>	-0.14	-4.76	1.86	-2.90
<b>P6</b>	0.23	-5.13	2.35	-2.78

<sup>a</sup> Onset potential of anodic scan. <sup>b</sup> Optical bandgap (in acetone for **P1** and **P2**, in  $\text{CH}_2\text{Cl}_2$  for **P3**, **P4**, and **P6**, and in film for **P5**). <sup>c</sup> The LUMO energy levels were calculated from the HOMO levels and the optical bandgaps. <sup>d</sup> Due to the different solubility characteristics, **P5** was the only material that could be measured in film.



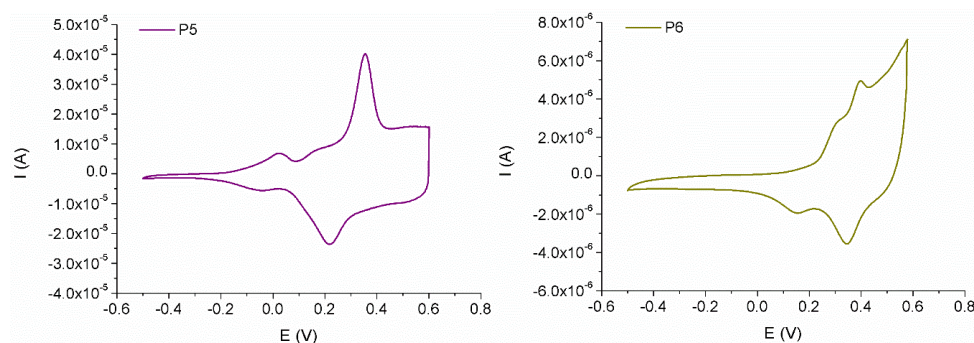


**Figure S7:** Oxidation scans of the synthesized polymers **P1–P6**.

## 2.5.7 Thermal analysis

### TGA

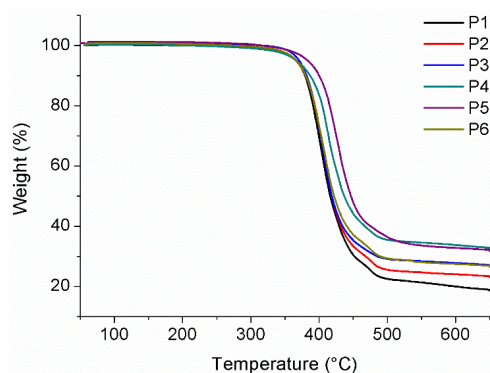


**Figure S8:** TGA profiles of the synthesized polymers **P1–P6**.

### RHC

**Table S2:** Thermal properties of the synthesized polymers **P1–P6**, after the first RHC heating cycle.

Polymer	$T_g$ (°C)	$T_m$ (°C)	$\Delta H$ (J/g)
<b>P1</b>	-18	92	3.2
<b>P2</b>	-20	96	6.7 ( $\sim 0.3 \cdot 17.8 + 0.7 \cdot 3.2 = 7.6$ )
<b>P3</b>	-26	116	10.7 ( $\sim 0.5 \cdot 17.8 + 0.5 \cdot 3.2 = 10.5$ )
<b>P4</b>	-33	112	12.5 ( $\sim 0.7 \cdot 17.8 + 0.3 \cdot 3.2 = 13.4$ )
<b>P5</b>	/	130	17.8
<b>P6</b>	-17	119	10.8 ( $\sim 0.5 \cdot 17.8 + 0.5 \cdot 3.2 = 10.5$ )

**Table S3:** Thermal properties of the synthesized polymers **P1–P6**, after the second RHC heating cycle (after cooling at 20 K/min).

Polymer	$T_g$ (°C)	$T_m$ (°C)	$\Delta H$ (J/g)
<b>P1</b>	-16	/	/
<b>P2</b>	-17	83	2.9
<b>P3</b>	-26	114	7.7
<b>P4</b>	-23	106	8.4
<b>P5</b>	-48	125	12.5
<b>P6</b>	-15	94	4.4

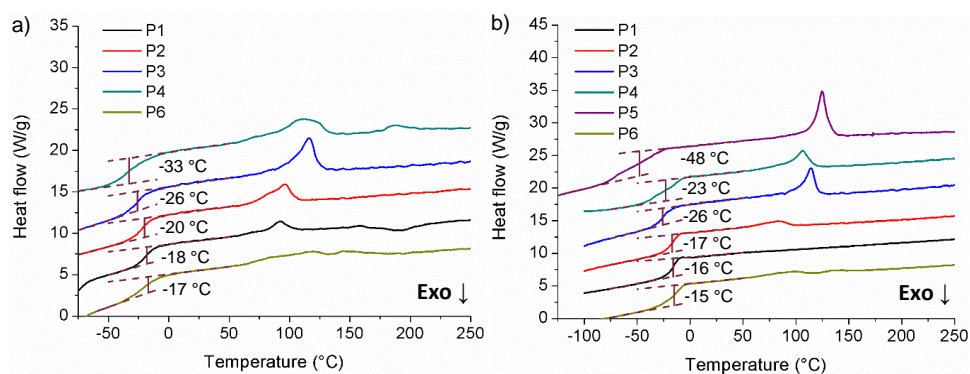


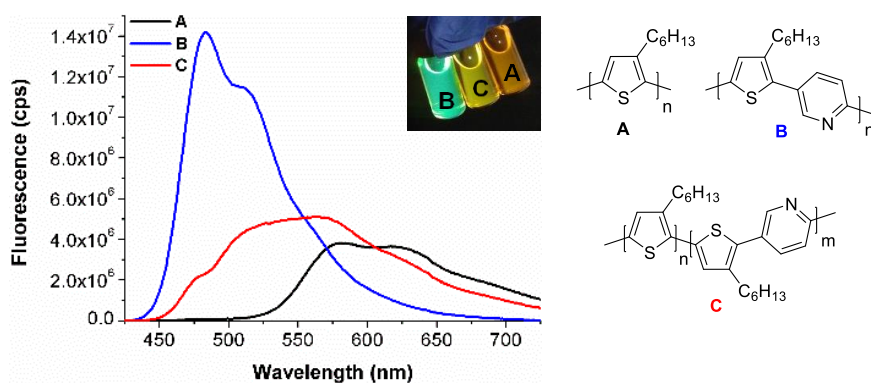
**Figure S9:** Determination of the glass transition temperatures from the RHC heating profiles of **P1–P6**, obtained after a) a first heating cycle at 500 K/min, and b) a second heating cycle at 500 K/min (after preceding cooling at 20 K/min). The curves are shifted vertically for clarity.

### 2.5.8 References

- [1] Bard, A. J.; Faulkner, L. R. *Electrochemical Methods: Fundamentals and Applications, 2nd Edition*; Wiley, 2001.
- [2] Trasatti, S. *Pure Appl. Chem.* **1986**, *58*, 955–966.
- [3] Ghooos, T.; Brassinne, J.; Fustin, C.-A.; Gohy, J.-F.; Defour, M.; Van den Brande, N.; Van Mele, B.; Lutsen, L.; Vanderzande, D. J.; Maes, W. *Polymer* **2013**, *54*, 6293–6304.

## Chapter 3

### Synthesis of highly fluorescent all-conjugated alternating donor-acceptor (block) copolymers via Kumada catalyst-transfer condensation polymerization



S. Govaerts, P. Verstappen, H. Penxten, M. Defour, B. Van Mele, L. Lutsen, D. Vanderzande and W. Maes, *Macromolecules*, **2016**, *49*, 6411–6419.

## **ABSTRACT**

Although controlled polymerization procedures for conjugated polymers have considerable advantages with respect to molar mass and end group control, the material scope has been very limited, in particular considering block copolymers and donor-acceptor type all-conjugated polymers, imposing considerable challenges upon the synthetic polymer community. In this work, a push-pull monomer consisting of a thiophene (donor) and a pyridine (acceptor) unit is synthesized and subsequently polymerized via Kumada catalyst-transfer condensation polymerization using a nickel catalyst. In this way, an alternating donor-acceptor copolymer is obtained via a chain-growth mechanism. Furthermore, an all-conjugated block copolymer containing a poly(3-hexylthiophene) block and the alternating copolymer is successfully prepared in a one-pot procedure as well. The diblock structure is confirmed by comparison of the thermal, electrochemical and spectroscopic properties of the block copolymer and its constituting polymer parts.

### 3.1 INTRODUCTION

Since the discovery that polyacetylene shows high conductivities after doping with halides,<sup>[1]</sup> the development of conjugated polymers has risen rapidly. Throughout the years, different classes were synthesized and investigated in several organic electronic applications, such as light-emitting diodes, transistors, photovoltaics, (bio)sensors, ...<sup>[2]</sup> One of the most studied conjugated polymers is poly(3-hexylthiophene) (P3HT), which played an important role as workhorse material to gain fundamental insights into the working principles of organic photovoltaics (OPV's).<sup>[3,4]</sup> Power conversion efficiencies up to 5% have been obtained when applying P3HT as the electron donor and [6,6]-phenyl-C<sub>61</sub>-butyric acid methyl ester (PC<sub>61</sub>BM) as the electron acceptor in polymer solar cell devices.<sup>[5]</sup> Nowadays, P3HT is outperformed by a particular class of conjugated polymers, the low bandgap donor-acceptor (D-A) alternating copolymers, which allow a more optimal harvesting of the solar spectrum.<sup>[6,7]</sup> These D-A or push-pull copolymers are generally synthesized by transition metal catalyzed polycondensation reactions, whereof the Stille and Suzuki polymerizations are the most well-known examples.<sup>[8-10]</sup> The polymerization mechanism of these reactions is based on the formation of a new carbon-carbon bond through cross-coupling of an organohalide and an organometallic compound with the aid of a transition metal catalyst. The catalytic cycle involves three main steps, i.e. oxidative addition, transmetalation and reductive elimination. The polymerizations follow a step-growth mechanism and high molar mass polymers can only be obtained at high conversions after long reaction times. As a result, rather poor control over the polymer molar mass, dispersity and end groups is achieved, often affording ill-defined materials. On the other hand, controlled chain-growth transition metal catalyzed polycondensations

allow precise control over the above-mentioned polymer characteristics and high molar mass polymers can already be obtained at low conversions. On top of that, they enable the synthesis of fully conjugated block copolymers and other advanced macromolecular structures via one-pot polymerizations. Such materials can give rise to interesting morphological structures and enhanced light absorption, beneficial for their use in for example polymer solar cells.<sup>[11-18]</sup>

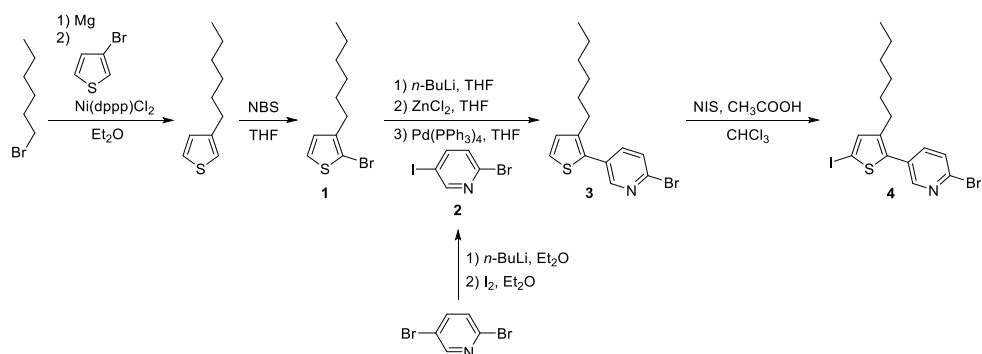
In 2004, Yokozawa *et al.* and McCullough *et al.* found that the nickel-catalyzed Kumada polymerization of 2-bromo-5-chloromagnesio-3-hexylthiophene, obtained after the Grignard metathesis (GRIM) reaction of 2-bromo-3-hexyl-5-iodothiophene with an alkylmagnesium chloride reagent, followed such a controlled chain-growth mechanism.<sup>[19,20]</sup> This chain-growth mechanism results from the fact that the Ni(0) species eliminated after the reductive elimination remains associated to the growing polymer chain, whereafter it is transferred to the next C-Br bond in the same polymer chain to undergo a new oxidative addition step.<sup>[21]</sup> Since 2004, a lot of research has been done on this type of polymerization,<sup>[15,22-30]</sup> generally referred to as Kumada catalyst-transfer condensation polymerization (KCTCP), but up until now there are only two examples known wherein one has been able to synthesize an alternating copolymer in a controlled way by performing KCTCP.<sup>[18,31]</sup> In these particular cases, a polymer consisting of two donor-type (electron rich) components was obtained. It would obviously be very interesting to extend this approach to the synthesis of low bandgap D-A alternating copolymers as this opens the door to a wide range of applications. Since both polythiophenes and polypyridines have already been synthesized in a controlled way via KCTCP, we chose to create a push-pull monomer consisting of a thiophene (D) and a pyridine (A) unit.<sup>[19,20,24,32]</sup>

In this work, the polymer synthesis and characterization will be discussed, as well as the tests performed to analyze the controlled character of the polymerization. Furthermore, the synthesis and characterization of an all-conjugated block copolymer, containing the alternating copolymer structure, will be elucidated.

## **3.2 RESULTS AND DISCUSSION**

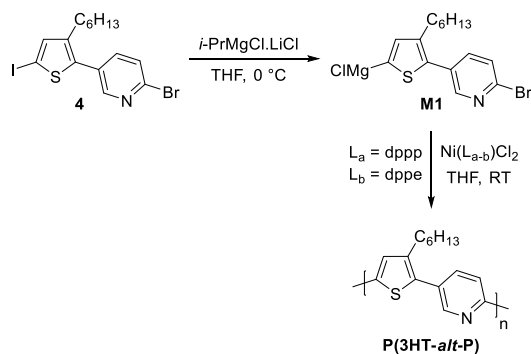
### **3.2.1 Monomer synthesis**

To obtain a conjugated D-A alternating copolymer via KCTCP, we opted for a precursor monomer consisting of a pyridine unit as electron deficient building block and a thiophene unit as the electron rich part. For the synthesis of the thiophene component, a Kumada coupling between 3-bromothiophene and hexylmagnesium bromide was performed, followed by bromination at the 2-position, which resulted in 2-bromo-3-hexylthiophene (**1**) (Scheme 1). The pyridine unit on the other hand was synthesized by selectively exchanging the bromine at the 5-position of 2,5-dibromopyridine with iodine, affording 2-bromo-5-iodopyridine (**2**). Afterwards, the pyridine unit was coupled onto the thiophene through a Negishi coupling, whereby 2-bromo-5-(3'-hexylthiophen-2'-yl)pyridine (**3**) was obtained. The 'para' coupling pattern is important to make sure that the final polymer is fully conjugated. In a last step, compound **3** was iodinated at the 5-position of the thiophene unit to end up with 2-bromo-5-(3'-hexyl-5'-iodothiophen-2'-yl)pyridine (**4**) as the precursor monomer.



**Scheme 1:** Precursor monomer synthesis.

Once the precursor monomer **4** was obtained, the active monomer **M1** could be formed via a GRIM reaction (Scheme 2). This was done prior to the polymerization by adding 1.0 equivalents of *i*-PrMgCl.LiCl to **4** in dry THF at 0 °C, whereby a concentration of 0.1 M was maintained, and letting it react for 1 h. During the GRIM reaction, the iodine end group of **4** was selectively replaced by a magnesium chloride group and the bromine end group remained intact as confirmed by a water quenching test and subsequent <sup>1</sup>H NMR analysis. Moreover, complete conversion of the precursor monomer **4** to the active monomer **M1** was observed. The above conditions for the GRIM reaction (0 °C, 1 h and [**M1**] = 0.1 M) were therefore used for all polymerizations described below.



**Scheme 2:** Synthesis of the **P(3HT-*alt*-P)** copolymer via KCTCP.

### 3.2.2 Alternating copolymer synthesis

Since both polypyridines and polythiophenes have been prepared before in a controlled way via KCTCP using Ni(dppp)Cl<sub>2</sub> as the catalyst,<sup>[19,20,24]</sup> these conditions were also used for the synthesis of the targeted alternating polymer poly[(3-hexylthiophene-5,2-diyl)-*alt*-(pyridine-5,2-diyl)] **P(3HT-*alt*-P)** (Scheme 2). A first polymerization test was performed by adding the *in situ* formed monomer **M1** to 1 mol% of Ni(dppp)Cl<sub>2</sub> in dry THF ([**M1**] = 0.075 M) at RT (Table 1, Test 1). Aliquots of the polymerization mixture were taken at different time intervals and analyzed by gel permeation chromatography (GPC) to determine the molar mass ( $M_n$ ), conversion ( $p$ ) and dispersity ( $\mathcal{D}$ ). These values are important to gain more insight into the polymerization mechanism, for instance by plotting  $M_n$  versus  $p$  and  $\ln([\mathbf{M1}]_0/[\mathbf{M1}])$  versus time. If both of these plots show a linear correlation, the polymerization proceeds via a controlled chain-growth mechanism.<sup>[19,26,33]</sup> From the GPC results, however, no clear plots could be obtained since the molar mass of the polymer was already ~20 000 g/mol after 1 minute and did not increase significantly thereafter (Figure S7, Supporting Information). So, to be able to investigate the polymerization mechanism, the polymerization speed had to be decreased. This was done by lowering the concentration and temperature during different polymerization tests. Nevertheless, the same result was obtained (Table 1, Tests 2-7). When the concentration became too low, no polymer was formed at all (Table 1, Test 8). Then, another polymerization test was performed with a different nickel catalyst, Ni(dppe)Cl<sub>2</sub>, under the same conditions as the initial polymerization test (Table 1, Test 9). Again, a molar mass of ~20 000 g/mol was obtained after 1 minute, which did not increase substantially afterwards (Figure S8, Supporting Information). From all of these polymerization tests, it can be concluded that the polymerization

does not proceed in a controlled way, since the polymer chains do not continue to grow any further once a  $M_n$  of  $\sim 20\,000$  g/mol is achieved, although there is still monomer present in the polymerization mixture.

**Table 1:** KCTCP of **M1** under different reaction conditions.

Test	Catalyst (1 mol%)	Temperature	[ <b>M1</b> ] (M)	$M_n \times 10^4$ (g/mol)	$\mathcal{D}$
1	Ni(dppp)Cl <sub>2</sub>	RT	0.075	2.6 <sup>a</sup>	1.28
2	Ni(dppp)Cl <sub>2</sub>	0 °C	0.075	2.1	1.29
3	Ni(dppp)Cl <sub>2</sub>	RT	0.03	1.7	1.40
4	Ni(dppp)Cl <sub>2</sub>	0 °C	0.01	1.8	1.37
5	Ni(dppp)Cl <sub>2</sub>	RT	0.0075	1.9	1.19
6	Ni(dppp)Cl <sub>2</sub>	RT	0.005	2.3	1.23
7	Ni(dppp)Cl <sub>2</sub>	RT	0.0045	2.2	1.36
8	Ni(dppp)Cl <sub>2</sub>	RT	0.002	/	/
9	Ni(dppe)Cl <sub>2</sub>	RT	0.075	2.3 <sup>a</sup>	1.29

<sup>a</sup> After purification by Soxhlet extraction.

This observation motivated further analysis to obtain more insights in the polymerization mechanism. To this extent, new polymerization tests were performed whereby each time the same amount of **M1** (0.20 mmol) was used under the same reactions conditions ( $[\mathbf{M1}] = 0.05$  M and RT) and only the amount of Ni(dppp)Cl<sub>2</sub> catalyst was altered (1, 2.5, 5 and 10 mol%). The results of those tests are depicted in Figure 1. It is clear that for all different catalyst amounts roughly the same  $M_n$  values ( $\sim 18\,000$  g/mol) were obtained. The same can be said for the dispersities, which all lie around 1.4. This confirms our previous assumption that the polymerization does not happen in a controlled way. On the other hand, the low dispersities and high molar masses at low conversions point out that the polymerization follows a chain-growth mechanism. It can be concluded that the polymerization of **P(3HT-*alt*-P)** proceeds via a non-controlled

chain-growth mechanism, whereby the growing polymer chains are terminated once they have reached a  $M_n$  value of  $\sim 20\,000$  g/mol.

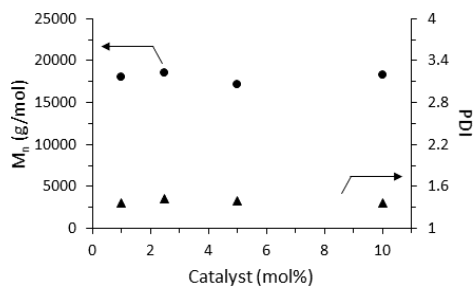
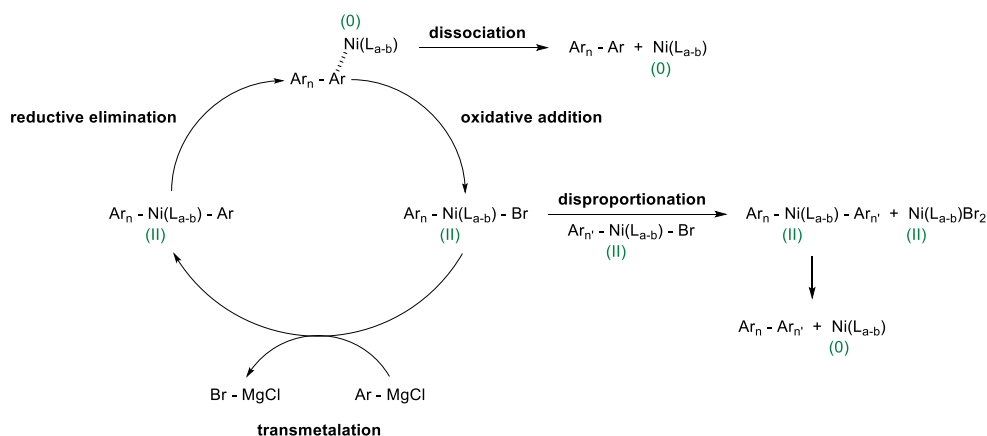


**Figure 1:** Relation between the amount of catalyst used and the resulting molar mass and dispersity.

Since these termination reactions have a strong influence on the polymerization characteristics of **P(3HT-*alt*-P)**, it would be interesting to reveal which type of termination reaction is dominant. In case of KCTCP, the association of the catalyst to the growing polymer chain after reductive elimination is essential to obtain the controlled chain-growth character. This means that there are two types of termination reactions possible, i.e. disproportionation and dissociation (Scheme 3).<sup>[29]</sup>



**Scheme 3:** Catalytic cycle of KCTCP with its possible termination reactions.<sup>[29]</sup>

When disproportionation is the dominant termination reaction, it goes in competition with the transmetalation step, which results into a degree of polymerization ( $X_n$ ) that is defined by the ratio of the rate of transmetalation ( $R_{TM}$ ) and the rate of disproportionation ( $R_{disp}$ ). If, however, dissociation is the dominant termination reaction,  $X_n$  is determined by the ratio of the rate of oxidative addition ( $R_{OA}$ ) and the rate of dissociation ( $R_{diss}$ ). This results into the following equations:

- If disproportionation is dominant:

$$X_n = \frac{R_{TM}}{R_{disp}} = \frac{k_{TM}[In]_0[M]_0}{k_{disp}[In]_0[In]_0} \quad (1)$$

- If dissociation is dominant:

$$X_n = \frac{R_{OA}}{R_{diss}} = \frac{k_{OA}[In]_0}{k_{diss}[In]_0} \quad (2)$$

whereby  $[In]_0$  is the initial initiator concentration,  $[M]_0$  is the initial monomer concentration and  $k_{TM}$ ,  $k_{disp}$ ,  $k_{OA}$  and  $k_{diss}$  are the rate constants for transmetalation, disproportionation, oxidative addition and dissociation, respectively.<sup>[29]</sup> Out of these equations, it can be deduced that if disproportionation is dominant, the degree of polymerization (and hence the molar mass) is dependent of  $[M]_0/[In]_0$ . On the contrary, when dissociation is the dominant termination reaction,  $X_n$  is independent of  $[M]_0/[In]_0$ . All polymerization tests, wherein first only  $[M]_0$  was altered (Table 1) and afterwards only  $[In]_0$  was varied (Figure 1), clearly show that the molar mass is independent of  $[M]_0/[In]_0$ . This points out that dissociation is most likely the dominant termination reaction in our non-controlled chain-growth polymerization of **P(3HT-*alt*-P)**. These results are in agreement with previous findings that difficulties arise in the KCTCP of n-type monomers due to the fact that they have a weaker n-donor ability to stabilize

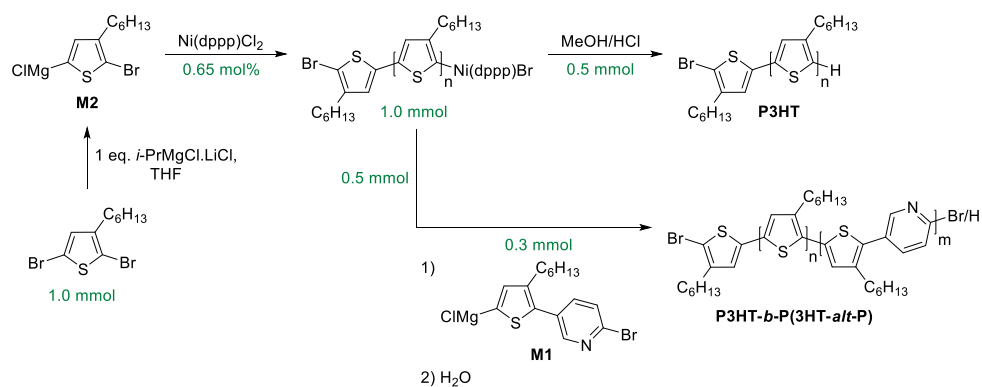
the polymer-nickel complex after reductive elimination, leading to shorter lifetimes of the growing polymer chains.<sup>[34]</sup> This could explain why no polymer is formed at all when the concentrations are too low (Table 1, Test 8), because in this case it takes too long to find another monomer unit in the vicinity to react with, causing the Ni catalyst to dissociate from the growing entity.

Another way to obtain more insights into the polymerization mechanism is to investigate the end groups of the polymer chains by performing MALDI-TOF (matrix-assisted laser desorption ionization - time of flight) mass spectrometry measurements. From literature, it is known that only polymer chains with Br/H end groups are formed in case of a controlled chain-growth mechanism.<sup>[35]</sup> When termination reactions occur, however, also polymer chains with Br/Br or H/H end groups are formed.<sup>[36]</sup> In our case, dissociation seems to be the dominant termination reaction, which results in polymer chains with Br/Br end groups. The MALDI-TOF spectrum of **P(3HT-*alt*-P)** (Table 1, Test 9) is displayed in Figure S9 (Supporting Information). It is clear that there are two main distributions present. The smaller signals correspond to polymer chains with Br/H end groups, whereas the most intense signals can be attributed to polymer chains with Br/Br end groups. These observations confirm the non-controlled chain-growth character of the KCTCP of **P(3HT-*alt*-P)**, due to dissociation of the nickel catalyst.

### 3.2.3 Block copolymer synthesis

It is well established in literature that the KCTCP of poly(3-hexylthiophene) follows a controlled chain-growth mechanism, enabling the synthesis of all-conjugated block copolymers by sequential addition of another active monomer species via a one-pot KCTCP procedure.<sup>[19,22,26,29,37]</sup> For this reason, we decided to start with an *in situ* formed **P3HT** block that is used as macro-initiator for the polymerization

of **P(3HT-*alt*-P)** as the second block in order to end up with an all-conjugated **P3HT-*b*-P(3HT-*alt*-P)** block copolymer (Scheme 4). This was done by first performing a GRIM reaction on 2,5-dibromo-3-hexylthiophene with one equivalent of *i*-PrMgCl.LiCl at 0 °C for 1 h, resulting in 2-bromo-5-chloromagnesio-3-hexylthiophene as active monomer **M2**. Then, this monomer was polymerized with 0.65 mol% of Ni(dppp)Cl<sub>2</sub> at RT ([**M2**] = 0.075 M). After a polymerization time of 15 min, half of the polymerization mixture was cannulated to another flask and quenched with a MeOH/HCl mixture, which resulted into the **P3HT** reference homopolymer. To the other half of the polymerization mixture, the *in situ* prepared active monomer **M1** was added to create the second block. After a polymerization time of 30 min at RT the polymerization mixture was quenched with water, yielding poly{[3-hexylthiophene-5,2-diyl]-*block*-[(3-hexylthiophene-5,2-diyl)-*alt*-(pyridine-5,2-diyl)]} **P3HT-*b*-P(3HT-*alt*-P)**. Both the **P3HT** homopolymer and the **P3HT-*b*-P(3HT-*alt*-P)** block copolymer were purified by Soxhlet extraction with MeOH, acetone, hexane and chloroform (dissolving the polymer), respectively. All polymeric material was found to be soluble in THF and CHCl<sub>3</sub>.



**Scheme 4:** Synthesis of the **P3HT-*b*-P(3HT-*alt*-P)** copolymer.

A first test performed to check whether a block copolymer was indeed formed, was the analysis of both **P3HT** and **P3HT-*b*-P(3HT-*alt*-P)** by GPC. The resulting GPC profiles clearly show a shift to higher  $M_n$  values, while maintaining a unimodal curve (Figure 2). The **P3HT** homopolymer was characterized by a  $M_n$  value of 23 000 g/mol and a  $\mathcal{D}$  of 1.15, while the **P3HT-*b*-P(3HT-*alt*-P)** block copolymer showed a  $M_n$  value of 41 000 g/mol and a  $\mathcal{D}$  of 1.37. These  $M_n$  values correspond reasonably well to what was expected. By using 0.65 mol% of Ni(dppp)Cl<sub>2</sub>, a  $M_n$  value of ~25 000 g/mol (~150 monomer units of 166 g/mol) was foreseen for **P3HT**. This value was targeted since we aimed at a doubling of the molar mass for the block copolymer and it was already established that the **P(3HT-*alt*-P)** polymer chains always grew till a length of ~20 000 g/mol.

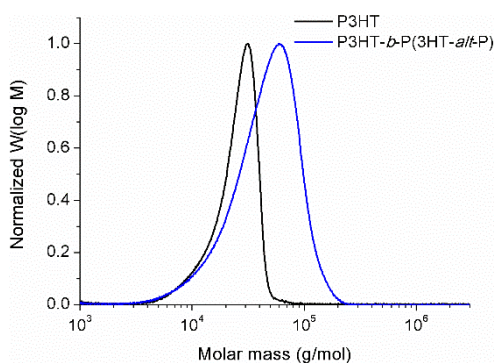


**Figure 2:** GPC profiles of the **P3HT** homopolymer and the **P3HT-*b*-P(3HT-*alt*-P)** copolymer.

The fact that a unimodal curve was obtained for the block copolymer indicates that the 'living' **P3HT** polymer chains grew further to end up with **P3HT-*b*-P(3HT-*alt*-P)** chains. This could be confirmed by studying both materials via <sup>1</sup>H NMR spectroscopy. First, the  $\alpha$ -CH<sub>2</sub> region of the hexyl side chains of the **P3HT** homopolymer was analyzed (Figure 3a). Three different triplets were distinguished, whereof the biggest signal (**a**) at 2.80 ppm could be ascribed to the

$\alpha$ -CH<sub>2</sub> protons of the internal **P3HT** units, whereas the two smaller signals correspond to the  $\alpha$ -CH<sub>2</sub> protons of the two external thiophene units with a hydrogen end group (signal **b** at 2.62 ppm) and a bromine end group (signal **c** at 2.58 ppm), according to McCullough *et al.*<sup>[37]</sup> Then, an overlay of the <sup>1</sup>H NMR spectra of the  $\alpha$ -CH<sub>2</sub> regions of **P3HT** and **P3HT-*b*-P(3HT-*alt*-P)** was studied (Figure 3b). From this overlay, it is clear that signal **b** of **P3HT** disappeared (or at least largely reduced), suggesting that (most of) the **P3HT** polymer chains reacted further to give the block copolymer. Besides this, another signal (**d** at 2.75 ppm) appeared in the spectrum of the **P3HT-*b*-P(3HT-*alt*-P)** copolymer, which could be ascribed to the  $\alpha$ -CH<sub>2</sub> protons of the hexyl side chains of the second block.

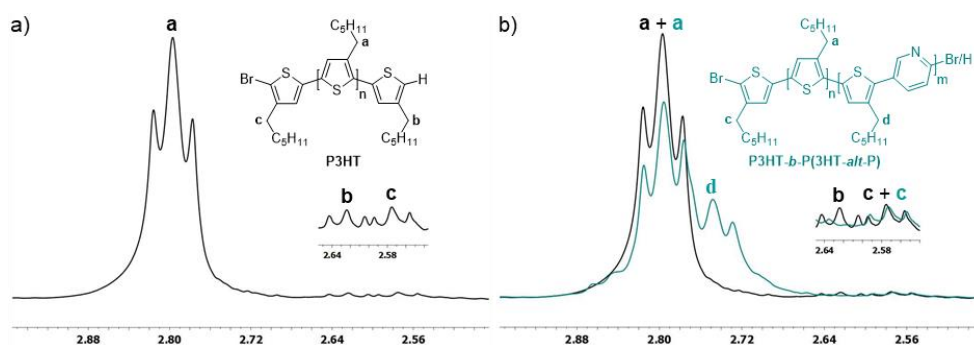


**Figure 3:** a) <sup>1</sup>H NMR spectrum of the  $\alpha$ -CH<sub>2</sub> region of **P3HT**; b) Overlay of the <sup>1</sup>H NMR spectra of the  $\alpha$ -CH<sub>2</sub> regions of **P3HT** and **P3HT-*b*-P(3HT-*alt*-P)**.

As we cannot exclude from the NMR analysis that minor amounts of non-chain-extended **P3HT** are still present in the block copolymer sample, as might be inferred from the tailing at the low molar mass side of the GPC profile (Figure 2), preparative GPC was used to remove the low-molar mass part. The two separate fractions obtained were then analyzed by GPC and <sup>1</sup>H NMR spectroscopy, from

which it can be concluded that ~3–4% of **P3HT** is present in the block copolymer (Figure S10-12, Supporting Information).

Also the other order of monomer addition was investigated (starting from **P(3HT-*alt*-P)**), but in this case no block copolymer was formed. This is not surprising since it was already established that the growing **P(3HT-*alt*-P)** polymer chains are terminated once they have reached a  $M_n$  value of ~20 000 g/mol after just a few minutes. This observation, together with the successful block copolymerization starting from a **P3HT** block, further strengthens our hypothesis that the **P(3HT-*alt*-P)** copolymer is formed via a non-controlled chain-growth polymerization.

#### **3.2.4 Thermal, electrochemical and optical characterization**

First of all, the thermal properties of the synthesized materials were analyzed by performing rapid heat-cool calorimetry (RHC) measurements on the **P(3HT-*alt*-P)** copolymer, the **P3HT** homopolymer and the **P3HT-*b*-P(3HT-*alt*-P)** copolymer. Also a blend of **P3HT** and **P(3HT-*alt*-P)** was made for comparison and characterized in the same way. This blend was created by mixing 40% of **P(3HT-*alt*-P)** with 60% of **P3HT**, approaching the constitution of the block copolymer (based on integration of the  $^1\text{H}$  NMR spectrum of **P3HT-*b*-P(3HT-*alt*-P)**). RHC was chosen above regular differential scanning calorimetry (DSC) because of its increased sensitivity to thermal transitions as a result of the fast scanning rates and the low sample amounts required.<sup>[38]</sup> The results of the RHC measurements are shown in Figure 4. The **P3HT** homopolymer shows a melting peak around 228 °C, with a melting enthalpy of 24.4 J/g, as expected for this molar mass range.<sup>[39]</sup> No clear glass transition temperature of **P3HT** can be detected. The **P(3HT-*alt*-P)** copolymer, on the other hand, shows no melting at

all and a clear glass transition temperature ( $T_g$ ) around 122 °C (see also Figure S13, Supporting Information), suggesting that the alternating copolymer is completely amorphous. The incorporation of the pyridine moieties apparently impedes efficient packing of the polymer chains in a crystal lattice. Some enthalpic relaxation can be observed on top of the glass transition due to the different heating and cooling rates applied. In the blend of **P(3HT-*alt*-P)** and **P3HT**, the melting peak of **P3HT** is slightly shifted to lower temperature (224 °C), suggesting that the **P3HT** crystals formed in the blend are a bit less stable. The melting enthalpy of the blend is 13.5 J/g, which corresponds to approximately 60% of the melting enthalpy of **P3HT**, in good agreement with the composition of the blend. The  $T_g$  of the blend is difficult to determine, but lower than the glass transition of **P(3HT-*alt*-P)** (likely around 112 °C or lower). The block copolymer shows both a (considerably broadened) melting peak with a maximum at 217 °C and an even lower and also broadened  $T_g$  around 70 °C (see also Figure S13, Supporting Information). The melting enthalpy of the block amounts to only 8.5 J/g, definitely lower than 60% of the melting enthalpy of **P3HT**. This lower melting enthalpy, together with the decreased melting temperature and the broad melting trajectory, points out that the **P(3HT-*alt*-P)** block hinders the crystallization of the **P3HT** block to a larger extent than in the blend, resulting in less perfect and less stable crystals. The lower and broader  $T_g$  around 70 °C probably indicates the plasticizing (interphase) effect of the **P3HT**-rich domains on the **P(3HT-*alt*-P)**-rich domains in the microphase separated block copolymer. Thermogravimetric analysis (TGA) of the synthesized materials was performed as well. These measurements revealed that the main degradation starts around 350 °C for all polymers (Figure S14, Supporting Information).

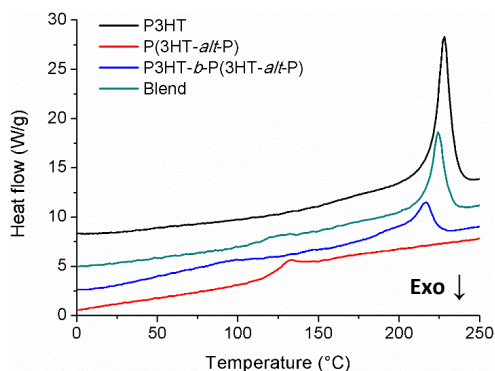


**Figure 4:** RHC heating profiles, obtained at 500 K/min after cooling at 20 K/min (2<sup>nd</sup> heating), of **P3HT**, **P(3HT-*alt*-P)**, **P3HT-*b*-P(3HT-*alt*-P)** and the physical blend of **P3HT** and **P(3HT-*alt*-P)** (curves shifted vertically for clarity).

The electrochemical properties of the synthesized materials, of relevance for their possible application in organic electronics, were investigated via cyclic voltammetry. The resulting voltammograms are depicted in Figure 5. From the overlay of the oxidation scans of all materials (Figure 5a), it is clear that the oxidation characteristics of both **P3HT** and **P(3HT-*alt*-P)** are present in the oxidation profile of the block copolymer and the blend. The oxidation profile of the blend is almost an exact superposition of the voltammograms of the two individual polymer components, with two sharp and nicely separated **P3HT** oxidations and one peak of **P(3HT-*alt*-P)**. In case of the block copolymer, the two oxidation peaks of **P3HT** are less sharp and not so well separated. The reduction characteristics of both constituting polymers are also observed in the reduction profiles of the block copolymer and blend (Figure 5b).

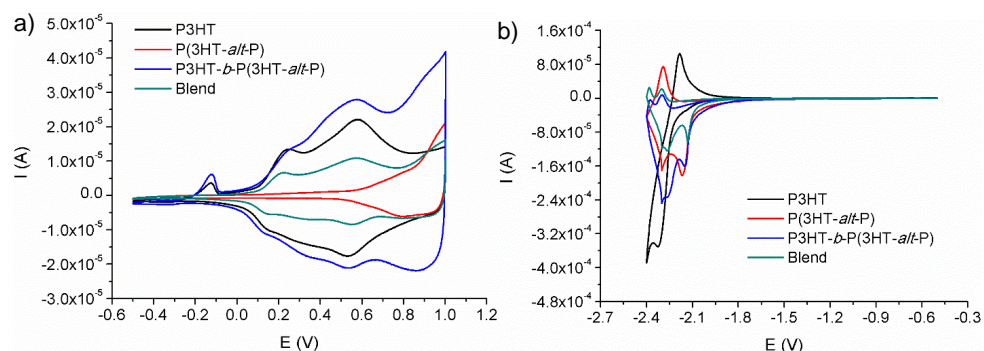


**Figure 5:** Overlay of the oxidation (a) and reduction (b) scans of **P3HT**, **P(3HT-*alt*-P)**, **P3HT-*b*-P(3HT-*alt*-P)** and the physical blend of **P3HT** and **P(3HT-*alt*-P)** as determined by cyclic voltammetry.

The frontier orbital energy levels of all materials can be obtained from the above voltammograms by determining the onset potentials. The results are presented in Table 2. The HOMO levels (derived from the oxidative onset potentials) of **P3HT**, the block copolymer and the blend are nearly the same, whereas the HOMO of the alternating copolymer lies significantly deeper. The LUMO levels (derived from the reductive onset potentials) of all pyridine-containing polymers are similar, whereas **P3HT** shows a slightly higher LUMO. The largest electrochemical bandgap is observed for the alternating D-A copolymer.

**Table 2:** Electrochemical properties of **P3HT**, **P(3HT-*alt*-P)**, **P3HT-*b*-P(3HT-*alt*-P)** and the physical blend of **P3HT** and **P(3HT-*alt*-P)** (60/40).

Polymer	$E_{\text{onset, ox}}$ (V) <sup>a</sup>	HOMO (eV)	$E_{\text{onset, red}}$ (V) <sup>a</sup>	LUMO (eV)	$E_{\text{g, EC}}$ (eV) <sup>b</sup>	$E_{\text{g, opt}}$ (eV) <sup>c</sup>
<b>P3HT</b>	0.12	-5.08	-2.23	-2.73	2.35	2.03
<b>P(3HT-<i>alt</i>-P)</b>	0.57	-5.53	-2.10	-2.86	2.67	2.17
<b>P3HT-<i>b</i>-P(3HT-<i>alt</i>-P)</b>	0.11	-5.07	-2.10	-2.86	2.21	2.06
Blend	0.11	-5.07	-2.09	-2.87	2.20	2.06

<sup>a</sup> Onset potential of anodic/cathodic scan. <sup>b</sup> Electrochemical bandgap. <sup>c</sup> Optical bandgap.

To obtain insight into the optical properties of the synthesized materials and to further prove that indeed a block copolymer was formed, the synthesized polymer materials and the physical blend were also studied by UV-vis absorption and fluorescence spectroscopy. The UV-vis absorption spectra of all materials in solution ( $\text{CHCl}_3$ ) are depicted in Figure 6. It is clear that the wavelength at maximal absorbance ( $\lambda_{\text{max}}$ ) of the block copolymer (424 nm) lies in between those of **P(3HT-*alt*-P)** (413 nm) and **P3HT** (453 nm), whereby the absorbance profile of the block copolymer overlaps with those of the two constituting polymers, but lies more closely toward that of **P(3HT-*alt*-P)**. The absorption spectrum of the blend is quite similar to that of the block copolymer, with the difference that a shoulder is observed in the **P3HT** region and  $\lambda_{\text{max}}$  is slightly blue-shifted (422 nm).

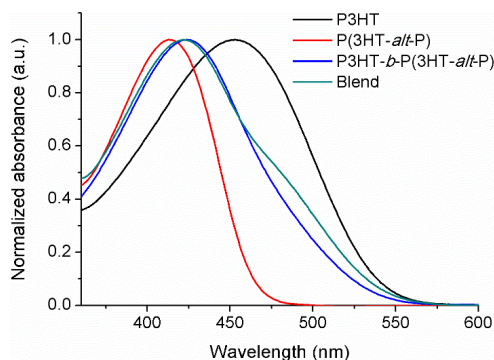


**Figure 6:** UV-vis absorption spectra of **P3HT**, **P(3HT-*alt*-P)**, **P3HT-*b*-P(3HT-*alt*-P)** and the physical blend of **P3HT** and **P(3HT-*alt*-P)**.

Finally, the fluorescence properties of the polymers were investigated as well. A green-yellow fluorescence was observed for the **P(3HT-*alt*-P)** copolymer, while the **P3HT** homopolymer shows an orange fluorescence and the **P3HT-*b*-P(3HT-*alt*-P)** copolymer a yellow-orange fluorescence (Figure S15, Supporting Information). These visual observations were confirmed by the fluorescence

spectra of the materials in  $\text{CHCl}_3$  solution, which are illustrated in Figure 7. From these spectra it can be determined that the **P(3HT-*alt*-P)** copolymer has an emission maximum at 483 nm, the **P3HT** homopolymer at 582 nm and the **P3HT-*b*-P(3HT-*alt*-P)** copolymer at 563 nm (Table 3). In contrast to the absorption spectra, there is a clear difference between the fluorescence spectrum of the block copolymer and that of the blend. The fluorescence spectrum of the blend ( $\lambda_{\text{max}} = 483$  nm) is mainly determined by the fluorescence spectrum of the **P(3HT-*alt*-P)** copolymer, with only a small contribution from **P3HT**. On the other hand, the fluorescence spectrum of the block copolymer is much broader and definitely not just a superposition of the fluorescence spectra of the two polymer components. This again confirms the successful formation of an all-conjugated block copolymer, which could also visually be established by means of paper chromatography (Figure S16, Supporting Information).

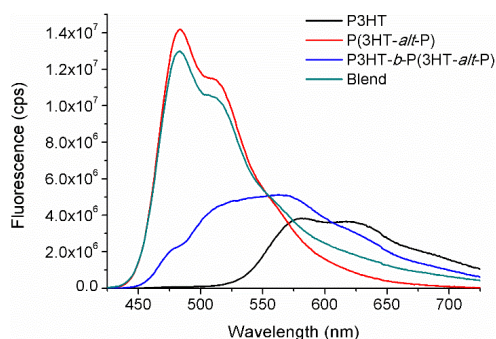


**Figure 7:** Fluorescence spectra of **P3HT**, **P(3HT-*alt*-P)**, **P3HT-*b*-P(3HT-*alt*-P)** and the physical blend of **P3HT** and **P(3HT-*alt*-P)** ( $\lambda_{\text{exc}} = 373$  nm).

In addition to the fluorescence spectra, the quantum yields were determined as well (Table 3). A very high quantum yield of 89% was obtained for the **P(3HT-*alt*-P)** copolymer. For **P3HT**, a value of 43% was found, which corresponds to

previous literature data.<sup>[40]</sup> The quantum yield of the block copolymer amounted to 62%, which lies nicely in between the values of the two polymer constituents.

**Table 3:** Optical properties of **P3HT**, **P(3HT-*alt*-P)** and **P3HT-*b*-P(3HT-*alt*-P)** in CHCl<sub>3</sub> solution.

Polymer	Absorbance $\lambda_{\max}$ (nm)	Fluorescence $\lambda_{\max}$ (nm)	Quantum yield (%)
<b>P3HT</b>	453	582	43
<b>P(3HT-<i>alt</i>-P)</b>	413	483	89
<b>P3HT-<i>b</i>-P(3HT-<i>alt</i>-P)</b>	424	563	62

### 3.3 CONCLUSIONS

We have shown that an alternating donor-acceptor copolymer (**P(3HT-*alt*-P)**) can be synthesized via Kumada catalyst-transfer condensation polymerization using a nickel catalyst, thereby requiring no toxic tin compounds as is the case for Stille polymerizations. Through several polymerization tests, varying the monomer concentration and the amount of catalyst (separately), it was proven that the KCTCP in this case follows a non-controlled chain-growth mechanism due to dissociation of the nickel catalyst. Nevertheless, rather narrow dispersities and reasonable molar masses of ~20 000 g/mol could already be obtained after one minute. Moreover, a new all-conjugated block copolymer (**P3HT-*b*-P(3HT-*alt*-P)**) was also successfully formed in a one-pot KCTCP procedure by using an *in situ* formed poly(3-hexylthiophene) (**P3HT**) block to initiate the polymerization of the donor-acceptor alternating copolymer as the second block. This was confirmed by GPC and <sup>1</sup>H NMR analysis.

The thermal, electrochemical and optical properties of the three polymers and a blend of **P3HT** and **P(3HT-*alt*-P)** were investigated. From the thermal analysis it

was clear that the presence of the **P(3HT-*alt*-P)** part in the block copolymer hinders the crystallization of the **P3HT** block. With respect to the optical properties, a clear distinction could be made between the block copolymer and a physical blend of the two polymer components by comparing the fluorescence spectra and quantum yields. The fluorescence spectrum of the block copolymer is not just a superposition of the two polymer parts and definitely differs from the spectrum of the blend, further proving the successful synthesis of the block copolymer. The block copolymer showed a quantum yield of 62%, nicely in between the values for **P3HT** and **P(3HT-*alt*-P)** (43% and 89%, respectively).

The synthesized materials show promising characteristics to be used in organic electronics. The deeper HOMO of the all-conjugated alternating copolymer is for instance an asset in polymer solar cells, as it allows to achieve higher open-circuit voltages.<sup>[41]</sup> On the other hand, the block copolymer is attractive toward the development of charge-selective interlayers for organic photovoltaics.<sup>[42]</sup> In this respect, it would be interesting to functionalize the side chains to enable the synthesis of conjugated polyelectrolytes.<sup>[43]</sup> The high fluorescence quantum yield for the alternating donor-acceptor copolymer renders this material an attractive candidate for sensor and/or bio-imaging applications (for instance in nanoparticle form).<sup>[44,45]</sup> Efforts in this direction are currently ongoing, while other donor-acceptor combinations will be explored as well.

### 3.4 REFERENCES

- [1] Shirakawa, H.; Louis, E. J.; MacDiarmid, A. G.; Chiang, C. K.; Heeger, A. *J. J. Chem. Soc. Chem. Commun.* **1977**, 578–580.
- [2] Skotheim, T. A.; Reynolds, J. *Conjugated Polymers: Theory, Synthesis, Properties, and Characterization (Handbook of Conducting Polymers, Third Edition)*; CRC Press, 2006.
- [3] Dang, M. T.; Hirsch, L.; Wantz, G. *Adv. Mater.* **2011**, *23*, 3597–3602.
- [4] Marrocchi, A.; Lanari, D.; Facchetti, A.; Vaccaro, L. *Energy Environ. Sci.* **2012**, *5*, 8457–8474.
- [5] Ma, W.; Yang, C.; Gong, X.; Lee, K.; Heeger, A. J. *Adv. Funct. Mater.* **2005**, *15*, 1617–1622.
- [6] Lu, L.; Zheng, T.; Wu, Q.; Schneider, A. M.; Zhao, D.; Yu, L. *Chem. Rev.* **2015**, *115*, 12666–12731.
- [7] Mazzi, K. A.; Luscombe, C. K. *Chem. Soc. Rev.* **2015**, *44*, 78–90.
- [8] Xu, S.; Kim, E. H.; Wei, A.; Negishi, E. *Sci. Technol. Adv. Mater.* **2014**, *15*, 044201–044223.
- [9] Bao, Z.; Chan, W. K.; Yu, L. *J. Am. Chem. Soc.* **1995**, *117*, 12426–12435.
- [10] Suzuki, A. *J. Organomet. Chem.* **1999**, *576*, 147–168.
- [11] Roncali, J.; Leriche, P.; Cravino, A. *Adv. Mater.* **2007**, *19*, 2045–2060.
- [12] Zhang, Y.; Tajima, K.; Hirota, K.; Hashimoto, K. *J. Am. Chem. Soc.* **2008**, *130*, 7812–7813.
- [13] Topham, P. D.; Parnell, A. J.; Hiorns, R. C. *J. Polym. Sci. Part B Polym. Phys.* **2011**, *49*, 1131–1156.

- [14] Ouhib, F.; Tomassetti, M.; Manca, J.; Piersimoni, F.; Spoltore, D.; Bertho, S.; Moons, H.; Lazzaroni, R.; Desbief, S.; Jérôme, C.; Detrembleur, C. *Macromolecules* **2013**, *46*, 785–795.
- [15] Boon, F.; Hergué, N.; Deshayes, G.; Moerman, D.; Desbief, S.; De Winter, J.; Gerbaux, P.; Geerts, Y. H.; Lazzaroni, R.; Dubois, P. *Polym. Chem.* **2013**, *4*, 4303–4307.
- [16] Lee, Y.; Gomez, E. D. *Macromolecules* **2015**, *48*, 7385–7395.
- [17] Wang, J.; Higashihara, T. *Polym. Chem.* **2013**, *4*, 5518–5526.
- [18] Qiu, Y.; Fortney, A.; Tsai, C.-H.; Baker, M. A.; Gil, R. R.; Kowalewski, T.; Noonan, K. J. T. *ACS Macro Lett.* **2016**, *5*, 332–336.
- [19] Yokoyama, A.; Miyakoshi, R.; Yokozawa, T. *Macromolecules* **2004**, *37*, 1169–1171.
- [20] Sheina, E. E.; Liu, J.; Iovu, M. C.; Laird, D. W.; McCullough, R. D. *Macromolecules* **2004**, *37*, 3526–3528.
- [21] Tkachov, R.; Senkovskyy, V.; Komber, H.; Sommer, J.-U.; Kiriya, A. *J. Am. Chem. Soc.* **2010**, *132*, 7803–7810.
- [22] Geng, Y.; Huang, L.; Wu, S.; Wang, F. *Sci. China Chem.* **2010**, *53*, 1620–1633.
- [23] Kiriya, A.; Senkovskyy, V.; Sommer, M. *Macromol. Rapid Commun.* **2011**, *32*, 1503–1517.
- [24] Nanashima, Y.; Yokoyama, A.; Yokozawa, T. *Macromolecules* **2012**, *45*, 2609–2613.
- [25] Palermo, E. F.; McNeil, A. J. *Macromolecules* **2012**, *45*, 5948–5955.
- [26] Willot, P.; Govaerts, S.; Koeckelberghs, G. *Macromolecules* **2013**, *46*, 8888–8895.
- [27] Wang, J.; Ueda, M.; Higashihara, T. *ACS Macro Lett.* **2013**, *2*, 506–510.

- [28] Magurudeniya, H. D.; Kularatne, R. S.; Rainbolt, E. A.; Bhatt, M. P.; Murphy, J. W.; Sheina, E. E.; Gnade, B. E.; Biewer, M. C.; Stefan, M. C. *J. Mater. Chem. A* **2014**, *2*, 8773–8781.
- [29] Willot, P.; Moerman, D.; Leclère, P.; Lazzaroni, R.; Baeten, Y.; Van der Auweraer, M.; Koeckelberghs, G. *Macromolecules* **2014**, *47*, 6671–6678.
- [30] Bhatt, M. P.; Magurudeniya, H. D.; Sista, P.; Sheina, E. E.; Jeffries-EL, M.; Janesko, B. G.; McCullough, R. D.; Stefan, M. C. *J. Mater. Chem. A* **2013**, *1*, 12841–12849.
- [31] Ono, R. J.; Kang, S.; Bielawski, C. W. *Macromolecules* **2012**, *45*, 2321–2326.
- [32] Nanashima, Y.; Shibata, R.; Miyakoshi, R.; Yokoyama, A.; Yokozawa, T. *J. Polym. Sci. Part A Polym. Chem.* **2012**, *50*, 3628–3640.
- [33] Qiu, J.; Charleux, B.; Matyjaszewski, K. *Polimery* **2001**, *46*, 453–460.
- [34] Yokozawa, T.; Nanashima, Y.; Ohta, Y. *ACS Macro Lett.* **2012**, *1*, 862–866.
- [35] Miyakoshi, R.; Yokoyama, A.; Yokozawa, T. *J. Am. Chem. Soc.* **2005**, *127*, 17542–17547.
- [36] Liu, J.; Loewe, R. S.; McCullough, R. D. *Macromolecules* **1999**, *32*, 5777–5785.
- [37] Iovu, M. C.; Sheina, E. E.; Gil, R. R.; McCullough, R. D. *Macromolecules* **2005**, *38*, 8649–8656.
- [38] Wouters, S.; Demir, F.; Beenaerts, L.; Van Assche, G. *Thermochim. Acta* **2012**, *530*, 64–72.
- [39] Spoltore, D.; Vangerven, T.; Verstappen, P.; Piersimoni, F.; Bertho, S.; Vandewal, K.; Van den Brande, N.; Defour, M.; Van Mele, B.; De Sio, A.;

- Parisi, J.; Lutsen, L.; Vanderzande, D.; Maes, W.; Manca, J. V. *Org. Electron.* **2015**, *21*, 160–170.
- [40] Li, Y.; Vamvounis, G.; Holdcroft, S. *Macromolecules* **2002**, *35*, 6900–6906.
- [41] Zhou, H.; Yang, L.; You, W. *Macromolecules* **2012**, *45*, 607–632.
- [42] Kesters, J.; Govaerts, S.; Pirotte, G.; Drijkoningen, J.; Chevrier, M.; Van den Brande, N.; Liu, X.; Fahlman, M.; Van Mele, B.; Lutsen, L.; Vanderzande, D.; Manca, J.; Clément, S.; Von Hauff, E.; Maes, W. *ACS Appl. Mater. Interfaces* **2016**, *8*, 6309–6314.
- [43] Ghoo, T.; Van den Brande, N.; Defour, M.; Brassinne, J.; Fustin, C.-A.; Gohy, J.-F.; Hoepfener, S.; Schubert, U. S.; Vanormelingen, W.; Lutsen, L.; Vanderzande, D. J.; Van Mele, B.; Maes, W. *Eur. Polym. J.* **2014**, *53*, 206–214.
- [44] Ethirajan, A.; D’Olieslaeger, L.; Vandenberg, J.; Lutsen, L.; D’Olieslaeger, M.; Vanderzande, D.; Junkers, T. *Macromol. Chem. Phys.* **2013**, *214*, 1859–1864.
- [45] Huynh, T.-P.; Sharma, P. S.; Sosnowska, M.; D’Souza, F.; Kutner, W. *Prog. Polym. Sci.* **2015**, *47*, 1–25.

## 3.5 SUPPORTING INFORMATION

### 3.5.1 Reagents and instrumentation

All reagents and chemicals were obtained from commercial sources and used without further purification. Diethyl ether and THF were dried using a solvent purification system (MBraun MB-SPS 800). NMR chemical shifts ( $\delta$ , in ppm) were determined relative to the residual  $^1\text{H}$  signal of  $\text{CHCl}_3$  (7.26 ppm) or the  $^{13}\text{C}\{^1\text{H}\}$  (proton decoupled  $^{13}\text{C}$  NMR spectroscopy) resonance shift of  $\text{CDCl}_3$  (77.16 ppm). High resolution ESI-MS was performed using a LTQ Orbitrap Velos Pro mass spectrometer equipped with an atmospheric pressure ionization source operating in the nebulizer assisted electrospray mode. The instrument was calibrated in the  $m/z$  range 220–2000 using a standard solution containing caffeine, MRFA and Ultramark 1621. Analysis of the molar masses and distributions of the polymer samples was performed on a Tosoh EcoSEC System, comprising of an autosampler, a PSS guard column SDV (50 x 7.5 mm), followed by three PSS SDV analytical linear XL columns (5  $\mu\text{m}$ , 300 x 7.5 mm) and a UV-detector using THF as the eluent at 40 °C with a flow rate of 1.0 mL/min. The SEC system was calibrated using linear narrow polystyrene standards ranging from 474 to  $7.5 \times 10^6$  g/mol ( $K = 14.1 \times 10^{-5}$  dL/g and  $\alpha = 0.70$ ). Preparative size exclusion chromatography (prep-SEC) was performed on a JAI LC-9110 NEXT system equipped with JAIGEL 2H and 3H columns (eluent  $\text{CHCl}_3$ , flow rate 3.5 mL/min). MALDI-TOF mass spectra were recorded on a Bruker Daltonics Ultraflex II ToF/ToF. 1  $\mu\text{L}$  of the matrix solution (4 mg/mL DCTB (*trans*-2-[3-(4-*tert*-butylphenyl)-2-methyl-2-propenyldene] malononitrile) in  $\text{CHCl}_3$ ) was spotted onto an MTP Anchorchip 600/384 MALDI plate. The spot was allowed to dry and 1  $\mu\text{L}$  of the analyte solution (0.5 mg/mL in  $\text{CHCl}_3$ ) was spotted on top of the matrix.

Background corrected UV-Vis absorption spectra were recorded on a Cary 5000 UV-Vis-NIR spectrophotometer from Agilent using a band width of 2 nm, full slit height and a scan speed of 600 nm/min. Fully corrected steady-state emission spectra were recorded on a Fluorolog 3-2-2 Tau from Horiba Jobin Yvon, using a band pass of 2 nm and an increment of 1. Samples were dissolved in chloroform. The absorbance at the excitation wavelength was adjusted between 0.01 and 0.1 AU. Absorption and emission spectra were collected at room temperature without deoxygenation. 9,10-Diphenylanthracene dissolved in cyclohexane was used as the reference (quantum yield = 0.90).<sup>[1]</sup> Calculated quantum yield values were corrected for refractive index variation between solvents. Electrochemical measurements were performed with an Eco Chemie Autolab PGSTAT 30 potentiostat using a three-electrode microcell setup with a platinum wire working electrode, a platinum wire counter electrode, a Ag/AgNO<sub>3</sub> reference electrode (silver wire in 0.01 M AgNO<sub>3</sub> / 0.1 M NBu<sub>4</sub>PF<sub>6</sub> in anhydrous acetonitrile) and (argon degassed) anhydrous acetonitrile containing 0.1 M NBu<sub>4</sub>PF<sub>6</sub> as the electrolyte. The system was calibrated against ferrocene/ferrocenium. Experiments were carried out under a constant flow of argon over the electrolyte surface. The polymer samples were dissolved in CS<sub>2</sub>. The working electrode was dipped into this solution and dried at room temperature in air before the measurement. Cyclic voltammograms were recorded at a scan rate of 100 mV/s. The HOMO-LUMO energy levels of the polymers were estimated using the obtained CV data. For the conversion of V to eV, the onset potentials of the first oxidation/reduction peaks were used and referenced to ferrocene/ferrocenium, which has an ionization potential of -4.98 eV vs. vacuum. This correction factor is based on a value of 0.31 eV for Cp<sub>2</sub>Fe/Cp<sub>2</sub>Fe<sup>+</sup> vs. a saturated calomel electrode (SCE)<sup>[2]</sup> and a value of 4.68 eV for SCE vs. vacuum:<sup>[3]</sup>

## Synthesis of highly fluorescent alternating donor-acceptor copolymers via KCTCP

$$E_{\text{HOMO}} (\text{eV}) = -4.98 - E_{\text{onset, ox}}^{\text{Ag/AgNO}_3} (\text{V}) + E_{\text{onset, Fc/Fc}^+}^{\text{Ag/AgNO}_3} (\text{V})$$

$$E_{\text{LUMO}} (\text{eV}) = -4.98 - E_{\text{onset, red}}^{\text{Ag/AgNO}_3} (\text{V}) + E_{\text{onset, Fc/Fc}^+}^{\text{Ag/AgNO}_3} (\text{V})$$

The accuracy of measuring redox potentials by CV is about 0.01–0.02 V. Reproducibility can be less because the potentials depend on concentration and temperature. Rapid heat–cool calorimetry (RHC) experiments were performed on a prototype RHC of TA Instruments, equipped with liquid nitrogen cooling and specifically designed for operation at high scanning rates. RHC measurements were performed at 500 K/min (after cooling at 20 K/min) using aluminum crucibles filled with samples of 200–250  $\mu\text{g}$ , using helium (10 mL/min) as a purge gas. TGA experiments were performed at 20 K/min in platinum crucibles on a TA Instruments Q5000 TGA using nitrogen (50 mL/min) as purge gas.

### **3.5.2 Monomer synthesis**

2,5-Dibromo-3-hexylthiophene was synthesized according to a literature procedure.<sup>[4,5]</sup>

#### **2-bromo-3-hexylthiophene (1)**<sup>[6]</sup>

A solution of 3-hexylthiophene (7.57 g, 45.0 mmol) in tetrahydrofuran (75 mL) was cooled to 0 °C and protected from light. *N*-bromosuccinimide (8.01 g, 45.0 mmol) was added in portions and the mixture was stirred for 2 h at room temperature and under N<sub>2</sub> atmosphere. The reaction was quenched with H<sub>2</sub>O, extracted with diethyl ether (3x) and washed subsequently with a saturated Na<sub>2</sub>S<sub>2</sub>O<sub>3</sub> solution and H<sub>2</sub>O. The organic layer was then dried with MgSO<sub>4</sub>, filtered and evaporated under reduced pressure. The product was purified by column chromatography (silica gel, petroleum ether), resulting in a colorless oil (7.98 g, 72%). <sup>1</sup>H NMR (300 MHz, CDCl<sub>3</sub>):  $\delta$  = 7.18 (d, *J* = 5.6 Hz, 1H), 6.79 (d, *J* = 5.6

Hz, 1H), 2.60–2.52 (m, 2H), 1.63–1.52 (m, 2H), 1.37–1.25 (m, 6H), 0.89 (t,  $J = 6.7$  Hz, 3H).

### **2-bromo-5-iodopyridine (2)**<sup>[7,8]</sup>

*n*-Butyllithium (9.29 mL, 23.2 mmol; 2.5 M in hexanes) was added dropwise to a solution of 2,5-dibromopyridine (5.00 g, 21.1 mmol) in dry diethyl ether (250 mL) at  $-78$  °C and under Ar atmosphere. After stirring for 30 min at  $-78$  °C, an ice-cooled solution of iodine (5.89 g, 23.2 mmol) in dry diethyl ether (50 mL) was added via cannula. The mixture was then stirred for 2 h, whereby it slowly heated up to  $-40$  °C. The reaction was quenched with a saturated  $\text{Na}_2\text{S}_2\text{O}_3$  solution and extracted with diethyl ether (3x). The resulting organic layer was washed with brine and dried with  $\text{MgSO}_4$ . After filtration and evaporation to dryness, the crude product was purified via column chromatography (silica gel, petroleum ether/ethyl acetate 80/20). The product was finally obtained as a white solid (5.49 g, 92%).  $^1\text{H}$  NMR (400 MHz,  $\text{CDCl}_3$ ):  $\delta = 8.59$  (d,  $J = 2.4$  Hz, 1H), 7.82 (dd,  $J = 8.3$  Hz and 2.4 Hz, 1H), 7.29 (dd,  $J = 8.3$  Hz and 0.5 Hz, 1H).

### **2-bromo-5-(3'-hexylthiophen-2'-yl)pyridine (3)**

*n*-Butyllithium (6.34 mL, 15.8 mmol; 2.5 M in hexanes) was added dropwise to a solution of 2-bromo-3-hexylthiophene (**1**) (3.56 g, 14.4 mmol) in dry tetrahydrofuran (6 mL) at  $-78$  °C and under Ar atmosphere. The mixture was stirred for 1 h at  $-78$  °C, during which zinc chloride (2.36 g, 17.3 mmol) was weighed in a flame-dried three-neck flask, dried under vacuum, brought under Ar atmosphere and dissolved in dry tetrahydrofuran (17 mL). This solution was then added via cannula to the lithiated thiophene at  $-78$  °C and the mixture was allowed to gradually heat up to room temperature over 2 h. Meanwhile, 2-bromo-5-iodopyridine (**2**) (3.68 g, 13.0 mmol) was dissolved in dry tetrahydrofuran (13

## Synthesis of highly fluorescent alternating donor-acceptor copolymers via KCTCP

mL) and purged with N<sub>2</sub>, after which Pd(PPh<sub>3</sub>)<sub>4</sub> (0.266 g, 0.230 mmol, 1.6 mol%) was added in one portion and the mixture was again purged with N<sub>2</sub>. The formed zinc intermediate was then added to this solution via cannula, the mixture was again purged with N<sub>2</sub> and then it was refluxed overnight. The mixture was cooled down to room temperature, quenched with a saturated NaHCO<sub>3</sub> solution and extracted with chloroform (3x). The resulting organic layer was dried with MgSO<sub>4</sub>, filtered and evaporated to dryness. The crude product was finally purified with column chromatography (silica gel, petroleum ether/dichloromethane 50/50), yielding a yellow oil (2.12 g, 50%). <sup>1</sup>H NMR (400 MHz, CDCl<sub>3</sub>): δ = 8.43 (dd, *J* = 2.5 and 0.7 Hz, 1H), 7.58 (dd, *J* = 8.2 and 2.5 Hz, 1H), 7.52 (dd, *J* = 8.2 and 0.7 Hz, 1H), 7.31 (d, *J* = 5.2 Hz, 1H), 7.01 (d, *J* = 5.2 Hz, 1H), 2.65–2.56 (m, 2H), 1.63–1.54 (m, 2H), 1.32–1.22 (m, 6H), 0.86 (t, *J* = 6.9 Hz, 3H); <sup>13</sup>C{<sup>1</sup>H} NMR (75 MHz, CDCl<sub>3</sub>): δ = 150.0 (CH), 140.74 (C), 140.67 (C), 139.1 (CH), 132.2 (C), 130.4 (C), 130.0 (CH), 128.0 (CH), 125.4 (CH), 31.7 (CH<sub>2</sub>), 31.1 (CH<sub>2</sub>), 29.2 (CH<sub>2</sub>), 28.8 (CH<sub>2</sub>), 22.7 (CH<sub>2</sub>), 14.2 (CH<sub>3</sub>); ESI-HRMS: found 324.0389, calcd 324.0422 (MH<sup>+</sup>).

### **2-bromo-5-(3'-hexyl-5'-iodothiophen-2'-yl)pyridine (4)**

2-Bromo-5-(3'-hexylthiophen-2'-yl)pyridine (**3**) (2.12 g, 6.54 mmol) was dissolved in chloroform (70 mL) and acetic acid (35 mL), and the solution was protected from light. Then, *N*-iodosuccinimide (2.48 g, 11.0 mmol) was added portion wise and the mixture was stirred overnight at room temperature and under N<sub>2</sub> atmosphere. The reaction was quenched with a saturated NaHCO<sub>3</sub> solution, extracted with hexanes (3x), washed with a saturated Na<sub>2</sub>S<sub>2</sub>O<sub>3</sub> solution and dried with MgSO<sub>4</sub>. After filtration, the solvent was evaporated under reduced pressure and the crude material was purified by column chromatography (silica gel,

petroleum ether/dichloromethane 50/50). The product was obtained as a yellow oil (2.56 g, 87%).  $^1\text{H}$  NMR (400 MHz,  $\text{CDCl}_3$ ):  $\delta$  = 8.37 (dd,  $J$  = 2.1 and 1.1 Hz, 1H), 7.53–7.51 (m, 2H), 7.15 (s, 1H), 2.59–2.50 (m, 2H), 1.59–1.50 (m, 2H), 1.30–1.21 (m, 6H), 0.86 (t,  $J$  = 6.9 Hz, 3H);  $^{13}\text{C}\{^1\text{H}\}$  NMR (75 MHz,  $\text{CDCl}_3$ ):  $\delta$  = 149.8 (CH), 142.6 (C), 141.3 (C), 139.6 (CH), 138.8 (CH), 138.2 (C), 129.2 (C), 128.0 (CH), 73.4 (C), 31.6 ( $\text{CH}_2$ ), 31.0 ( $\text{CH}_2$ ), 29.1 ( $\text{CH}_2$ ), 28.4 ( $\text{CH}_2$ ), 22.7 ( $\text{CH}_2$ ), 14.2 ( $\text{CH}_3$ ); ESI-HRMS: found 449.9350, calcd 449.9388 ( $\text{MH}^+$ ).

### 3.5.3 Alternating copolymer synthesis

#### Polymerization test 1

2-Bromo-5-(3'-hexyl-5'-iodothiophen-2'-yl)pyridine (**4**) (0.225 g, 0.500 mmol), dried overnight under vacuum using  $\text{P}_2\text{O}_5$  prior to use, was loaded in a three-neck flask and brought under Ar atmosphere, after which dry THF (5 mL) was added via cannula. *i*-PrMgCl.LiCl (0.385 mL, 0.500 mmol; 1.30 M in THF) was added dropwise to this solution at 0 °C to start the Grignard metathesis reaction. After stirring for 1 h at 0 °C, this mixture was cannulated to another three-neck flask containing Ni(dppp) $\text{Cl}_2$  (2.71 mg, 5.00  $\mu\text{mol}$ ) and dry THF (2 mL), at RT and under Ar atmosphere. After the start of the polymerization, aliquots were taken at different time intervals and analyzed by gel permeation chromatography (GPC). The polymerization was stopped after 30 min by adding water (0.5 mL). Then, the polymerization mixture was precipitated in methanol, whereafter the precipitate was filtered over a Soxhlet thimble and subsequently purified by means of Soxhlet extractions with methanol, acetone, hexanes and chloroform (dissolving the polymer), respectively. The solvent was evaporated under reduced pressure, after which the polymer was redissolved in pyridine (2 mL) and again precipitated in methanol. The precipitate was filtered off over a PTFE membrane (47 mm/0.45

µm) and dried overnight under vacuum, affording an orange solid (34.1 mg, 28%). <sup>1</sup>H NMR (400 MHz, CDCl<sub>3</sub>): δ = 8.67 (d, *J* = 1.8 Hz, 1H), 7.79 (dd, *J* = 8.2 and 1.8 Hz, 1H), 7.68 (d, *J* = 8.2 Hz, 1H), 7.53 (s, 1H), 2.79–2.71 (m, 2H), 1.78–1.69 (m, 2H), 1.45–1.32 (m, 6H), 0.94 (t, *J* = 6.7 Hz, 3H); UV-Vis (CHCl<sub>3</sub>): λ<sub>max</sub> = 413 nm, UV-Vis (film): λ<sub>max</sub> = 437 nm; GPC (THF, PS standards): *M*<sub>n</sub> = 2.6 × 10<sup>4</sup> g/mol, *M*<sub>w</sub> = 3.4 × 10<sup>4</sup> g/mol, *D* = 1.28.

### **Polymerization test 9**

Similar to polymerization test 1, but Ni(dppe)Cl<sub>2</sub> (2.64 mg, 5.00 µmol) was used instead of Ni(dppp)Cl<sub>2</sub>. The polymer was obtained as an orange solid (35.0 mg, 29%). GPC (THF, PS standards): *M*<sub>n</sub> = 2.3 × 10<sup>4</sup> g/mol, *M*<sub>w</sub> = 3.0 × 10<sup>4</sup> g/mol, *D* = 1.29.

### **Variable catalyst amounts**

2-Bromo-5-(3'-hexyl-5'-iodothiophen-2'-yl)pyridine (**4**) (90.0 mg, 0.200 mmol), dried overnight under vacuum using P<sub>2</sub>O<sub>5</sub> prior to use, was loaded in a three-neck flask and brought under Ar atmosphere, after which dry THF (2 mL) was added via cannula. *i*-PrMgCl.LiCl (0.154 mL, 0.200 mmol, 1.30 M in THF) was added dropwise to this solution at 0 °C to start the Grignard metathesis reaction. After stirring for 1 h at 0 °C, this mixture was cannulated to another three-neck flask containing each time a different amount of Ni(dppp)Cl<sub>2</sub> (1 mol%: 1.08 mg, 2.00 µmol; 2.5 mol%: 2.71 mg, 5.00 µmol; 5 mol%: 5.42 mg, 10.0 µmol; 10 mol%: 10.8 mg, 20.0 µmol) and dry THF (2 mL), at RT and under Ar atmosphere. The polymerization mixture was stirred for 30 min at RT, whereafter it was quenched with 0.5 mL of water and precipitated in methanol. The precipitate was filtered over a Soxhlet thimble and subsequently purified by means of Soxhlet extractions with methanol, acetone, hexanes and chloroform (dissolving the polymer),

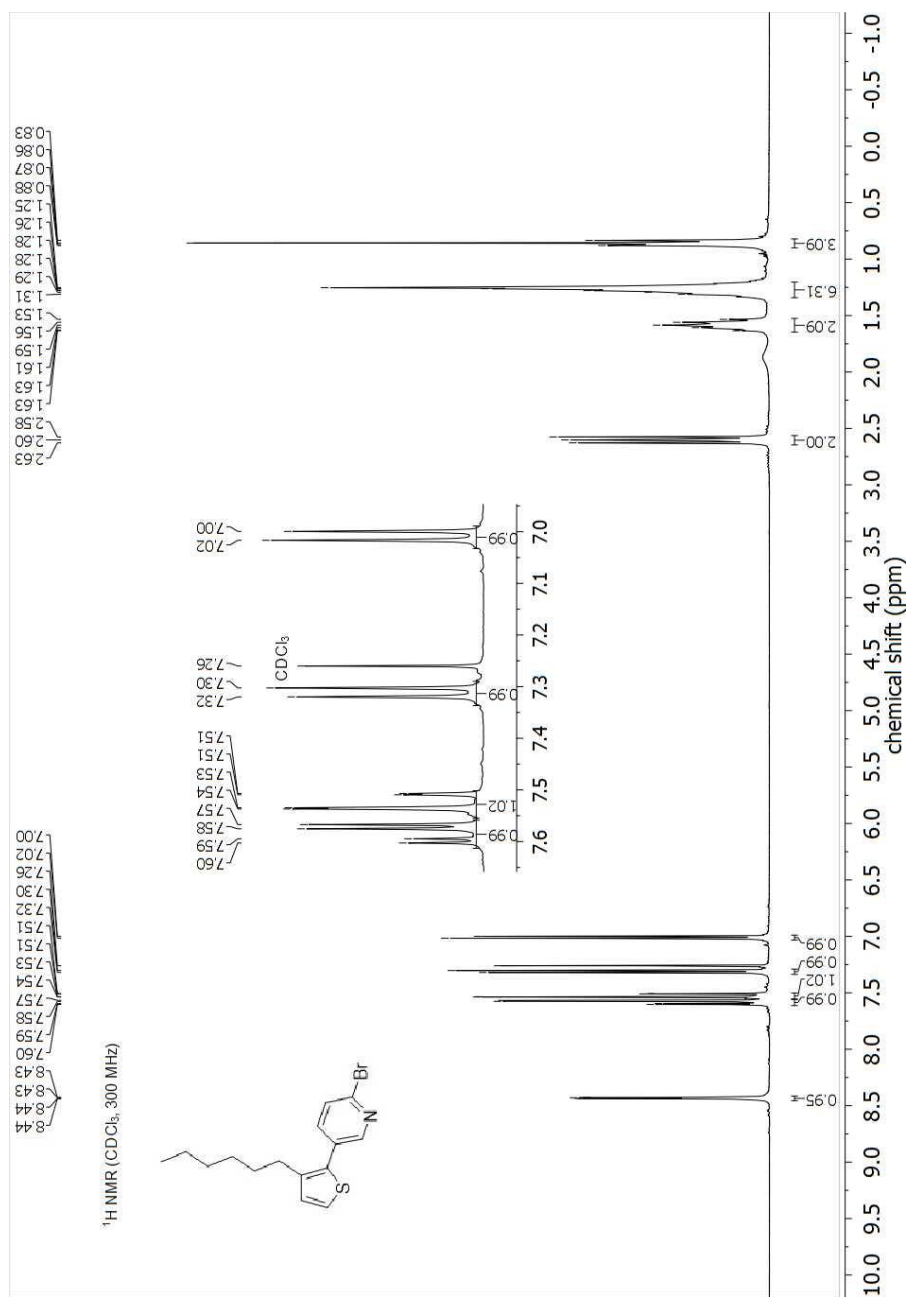
respectively. The solvent was evaporated under reduced pressure, after which the polymer was characterized by GPC.

#### 3.5.4 Block copolymer synthesis

2,5-Dibromo-3-hexylthiophene (0.326 g, 1.00 mmol) was loaded in a three-neck flask and brought under Ar atmosphere. Then, dry THF (10 mL) was added via cannula, after which the solution was cooled down to 0 °C. *i*-PrMgCl.LiCl (0.769 mL, 1.00 mmol; 1.30 M in THF) was added dropwise to this solution to start the first Grignard metathesis reaction (GRIM 1). Meanwhile, 2-bromo-5-(3'-hexyl-5'-iodothiophen-2'-yl)pyridine (**4**) (0.135 g, 0.300 mmol), dried overnight under vacuum using P<sub>2</sub>O<sub>5</sub> prior to use, was also loaded in a three-neck flask, brought under Ar atmosphere and dissolved in dry THF (3 mL). 15 Min after the start of GRIM 1, *i*-PrMgCl.LiCl (0.231 mL, 0.300 mmol; 1.30 M in THF) was added dropwise to this solution at 0 °C to start the second Grignard metathesis reaction (GRIM 2). Both GRIM reactions were stirred for 1 h at 0 °C. After GRIM 1, the thiophene mixture was cannulated to another three-neck flask containing Ni(dppp)Cl<sub>2</sub> (3.52 mg, 6.50 μmol) and dry THF (3 mL), at RT and under Ar atmosphere. This polymerization mixture was then stirred for 15 min at RT, whereafter half of it (6.5 mL) was quenched with a MeOH/HCl mixture (1 mL, 1 M), while to the other half of the mixture the thiophene-pyridine mixture of GRIM 2 was added at RT. The block copolymerization was stopped after 30 min by quenching with 1 mL of water. Both the **P3HT** homopolymer and the **P3HT-*b*-P(3HT-*alt*-P)** copolymer were precipitated in methanol and filtered over a Soxhlet thimble. Both materials were subsequently purified by means of Soxhlet extractions with methanol, acetone, hexanes and chloroform (dissolving the polymer), respectively. The solvent was evaporated under reduced pressure, after which the polymers were

Synthesis of highly fluorescent alternating donor-acceptor copolymers via KCTCP

redissolved in chloroform (2 mL) and again precipitated in methanol. The precipitates were filtered off over a PTFE membrane (47 mm/0.45  $\mu\text{m}$ ) and dried overnight under vacuum, affording 24.5 mg of **P3HT** and 63.3 mg of the **P3HT-*b*-P(3HT-*alt*-P)** copolymer (41%).  $^1\text{H}$  NMR (400 MHz,  $\text{CDCl}_3$ ):  $\delta$  = 8.67 (br, 0.6H), 7.79 (d,  $J$  = 8.2 Hz, 0.6H), 7.68 (d,  $J$  = 8.2 Hz, 0.6H), 7.53 (s, 0.6H), 6.92 (s, 1.4H), 2.91–2.63 (m, 4H), 1.79–1.63 (m, 4H), 1.50–1.33 (m, 12H), 0.99–0.90 (m, 6H); UV-Vis ( $\text{CHCl}_3$ ):  $\lambda_{\text{max}}$  = 424 nm, UV-Vis (film):  $\lambda_{\text{max}}$  = 447 nm; GPC (THF, PS standards):  $M_n$  =  $4.1 \times 10^4$  g/mol,  $M_w$  =  $5.6 \times 10^4$  g/mol,  $D$  = 1.37.

3.5.5  $^1\text{H}$  NMR spectra**Figure S1:**  $^1\text{H}$  NMR spectrum of 2-bromo-5-(3'-hexylthiophen-2'-yl)pyridine (**3**).

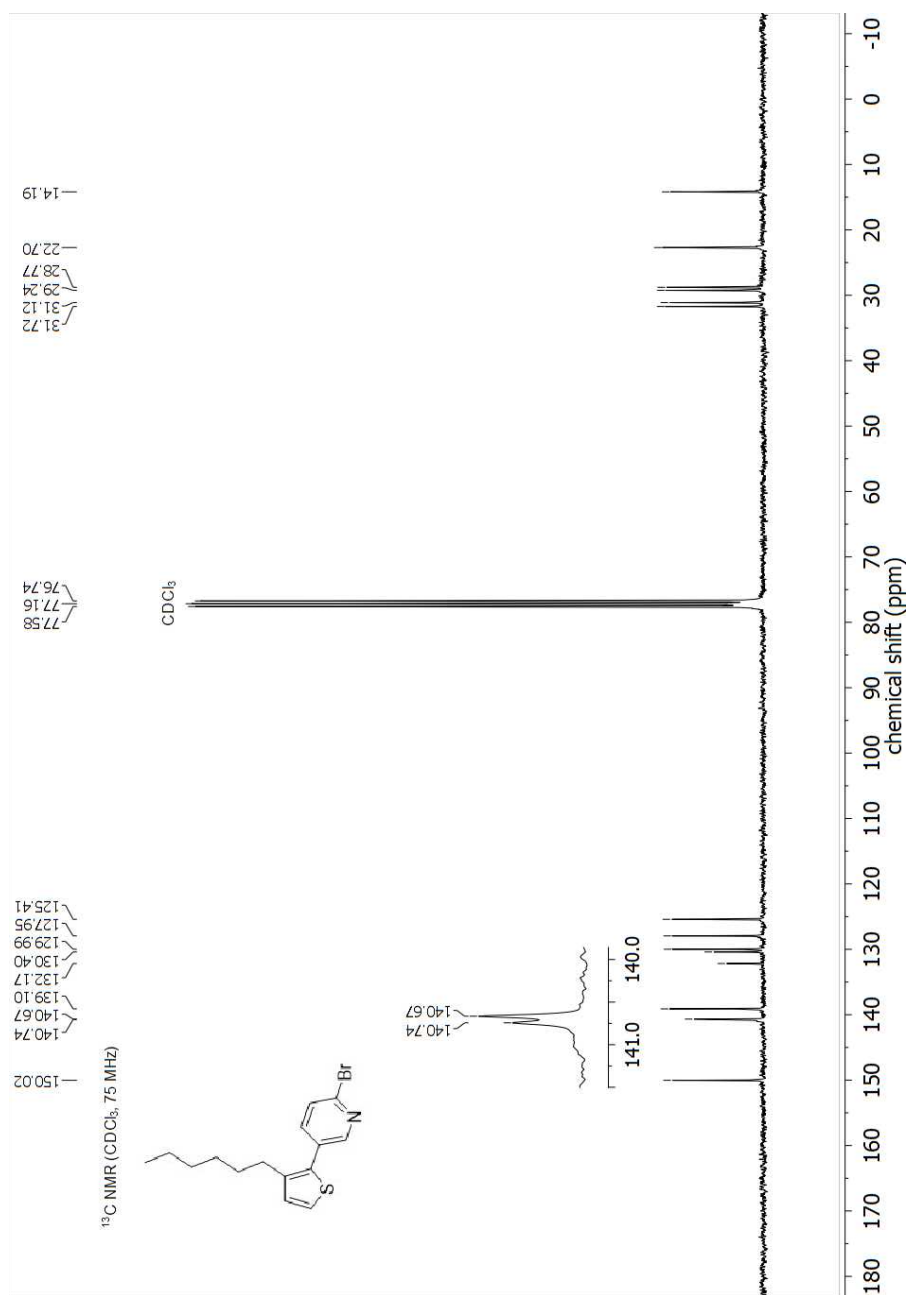


**Figure S2:** <sup>13</sup>C NMR spectrum of 2-bromo-5-(3'-hexylthiophen-2'-yl)pyridine (**3**).

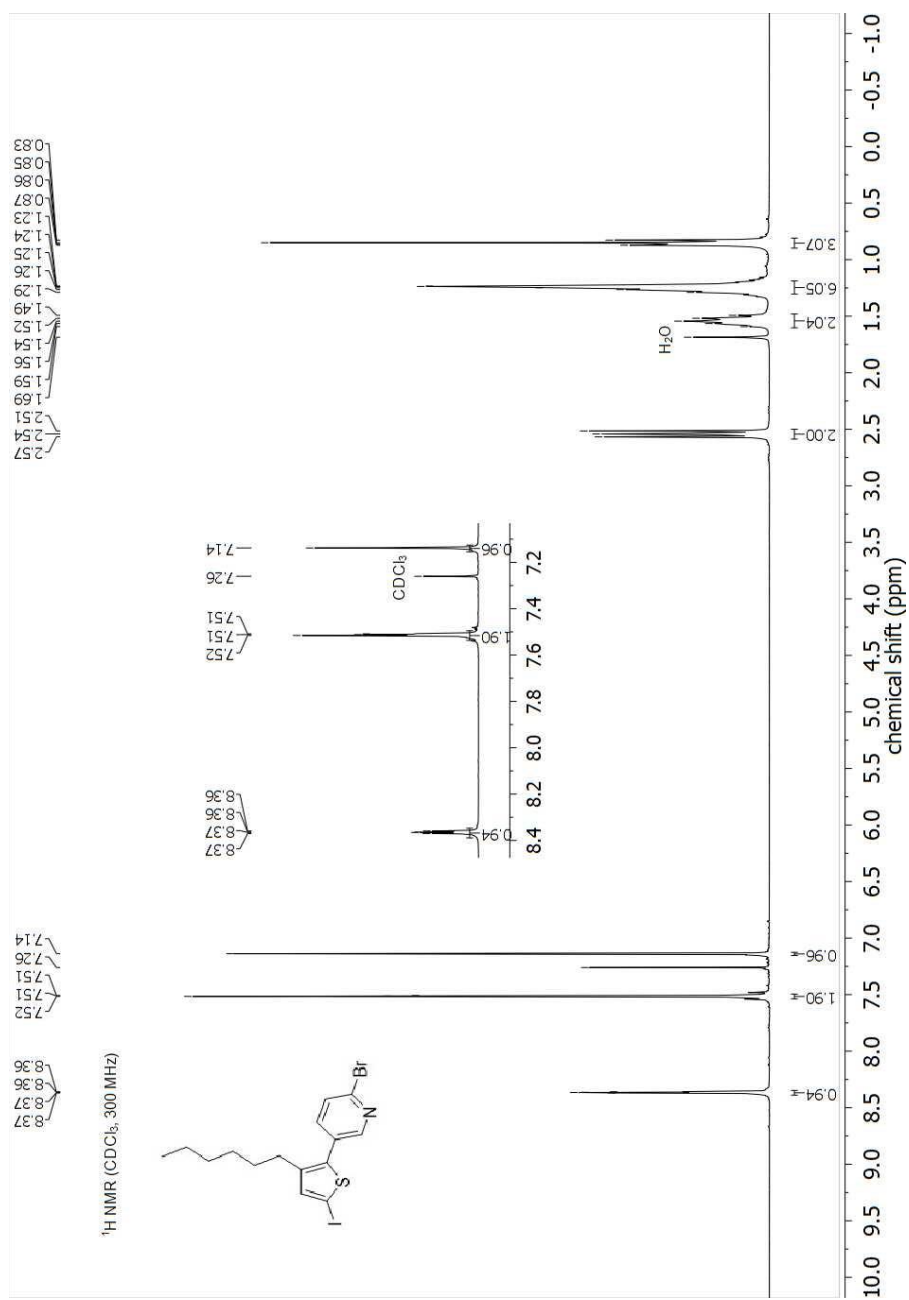


**Figure S3:** <sup>1</sup>H NMR spectrum of 2-bromo-5-(3'-hexyl-5'-iodothiophen-2'-yl)pyridine (**4**).

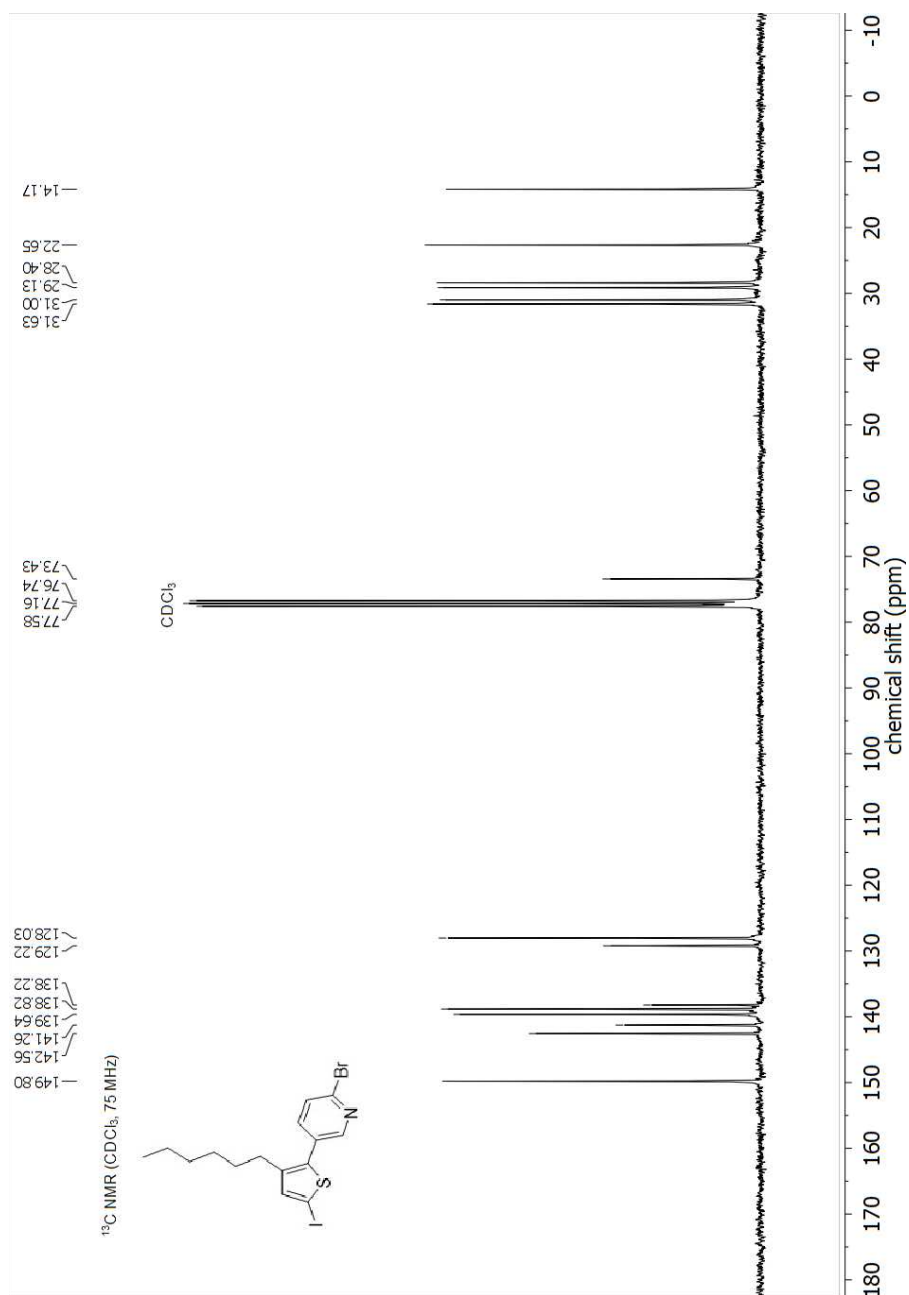


**Figure S4:** <sup>13</sup>C NMR spectrum of 2-bromo-5-(3'-hexyl-5'-iodothiophen-2'-yl)pyridine (**4**).

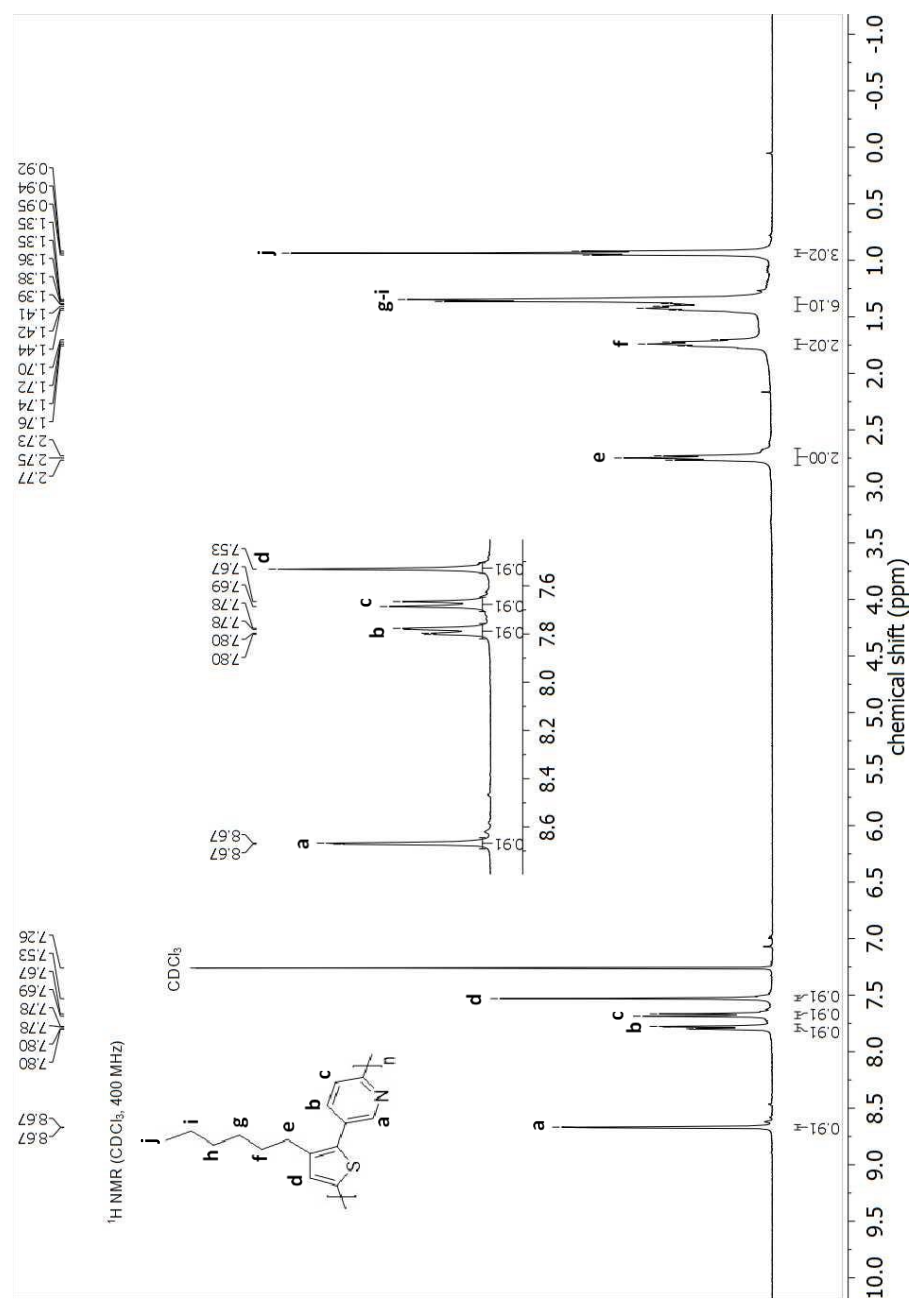


**Figure S5:** <sup>1</sup>H NMR spectrum of poly[(3-hexylthiophene-5,2-diyl)-alt-(pyridine-5,2-diyl)] (P(3HT-alt-P)).

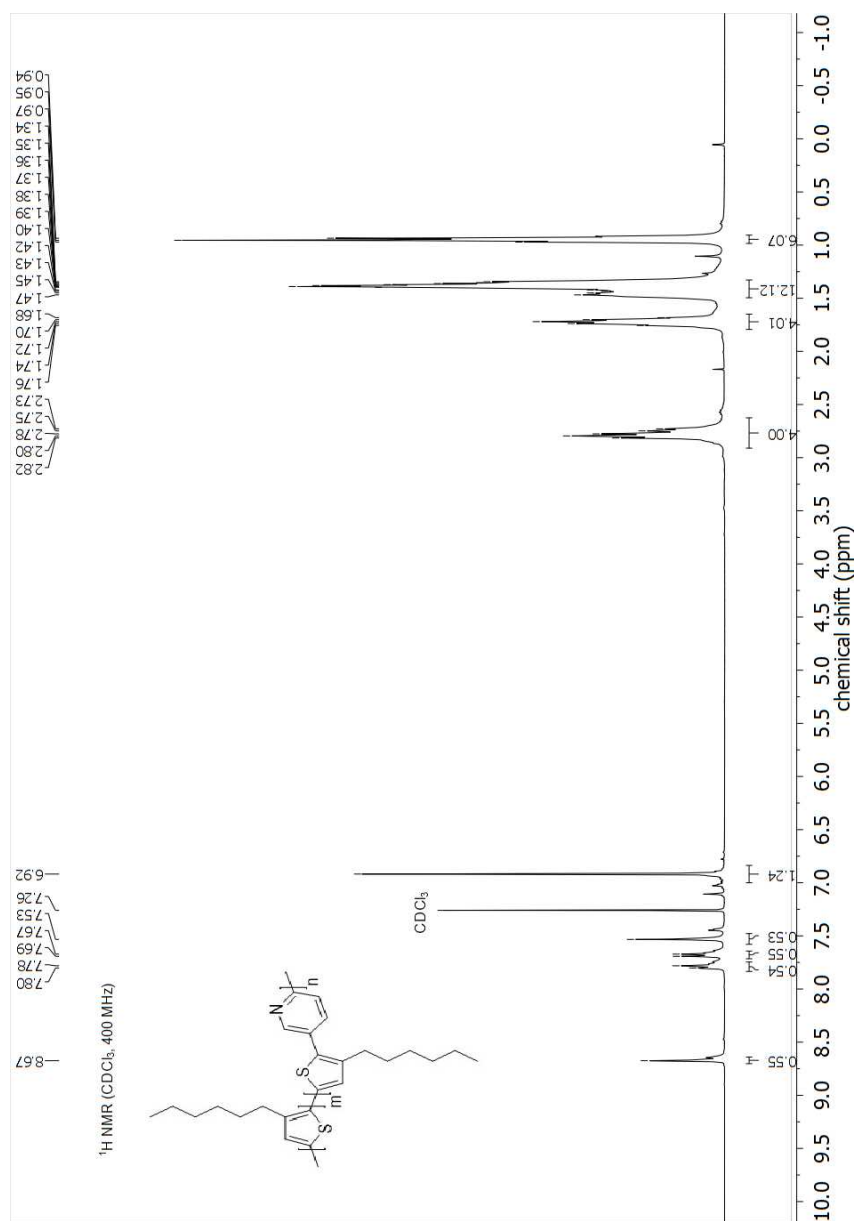


**Figure S6:** <sup>1</sup>H NMR spectrum of poly{[3-hexylthiophene-5,2-diy]-(3-hexylthiophene-5,2-diy)-alt-(pyridine-5,2-diy)} (P3HT-b-P(3HT-alt-P)).

### 3.5.6 Polymerization plots

#### Polymerization test 1

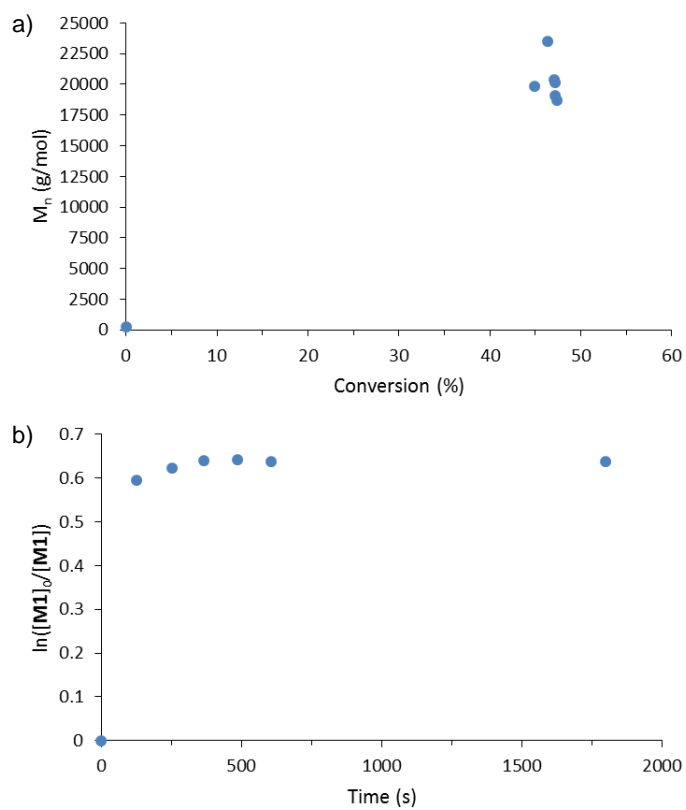


**Figure S7:** a) Relation between  $M_n$  and conversion; b) Relation between  $\ln([M1]_0/[M1])$  and time. The polymerization test was run with 1 mol% of  $Ni(dppp)Cl_2$  at RT and  $[M1] = 0.075$  M.

**Polymerization test 9**

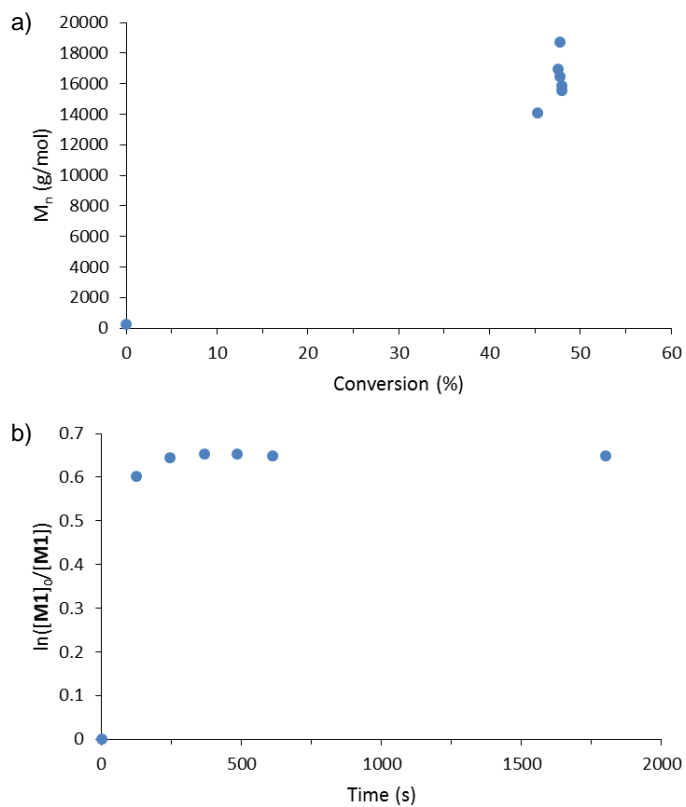


**Figure S8:** a) Relation between  $M_n$  and conversion; b) Relation between  $\ln([M1]_0/[M1])$  and time. The polymerization test was run with 1 mol% of Ni(dppe)Cl<sub>2</sub> at RT and  $[M1] = 0.075$  M.

## 3.5.7 MALDI-TOF measurements

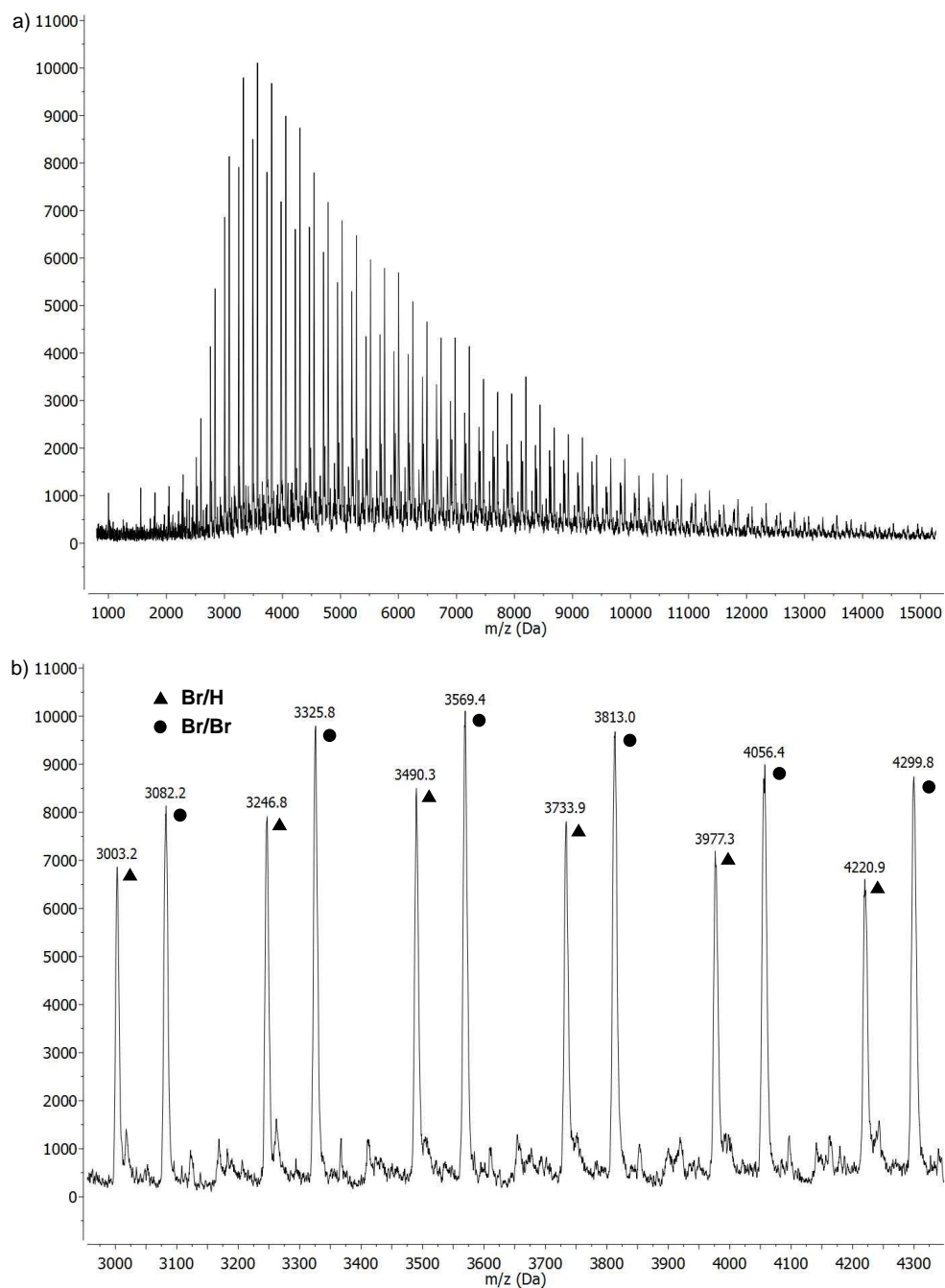


**Figure S9:** a) MALDI-TOF MS spectrum of **P(3HT-*alt*-P)**; b) Enlarged region ( $m/z$  3000–4300) of the MALDI-TOF MS spectrum of **P(3HT-*alt*-P)**.

### 3.5.8 Study of the block copolymer purity

#### GPC

Preparative size exclusion chromatography was performed to cut off the low-molar mass tail of the block copolymer (to evaluate the possible presence of non-chain-extended **P3HT**). The prep-SEC profile is shown in Figure S10. Two fractions (**F1** and **F2**) were collected and evaporated to dryness. The weight percentage of **F2** equals to 19%.

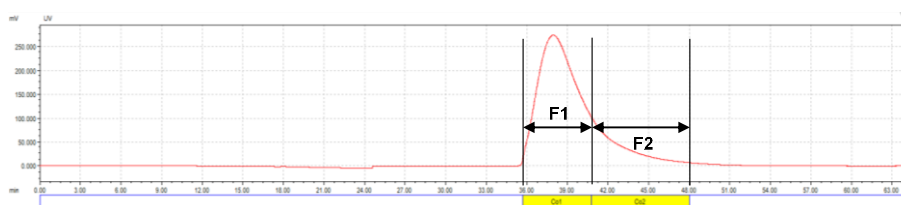


**Figure S10:** Prep-SEC profile of the **P3HT-*b*-P(3HT-*alt*-P)** copolymer. The tail was cut off at 40.75 min.

Both fractions were then analyzed by analytical GPC and  $^1\text{H}$  NMR spectroscopy. From the GPC profiles (Figure S11), it is clear that fraction **F1** (green curve) no longer contains any of the low molar mass polymer species. This fraction can thus be considered as the pure block copolymer.

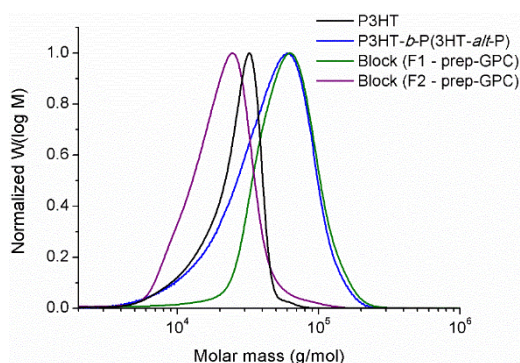


**Figure S11:** GPC profiles of the **P3HT** homopolymer, the **P3HT-*b*-P(3HT-*alt*-P)** copolymer and the two fractions (**F1** and **F2**) after prep-SEC purification of the block copolymer.

**<sup>1</sup>H NMR**

By comparing the aromatic regions of the <sup>1</sup>H NMR spectra of both fractions (Figure S12), the amount of **P3HT** in the low-molar mass fraction **F2** was determined to be less than 20%. This finding, together with the weight percentage of 19% for **F2**, results in the conclusion that only 3-4% of **P3HT** is present in the block copolymer after the synthesis and standard purification procedure.

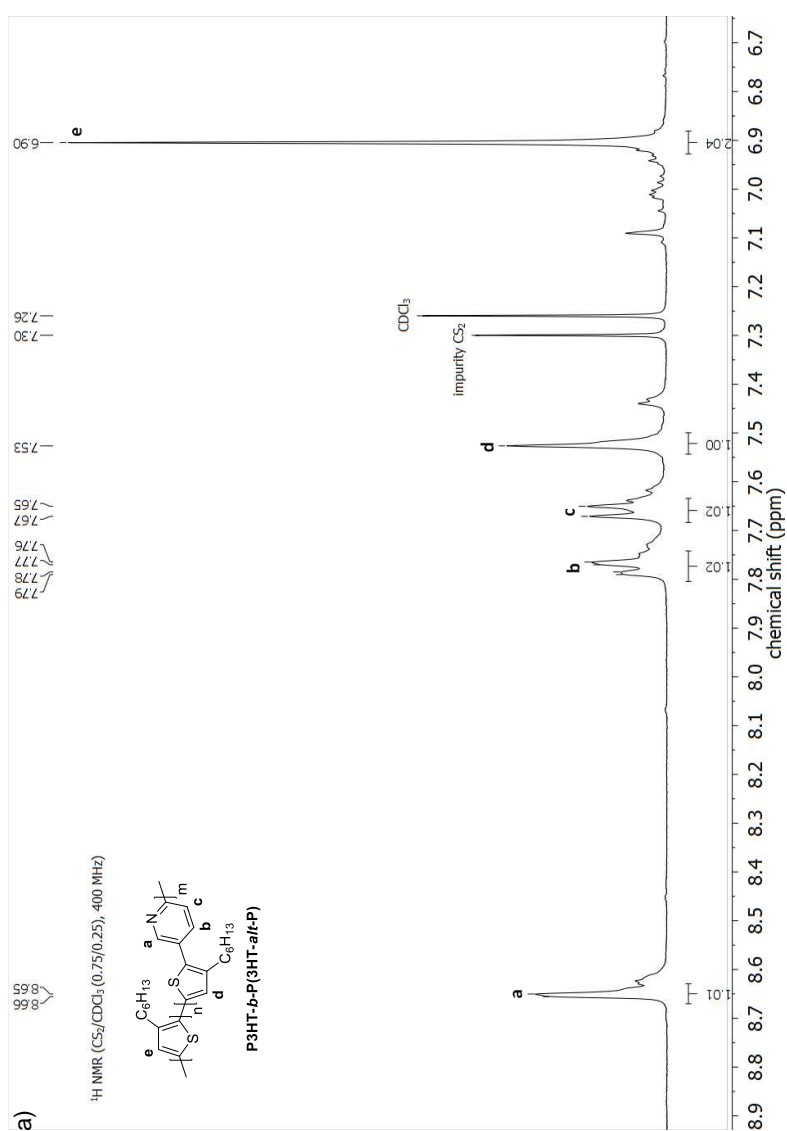


**Figure S12:** Aromatic regions of the <sup>1</sup>H NMR spectra of a) **F1** and b) **F2**.

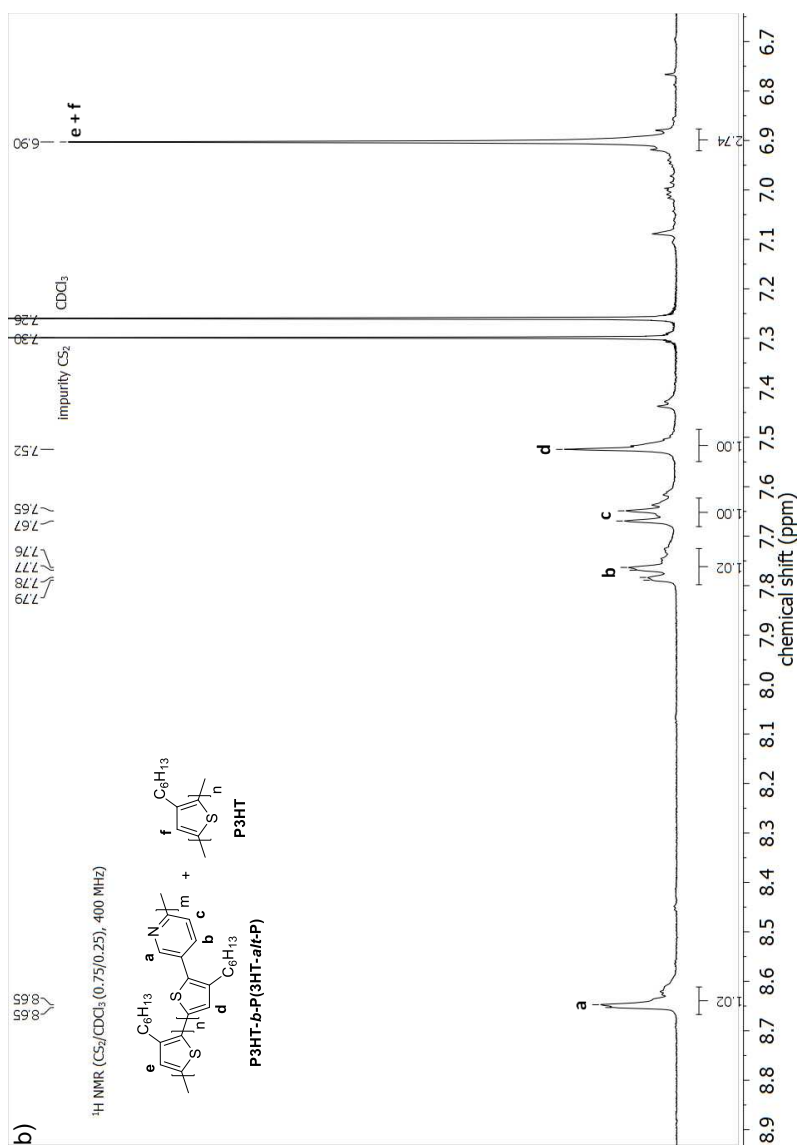


**Figure S12:** Aromatic regions of the  $^1\text{H NMR}$  spectra of a) **F1** and b) **F2**.

### 3.5.9 Thermal analysis

#### RHC

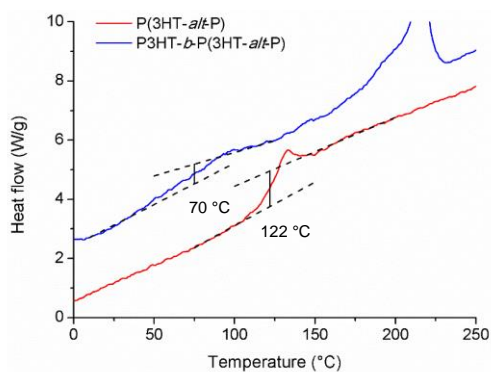


**Figure S13:** Determination of the glass transition temperatures from the RHC (2<sup>nd</sup>) heating profiles of **P(3HT-*alt*-P)** and **P3HT-*b*-P(3HT-*alt*-P)** (curves shifted vertically for clarity).

#### TGA

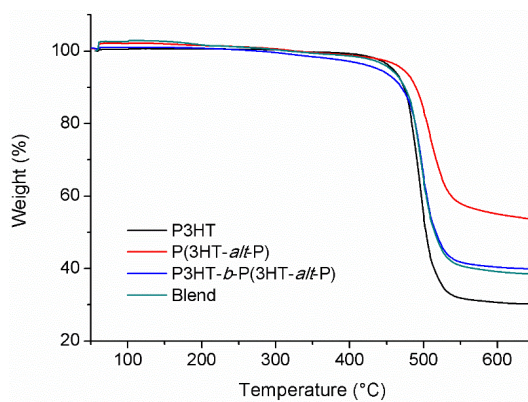


**Figure S14:** TGA profiles of **P3HT**, **P(3HT-*alt*-P)**, **P3HT-*b*-P(3HT-*alt*-P)** and the physical blend of **P3HT** and **P(3HT-*alt*-P)** (60/40).

### 3.5.10 Polymer fluorescence



**Figure S15:** Fluorescence of **P(3HT-*alt*-P)** (left), **P3HT-*b*-P(3HT-*alt*-P)** (middle) and **P3HT** (right) in chloroform solution under a UV lamp at 365 nm.

### 3.5.11 Paper chromatography

Solutions of **P3HT**, **P(3HT-*alt*-P)**, **P3HT-*b*-P(3HT-*alt*-P)** and the blend of **P3HT** and **P(3HT-*alt*-P)** (60/40) were spotted on chromatography paper (Figure S13a). If all materials are spotted onto the same line and chloroform is used as the eluent, the chromatogram as shown in Figure S13b is obtained. In both cases, a clear distinction can be made between the block copolymer and the blend, whereby the blend is just a superposition of the two polymer constituents.

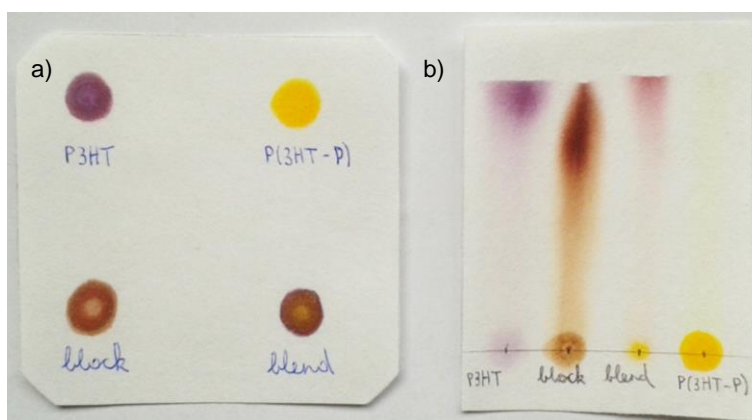


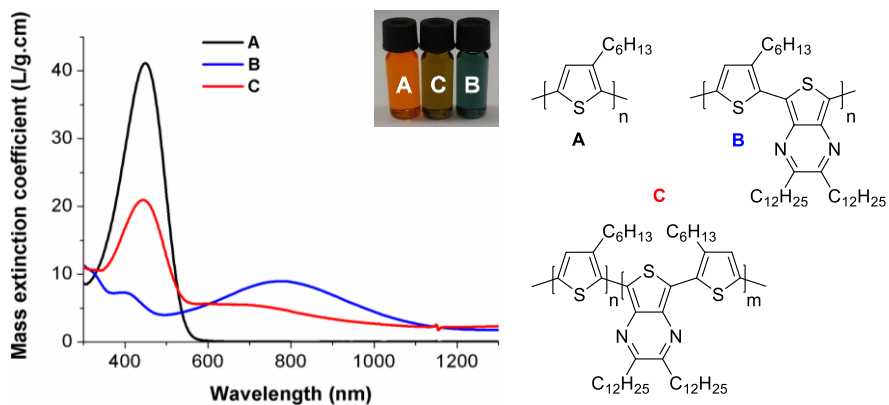
**Figure S16:** a) Spots of the different polymer materials on chromatography paper; b) Paper chromatogram of the different polymer materials (eluent =  $\text{CHCl}_3$ ).

### 3.5.12 References

- [1] Hamai, S.; Hirayama, F. *J. Phys. Chem.* **1983**, *87*, 83–89.
- [2] Bard, A. J.; Faulkner, L. R. *Electrochemical Methods: Fundamentals and Applications, 2nd Edition*; Wiley, 2001.
- [3] Trasatti, S. *Pure Appl. Chem.* **1986**, *58*, 955–966.
- [4] Pal, B.; Yen, W.-C.; Yang, J.-S.; Su, W.-F. *Macromolecules* **2007**, *40*, 8189–8194.
- [5] Yang, Y.-L.; Lee, Y.-H.; Lee, Y.-P.; Chiang, C.-J.; Shen, C.; Wu, C.-C.; Ohta, Y.; Yokozawa, T.; Dai, C.-A. *Polym. Int.* **2014**, *63*, 2068–2075.
- [6] Yokoyama, A.; Miyakoshi, R.; Yokozawa, T. *Macromolecules* **2004**, *37*, 1169–1171.
- [7] Wang, X.; Rabbat, P.; O’Shea, P.; Tillyer, R.; Grabowski, E. J. J.; Reider, P. J. *Tetrahedron Lett.* **2000**, *41*, 4335–4338.
- [8] Engtrakul, C.; Sita, L. R. *Nano Lett.* **2001**, *1*, 541–549.

# Chapter 4

## Synthesis of all-conjugated alternating thiophene-thieno[3,4-*b*]pyrazine (block) copolymers via Kumada catalyst-transfer condensation polymerization



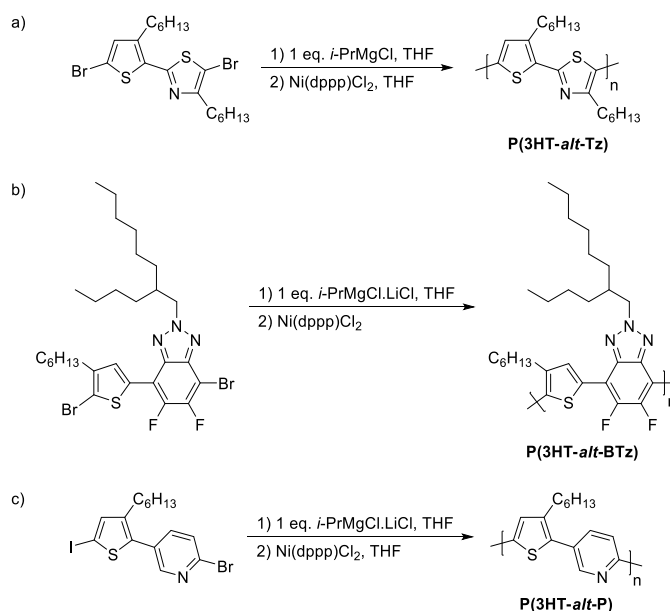
## **ABSTRACT**

Since alternating donor-acceptor conjugated polymers with a controllable molar mass and dispersity can be advantageous for application in organic electronics, the Kumada catalyst-transfer condensation polymerization of such alternating copolymers is further investigated in this work. This is done by first synthesizing a push-pull monomer combining a strong thienopyrazine acceptor unit with a regular thiophene donor unit, enabling absorption over a broad wavelength range. Then, this monomer is polymerized via Kumada catalyst-transfer condensation polymerization with Ni(dppp)Cl<sub>2</sub>, resulting in the alternating donor-acceptor copolymer in a non-controlled chain-growth manner. Furthermore, an all-conjugated block copolymer, consisting of poly(3-hexylthiophene) as the first block and the alternating copolymer as the second block, is synthesized as well in a one-pot procedure. The obtained polymers are carefully characterized and the block copolymer formation is confirmed.

## 4.1 INTRODUCTION

Low bandgap alternating donor-acceptor (D-A) copolymers are nowadays preferred as the donor material in the photoactive layer of bulk heterojunction (BHJ) organic solar cells due to their extended absorption profiles, allowing a better overlap with the solar spectrum.<sup>[1,2]</sup> These D-A or push-pull copolymers are generally synthesized via Stille or Suzuki cross-coupling polymerizations, which follow a step-growth mechanism.<sup>[3-5]</sup> This implies that high molar mass polymers can only be obtained at high conversions, resulting in a rather poor control over the polymer molar mass, dispersity and end groups. Since it has already been established that the molar mass and dispersity can have a strong influence on the efficiencies of BHJ polymer solar cells,<sup>[6-10]</sup> it would be very interesting if these parameters could be more carefully controlled. A well-established polymerization method that allows precise control over the above-mentioned polymer characteristics is the nickel-catalyzed Kumada catalyst-transfer condensation polymerization (KCTCP), which was proven to follow a controlled chain-growth mechanism for the synthesis of poly(3-hexylthiophene) (P3HT).<sup>[11,12]</sup> After this discovery, a lot of research has been performed on this polymerization method.<sup>[13-15]</sup> Until recently, there were, however, only two examples known wherein an alternating donor-acceptor copolymer could be synthesized via KCTCP.<sup>[16,17]</sup> In both cases the same strategy was used, i.e. the KCTCP of a monomer that already comprises both the donor and the acceptor building blocks (Scheme 1a and 1b). This resulted in the desired alternating D-A copolymers, but it was only proven for the **P(3HT-*alt*-BTz)** copolymer that the KCTCP indeed followed a controlled chain-growth mechanism.<sup>[17]</sup> To further explore this promising route, we started with the synthesis of a push-pull monomer consisting of a thiophene (D) and a

pyridine (A) unit. As described in previous work, this monomer could be polymerized via KCTCP in a non-controlled chain-growth manner, leading to the desired alternating D-A copolymer with a number-average molar mass ( $M_n$ ) of  $\sim 20.0$  kg/mol (Scheme 1c).<sup>[18]</sup> Although no complete control over the polymerization was obtained, it remains interesting to investigate whether this approach can be extended to a monomer system with a stronger acceptor unit, affording a red-shifted absorption. Since poly(thienopyrazines) have already been synthesized via KCTCP and they show an absorption profile extending into the near-infrared (NIR) region,<sup>[19]</sup> this building block was chosen as the acceptor unit. As such, the synthesis of a push-pull monomer comprising a thiophene (D) and a thieno[3,4-*b*]pyrazine (A) unit was pursued. The alternating and block copolymer synthesis of this monomer via KCTCP as well as their characterization will be discussed.



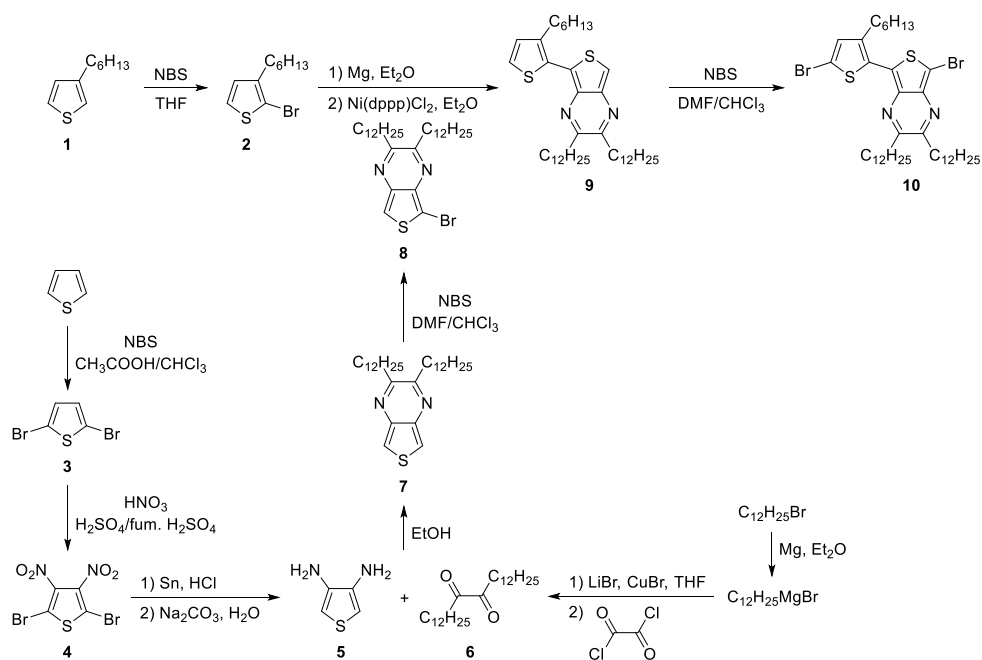
**Scheme 1:** Synthesis of alternating D-A copolymers via KCTCP.<sup>[16-18]</sup>

## 4.2 RESULTS AND DISCUSSION

### 4.2.1 Monomer synthesis

First of all, the push-pull precursor monomer consisting of a thiophene and a thieno[3,4-*b*]pyrazine unit, equipped with two dodecyl side chains for solubility reasons,<sup>[19]</sup> was prepared (Scheme 2). This was done by synthesizing both building blocks separately and then coupling them. For the synthesis of the thiophene unit, a Kumada coupling between 3-bromothiophene and hexylmagnesium bromide was performed, yielding 3-hexylthiophene (**1**). This compound was then monobrominated by adding 1 equivalent (eq.) of NBS, resulting in 2-bromo-3-hexylthiophene (**2**) as the donor part. For the synthesis of the thieno[3,4-*b*]pyrazine unit, a literature procedure was followed.<sup>[20]</sup> This protocol starts from a non-substituted thiophene ring, which is first dibrominated, thereby obtaining 2,5-dibromothiophene (**3**). This compound was then nitrated at the 3- and 4-position (**4**) according to another literature procedure,<sup>[21]</sup> avoiding the use of fuming nitric acid and affording a higher yield. Subsequently, these nitro groups were reduced to amines, resulting in 3,4-diaminothiophene (**5**). To create the desired thieno[3,4-*b*]pyrazine, the  $\alpha$ -dione **6** still had to be prepared. This was done by first preparing the Gilman reagent of dodecylbromide *in situ* and then adding oxalyl chloride. Afterwards, a condensation reaction between compounds **5** and **6** was performed and 2,3-didodecylthieno[3,4-*b*]pyrazine (**7**) was obtained. This compound was then monobrominated, finally yielding 5-bromo-2,3-didodecylthieno[3,4-*b*]pyrazine (**8**) as the acceptor part. As both the donor (**2**) and acceptor (**8**) units were now obtained, they still had to be coupled to each other. A Kumada coupling was performed to obtain compound **9**, whereafter this was dibrominated to end up with 5-bromo-7-(5-bromo-3-

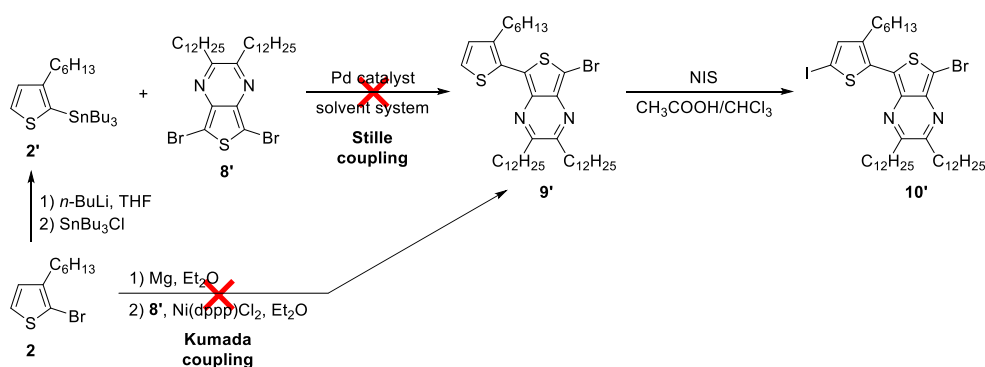
hexylthiophen-2-yl)-2,3-didodecylthieno[3,4-*b*]pyrazine (**10**) as the push-pull precursor monomer. During the purification and storage of precursor monomer **10**, it was observed that this compound readily degrades, explaining the solvent removal under reduced pressure without heating (Supporting Information). A better way to ensure that most of the precursor monomer is still intact, is to perform the last dibromination step just before the polymerization reaction, since compound **9** is clearly more stable.



**Scheme 2:** Synthesis of precursor monomer **10**.

Prior to the development of the above synthesis route (Scheme 2), some other protocols were attempted as well. In an initial effort, we tried to end up with a precursor monomer with an iodine on the thiophene part and a bromide on the thienopyrazine building block (similar to the precursor monomer of **P(3HT-*alt*-P)** in Scheme 1c) to guarantee a selective GRIM reaction. Hence, the dibrominated thieno[3,4-*b*]pyrazine (**8'**) was synthesized by adding 2 eq. of NBS to compound

**7**, which would lead to the monobrominated species (**9'**) after the coupling reaction (Scheme 3). Since the Stille coupling gave good yields for the synthesis of dicoupled thiophene-thienopyrazine-thiophene (T-TP-T) products,<sup>[22]</sup> these reaction conditions were explored first. To this extent, the stannylated thiophene (**2'**) had to be synthesized first. Afterwards, a Pd catalyst was added to equimolar amounts of **2'** and **8'** to obtain the desired monocoupled T-TP compound **9'**. Different Pd catalysts, solvent systems and temperatures were tested, but in none of the cases the desired product was formed and only a small amount of the dicoupled T-TP-T was retrieved. Aiming to obtain more control over the coupling reaction, the Kumada coupling was explored next. In this case, equimolar amounts of **2** and **8'** were used. After reaction work-up and purification, again only the dicoupled T-TP-T was obtained, but in decent amounts this time. From these findings, it was concluded that the coupling reaction of the dibrominated thieno[3,4-*b*]pyrazine (**8'**) with the corresponding thiophene unit only afforded the dicoupled T-TP-T product. Furthermore, it was also established that the Kumada coupling gave much better results. This clarifies the choice for the monobrominated thieno[3,4-*b*]pyrazine (**8**) for the final Kumada coupling in Scheme 2.



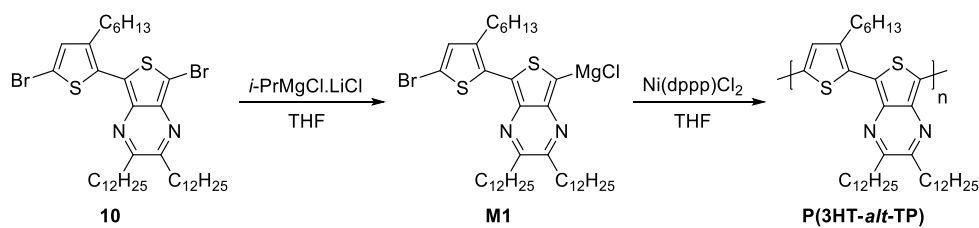
**Scheme 3:** Attempted synthesis of precursor monomer **10'**.

Prior to the polymerization, the obtained precursor monomer **10** still had to be activated by performing a GRIM reaction. This was done by reacting compound **10** with 1.0 eq. of *i*-PrMgCl.LiCl in dry THF (concentration of 0.1 M) at 0 °C for 1 hour. To analyze what happened during this GRIM reaction, a small amount of the resulting reaction mixture was quenched in water and analyzed by <sup>1</sup>H NMR spectroscopy. From this study, it could be concluded that the bromide end group at the thienopyrazine side was replaced by a magnesium chloride group, which is in agreement with the observations of Todd *et al.* that the end group at the acceptor side is replaced by a magnesium chloride group.<sup>[17]</sup> This means that during the GRIM reaction precursor monomer **10** is converted into active monomer **M1** according to Scheme 4.

#### 4.2.2 Polymer synthesis and characterization

Since both poly(thiophenes) and poly(thienopyrazines) have already been synthesized via KCTCP,<sup>[11,12,19]</sup> we decided to also use KCTCP for the synthesis of the alternating donor-acceptor copolymer. This was done by first creating the active monomer **M1** *in situ* via a GRIM reaction (0 °C, 1 h and [**M1**] = 0.1 M), whereafter it was added to the Ni(dppp)Cl<sub>2</sub> catalyst in dry THF ([**M1**] = 0.05 M) at room temperature (RT). The polymerization mixture was stirred overnight at RT and then quenched with a THF/HCl mixture, resulting in the targeted alternating copolymer poly[(3-hexylthiophene-5,2-diyl)-*alt*-(2,3-didodecylthieno[3,4-*b*]pyrazine-5,7-diyl)] **P(3HT-*alt*-TP)** (Scheme 4). The polymer was purified by repetitive Soxhlet extractions with MeOH, acetone, hexanes and chloroform, respectively. The resulting polymer had a *M<sub>n</sub>* of 6.9 kg/mol and a dispersity (*Đ*) of 1.29. This would mean that only ~11 monomer units (637 g/mol per monomer unit) have coupled to each other, which is a lot

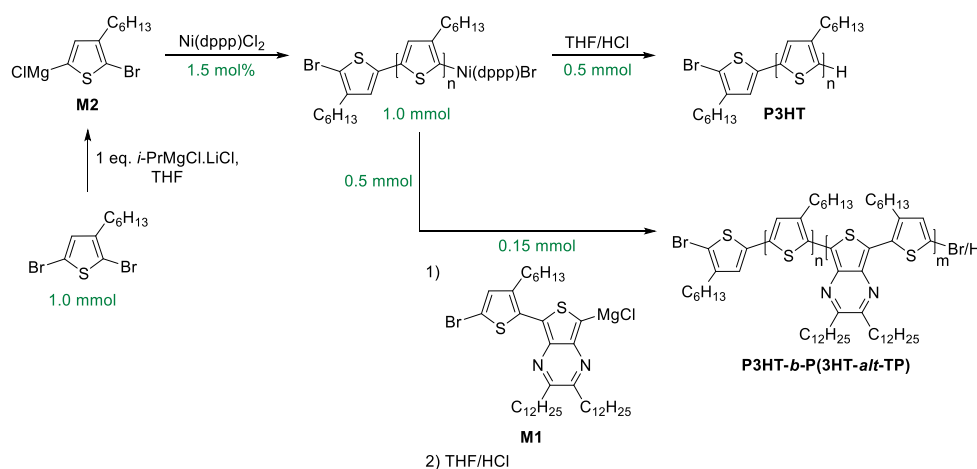
lower than the ~50 monomer units ( $M_n$  of ~30 kg/mol) aimed for by using 2.0 mol% of the Ni catalyst. This obviously does not take into account the error on the  $M_n$  derived from GPC (gel permeation chromatography) analysis. The obtained molar mass of the alternating copolymer is anyway lower than expected in case of a controlled chain-growth polymerization, which suggests that the polymerization does not proceed in a controlled way. This is most probably caused by dissociation of the Ni catalyst from the polymer chains, which proved to be the dominant termination reaction in the KCTCP of poly(thienopyrazines) and the alternating thiophene-pyridine copolymer **P(3HT-*alt*-P)**.<sup>[18,19]</sup>



**Scheme 4:** Synthesis of the **P(3HT-*alt*-TP)** copolymer via KCTCP.

To further investigate the chain-growth character of the KCTCP of **P(3HT-*alt*-TP)**, a block copolymerization starting from a **P3HT** macro-initiator was pursued (Scheme 5). First of all, the **P3HT** block was synthesized *in situ* via KCTCP. This was done by first activating the 2,5-dibromo-3-hexylthiophene precursor monomer with 1 eq. of *i*-PrMgCl.LiCl at 0 °C for 1 hour, yielding 2-bromo-5-chloromagnesio-3-hexylthiophene as the active monomer **M2**. This monomer was then polymerized by adding it to 1.5 mol% of Ni(dppp)Cl<sub>2</sub> in dry THF ([**M2**] = 0.075 M) at RT. After 15 minutes, half of the resulting polymerization mixture was cannulated to another flask and quenched with a THF/HCl mixture, thereby obtaining the **P3HT** reference homopolymer. To the other half of the polymerization mixture, the *in situ* prepared active monomer **M1** was added to

initiate the polymerization of the second **P(3HT-*alt*-TP)** block. The block copolymerization was allowed to proceed overnight at RT, whereupon it was quenched with a THF/HCl mixture to yield the desired block copolymer poly{[3-hexylthiophene-5,2-diyl]-*block*-[(3-hexylthiophene-5,2-diyl)-*alt*-(2,3-didodecylthieno[3,4-*b*]pyrazine-5,7-diyl)]} **P3HT-*b*-P(3HT-*alt*-TP)**.



**Scheme 5:** Synthesis of the **P3HT-*b*-P(3HT-*alt*-TP)** copolymer.

After purification by repetitive Soxhlet extractions with MeOH, acetone, hexanes and chloroform, respectively, the **P3HT** homopolymer and **P3HT-*b*-P(3HT-*alt*-TP)** block copolymer were analyzed by GPC. The resulting GPC profiles are depicted in Figure 1 and clearly show a shift to higher  $M_n$  values when going from the homopolymer to the block copolymer. The **P3HT** homopolymer showed a  $M_n$  value of 7.2 kg/mol and a  $D$  of 1.09, while the **P3HT-*b*-P(3HT-*alt*-TP)** copolymer was characterized by a  $M_n$  value of 14 kg/mol and a  $D$  of 1.21. This means that the second block has a  $M_n$  of only  $\sim 7$  kg/mol, which corresponds nicely to the maximum obtainable length of the alternating copolymer **P(3HT-*alt*-TP)** as shown above. Although the KCTCP of **P(3HT-*alt*-TP)** does not proceed in a

controlled way, the fact that a block copolymer can be synthesized from a **P3HT** macro-initiator further strengthens our hypothesis that this polymerization follows a chain-growth mechanism.

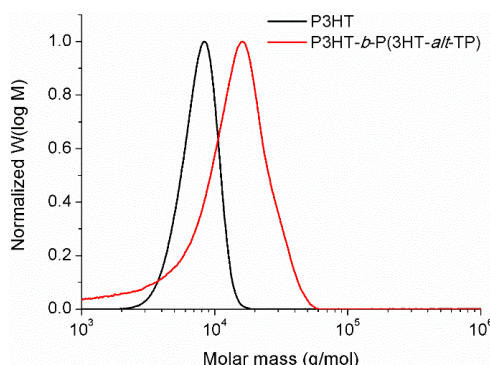


**Figure 1:** GPC profiles of the **P3HT** homopolymer and **P3HT-*b*-P(3HT-*alt*-TP)** copolymer.

The unimodal GPC profile of the **P3HT-*b*-P(3HT-*alt*-TP)** copolymer suggests that almost all **P3HT** polymer chains grew further upon addition of the **M1** monomer. This was confirmed by analyzing both materials via  $^1\text{H}$  NMR spectroscopy. For the hexyl side chains of the **P3HT** homopolymer, the large triplet at 2.80 ppm (**a**) can be assigned to the  $\alpha\text{-CH}_2$  protons of the internal **P3HT** units, while the two smaller triplets at 2.63 ppm (**b**) and 2.58 ppm (**c**) can be ascribed to the  $\alpha\text{-CH}_2$  protons of the two external **P3HT** units with a hydrogen and a bromide end group, respectively (Figure 2a).<sup>[23]</sup> If an overlay is made between the  $^1\text{H}$  NMR spectra of the  $\alpha\text{-CH}_2$  regions of **P3HT** and **P3HT-*b*-P(3HT-*alt*-TP)**, it can be established that signal **b** disappeared in the spectrum of the block copolymer (Figure 2b). This suggests that the **P3HT** polymer chains indeed reacted further with **M1** to end up with an all-conjugated block copolymer.

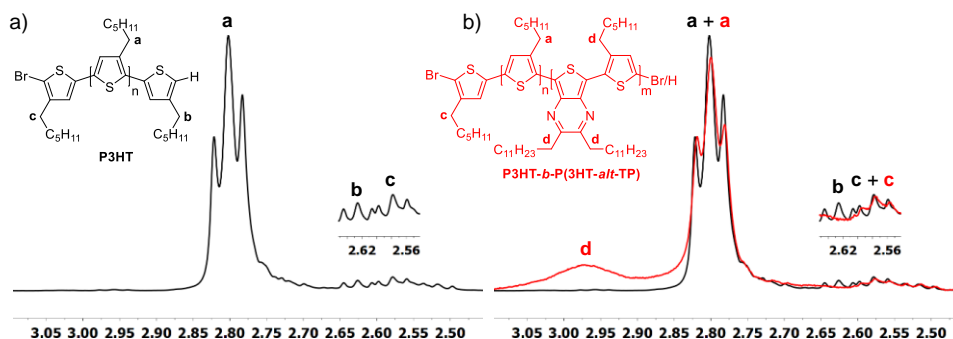


**Figure 2:** a)  $^1\text{H}$  NMR spectrum of the  $\alpha\text{-CH}_2$  region of **P3HT**; b) Overlay of the  $^1\text{H}$  NMR spectra of the  $\alpha\text{-CH}_2$  regions of **P3HT** and **P3HT-*b*-P(3HT-*alt*-TP)**.

The optical properties of the block copolymer and its constituting homopolymers were studied by UV-vis-NIR absorption spectroscopy in solution and thin film. From the absorption spectra in  $\text{CHCl}_3$  solution (Figure 3a), it is clear that the spectrum of the block copolymer shows two peaks with a  $\lambda_{\text{max}}$  (wavelength at maximal absorbance) of 443 and  $\sim 700$  nm. The low wavelength maximum arises from the contribution of the **P3HT** block, which is characterized by a  $\lambda_{\text{max}}$  of 449 nm. The broad peak, on the other hand, can be attributed to the **P(3HT-*alt*-TP)** block, which also shows a broad absorption peak ranging from about 500 to 1200 nm with a  $\lambda_{\text{max}}$  of 773 nm. Due to this, the block copolymer is characterized by a khaki colour in solution, which lies somewhere in between the typical orange colour of **P3HT** and the dark green colour of **P(3HT-*alt*-TP)** (Figure S9, Supporting Information). The absorption spectra of these materials in thin film show a clear red-shift for both homopolymers (Figure 3b), i.e. a rise in  $\lambda_{\text{max}}$  from 449 to 555 nm is observed for **P3HT**, while the **P(3HT-*alt*-TP)** copolymer shows a red-shift from 773 to 857 nm. The spectrum of the **P3HT-*b*-P(3HT-*alt*-TP)** block copolymer in thin film is still characterized by the two absorptions from the constituting homopolymers, whereby both peaks are also red-shifted. The

contribution from the **P(3HT-*alt*-TP)** block shows a maximum absorption red-shifted from  $\sim 700$  to  $\sim 800$  nm, whereas the peak from the **P3HT** block shows a similar bathochromic shift as the **P3HT** homopolymer (from 443 to 553 nm).

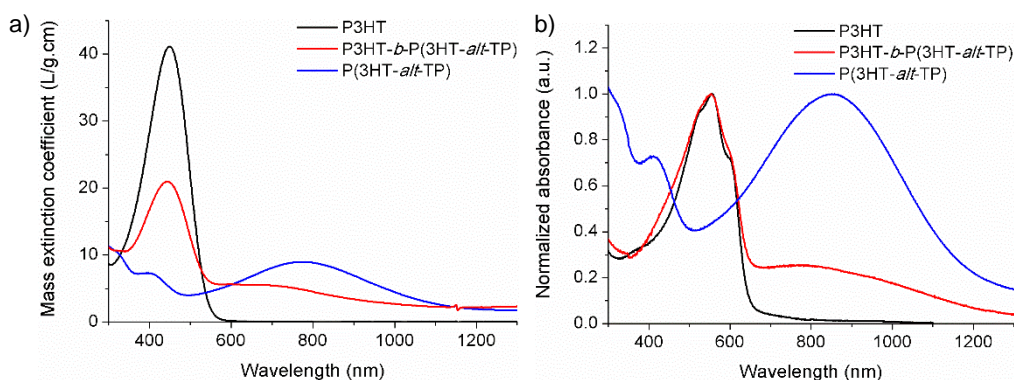


**Figure 3:** UV-vis-NIR absorption spectra of the synthesized polymers in a)  $\text{CHCl}_3$  solution and b) thin film.

To investigate whether the two blocks influence each other electronically, a UV-vis-NIR absorption spectrum of the block copolymer was simulated, assuming that the two blocks do not influence each other (Figure 4). This was done by superposition of the spectra of the two homopolymers, taking into account the mass percentages of both blocks. These mass percentages amount to 71% for the **P3HT** block and 29% for the **P(3HT-*alt*-TP)** block (or 50% for both blocks), based on the integration of the  $^1\text{H}$  NMR spectrum of **P3HT-*b*-P(3HT-*alt*-TP)** (or based on the  $M_n$  values of both blocks). In both cases, a difference between the simulated and recorded UV-vis-NIR absorption spectrum of the block copolymer is observed (mainly in the region around 600 nm). This means that there is some electronic interaction between both blocks, suggesting that the conjugation between both blocks is not interrupted. These findings further confirm the successful formation of an all-conjugated **P3HT-*b*-P(3HT-*alt*-TP)** copolymer.

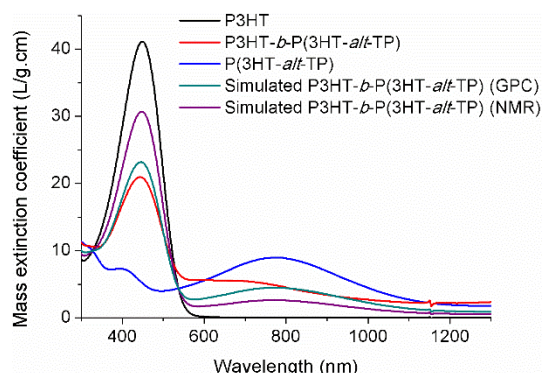


**Figure 4:** UV-vis-NIR absorption spectra of the **P3HT** and **P(3HT-*alt*-TP)** homopolymers and the recorded and simulated spectra of the **P3HT-*b*-P(3HT-*alt*-TP)** block copolymer.

### 4.3 CONCLUSIONS

We were able to extend the (small) list of alternating donor-acceptor copolymers that can be synthesized via KCTCP by performing the KCTCP of a monomer that consists of both a thiophene (donor) and thieno[3,4-*b*]pyrazine (acceptor) unit, resulting into a **P(3HT-*alt*-TP)** copolymer. From GPC analysis, it was found that the polymer did not grow beyond a molar mass of  $\sim 7$  kg/mol, while a rather narrow dispersity was obtained, suggesting that this polymerization follows a non-controlled chain-growth mechanism. This was confirmed by the successful synthesis of an all-conjugated block copolymer via a one-pot KCTCP procedure, whereby the *in situ* formed **P3HT** was used as a macro-initiator to start the polymerization of the alternating donor-acceptor copolymer. In this way, a **P3HT-*b*-P(3HT-*alt*-TP)** block copolymer was obtained, which was confirmed by GPC and  $^1\text{H}$  NMR analysis. From the investigation of the optical properties of the synthesized polymers by UV-vis-NIR absorption spectroscopy, it was clear that the absorption spectrum of the **P3HT-*b*-P(3HT-*alt*-TP)** block copolymer is

composed of the two contributions from its constituting **P3HT** and **P(3HT-*alt*-TP)** homopolymers. Besides this, also a difference between the simulated and recorded absorption spectrum of the block copolymer was observed, meaning that the two blocks influence each other electronically. The extended absorption of the alternating and block copolymer into the near-infrared renders these materials of particular interest for organic photovoltaics as well as photodetectors.

#### 4.4 REFERENCES

- [1] Lu, L.; Zheng, T.; Wu, Q.; Schneider, A. M.; Zhao, D.; Yu, L. *Chem. Rev.* **2015**, *115*, 12666–12731.
- [2] Mazziio, K. A.; Luscombe, C. K. *Chem. Soc. Rev.* **2015**, *44*, 78–90.
- [3] Xu, S.; Kim, E. H.; Wei, A.; Negishi, E. *Sci. Technol. Adv. Mater.* **2014**, *15*, 044201–044223.
- [4] Bao, Z.; Chan, W. K.; Yu, L. *J. Am. Chem. Soc.* **1995**, *117*, 12426–12435.
- [5] Suzuki, A. *J. Organomet. Chem.* **1999**, *576*, 147–168.
- [6] Spoltore, D.; Vangerven, T.; Verstappen, P.; Piersimoni, F.; Bertho, S.; Vandewal, K.; Van den Brande, N.; Defour, M.; Van Mele, B.; De Sio, A.; Parisi, J.; Lutsen, L.; Vanderzande, D.; Maes, W.; Manca, J. V. *Org. Electron.* **2015**, *21*, 160–170.
- [7] Vangerven, T.; Verstappen, P.; Drijkoningen, J.; Dierckx, W.; Himmelberger, S.; Salleo, A.; Vanderzande, D.; Maes, W.; Manca, J. V. *Chem. Mater.* **2015**, *27*, 3726–3732.
- [8] Bartelt, J. A.; Douglas, J. D.; Mateker, W. R.; El Labban, A.; Tassone, C. J.; Toney, M. F.; Fréchet, J. M. J.; Beaujuge, P. M.; McGehee, M. D. *Adv. Energy Mater.* **2014**, *4*, 1301733.

- [9] van Franeker, J. J.; Heintges, G. H. L.; Schaefer, C.; Portale, G.; Li, W.; Wienk, M. M.; van der Schoot, P.; Janssen, R. A. J. *J. Am. Chem. Soc.* **2015**, *137*, 11783–11794.
- [10] Li, W.; Yang, L.; Tumbleston, J. R.; Yan, L.; Ade, H.; You, W. *Adv. Mater.* **2014**, *26*, 4456–4462.
- [11] Yokoyama, A.; Miyakoshi, R.; Yokozawa, T. *Macromolecules* **2004**, *37*, 1169–1171.
- [12] Sheina, E. E.; Liu, J.; Iovu, M. C.; Laird, D. W.; McCullough, R. D. *Macromolecules* **2004**, *37*, 3526–3528.
- [13] Geng, Y.; Huang, L.; Wu, S.; Wang, F. *Sci. China Chem.* **2010**, *53*, 1620–1633.
- [14] Verheyen, L.; Leysen, P.; Van Den Eede, M.-P.; Ceunen, W.; Hardeman, T.; Koeckelberghs, G. *Polymer* **2017**, *108*, 521–546.
- [15] Kiriya, A.; Senkovskyy, V.; Sommer, M. *Macromol. Rapid Commun.* **2011**, *32*, 1503–1517.
- [16] Bronstein, H.; Hurhangee, M.; Fregoso, E. C.; Beatrup, D.; Soon, Y. W.; Huang, Z.; Hadipour, A.; Tuladhar, P. S.; Rossbauer, S.; Sohn, E.-H.; Shoaee, S.; Dimitrov, S. D.; Frost, J. M.; Ashraf, R. S.; Kirchartz, T.; Watkins, S. E.; Song, K.; Anthopoulos, T.; Nelson, J.; Rand, B. P.; Durrant, J. R.; McCulloch, I. *Chem. Mater.* **2013**, *25*, 4239–4249.
- [17] Todd, A. D.; Bielawski, C. W. *ACS Macro Lett.* **2015**, *4*, 1254–1258.
- [18] Govaerts, S.; Verstappen, P.; Penxten, H.; Defour, M.; Van Mele, B.; Lutsen, L.; Vanderzande, D.; Maes, W. *Macromolecules* **2016**, *49*, 6411–6419.
- [19] Willot, P.; Moerman, D.; Leclère, P.; Lazzaroni, R.; Baeten, Y.; Van der Auweraer, M.; Koeckelberghs, G. *Macromolecules* **2014**, *47*, 6671–6678.

- [20] Kenning, D. D.; Mitchell, K. A.; Calhoun, T. R.; Funfar, M. R.; Sattler, D. J.; Rasmussen, S. C. *J. Org. Chem.* **2002**, *67*, 9073–9076.
- [21] Wen, L.; Rasmussen, S. C. *J. Chem. Crystallogr.* **2007**, *37*, 387–398.
- [22] Zoombelt, A. P.; Leenen, M. A. M.; Fonrodona, M.; Nicolas, Y.; Wienk, M. M.; Janssen, R. A. J. *Polymer* **2009**, *50*, 4564–4570.
- [23] Iovu, M. C.; Sheina, E. E.; Gil, R. R.; McCullough, R. D. *Macromolecules* **2005**, *38*, 8649–8656.

## 4.5 SUPPORTING INFORMATION

### 4.5.1 Reagents and instrumentation

All reagents and chemicals were obtained from commercial sources and used without further purification. THF and Et<sub>2</sub>O were dried using a solvent purification system (MBraun MB-SPS 800). NMR chemical shifts ( $\delta$ , in ppm) were determined relative to the residual <sup>1</sup>H signal of CHCl<sub>3</sub> (7.26 ppm) or the <sup>13</sup>C{<sup>1</sup>H} (proton decoupled <sup>13</sup>C NMR spectroscopy) resonance shift of CDCl<sub>3</sub> (77.16 ppm). High resolution ESI-MS was performed using a LTQ Orbitrap Velos Pro mass spectrometer equipped with an atmospheric pressure ionization source operating in the nebulizer assisted electrospray mode. The instrument was calibrated in the *m/z* range 220–2000 using a standard solution containing caffeine, MRFA and Ultramark 1621. Analysis of the molar masses and distributions of the polymer samples was performed on a Tosoh EcoSEC System, comprising of an autosampler, a PSS guard column SDV (50 x 7.5 mm) followed by three PSS SDV analytical linear XL columns (5  $\mu$ m, 300 x 7.5 mm), and a UV detector using THF as the eluent at 40 °C with a flow rate of 1.0 mL/min. The SEC system was calibrated using linear narrow polystyrene standards ranging from 474 to 7.5 x 10<sup>6</sup> g/mol ( $K = 14.1 \times 10^{-5}$  dL/g and  $\alpha = 0.70$ ). Background corrected UV-Vis-NIR absorption spectra were recorded on a Cary 5000 UV-Vis-NIR spectrophotometer from Agilent using a band width of 2 nm, full slit height and a scan speed of 600 nm/min.

#### 4.5.2 Monomer synthesis

2,5-Dibromo-3-hexylthiophene,<sup>[1,2]</sup> 2-bromo-3-hexylthiophene (**2**)<sup>[3]</sup> and 2,3-didodecylthieno[3,4-*b*]pyrazine (**7**)<sup>[4,5]</sup> were synthesized according to literature procedures.

#### 5-bromo-2,3-didodecylthieno[3,4-*b*]pyrazine (**8**)

2,3-Didodecylthieno[3,4-*b*]pyrazine (**7**) (1.00 g, 2.11 mmol) was dissolved in a mixture of CHCl<sub>3</sub> (30 mL) and *N,N*-dimethylformamide (DMF) (50 mL), cooled to 0 °C and protected from light. *N*-bromosuccinimide (0.376 g, 2.11 mmol) was dissolved in DMF (10 mL) and added dropwise. The mixture was stirred overnight at RT under N<sub>2</sub> atmosphere. The reaction mixture was quenched with H<sub>2</sub>O, extracted with chloroform and the organic layer was washed with a saturated NaCl solution. The organic layer was then dried with MgSO<sub>4</sub>, filtered and evaporated under reduced pressure. The product was purified by column chromatography (silica gel, hexanes/CHCl<sub>3</sub> 20/80), resulting in a yellow-brown solid (0.650 g, 56%). <sup>1</sup>H NMR (400 MHz, CDCl<sub>3</sub>): δ = 7.85 (s, 1H), 2.97–2.83 (m, 4H), 1.86–1.74 (m, 4H), 1.47–1.24 (m, 36H), 0.90–0.86 (m, 6H); <sup>13</sup>C{<sup>1</sup>H} NMR (100 MHz, CDCl<sub>3</sub>): δ = 157.7, 156.7, 139.7, 115.7, 105.1, 35.6, 35.1, 31.9, 29.7, 29.49, 29.45, 29.4, 22.7, 14.2; ESI-HRMS: found 551.2987, calcd 551.3035 (MH<sup>+</sup>).

#### 2,3-didodecyl-5-(3-hexylthiophen-2-yl)thieno[3,4-*b*]pyrazine (**9**)

Magnesium (0.250 g, 10.3 mmol) was added to dry Et<sub>2</sub>O (35 mL), a little bit of iodine was added and the mixture was stirred under N<sub>2</sub> for ~10 min. 2-Bromo-3-hexylthiophene (**2**) (0.851 g, 0.687 mL, 3.44 mmol) was added dropwise to the activated magnesium at RT and the reaction mixture was heated to reflux for 1 h. The obtained Grignard reagent was added, via cannula, to a solution of 5-bromo-2,3-didodecylthieno[3,4-*b*]pyrazine (**8**) (1.71 g, 3.10 mmol) and Ni(dppp)Cl<sub>2</sub>

(16.8 mg, 31.0  $\mu$ mol, 1 mol%) in dry Et<sub>2</sub>O (30 mL) at RT and the brown mixture was refluxed overnight. The reaction mixture was then cooled to RT, quenched with a HCl solution (1 M) and extracted with chloroform. The combined organic layers were dried over magnesium sulfate and the volatiles were removed *in vacuo*. The residue was purified by column chromatography (silica gel, hexanes/CH<sub>2</sub>Cl<sub>2</sub> 75/25) to afford the product as an orange-brown solid (1.20 g, 61%). <sup>1</sup>H NMR (400 MHz, CDCl<sub>3</sub>):  $\delta$  = 7.76 (s, 1H), 7.36 (d, *J* = 5.2 Hz, 1H), 7.01 (d, *J* = 5.2 Hz, 1H), 2.97–2.83 (m, 6H), 1.90 (quint, *J* = 7.5 Hz, 2H), 1.79 (quint, *J* = 7.7 Hz, 2H), 1.69 (quint, *J* = 7.6 Hz, 2H), 1.50–1.25 (m, 42H), 0.90–0.85 (m, 9H); <sup>13</sup>C{<sup>1</sup>H} NMR (100 MHz, CDCl<sub>3</sub>):  $\delta$  = 156.2, 155.5, 141.0, 138.1, 129.3, 128.0, 126.5, 112.8, 35.2, 32.0, 31.7, 30.3, 30.1, 29.7, 29.6, 29.54, 29.50, 29.4, 28.5, 27.5, 22.7, 14.2; ESI-HRMS: found 639.4689, calcd 639.4746 (MH<sup>+</sup>).

**5-bromo-7-(5-bromo-3-hexylthiophen-2-yl)-2,3-didodecylthieno[3,4-*b*]pyrazine (10)**

2,3-Didodecyl-5-(3-hexylthiophen-2-yl)thieno[3,4-*b*]pyrazine (**9**) (1.17 g, 1.83 mmol) was dissolved in a mixture of CHCl<sub>3</sub> (25 mL) and DMF (45 mL), cooled to 0 °C and protected from light. *N*-bromosuccinimide (0.684 g, 3.84 mmol) was dissolved in DMF (20 mL) and added dropwise. The mixture was stirred overnight at RT and under N<sub>2</sub> atmosphere. The reaction was quenched with H<sub>2</sub>O, extracted with dichloromethane (DCM) and washed with a saturated Na<sub>2</sub>S<sub>2</sub>O<sub>3</sub> solution. The resulting organic layer was then dried with MgSO<sub>4</sub>, filtered and evaporated under reduced pressure (without heating). The product was purified by column chromatography (silica gel, hexanes/DCM 95/5), resulting in an orange-brown solid (0.926 g, 63%). <sup>1</sup>H NMR (400 MHz, CDCl<sub>3</sub>):  $\delta$  = 6.94 (s, 1H), 2.94–2.88 (m, 4H), 2.82–2.76 (m, 2H), 1.90 (quint, *J* = 7.4 Hz, 2H), 1.80 (quint, *J* = 7.6 Hz,

2H), 1.67 (quint,  $J = 7.5$  Hz, 2H), 1.49–1.25 (m, 42H), 0.90–0.86 (m, 9H);  $^{13}\text{C}\{^1\text{H}\}$  NMR (100 MHz,  $\text{CDCl}_3$ ):  $\delta = 155.8, 152.5, 143.7, 140.5, 132.5, 132.3, 127.8, 126.0, 117.2, 109.3, 100.5, 34.4, 31.9, 31.6, 31.5, 30.7, 29.7, 29.4, 27.3, 24.9, 22.7, 14.1$  (one unidentified carbon signal too much in the aromatic region); ESI-HRMS: found 795.2904, calcd 795.2956 ( $\text{MH}^+$ ).

#### 4.5.3 Polymer synthesis

##### **P(3HT-*alt*-TP)**

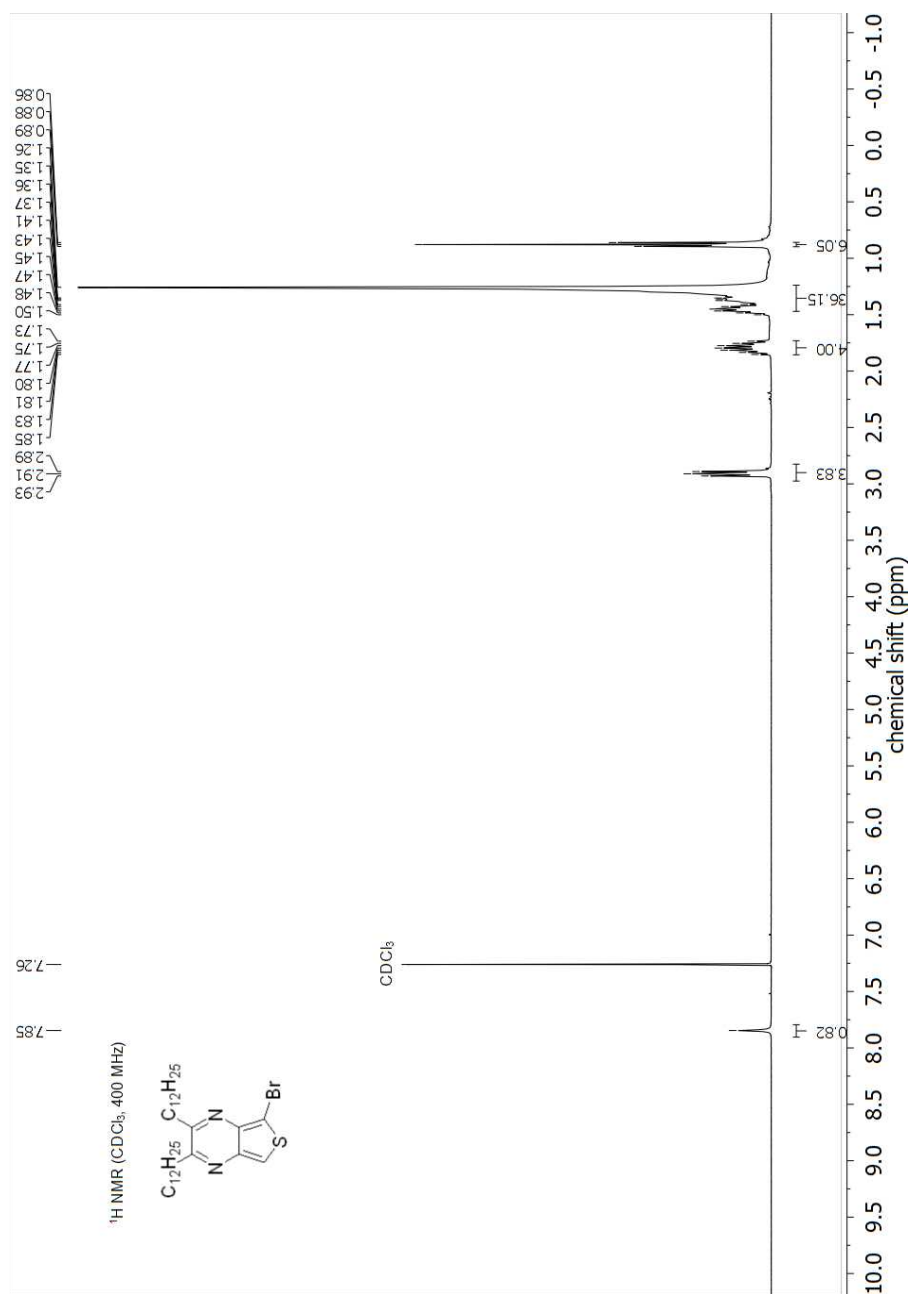
5-Bromo-7-(5-bromo-3-hexylthiophen-2-yl)-2,3-didodecylthieno[3,4-*b*]pyrazine (**10**) (0.199 g, 0.250 mmol) was loaded in a three-neck flask and brought under Ar atmosphere, after which dry THF (2.5 mL) was added via cannula. *i*-PrMgCl.LiCl (0.192 mL, 0.250 mmol; 1.30 M in THF) was added dropwise to this solution at 0 °C to start the GRIM reaction. After stirring for 1 h at 0 °C, this mixture was cannulated to another three-neck flask containing Ni(dppp)Cl<sub>2</sub> (2.71 mg, 5.00 μmol, 2.0 mol%) and dry THF (2.5 mL), at RT and under Ar atmosphere. The polymerization was allowed to stir overnight, before it was stopped by quenching with a THF/HCl mixture (0.5 mL; 1.0 M). The resulting polymerization mixture was then precipitated in methanol, whereafter the precipitate was filtered over a Soxhlet thimble and subsequently purified by means of Soxhlet extractions with methanol, acetone, hexanes and chloroform (dissolving the polymer), respectively. The solvent was evaporated under reduced pressure, after which the polymer was redissolved in chloroform (2 mL) and again precipitated in methanol. The precipitate was filtered off over a PTFE membrane (47 mm/0.45 μm) and dried overnight under vacuum, affording **P(3HT-*alt*-TP)** as a dark-green solid.  $^1\text{H}$  NMR (400 MHz,  $\text{CS}_2/\text{CDCl}_3$ ):  $\delta = 7.75$  (br, 1H), 2.98 (br, 6H), 2.01 (br, 4H), 1.88 (br, 2H), 1.60–1.25 (m, 42H), 0.92–0.84 (m, 9H); UV-Vis-NIR ( $\text{CHCl}_3$ ):

$\lambda_{max} = 828$  nm, UV-Vis-NIR (film):  $\lambda_{max} = 914$  nm; GPC (THF, PS standards):  $M_n = 6.9 \times 10^3$  g/mol,  $M_w = 9.0 \times 10^3$  g/mol,  $D = 1.29$ .

### **P3HT-*b*-P(3HT-*alt*-TP)**

2,5-Dibromo-3-hexylthiophene (0.326 g, 1.00 mmol) was loaded in a three-neck flask and brought under Ar atmosphere. Then, dry THF (10 mL) was added via cannula, after which the solution was cooled down to 0 °C. *i*-PrMgCl.LiCl (0.769 mL, 1.00 mmol; 1.30 M in THF) was added dropwise to this solution to start the first GRIM reaction (GRIM 1). Meanwhile, 5-bromo-7-(5-bromo-3-hexylthiophen-2-yl)-2,3-didodecylthieno[3,4-*b*]pyrazine (**10**) (0.120 g, 0.150 mmol) was also loaded in a three-neck flask, brought under Ar atmosphere and dissolved in dry THF (1.5 mL). 15 Min after the start of GRIM 1, *i*-PrMgCl.LiCl (0.115 mL, 0.150 mmol; 1.30 M in THF) was added dropwise to this solution at 0 °C to start the second GRIM reaction (GRIM 2). Both GRIM reactions were stirred for 1 h at 0 °C. After GRIM 1, the **M2** mixture was cannulated to another three-neck flask containing Ni(dppp)Cl<sub>2</sub> (8.13 mg, 15.0 μmol, 1.5 mol%) and dry THF (3 mL), at RT and under Ar atmosphere. This polymerization mixture was then stirred for 15 min at RT, whereafter half of it (6.5 mL) was quenched with a THF/HCl mixture (1.0 mL, 1.0 M), while to the other half of the mixture, the **M1** mixture was added at RT. The block copolymerization was allowed to stir overnight, before it was stopped by quenching with a THF/HCl mixture (1.0 mL, 1.0 M). The resulting **P3HT** homopolymer and the **P3HT-*b*-P(3HT-*alt*-TP)** block copolymer were both precipitated in methanol and filtered over a Soxhlet thimble. Both materials were subsequently purified by means of Soxhlet extractions with methanol, acetone, hexanes and chloroform (dissolving the polymer), respectively. The solvent was evaporated under reduced pressure, after which the polymers were redissolved in

chloroform (2 mL) and again precipitated in methanol. The precipitates were filtered off over a PTFE membrane (47 mm/0.45  $\mu\text{m}$ ) and dried overnight under vacuum, affording **P3HT** as a purple solid and **P3HT-*b*-P(3HT-*alt*-TP)** as a dark-purple solid.  $^1\text{H}$  NMR (400 MHz,  $\text{CS}_2/\text{CDCl}_3$ ):  $\delta$  = 7.75 (br, 0.1H), 6.94 (s, 1H), 2.98 (br, 0.6H), 2.80 (t,  $J$  = 7.4 Hz, 2H), 2.02 (br, 0.4H), 1.88 (br, 0.2H), 1.76–1.68 (m, 2H), 1.51–1.27 (m, 10.2H), 0.98–0.91 (m, 3.9H); UV-Vis-NIR ( $\text{CHCl}_3$ ):  $\lambda_{\text{max}}$  = 446 and 929 nm, UV-Vis-NIR (film):  $\lambda_{\text{max}}$  = 537 nm; GPC (THF, PS standards):  $M_n$  =  $1.4 \times 10^4$  g/mol,  $M_w$  =  $1.7 \times 10^4$  g/mol,  $D$  = 1.21.

4.5.4  $^1\text{H}$  NMR spectra**Figure S1:**  $^1\text{H}$  NMR spectrum of 5-bromo-2,3-didodecylthieno[3,4-*b*]pyrazine (**8**).

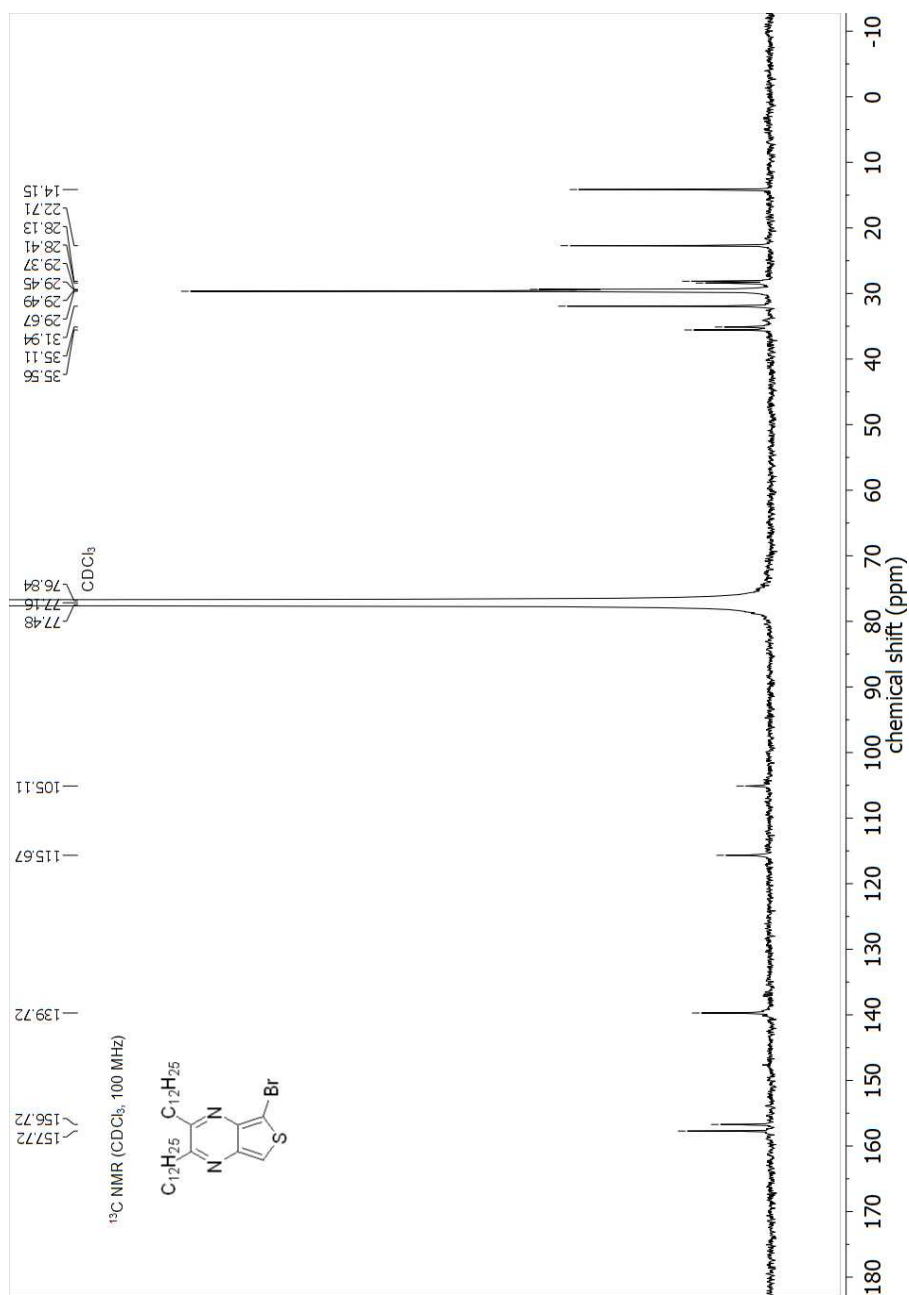


**Figure S2:** <sup>13</sup>C NMR spectrum of 5-bromo-2,3-didodecylthieno[3,4-*b*]pyrazine (**8**).

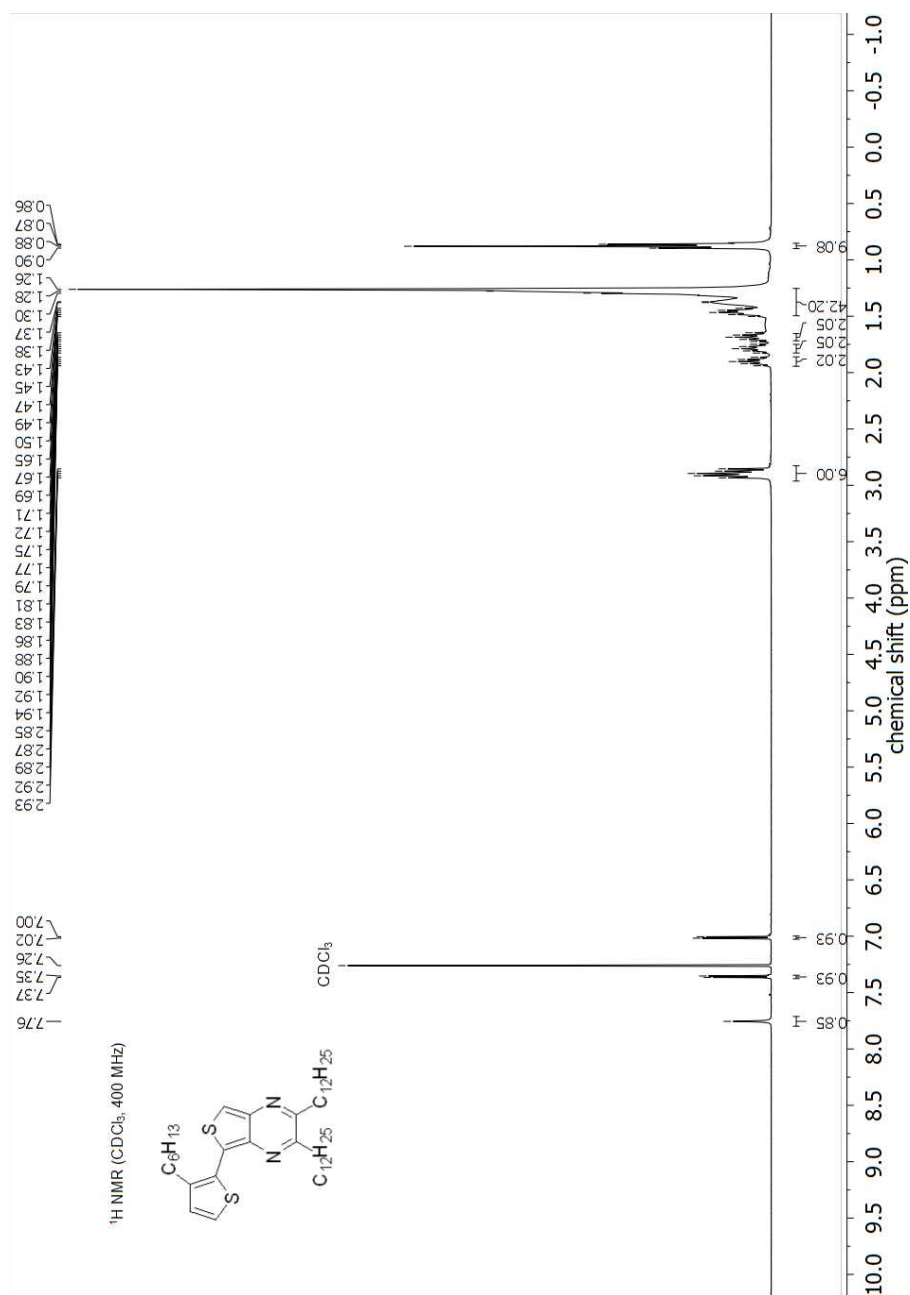


**Figure S3:** <sup>1</sup>H NMR spectrum of 2,3-didodecyl-5-(3-hexylthiophen-2-yl)thieno[3,4-b]pyrazine (**9**).

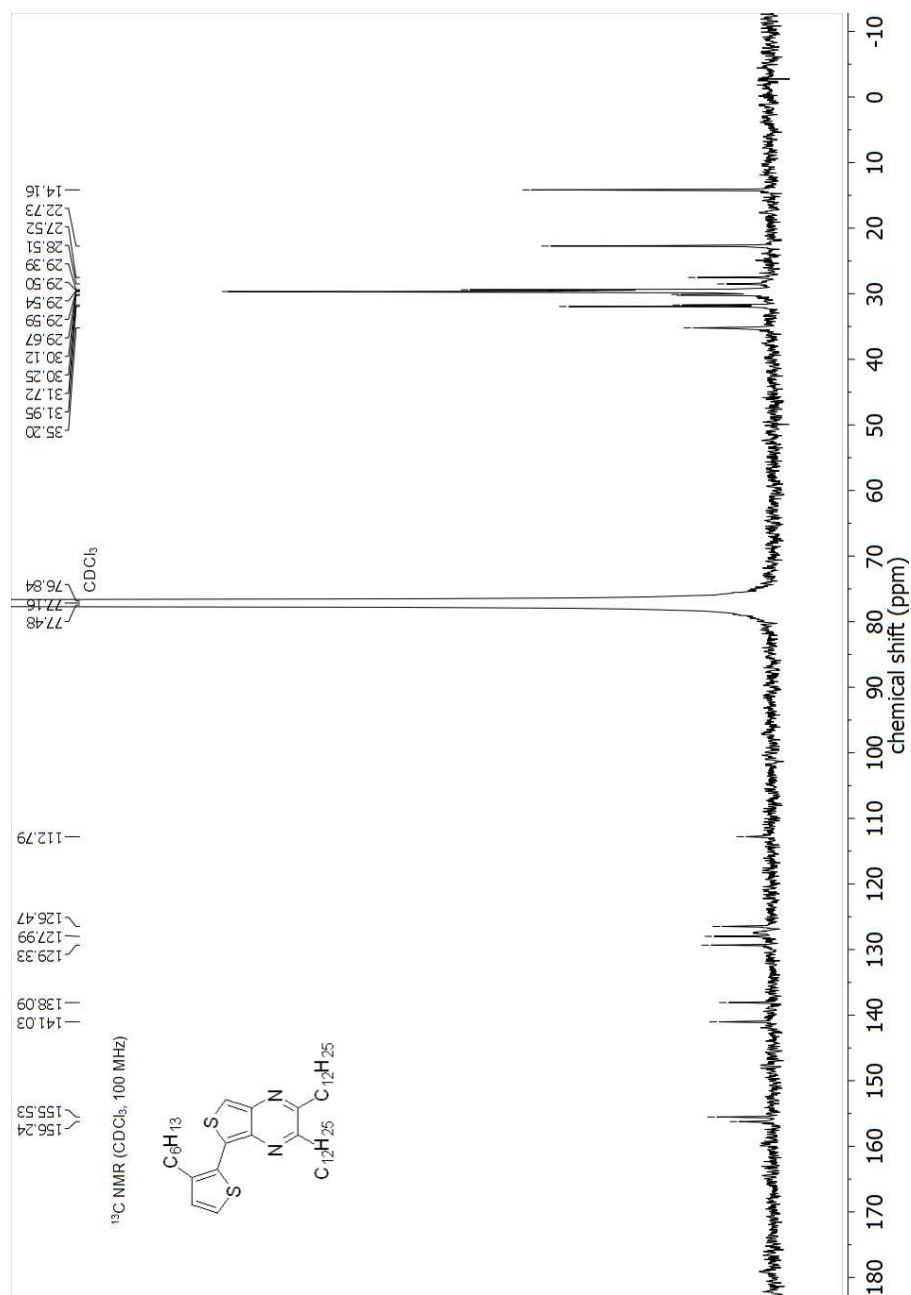


**Figure S4:** <sup>13</sup>C NMR spectrum of 2,3-didodecyl-5-(3-hexylthiophen-2-yl)thieno[3,4-*b*]pyrazine (**9**).

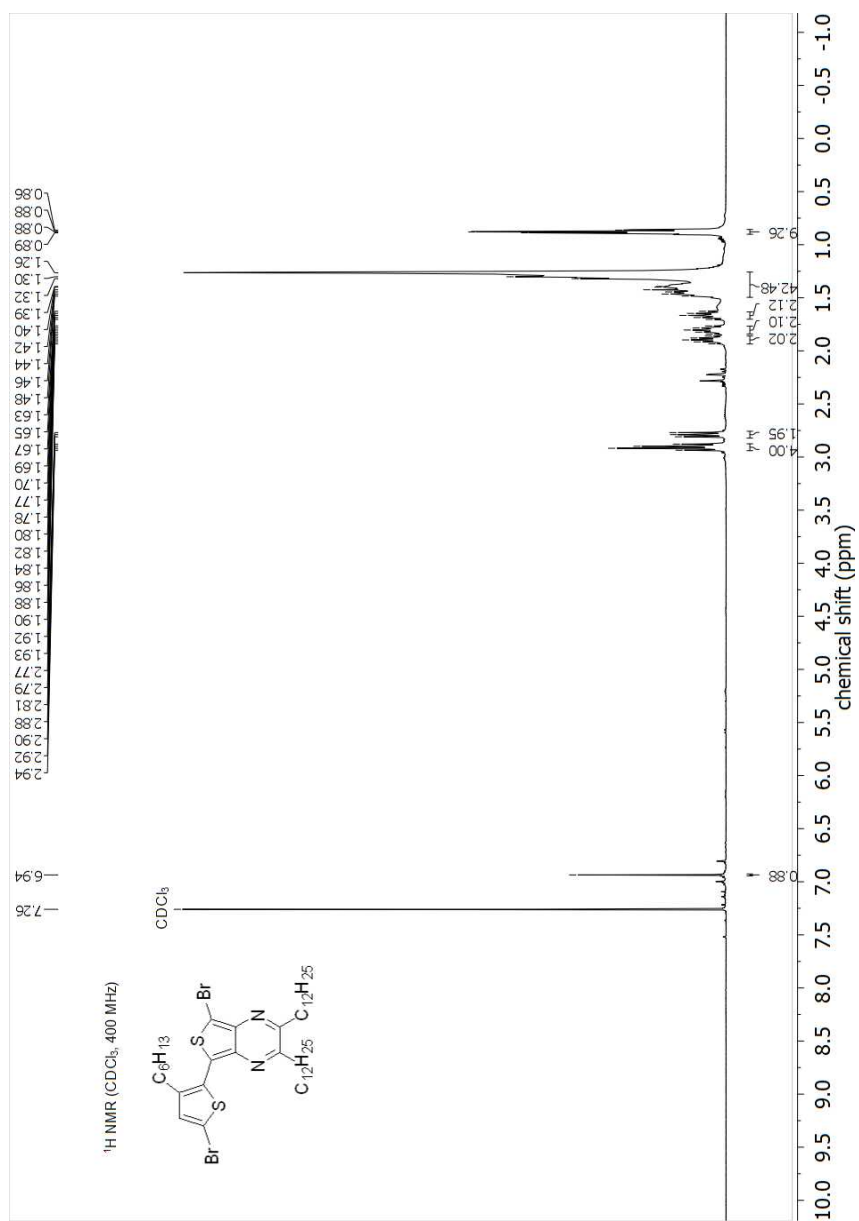


**Figure S5:** <sup>1</sup>H NMR spectrum of 5-bromo-7-(5-bromo-3-hexylthiophen-2-yl)-2,3-didodecylthieno[3,4-b]pyrazine (**10**).

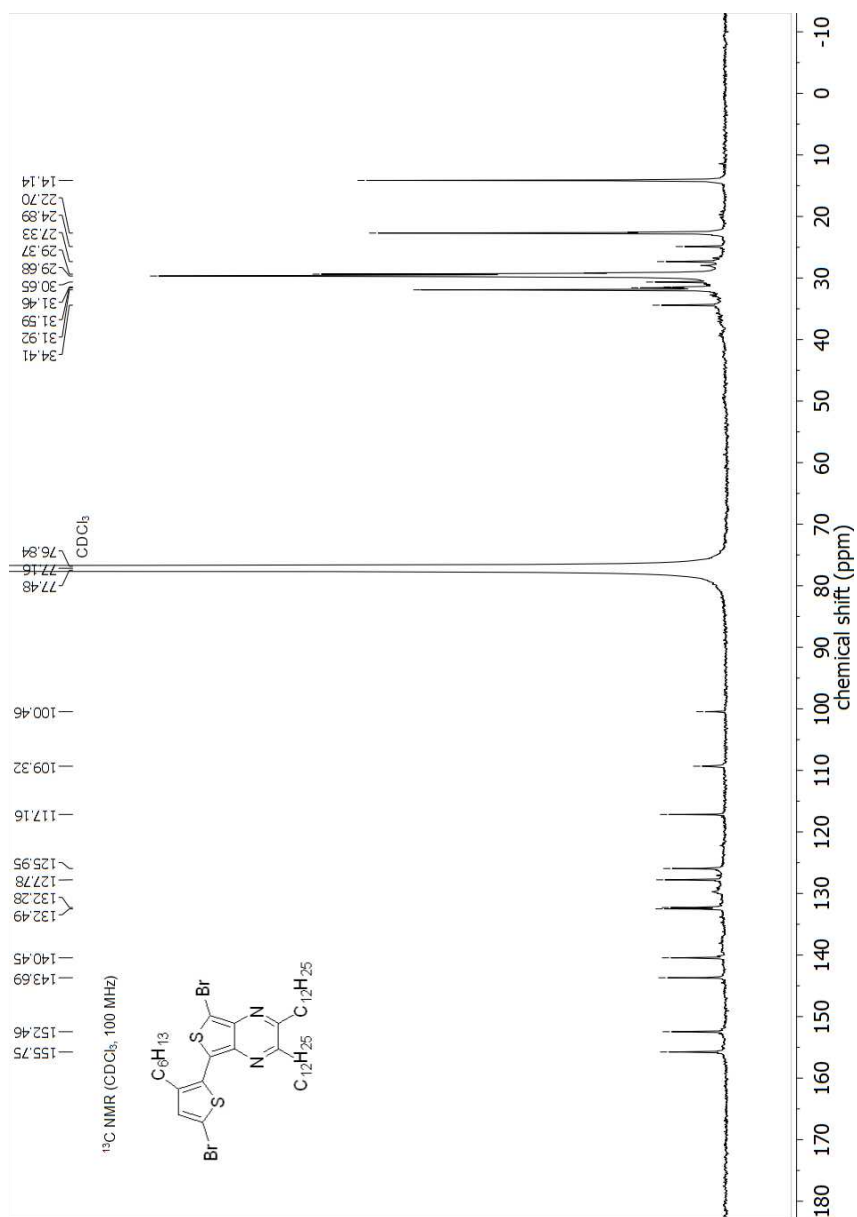


**Figure S6:** <sup>13</sup>C NMR spectrum of 5-bromo-7-(5-bromo-3-hexylthiophen-2-yl)-2,3-didodecylthieno[3,4-b]pyrazine (**10**).

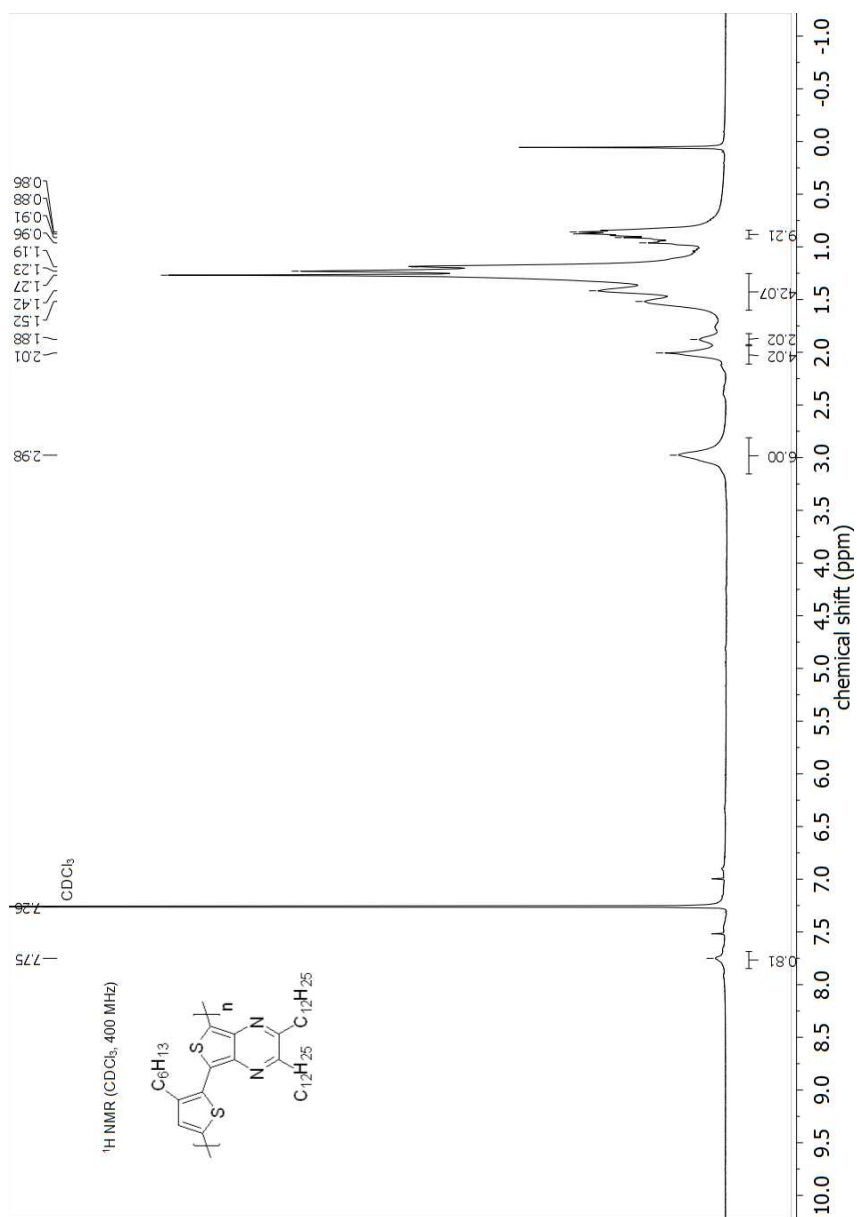


**Figure S7:** <sup>1</sup>H NMR spectrum of poly[(3-hexylthiophene-5,2-diy)-*alt*-(2,3-didodecylthieno[3,4-*b*]pyrazine-5,7-diy)] (**P(3HT-*alt*-TP)**).

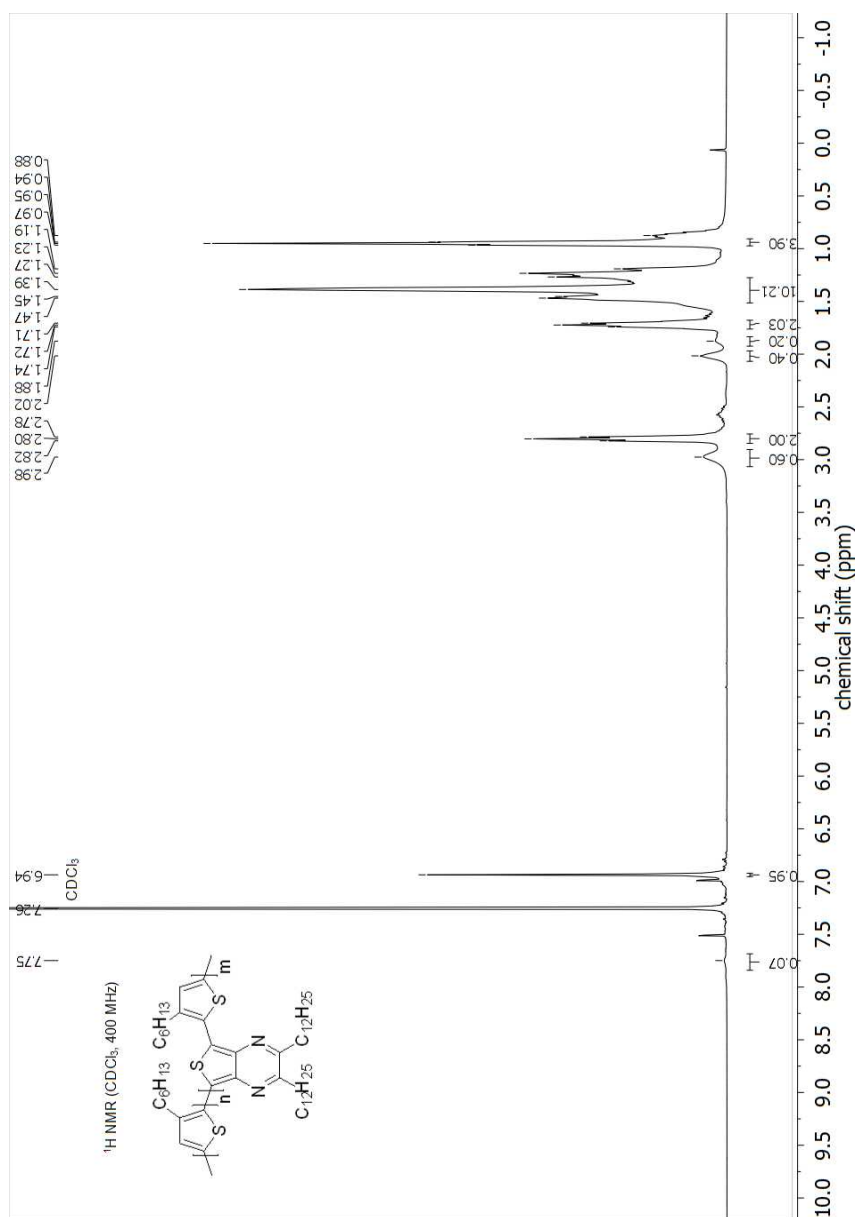


**Figure S8:** <sup>1</sup>H NMR spectrum of poly{[3-hexylthiophene-5,2-diy]-block-[3-hexylthiophene-5,2-diy]-*alt*-(2,3-didodecylthieno[3,4-*b*]pyrazine-5,7-diy)} (P3HT-*b*-P(3HT-*alt*-TP)).

#### 4.5.5 Polymer solutions



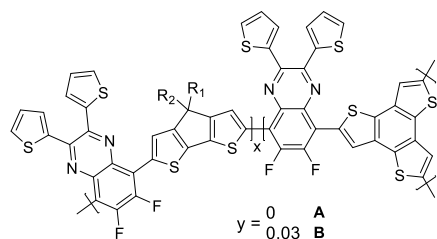
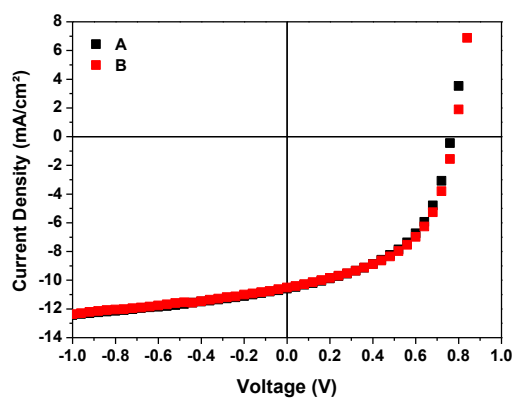
**Figure S9:** Vials containing **P3HT** (left), **P3HT-*b*-P(3HT-*alt*-TP)** (middle) and **P(3HT-*alt*-TP)** (right) in chloroform solution.

#### 4.5.6 References

- [1] Pal, B.; Yen, W.-C.; Yang, J.-S.; Su, W.-F. *Macromolecules* **2007**, *40*, 8189–8194.
- [2] Yang, Y.-L.; Lee, Y.-H.; Lee, Y.-P.; Chiang, C.-J.; Shen, C.; Wu, C.-C.; Ohta, Y.; Yokozawa, T.; Dai, C.-A. *Polym. Int.* **2014**, *63*, 2068–2075.
- [3] Yokoyama, A.; Miyakoshi, R.; Yokozawa, T. *Macromolecules* **2004**, *37*, 1169–1171.
- [4] Kenning, D. D.; Mitchell, K. A.; Calhoun, T. R.; Funfar, M. R.; Sattler, D. J.; Rasmussen, S. C. *J. Org. Chem.* **2002**, *67*, 9073–9076.
- [5] Wen, L.; Rasmussen, S. C. *J. Chem. Crystallogr.* **2007**, *37*, 387–398.

# Chapter 5

## The introduction of branching in a low bandgap alternating cyclopentadithiophene-quinoxaline copolymer



## ABSTRACT

Although many pathways have already been explored to further enhance the device efficiency and lifetime of organic photovoltaics, most of the results were obtained by using linear conjugated polymers as the donor material in the photoactive layer. More advanced conjugated polymer architectures have rarely been investigated. Conjugation in two or three dimensions could, however, afford several advantages, such as an isotropic charge transport, enhanced dielectric constants and more favorable active layer morphologies. To this extent, a small amount of a trifunctional benzotrithiophene core is added to the Stille polymerization of an alternating 4*H*-cyclopenta[2,1-*b*:3,4-*b'*]dithiophene-quinoxaline (donor-acceptor) copolymer, resulting into a branched copolymer. Comparison of the characteristics of the linear and branched alternating copolymers allows to confirm the incorporation of the benzotrithiophene core into some of the branched copolymer chains. Both copolymers are then applied as donor components in bulk heterojunction polymer solar cells with PC<sub>71</sub>BM as the acceptor to investigate the influence of the branching on the device performance.

## 5.1 INTRODUCTION

Over the last two decades, organic photovoltaics (OPVs) have received an increasing amount of interest as an alternative renewable energy source, in particular because they show some additional assets in comparison to competing photovoltaic technologies. Their low weight, flexibility, semi-transparency, and low-cost large area production make them suitable candidates for building and automotive-integrated applications, smart textiles, sunscreens, etc.<sup>[1-4]</sup> Due to the extensive research in this domain, the power conversion efficiency (PCE) of OPV devices could be elevated to values currently exceeding 12%.<sup>[5-7]</sup> This was achieved through the application of the bulk heterojunction (BHJ) concept, the development of a plethora of low bandgap organic semiconductors to improve the solar spectrum coverage, the use of optimized device architectures, and the introduction of suitable interlayer materials.<sup>[2,8-10]</sup> The BHJ concept increases the interfacial area between the electron donor and electron acceptor in the photoactive layer by intimately mixing them, leading to an enhanced charge separation. Most often, low bandgap alternating donor-acceptor copolymers are used as the electron donor materials, with fine-tuned electronic and optical properties through subtle structural variations, in combination with fullerene derivatives as the electron acceptor. During the past two years, however, non-fullerene OPVs have also attracted considerable attention.<sup>[11]</sup>

Although many pathways have already been explored to further enhance the polymer solar cell efficiency and stability, and very good devices have been realized, most of these results were obtained using linear conjugated polymers. More advanced conjugated polymer architectures – like star and hyperbranched

polymers – have rarely been investigated. Such materials could, however, afford several advantages, such as an isotropic charge transport and enhanced dielectric constants.<sup>[12-14]</sup> Furthermore, these more advanced polymer topologies could give rise to favorable active layer morphologies, which play a crucial role in BHJ OPV device performance. In 2012, a hyperbranched polythiophene was synthesized by Mangold *et al.*<sup>[12]</sup> This material showed lower-lying HOMO (highest occupied molecular orbital) and LUMO (lowest unoccupied molecular orbital) energy levels, and hence a higher open-circuit voltage ( $V_{oc}$ ) was achieved, thereby demonstrating the potential of branched conjugated polymers for OPV applications. More recently, Heintges *et al.* introduced branching in a low bandgap alternating donor-acceptor copolymer and studied its effect on the efficiency of OPV devices.<sup>[15]</sup> The incorporation of branching led to a severe decrease in polymer solubility and a more intimately mixed morphology of the photoactive layer, which resulted in elevated currents and higher efficiencies. However, more dedicated studies on other low bandgap copolymer systems are necessary to gain a better understanding of the effects of branching on the polymer properties and OPV device efficiencies.

In this work, we chose to start from a linear alternating donor-acceptor copolymer system with a very good solubility, affording PCEs of  $\sim 5\%$ , and with particular advantages in terms of structural characterization.<sup>[16,17]</sup> This push-pull copolymer consists of an asymmetrically dialkylated 4*H*-cyclopenta[2,1-*b*:3,4-*b'*]dithiophene (CPDT) as the electron rich building block and a thienyl-substituted quinoxaline (Qx) as the electron poor constituent. To end up with an all-conjugated branched copolymer, a trifunctional benzo[1,2-*b*:3,4-*b'*:5,6-*b''*]trithiophene (BTT) core was synthesized and added in a small amount to the Stille polymerization of CPDT and

Qx. Afterwards, both materials were characterized and applied as the donor component in BHJ OPV devices with PC<sub>71</sub>BM as the acceptor.

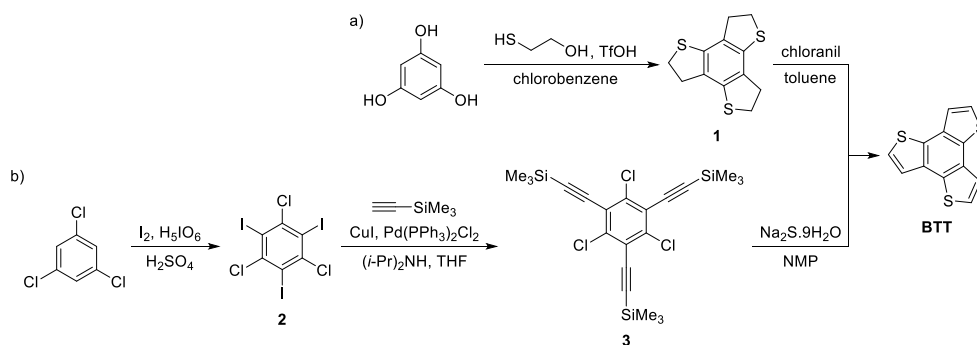
## 5.2 RESULTS AND DISCUSSION

### 5.2.1 Monomer synthesis

The distannylated CPDT monomer **M1** (2,6-bis(trimethylstannyl)-4-(2'-ethylhexyl)-4-octyl-4*H*-cyclopenta[2,1-*b*:3,4-*b'*]dithiophene) and dibrominated Qx monomer **M2** (5,8-dibromo-6,7-difluoro-2,3-bis(thiophen-2'-yl)quinoxaline) were synthesized as described before.<sup>[16,17]</sup> For the CPDT monomer, an optimized synthesis protocol was used, allowing a smooth introduction of asymmetric alkyl side chains.<sup>[18,19]</sup> On the other hand, the Qx monomer is substituted with two thienyl groups to slightly extend the absorption spectrum of the low bandgap alternating copolymer.<sup>[20]</sup> Furthermore, this Qx monomer is also equipped with two fluorine atoms. This results in a decrease in the HOMO level of the low bandgap alternating copolymer and hence an increase of the  $V_{OC}$  of the resulting OPV devices.<sup>[17]</sup>

For the synthesis of the trifunctional benzotrithiophene core, two different procedures were explored. First of all, the two-step synthesis route of Rungtaweeworanit *et al.* was followed to prepare BTT (Scheme 1a).<sup>[21]</sup> In a first step, 2-mercaptoethanol and trifluoromethanesulfonic acid (TfOH) were added to 1,3,5-trihydroxybenzene to obtain the ring-closed product **1**. In the second step, this compound was oxidized with chloranil to deliver the BTT core. The main drawback of this procedure was the very low overall yield (below 1%). Next to this, the three-step synthesis procedure of Kashiki *et al.* was also performed (Scheme 1b).<sup>[22,23]</sup> In this case, the starting material is 1,3,5-trichlorobenzene,

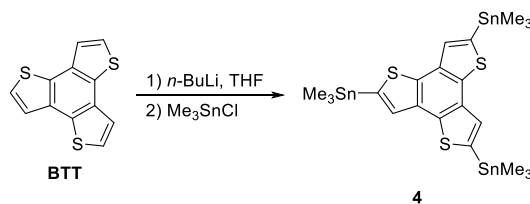
which was iodinated on the free positions to yield product **2**. Then, these iodide groups were replaced by trimethylsilylacetylene moieties by performing a Sonogashira cross-coupling, resulting in product **3**. In the last step, this product was ring-closed by adding sodium sulfide and letting it react overnight at 180 °C in *N*-methyl-2-pyrrolidone (NMP). *N,N*-dimethylformamide was explored as an alternative solvent, but this reaction did not afford any product. The reaction was also tested at lower temperatures and shorter reaction times under microwave irradiation in an attempt to elevate the reaction yield. The yields could not be improved, but it was observed that longer reaction times were beneficial to obtain more product. The overall reaction yield obtained with this three-step synthesis route was 20%, making this the method of choice for synthesizing larger quantities of the BTT core.



**Scheme 1:** Synthesis of BTT according to the procedure of a) Rungtaweearonit *et al.*<sup>[21]</sup> and b) Kashiki *et al.*<sup>[22,23]</sup>

To be able to introduce some branching during the polymerization, the BTT core still had to undergo one reaction to incorporate three reactive end groups. Since, in general, best results are obtained for Stille polymerizations by combining distannylated electron rich monomers with dihalogenated electron deficient monomers,<sup>[24]</sup> we decided to decorate the BTT core with three stannyl groups

(Scheme 2). This was done by first adding 1 equivalent (eq.) of *n*-BuLi at -10 °C to the BTT core and letting it react for 30 minutes, whereupon 1 eq. of trimethyltin chloride was added and the reaction was stirred for another 15 minutes. Afterwards, again 1 eq. of both reagents was added successively in the same way, followed by a final 3.5 eq. of *n*-BuLi and 4 eq. of trimethyltin chloride. This stepwise approach was followed to ensure good conversion to the tristannylated compound **4**. After purification by preparative size-exclusion chromatography (prep-SEC) and subsequent recrystallization, the pure trifunctional BTT core **4** was obtained. The yield of this reaction was, however, not impressive since there was still a considerable amount of mono- and distannylated product present in the reaction mixture after reaction work-up.

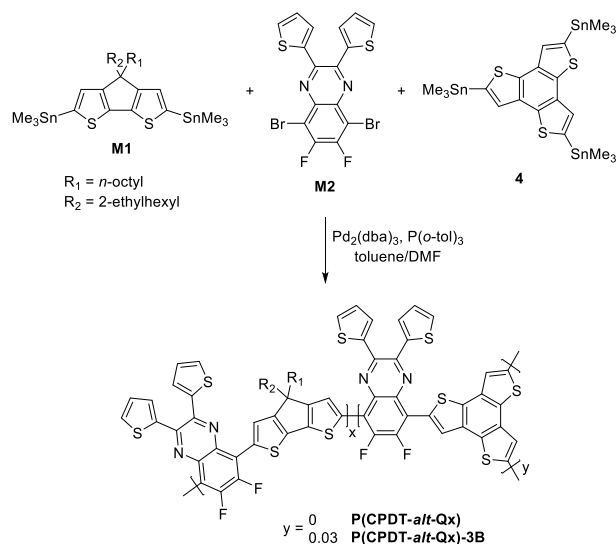


**Scheme 2:** Synthesis of the tristannylated BTT core.

### 5.2.2 Polymer synthesis and characterization

The linear **P(CPDT-*alt*-Qx)** copolymer (poly{(4-(2'-ethylhexyl)-4-octyl-4*H*-cyclopenta[2,1-*b*:3,4-*b'*]-dithiophene-2,6-diyl)-*alt*-(6,7-difluoro-2,3-bis[thiophen-2'-yl]quinoxaline-5,8-diyl)}) was synthesized by adding Pd<sub>2</sub>(dba)<sub>3</sub>/P(*o*-tol)<sub>3</sub> to equimolar amounts of **M1** and **M2** and leaving the reaction overnight at 110 °C (Scheme 3). Afterwards, the polymerization mixture was extracted with an aqueous sodium *N,N*-diethyldithiocarbamate solution to remove traces of the Pd catalyst.<sup>[25]</sup> Then, the polymer was precipitated in MeOH, filtered over a Soxhlet thimble and purified by Soxhlet extractions with MeOH, acetone,

hexanes and chloroform, respectively. The chloroform fraction was concentrated and precipitated in MeOH, finally yielding the linear **P(CPDT-*alt*-Qx)** copolymer as a greenish-black solid. The 3% branched **P(CPDT-*alt*-Qx)-3B** copolymer was obtained in the same way by replacing 3 mol% of **M1** with 3 mol% of **4**, also resulting in a greenish-black solid after purification. The obtained branched copolymer was still soluble in chloroform, but to a lesser extent, which suggests that indeed some branching occurred.



**Scheme 3:** Stille polymerization to achieve the linear and branched **P(CPDT-*alt*-Qx)** copolymers.

This decreased solubility was also observed during the preparation of SEC samples in chlorobenzene, since some of the branched copolymer remained on the filter, which was not the case for the linear copolymer. The results of the SEC measurements are depicted in Figure 1. In the SEC curve of the branched **P(CPDT-*alt*-Qx)-3B** copolymer, a broad shoulder arises in the high molar mass region. The appearance of these high molar masses can (to some extent) be attributed to aggregation of the polymer chains. This broadening leads to a rise in

dispersity ( $\mathcal{D}$ ) from 1.81 to 3.09 and also the number-average molar mass ( $M_n$ ) is elevated from 31 to 43 kg/mol. The dashed SEC profile depicted in Figure 1 belongs to the linear **P(CPDT-*alt*-Qx)** copolymer after prep-SEC, which was performed to remove the lower molar mass fraction. It has already been established that the molar mass and dispersity can strongly influence the performance of BHJ polymer solar cells.<sup>[26-30]</sup> It is this linear **P(CPDT-*alt*-Qx)** copolymer (after prep-SEC) with a  $M_n$  of 50 kg/mol and a  $\mathcal{D}$  of 1.42 that was used for all further characterizations and the preparation of the OPV devices. Due to the decreased solubility of the **P(CPDT-*alt*-Qx)-3B** copolymer, prep-SEC could not be performed on the branched copolymer.

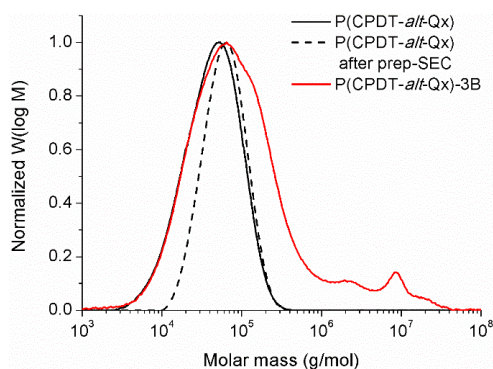


**Figure 1:** SEC profiles of the linear and branched **P(CPDT-*alt*-Qx)** copolymers.

The optical properties of the two polymers were analyzed by UV-vis-NIR absorption spectroscopy (Figure 2). As expected, the optical characteristics of the branched **P(CPDT-*alt*-Qx)-3B** copolymer do not differ much from that of the linear **P(CPDT-*alt*-Qx)** copolymer. The wavelength at maximal absorbance ( $\lambda_{\max}$ ) lies around 690 nm for all measurements (in solution and thin film; Table 1).

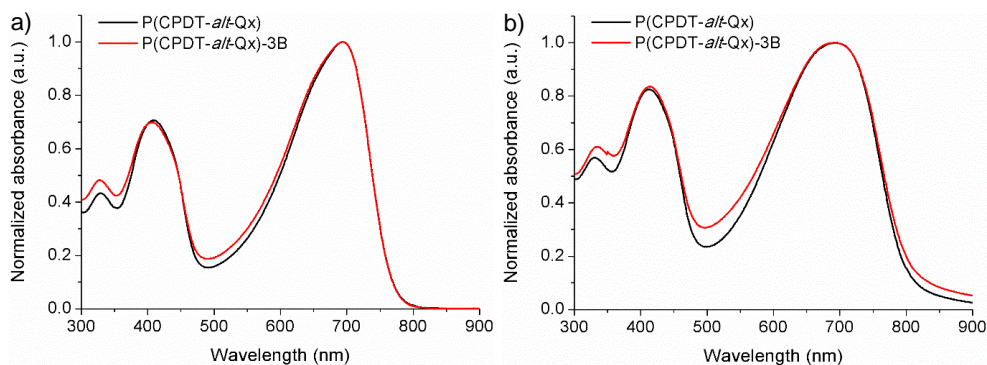


**Figure 2:** UV-vis-NIR absorption spectra of the linear and branched **P(CPDT-*alt*-Qx)** copolymers in a)  $\text{CHCl}_3$  solution and b) thin film.

The electrochemical properties of the polymers were investigated by cyclic voltammetry (CV) and the results are shown in Table 1. The HOMO and LUMO energy levels were estimated from the onset of the oxidation and reduction peaks, respectively. From these results, it is clear that the electrochemical properties of the linear **P(CPDT-*alt*-Qx)** and branched **P(CPDT-*alt*-Qx)-3B** copolymer are also pretty similar.

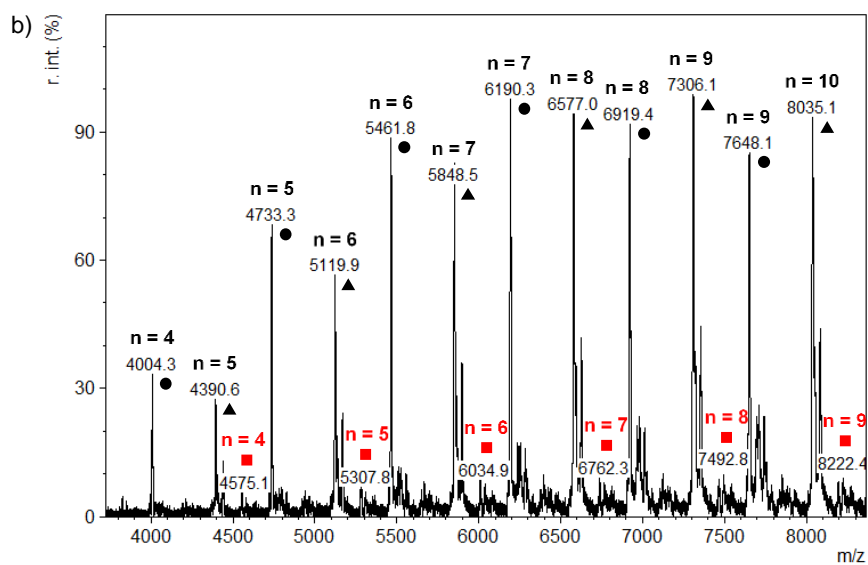
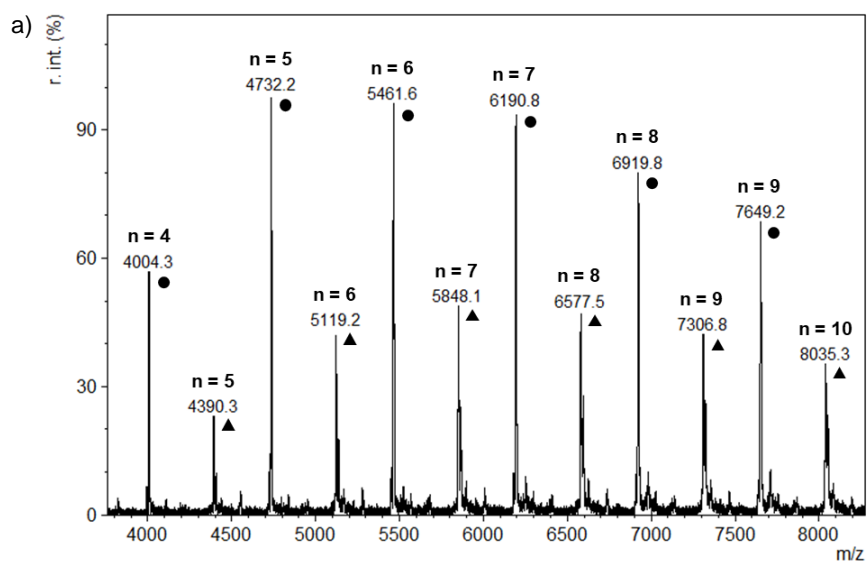
**Table 1:** Optical and electrochemical properties of the linear and branched **P(CPDT-*alt*-Qx)** copolymers.

Polymer	$\lambda_{\text{max, solution}}$ (nm)	$\lambda_{\text{max, film}}$ (nm)	$E_{\text{g, opt}}$ (eV) <sup>a</sup>	HOMO (eV) <sup>b</sup>	LUMO (eV) <sup>b</sup>	$E_{\text{g, EC}}$ (eV) <sup>c</sup>
<b>P(CPDT-<i>alt</i>-Qx)</b>	694	693	1.55	-5.27	-3.35	1.92
<b>P(CPDT-<i>alt</i>-Qx)-3B</b>	693	691	1.55	-5.30	-3.34	1.96

<sup>a</sup> Optical bandgap, determined by the onset of the solid-state UV-vis-NIR absorption spectrum. <sup>b</sup> Determined by CV from the onset potential of the anodic/cathodic scan. <sup>c</sup> Electrochemical bandgap.

One of the main reasons why we chose for **P(CPDT-*alt*-Qx)** to study the effect of branching was its very good solubility, which is particularly advantageous in terms of structural characterization. Both copolymers were thus also characterized

by  $^1\text{H}$  NMR spectroscopy (Figures S2–S3, Supporting Information). Since there is only 3% of the BTT core present in the branched **P(CPDT-*alt*-Qx)-3B** copolymer, no clear difference could, however, be observed. In a final attempt to prove that the BTT branching unit was indeed incorporated, MALDI-TOF (matrix-assisted laser desorption ionization - time of flight) mass spectrometry measurements were performed on both copolymers. For the linear **P(CPDT-*alt*-Qx)** copolymer, two main distributions are present (Figure 3a). The distribution with the highest intensity (marked by the black dots) corresponds to the linear polymer chains with two methylated Qx end groups. The other distribution (marked by the black triangles) can be correlated to the linear polymer chains with a methylated Qx and a destannylated CPDT unit as the end groups (Figure 3c). In case of the branched **P(CPDT-*alt*-Qx)-3B** copolymer, these two distributions are again mainly represented. An important observation was, however, the appearance of another distribution amongst the smaller intensity peaks, marked by the red squares (Figure 3b). This distribution could be assigned to the branched polymer chains with an integrated BTT core and two methylated Qx units and one CPDT unit as the end groups (Figure 3c). From these differences in the MALDI-TOF MS spectra, it could be concluded that the BTT core was indeed incorporated in some of the polymer chains of the **P(CPDT-*alt*-Qx)-3B** copolymer.



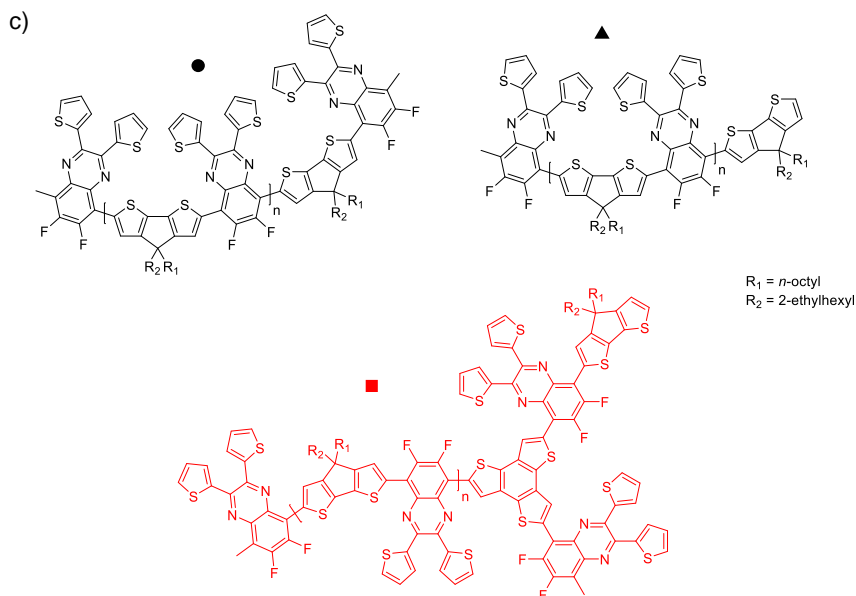


**Figure 3:** MALDI-TOF MS spectra of a) **P(CPDT-*alt*-Qx)** and b) **P(CPDT-*alt*-Qx)-3B**, whereby the relative intensity (r. int.) in % is expressed in function of the mass-to-charge ratio ( $m/z$ ) in Da. The chemical structures of the assigned peaks are represented in c). For the structures depicted with a red square, the position of the branching point is tentatively assigned.

### 5.2.3 Photovoltaic properties

Since the multidimensional conjugation and the aggregation tendency of the branched copolymer could lead to more isotropic charge transport and favorable active layer morphologies, it was investigated which influence branching has on the photovoltaic properties. To this extent, BHJ organic solar cells with a standard device architecture consisting of glass/ITO/PEDOT:PSS/polymer:PC<sub>71</sub>BM/Ca/Al were prepared and characterized. Devices based on the linear **P(CPDT-*alt*-Qx)** copolymer were previously optimized.<sup>[16]</sup> One of the best results was obtained for a 1:3 polymer:PC<sub>71</sub>BM ratio and spin-coating from a chloroform + 10% *ortho*-dichlorobenzene solution of the two components (Table 2). These processing conditions were also used for the device optimization of the branched **P(CPDT-**

***alt-Qx*-3B** copolymer. The OPV results are summarized in Table 2 and Figure 4. The  $V_{OC}$  values were almost identical, which could be expected due to the similar backbone of the linear and branched copolymer. Also the FF (fill factor) and  $J_{SC}$  (short-circuit current density) values did not differ much, leading to pretty similar PCE values of 3.92 and 4.00% for the average performing devices containing **P(CPDT-*alt-Qx*)** and **P(CPDT-*alt-Qx*)-3B**, respectively.

**Table 2:** Photovoltaic parameters for the linear and branched copolymers in BHJ solar cells with a standard configuration glass/ITO/PEDOT:PSS/polymer:PC<sub>71</sub>BM/Ca/Al.

Polymer	Processing solvent <sup>a</sup>	$V_{OC}$ (V)	$J_{SC}$ (mA/cm <sup>2</sup> )	FF	Avg. $\eta$ (%) <sup>b</sup>	Best $\eta$ (%)
<b>P(CPDT-<i>alt-Qx</i>)</b>	CF + 10% ODCB	0.77 $\pm 0.00$	10.05 $\pm 0.38$	0.51 $\pm 0.00$	3.92 $\pm 0.15$	4.04
<b>P(CPDT-<i>alt-Qx</i>)-3B</b>	CF + 10% ODCB	0.78 $\pm 0.00$	9.91 $\pm 0.42$	0.52 $\pm 0.00$	4.00 $\pm 0.17$	4.20

<sup>a</sup> CF = chloroform and ODCB = *ortho*-dichlorobenzene. <sup>b</sup> Average PCE over at least 4 devices.

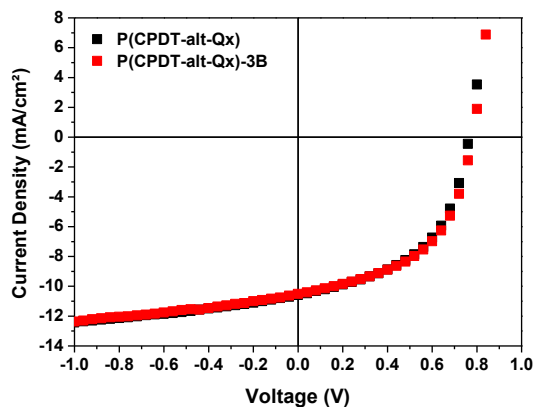


**Figure 4:**  $J$ - $V$  curves under illumination for average performing BHJ photovoltaic devices based on **P(CPDT-*alt-Qx*)** and **P(CPDT-*alt-Qx*)-3B**.

Atomic force microscopy (AFM) topography imaging was then performed to investigate whether the incorporation of the BTT core had an influence on the

morphology of the photoactive layer. From the resulting images in Figure 5, it is clear that in both cases a finely intermixed polymer:PC<sub>71</sub>BM network was obtained and no significant morphological changes were observed between the photoactive layers based on the linear and branched copolymer, which is in agreement with their similar solar cell performances (Table 2).

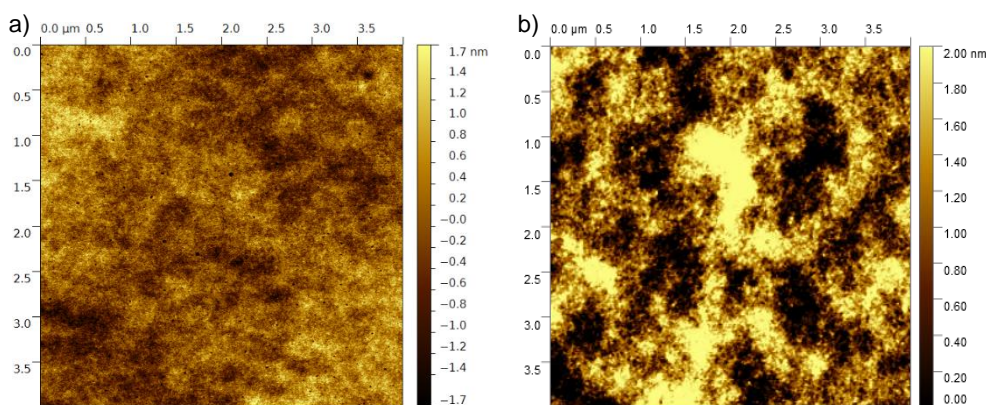


**Figure 5:** AFM topography images (4 x 4  $\mu\text{m}$ ) of the photoactive layers of the BHJ solar cells based on a) **P(CPDT-*alt*-Qx)**:PC<sub>71</sub>BM and b) **P(CPDT-*alt*-Qx)-3B**:PC<sub>71</sub>BM.

### 5.3 CONCLUSIONS

The introduction of branches in a linear alternating donor-acceptor copolymer (**P(CPDT-*alt*-Qx)**) was achieved by adding a small amount (3%) of a trifunctional benzotrithiophene core to the Stille polymerization of 4*H*-cyclopenta[2,1-*b*:3,4-*b'*]dithiophene and quinoxaline, resulting in the branched **P(CPDT-*alt*-Qx)-3B** copolymer. Both copolymers were characterized and, as expected, their optical and electrochemical properties did not differ much. The SEC profile of the branched copolymer did, however, show the appearance of a broad shoulder in the high molar mass region, resulting in an increase in molar mass and dispersity

when going from the linear to the branched copolymer. Together with the differences in the MALDI-TOF MS spectra, this led to the conclusion that the benzotrithiophene core was indeed incorporated to some extent in the copolymer chains.

Both copolymers were then applied as the donor component in BHJ organic solar cells with a standard device architecture to investigate the influence of branching on the device performance. From these measurements, it was clear that all photovoltaic parameters ( $V_{oc}$ ,  $J_{sc}$ , FF) remained almost identical upon incorporation of the BTT core. On top of that, no significant morphological changes were observed in the AFM topography images of the photoactive layers containing **P(CPDT-*alt*-Qx)**:PC<sub>71</sub>BM and **P(CPDT-*alt*-Qx)-3B**:PC<sub>71</sub>BM. Both findings are consistent with the pretty similar average power conversion efficiencies of 3.92 and 4.00% for the devices based on the linear and branched copolymer, respectively. Since the incorporation of only 3% of the benzotrithiophene core did not really have an impact on the polymer or photovoltaic properties, it would be interesting to investigate whether the implementation of a higher amount of the branching unit would lead to more significant differences.

## 5.4 REFERENCES

- [1] Cao, W.; Xue, J. *Energy Environ. Sci.* **2014**, *7*, 2123–2144.
- [2] Lu, L.; Zheng, T.; Wu, Q.; Schneider, A. M.; Zhao, D.; Yu, L. *Chem. Rev.* **2015**, *115*, 12666–12731.
- [3] Mazzio, K. A.; Luscombe, C. K. *Chem. Soc. Rev.* **2015**, *44*, 78–90.
- [4] Darling, S. B.; You, F. *RSC Adv.* **2013**, *3*, 17633–17648.

- [5] Li, S.; Ye, L.; Zhao, W.; Zhang, S.; Mukherjee, S.; Ade, H.; Hou, J. *Adv. Mater.* **2016**, *28*, 9423–9429.
- [6] Yang, Y.; Zhang, Z.-G.; Bin, H.; Chen, S.; Gao, L.; Xue, L.; Yang, C.; Li, Y. *J. Am. Chem. Soc.* **2016**, *138*, 15011–15018.
- [7] Liu, Y.; Zhao, J.; Li, Z.; Mu, C.; Ma, W.; Hu, H.; Jiang, K.; Lin, H.; Ade, H.; Yan, H. *Nat. Commun.* **2014**, *5*, 5293.
- [8] He, Z.; Zhong, C.; Su, S.; Xu, M.; Wu, H.; Cao, Y. *Nat. Photonics* **2012**, *6*, 591–595.
- [9] Hu, H.; Jiang, K.; Yang, G.; Liu, J.; Li, Z.; Lin, H.; Liu, Y.; Zhao, J.; Zhang, J.; Huang, F.; Qu, Y.; Ma, W.; Yan, H. *J. Am. Chem. Soc.* **2015**, *137*, 14149–14157.
- [10] Houston, J. E.; Richeter, S.; Clément, S.; Evans, R. C. *Polym. Int.* **2017**, DOI: 10.1002/pi.5397.
- [11] Liang, N.; Jiang, W.; Hou, J.; Wang, Z. *Mater. Chem. Front.* **2017**, *1*, 1291–1303.
- [12] Mangold, H. S.; Richter, T. V.; Link, S.; Würfel, U.; Ludwigs, S. *J. Phys. Chem. B* **2012**, *116*, 154–159.
- [13] Roncali, J.; Leriche, P.; Cravino, A. *Adv. Mater.* **2007**, *19*, 2045–2060.
- [14] Guo, M.; Hayakawa, T.; Kakimoto, M.; Goodson, T. *J. Phys. Chem. B* **2011**, *115*, 13419–13432.
- [15] Heintges, G. H. L.; van Franeker, J. J.; Wienk, M. M.; Janssen, R. A. J. *Chem. Commun.* **2016**, *52*, 92–95.
- [16] Verstappen, P.; Kesters, J.; D’Olieslaeger, L.; Drijkoningen, J.; Cardinaletti, I.; Vangerven, T.; Bruijnaers, B. J.; Willems, R. E. M.; D’Haen, J.; Manca, J. V.; Lutsen, L.; Vanderzande, D. J. M.; Maes, W. *Macromolecules* **2015**, *48*, 3873–3882.

- [17] Verstappen, P.; Kesters, J.; Vanormelingen, W.; Heintges, G. H. L.; Drijkoningen, J.; Vangerven, T.; Marin, L.; Koudjina, S.; Champagne, B.; Manca, J.; Lutsen, L.; Vanderzande, D.; Maes, W. *J. Mater. Chem. A* **2015**, *3*, 2960–2970.
- [18] Vanormelingen, W.; Verstappen, P.; Maes, V.; Bevk, D.; Lutsen, L.; Vanderzande, D.; Maes, W. *Synlett* **2013**, *24*, 2389–2392.
- [19] Van Mierloo, S.; Adriaenssens, P. J.; Maes, W.; Lutsen, L.; Cleij, T. J.; Botek, E.; Champagne, B.; Vanderzande, D. *J. Org. Chem.* **2010**, *75*, 7202–7209.
- [20] Marin, L.; Lutsen, L.; Vanderzande, D.; Maes, W. *Org. Biomol. Chem.* **2013**, *11*, 5866–5876.
- [21] Rungtaweivoranit, B.; Butsuri, A.; Wongma, K.; Sadorn, K.; Neranon, K.; Nerungsi, C.; Thongpanchang, T. *Tetrahedron Lett.* **2012**, *53*, 1816–1818.
- [22] Kashiki, T.; Shinamura, S.; Kohara, M.; Miyazaki, E.; Takimiya, K.; Ikeda, M.; Kuwabara, H. *Org. Lett.* **2009**, *11*, 2473–2475.
- [23] Sonoda, M.; Inaba, A.; Itahashi, K.; Tobe, Y. *Org. Lett.* **2001**, *3*, 2419–2421.
- [24] Bao, Z.; Chan, W. K.; Yu, L. *J. Am. Chem. Soc.* **1995**, *117*, 12426–12435.
- [25] Shahid, M.; Ashraf, R. S.; Huang, Z.; Kronemeijer, A. J.; McCarthy-Ward, T.; McCulloch, I.; Durrant, J. R.; Siringhaus, H.; Heeney, M. *J. Mater. Chem.* **2012**, *22*, 12817–12823.
- [26] Spoltore, D.; Vangerven, T.; Verstappen, P.; Piersimoni, F.; Bertho, S.; Vandewal, K.; Van den Brande, N.; Defour, M.; Van Mele, B.; De Sio, A.; Parisi, J.; Lutsen, L.; Vanderzande, D.; Maes, W.; Manca, J. V. *Org. Electron.* **2015**, *21*, 160–170.

- [27] Vangerven, T.; Verstappen, P.; Drijkoningen, J.; Dierckx, W.; Himmelberger, S.; Salleo, A.; Vanderzande, D.; Maes, W.; Manca, J. V. *Chem. Mater.* **2015**, *27*, 3726–3732.
- [28] Bartelt, J. A.; Douglas, J. D.; Mateker, W. R.; El Labban, A.; Tassone, C. J.; Toney, M. F.; Fréchet, J. M. J.; Beaujuge, P. M.; McGehee, M. D. *Adv. Energy Mater.* **2014**, *4*, 1301733.
- [29] Li, W.; Yang, L.; Tumbleston, J. R.; Yan, L.; Ade, H.; You, W. *Adv. Mater.* **2014**, *26*, 4456–4462.
- [30] van Franeker, J. J.; Heintges, G. H. L.; Schaefer, C.; Portale, G.; Li, W.; Wienk, M. M.; van der Schoot, P.; Janssen, R. A. J. *J. Am. Chem. Soc.* **2015**, *137*, 11783–11794.

## 5.5 SUPPORTING INFORMATION

### 5.5.1 Reagents and instrumentation

All reagents and chemicals were obtained from commercial sources and used without further purification. THF, DMF and toluene were dried using a solvent purification system (MBraun MB-SPS 800). Microwave synthesis was performed using a CEM Discover SP synthesis platform.  $^1\text{H}$  NMR chemical shifts ( $\delta$ , in ppm) were determined relative to the residual  $^1\text{H}$  signal of  $\text{CHCl}_3$  (7.26 ppm). Analysis of the molar masses and distributions of the polymer samples was performed by size-exclusion chromatography (SEC), using a Spectra Series P100 pump equipped with two mixed-B columns (10  $\mu\text{m}$ , 2 cm  $\times$  30 cm, Polymer Laboratories) and an Agilent 1100 diode array detector with chlorobenzene as an eluent at 60  $^\circ\text{C}$  and a flow rate of 1.0 mL/min. The SEC system was calibrated using linear narrow polystyrene standards ranging from 474 to  $7.5 \times 10^6$  g/mol ( $K = 14.1 \times 10^{-5}$  dL/g and  $\alpha = 0.70$ ). Prep-SEC was performed on a JAI LC-9110 NEXT system equipped with JAIGEL 2H and 3H columns (eluent  $\text{CHCl}_3$ , flow rate 3.5 mL/min). MALDI-TOF mass spectra were recorded on a Bruker Daltonics Ultraflex II ToF/ToF. 1  $\mu\text{L}$  of the matrix solution (4 mg/mL DCTB (*trans*-2-[3-(4-*tert*-butylphenyl)-2-methyl-2-propenylidene]malononitrile) in  $\text{CHCl}_3$ ) was spotted onto an MTP Anchorchip 600/384 MALDI plate. The spot was allowed to dry and 1  $\mu\text{L}$  of the analyte solution (0.5 mg/mL in  $\text{CHCl}_3$ ) was spotted on top of the matrix. Background corrected UV-Vis-NIR absorption spectra were recorded on a Cary 5000 UV-Vis-NIR spectrophotometer from Agilent using a band width of 2 nm, full slit height and a scan speed of 600 nm/min. Electrochemical measurements were performed with an Eco Chemie Autolab PGSTAT 30 potentiostat using a three-electrode microcell setup with a platinum wire working electrode, a platinum wire

counter electrode, a Ag/AgNO<sub>3</sub> reference electrode (silver wire in 0.01 M AgNO<sub>3</sub> / 0.1 M NBu<sub>4</sub>PF<sub>6</sub> in anhydrous acetonitrile) and (argon degassed) anhydrous acetonitrile containing 0.1 M NBu<sub>4</sub>PF<sub>6</sub> as the electrolyte. The system was calibrated against ferrocene/ferrocenium. Experiments were carried out under a constant flow of argon over the electrolyte surface. The polymer samples were dissolved in CHCl<sub>3</sub>. The working electrode was dipped into this solution and dried at room temperature in air before the measurement. Cyclic voltammograms were recorded at a scan rate of 100 mV/s. The HOMO-LUMO energy levels of the polymers were estimated using the obtained CV data. For the conversion of V to eV, the onset potentials of the first oxidation/reduction peaks were used and referenced to ferrocene/ferrocenium, which has an ionization potential of -4.98 eV vs. vacuum. This correction factor is based on a value of 0.31 eV for Cp<sub>2</sub>Fe/Cp<sub>2</sub>Fe<sup>+</sup> vs. a saturated calomel electrode (SCE)<sup>[1]</sup> and a value of 4.68 eV for SCE vs. vacuum:<sup>[2]</sup>

$$E_{\text{HOMO}} \text{ (eV)} = -4.98 - E_{\text{onset, ox}}^{\text{Ag/AgNO}_3} \text{ (V)} + E_{\text{onset, Fc/Fc}^+}^{\text{Ag/AgNO}_3} \text{ (V)}$$

$$E_{\text{LUMO}} \text{ (eV)} = -4.98 - E_{\text{onset, red}}^{\text{Ag/AgNO}_3} \text{ (V)} + E_{\text{onset, Fc/Fc}^+}^{\text{Ag/AgNO}_3} \text{ (V)}$$

The accuracy of measuring redox potentials by CV is about 0.01–0.02 V. Reproducibility can be less because the potentials depend on concentration and temperature.

### 5.5.2 Photovoltaic device fabrication and characterization

*Device fabrication:* Bulk heterojunction polymer solar cells were fabricated using the standard architecture glass/ITO/PEDOT:PSS/polymer:PC<sub>71</sub>BM/Ca/Al. Prior to device construction, the prepatterned indium tin oxide (ITO, Kintec, 100 nm, 20 Ohm/sq) containing glass substrates were thoroughly cleaned using soap, demineralized water, acetone, isopropanol and a UV/O<sub>3</sub> treatment. Consequently,

a thin layer of PEDOT:PSS [poly(3,4-ethylenedioxythiophene):poly(styrenesulfonic acid), Heraeus Clevios] was deposited by spin-coating with a thickness of ~30 nm, followed by an annealing step at 130 °C for 15 mins to remove residual water. Further processing was carried out under nitrogen atmosphere in a glovebox ( $O_2/H_2O < 0.1$  ppm). The polymer:PC<sub>71</sub>BM active layer blend solution was spin-coated on top of PEDOT:PSS at a total concentration of 5 mg/mL in CF (+ 10% ODCB) with a polymer:fullerene ratio of 1:3. Finally, the devices were finished off with Ca/Al (~30/80 nm). In this way an active area of ~3 mm<sup>2</sup> was obtained.

*Device characterization:* The *J-V* curves under illumination and dark conditions for the polymer solar cells were obtained using a Newport class A solar simulator (model 91195A) calibrated with a silicon solar cell to give an AM 1.5G spectrum. AFM experiments were performed with a JPK NanoWizard 3 AFM (JPK Instruments AG, Berlin, Germany) using AC mode in air. Silicon ACTA-50 tips from AppNano with cantilever length ~125 mm, spring constant ~40 N/m and resonance frequency ~300 kHz were used. The scan angle, set point height, gain values and scan rate were adjusted according to the calibration of the AFM tip.

### 5.5.3 Monomer synthesis

2,6-Bis(trimethylstannyl)-4-(2'-ethylhexyl)-4-octyl-4*H*-cyclopenta[2,1-*b*:3,4-*b'*]dithiophene (**M1**),<sup>[3]</sup> 5,8-dibromo-6,7-difluoro-2,3-bis(thiophen-2'-yl)quinoxaline (**M2**)<sup>[4]</sup> and benzo[1,2-*b*:3,4-*b'*:5,6-*b''*]trithiophene (BTT)<sup>[5,6]</sup> were synthesized according to literature procedures.

**2,5,8-tris(trimethylstannyl)benzo[1,2-*b*:3,4-*b'*:5,6-*b''*]trithiophene (4)**

BTT (0.200 g, 0.81 mmol) was dissolved in dry THF (10 mL) and the solution was cooled down to -10 °C, followed by a dropwise addition of *n*-BuLi (0.32 mL, 0.81 mmol, 2.5 M in hexanes). After stirring for 30 min at -10 °C, trimethyltin chloride (0.81 mL, 0.81 mmol, 1.0 M in hexanes) was added dropwise and the mixture was stirred for another 15 min at -10 °C. Then, again 1 equivalent of *n*-BuLi (0.32 mL, 0.81 mmol, 2.5 M in hexanes) and trimethyltin chloride (0.81 mL, 0.81 mmol, 1.0 M in hexanes) were added successively in the same way, whereupon a final 3.5 equivalents of *n*-BuLi (1.14 mL, 2.84 mmol, 2.5 M in hexanes) and 4 equivalents of trimethyltin chloride (3.25 mL, 3.25 mmol, 1.0 M in hexanes) were added. The resulting solution was allowed to gently warm to room temperature overnight. The reaction was quenched with water and the mixture was extracted with diethyl ether. The organic phase was washed with brine, dried with MgSO<sub>4</sub>, filtered and the solvents were evaporated under reduced pressure. The crude mixture was purified via prep-SEC, followed by a recrystallization from a MeOH/hexanes (4/1) mixture to yield the pure product as white needles (45 mg, 8%). <sup>1</sup>H NMR (400 MHz, CDCl<sub>3</sub>): δ 7.69 (s, 3H), 0.47 (s, 27H).

**5.5.4 Polymer synthesis**

**P(CPDT-*alt*-Qx)**

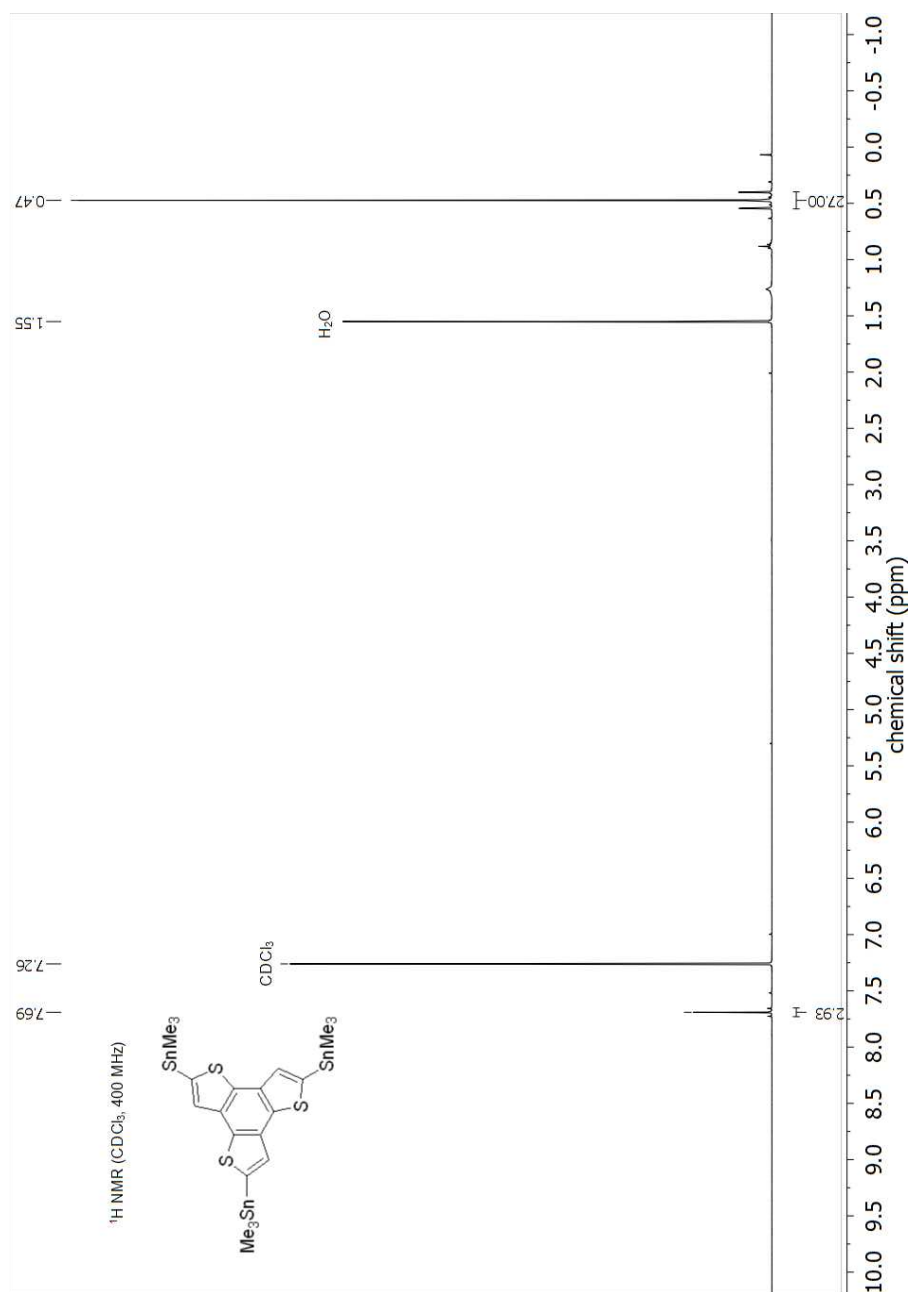
CPDT monomer **M1** (0.157 g, 0.216 mmol), Qx monomer **M2** (0.106 g, 0.216 mmol), Pd<sub>2</sub>(dba)<sub>3</sub> (4.94 mg, 5.40 μmol), and P(*o*-tol)<sub>3</sub> (6.57 mg, 21.6 μmol) were dissolved in a mixture of dry toluene (5.0 mL) and dry DMF (1.2 mL). The mixture was purged with N<sub>2</sub> for 15 min and heated to 110 °C for 15 h. The resulting polymer mixture was diluted with CHCl<sub>3</sub>, added to an aqueous solution of sodium *N,N*-diethyldithiocarbamate, and the mixture was stirred for 2 h at 60 °C. After

separation from the aqueous layer, the organic phase was concentrated *in vacuo*, precipitated in MeOH and filtered off over a Soxhlet thimble. Soxhlet extractions were performed with MeOH, acetone, hexanes, and CHCl<sub>3</sub> (dissolving the polymer). The solvent was then evaporated under reduced pressure, and the obtained polymer was subjected to prep-SEC to remove the low molar mass fractions. The resulting polymer was precipitated in MeOH, filtered off over a PTFE membrane (47 mm/0.45 μm) and dried overnight under vacuum, finally yielding **P(CPDT-*alt*-Qx)** as a greenish-black solid (99 mg, 63%). <sup>1</sup>H NMR (400 MHz, CDCl<sub>3</sub>): δ = 8.25–7.97 (m, 2H), 7.68–7.46 (m, 4H), 7.20–7.07 (m, 2H), 2.08 (br, 4H), 1.27–0.93 (m, 21H), 0.81 (t, *J* = 6.7 Hz, 3H), 0.75–0.63 (m, 6H); UV-Vis (CHCl<sub>3</sub>): λ<sub>max</sub> = 694 nm, UV-Vis (film): λ<sub>max</sub> = 693 nm; SEC (CB, PS standards): before prep-SEC: *M*<sub>n</sub> = 3.1 × 10<sup>4</sup> g/mol, *M*<sub>w</sub> = 5.5 × 10<sup>4</sup> g/mol, *D* = 1.81; after prep-SEC: *M*<sub>n</sub> = 5.0 × 10<sup>4</sup> g/mol, *M*<sub>w</sub> = 7.1 × 10<sup>4</sup> g/mol, *D* = 1.42.

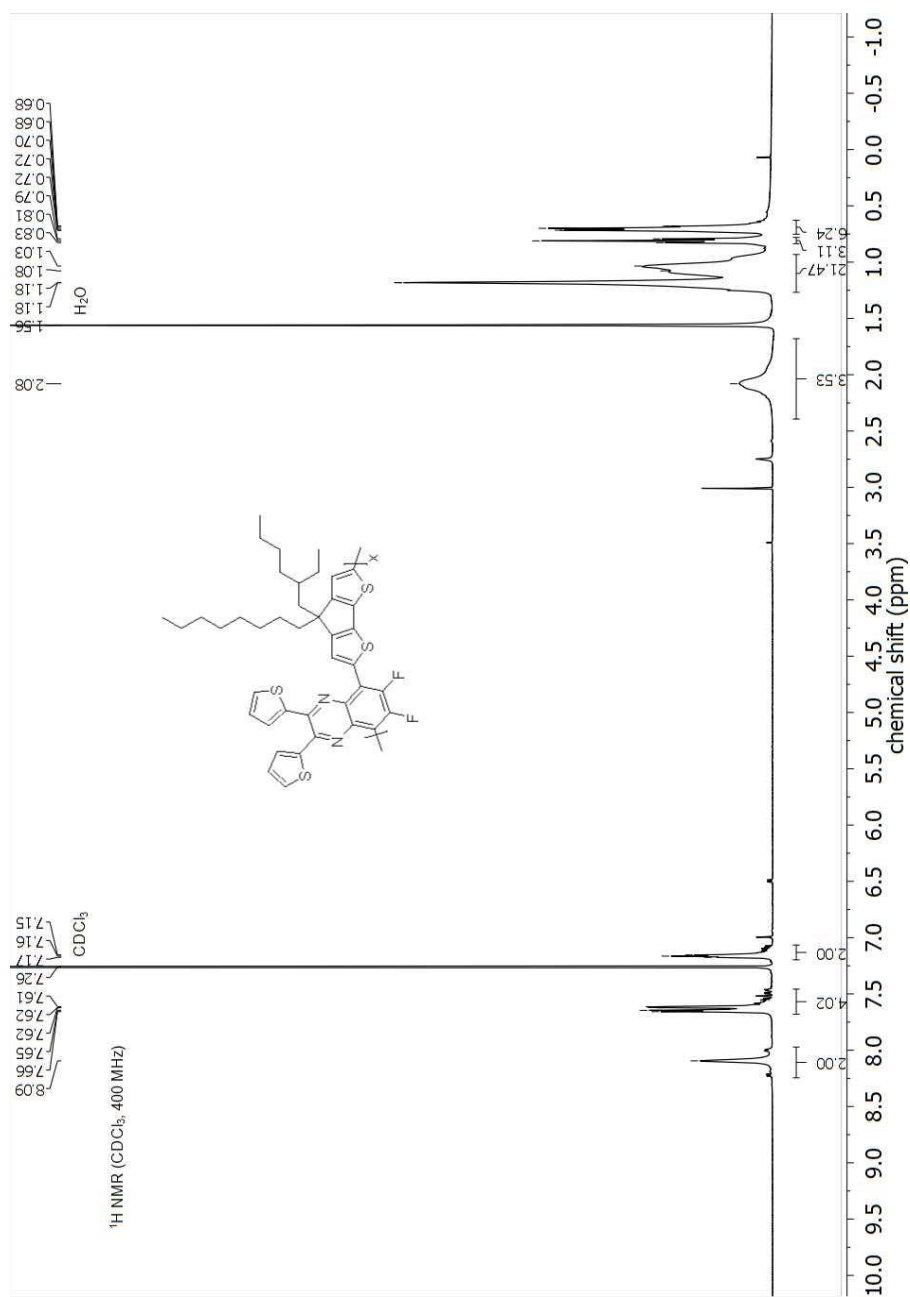
### **P(CPDT-*alt*-Qx)-3B**

Similar to the polymerization procedure of **P(CPDT-*alt*-Qx)**. CPDT monomer **M1** (0.084 g, 0.115 mmol), Qx monomer **M2** (0.058 g, 0.118 mmol), BTT core **4** (2.53 mg, 3.45 μmol), Pd<sub>2</sub>(dba)<sub>3</sub> (2.70 mg, 2.95 μmol), and P(*o*-tol)<sub>3</sub> (3.59 mg, 11.8 μmol) were dissolved in a mixture of dry toluene (2.0 mL) and dry DMF (0.4 mL). In this case, the polymer was not subjected to prep-SEC and the **P(CPDT-*alt*-Qx)-3B** copolymer was finally obtained as a greenish-black solid (76 mg, 89%). <sup>1</sup>H NMR (400 MHz, CDCl<sub>3</sub>): δ = 8.17–7.92 (m, 2H), 7.69–7.44 (m, 4H), 7.19–7.05 (m, 2H), 2.08 (br, 4H), 1.27–0.96 (m, 21H), 0.85 (t, *J* = 6.7 Hz, 3H), 0.78–0.68 (m, 6H); UV-Vis (CHCl<sub>3</sub>): λ<sub>max</sub> = 693 nm, UV-Vis (film): λ<sub>max</sub> = 691 nm; SEC (CB, PS standards): *M*<sub>n</sub> = 4.3 × 10<sup>4</sup> g/mol, *M*<sub>w</sub> = 13 × 10<sup>4</sup> g/mol, *D* = 3.09.

### 5.5.5 $^1\text{H}$ NMR spectra



**Figure S1:**  $^1\text{H}$  NMR spectrum of 2,5,8-tris(trimethylstannyl)benzo[1,2-*b*:3,4-*b'*:5,6-*b''*]trithiophene (**4**).

Figure S2: <sup>1</sup>H NMR spectrum of P(CPDT-*alt*-Qx).

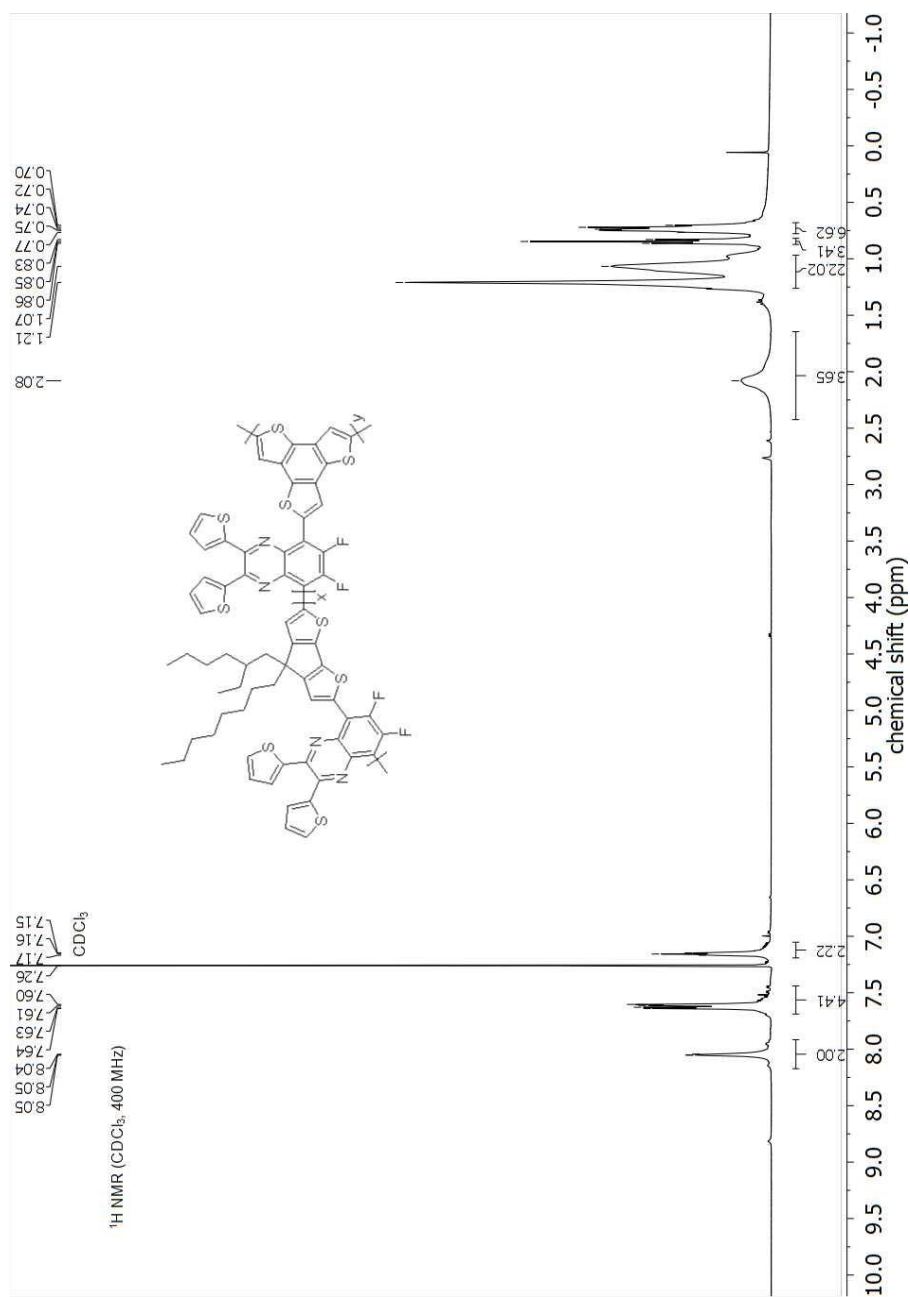


Figure S3: <sup>1</sup>H NMR spectrum of P(CPDT-*alt*-Qx)-3B.

### 5.5.6 References

- [1] Bard, A. J.; Faulkner, L. R. *Electrochemical Methods: Fundamentals and Applications, 2nd Edition*; Wiley, 2001.
- [2] Trasatti, S. *Pure Appl. Chem.* **1986**, *58*, 955–966.
- [3] Verstappen, P.; Kesters, J.; Vanormelingen, W.; Heintges, G. H. L.; Drijkoningen, J.; Vangerven, T.; Marin, L.; Koudjina, S.; Champagne, B.; Manca, J.; Lutsen, L.; Vanderzande, D.; Maes, W. *J. Mater. Chem. A* **2015**, *3*, 2960–2970.
- [4] Verstappen, P.; Kesters, J.; D’Olieslaeger, L.; Drijkoningen, J.; Cardinaletti, I.; Vangerven, T.; Bruijnaers, B. J.; Willems, R. E. M.; D’Haen, J.; Manca, J. V.; Lutsen, L.; Vanderzande, D. J. M.; Maes, W. *Macromolecules* **2015**, *48*, 3873–3882.
- [5] Rungtaweeworanit, B.; Butsuri, A.; Wongma, K.; Sadorn, K.; Neranon, K.; Nerungsi, C.; Thongpanchang, T. *Tetrahedron Lett.* **2012**, *53*, 1816–1818.
- [6] Kashiki, T.; Shinamura, S.; Kohara, M.; Miyazaki, E.; Takimiya, K.; Ikeda, M.; Kuwabara, H. *Org. Lett.* **2009**, *11*, 2473–2475.

---

# Chapter 6

## Summary and outlook

---

### 6.1 SUMMARY

Over the past two decades, organic photovoltaics (OPVs) have seen an increasing interest as an alternative renewable energy source, in particular because of some additional appealing features such as their light weight, flexibility, semi-transparency, and low-cost large area production. As a result of the extensive research in this domain, the power conversion efficiency (PCE) of OPV devices could be elevated to values currently exceeding 12%. To become viable for commercialization, however, organic solar cells still need to improve further in terms of production cost, efficiency, and stability. In this work, these last two parameters were addressed by three different approaches.

In a first part of this thesis, we have focused on the synthesis and characterization of ionic (co)polythiophenes, since the device efficiency can be boosted by incorporating these conjugated polyelectrolytes as cathode interlayers. Therefore, a series of imidazolium-substituted ionic (co)polythiophenes was synthesized via Kumada catalyst-transfer condensation polymerization (KCTCP) and subsequent introduction of the ionic moieties on the polymer side chains. Both the topology (i.e. homopolymers, random, and block copolymers) and the amount of ionic

groups were systematically varied. The polymers were fully characterized and then applied as cathode interlayers in polymer solar cells based on PCDTBT:PC<sub>71</sub>BM, thereby enhancing all photovoltaic parameters ( $V_{OC}$ ,  $J_{SC}$ , FF), which resulted into an average efficiency increase of ~15%. These findings were observed for the entire series of ionic (co)polythiophenes, indicating that the efficiency gain is a rather general phenomenon for this material class. On the other hand, the best photovoltaic responses were observed for the conjugated polyelectrolytes with a higher triethylene glycol side chain ratio and the block copolymer structure performed slightly better in comparison to the random copolymer with the same (50/50) monomer ratio.

Since the device efficiency is also influenced by the molar mass and dispersity of the donor material in the photoactive layer, it would be interesting if these parameters could be more carefully controlled. For this reason, the controlled synthesis of low bandgap alternating donor-acceptor copolymers was pursued via KCTCP in a second part of this thesis. A general approach was utilized, whereby a push-pull monomer consisting of a donor and an acceptor unit was synthesized first and subsequently polymerized via KCTCP using a nickel catalyst. As a proof of concept, first of all a thiophene was used as the donor component and a pyridine as the acceptor component, resulting into the alternating **P(3HT-*alt*-P)** copolymer after KCTCP. Moreover, a new all-conjugated block copolymer (**P3HT-*b*-P(3HT-*alt*-P)**) was also successfully formed in a one-pot KCTCP procedure by using an *in situ* formed poly(3-hexylthiophene) (**P3HT**) block to initiate the polymerization of the donor-acceptor alternating copolymer as the second block. The synthesized materials showed interesting fluorescence properties. To further explore this KCTCP of alternating donor-acceptor copolymers, another push-pull

monomer with a stronger acceptor unit (thienopyrazine) and the same donor unit (thiophene) was created and then polymerized via KCTCP, resulting into an alternating copolymer (**P(3HT-*alt*-TP)**) with a smaller bandgap. Furthermore, an all-conjugated **P3HT-*b*-P(3HT-*alt*-TP)** block copolymer was prepared in the same way. The synthesized copolymers showed interesting absorption profiles extending into the near-infrared region. In both cases, the alternating copolymers were obtained via a non-controlled chain-growth mechanism.

Finally, also the effect of branching was investigated since conjugation in two or three dimensions could lead to several advantages, such as isotropic charge transport, enhanced dielectric constants and favorable active layer morphologies. This pathway has rarely been explored and could have a significant impact on the device efficiency and stability. To this extent, a small amount of a trifunctional benzotrithiophene core was added to the Stille polymerization of an alternating cyclopentadithiophene-quinoxaline (donor-acceptor) copolymer, resulting in a branched copolymer (**P(CPDT-*alt*-Qx)-3B**). Afterwards, both the linear and branched alternating copolymers were characterized by MALDI-TOF MS, confirming the incorporation of the benzotrithiophene core in the copolymer chains. Furthermore, both copolymers were applied as the donor component in bulk heterojunction OPV devices with PC<sub>71</sub>BM as the acceptor component. From these measurements, it is clear that all photovoltaic parameters ( $V_{OC}$ ,  $J_{SC}$ , FF) remained almost identical upon incorporation of the benzotrithiophene core, which resulted into pretty similar average power conversion efficiencies of 3.92 and 4.00% for the devices based on the linear and branched copolymer, respectively.

## 6.2 OUTLOOK

In this work, we have demonstrated that the incorporation of imidazolium-substituted ionic (co)polythiophenes as cathode interlayers in BHJ organic solar cells is a successful way to boost the device efficiency by ~15%. Although this efficiency gain is a rather general phenomenon for this material class, the ionic block copolymer slightly outperforms the ionic random copolymer with the same (50/50) monomer ratio. Since it is known that control of the morphology is crucial for device performance and that block copolymers can self-assemble into nanostructured morphologies, it seems worthwhile to further explore this route to push the device efficiency to even higher values.

Another realization of this work is the successful synthesis of two different alternating donor-acceptor copolymers via KCTCP. Although the molar masses could not be controlled, pretty low dispersities were obtained and all-conjugated block copolymers could be successfully synthesized via a one-pot procedure. The **P3HT-*b*-P(3HT-*alt*-P)** block copolymer and especially the **P(3HT-*alt*-P)** alternating copolymer show high fluorescence quantum yields of 62 and 89%, respectively, making them attractive candidates for bio-imaging applications. The **P(3HT-*alt*-TP)** and **P3HT-*b*-P(3HT-*alt*-TP)** copolymers, on the other hand, show absorption profiles extended into the near-infrared, which renders them attractive for application in near-infrared organic electronics. Further efforts in this direction should be undertaken. With respect to the optimization of this polymerization approach, it remains interesting to explore other donor-acceptor combinations as well as other catalyst systems.

Finally, also a branched donor-acceptor copolymer could be successfully obtained by adding a trifunctional core to the Stille polymerization of the respective donor and acceptor monomers. Since the incorporation of only 3% of the benzotrithiophene core did not really have an impact on the polymer or photovoltaic properties, it would be interesting to investigate whether the implementation of a higher amount of the branching unit would lead to more significant differences. On top of that, this interesting route to improve the device efficiency and stability should be explored further on other polymer systems.

### **6.3 NEDERLANDSE SAMENVATTING**

In de afgelopen decennia hebben organische zonnecellen een toenemende interesse genoten als een alternatieve hernieuwbare energiebron, in het bijzonder omwille van enkele bijkomende aantrekkelijke karakteristieken zoals hun gering gewicht, flexibiliteit en semi-transparant karakter. Door het uitgebreide onderzoek in dit domein kon de efficiëntie van organische zonnecellen verhoogd worden tot waarden die momenteel de 12% overschrijden. Om commercieel succesvol te kunnen zijn, moeten organische zonnecellen echter nog verder verbeteren betreffende de productiekosten, efficiëntie en stabiliteit. In dit werk werden de twee laatste parameters aangepakt op drie verschillende manieren.

In een eerste deel van dit proefschrift hebben we ons toegelegd op de synthese en karakterisatie van ionische (co)polythiofenen aangezien de efficiëntie van organische zonnecellen verhoogd kan worden door de incorporatie van dergelijke geconjugeerde polyelektrolyten als kathode-interlagen. Vandaar dat een reeks van imidazolium-gesubstitueerde ionische (co)polythiofenen gesynthetiseerd werd via een Kumada katalysator-transfer condensatie polymerisatie (KKTCP) en

introductie van de ionische groepen in de polymeerzijketens. Zowel de topologie (d.i. homopolymeren, willekeurige en blokcopolymeren) als het aantal ionische groepen werd systematisch gevarieerd. De polymeren werden volledig gekarakteriseerd en vervolgens toegepast als kathode-interlagen in organische zonnecellen gebaseerd op PCDTBT:PC<sub>71</sub>BM. Dit gaf een verbetering van alle fotonische parameters ( $V_{OC}$ ,  $J_{SC}$ , FF), hetgeen uiteindelijk resulteerde in een gemiddelde efficiëntieverhoging van ~15%. Deze bevindingen werden vastgesteld voor de gehele reeks van ionische (co)polythiofenen, hetgeen erop wijst dat de stijging in efficiëntie veeleer een algemeen fenomeen is voor deze materiaalklasse. Anderzijds werden de beste fotonische resultaten waargenomen voor de geconjugeerde polyelektrolyten met een hogere verhouding aan triëthyleenglycol-zijstaarten en het blokcopolymeer presteerde lichtjes beter dan het willekeurige copolymeer met dezelfde (50/50) monomeerverhouding.

Aangezien de zonnecel-efficiëntie ook beïnvloed wordt door de molaire massa en dispersiteit van het donormateriaal in de foto-actieve laag, zou het interessant zijn indien we deze parameters nauwkeuriger zouden kunnen controleren. Vandaar dat in een tweede deel van dit proefschrift de gecontroleerde synthese van *low bandgap* alternerende donor-acceptor copolymeren werd nagestreefd via KKTCP. Hiervoor werd gebruik gemaakt van een algemene aanpak, waarbij een *push-pull* monomeer bestaande uit een donor- en een acceptoreenheid werd gesynthetiseerd en vervolgens gepolymeriseerd via KKTCP door gebruik te maken van een nikkel-katalysator. Als *proof of concept* werd er allereerst gebruik gemaakt van een thiofeen als donorcomponent en een pyridine als acceptorcomponent, resulterend in het alternerende **P(3HT-*alt*-P)** copolymeer

na KKTCP polymerisatie. Bovendien werd er ook een nieuw volledig geconjugueerd blokcopolymeer (**P3HT-*b*-P(3HT-*alt*-P)**) gecreëerd volgens een *one-pot* KKTCP procedure door gebruik te maken van een *in situ* gevormd poly(3-hexylthiofeen) (**P3HT**) blok om de polymerisatie van het donor-acceptor alternerende copolymeer te initiëren. De gesynthetiseerde materialen vertoonden interessante fluorescente eigenschappen. Om de KKTCP van alternerende donor-acceptor copolymeren nader te onderzoeken, werd ook nog een ander *push-pull* monomeer met een sterkere acceptoreenheid (thiënopirazine) en dezelfde donoreenheid (thiofeen) bereid en vervolgens gepolymeriseerd via KKTCP, resulterend in een alternerend copolymeer (**P(3HT-*alt*-TP)**) met een kleinere *bandgap*. Daarenboven werd ook een volledig geconjugueerd **P3HT-*b*-P(3HT-*alt*-TP)** blokcopolymeer bereid op dezelfde manier. De gesynthetiseerde copolymeren vertoonden interessante absorptieprofielen tot in het nabij infrarood gebied. In beide gevallen werden de alternerende copolymeren verkregen via een niet-gecontroleerd ketengroeimechanisme.

Tenslotte werd ook het effect van vertakkingen onderzocht, aangezien conjugatie in twee of drie dimensies kan leiden tot verscheidene voordelen, zoals een isotroop ladingstransport, verhoogde diëlektrische constanten en interessante morfologieën. Deze route is nauwelijks onderzocht en zou een significante invloed kunnen hebben op de zonneefficiëntie en -stabiliteit. Hiertoe werd een kleine hoeveelheid van een trifunctionele benzotrithiofeenkern toegevoegd aan de Stille polymerisatie van een alternerend cyclopentadithiofeen-quinoline (donor-acceptor) copolymeer, resulterend in een vertakt copolymeer (**P(CPDT-*alt*-Qx)-3B**). Vervolgens werden zowel het lineaire als het vertakte alternerende copolymeer gekarakteriseerd met behulp van MALDI-TOF MS, wat de incorporatie

van de benzotrithiofeenkern in de copolymeerketens bevestigde. Daarna werden beide copolymeren toegepast als donorcomponent in bulk heterojunctie organische zonnecellen met PC<sub>71</sub>BM als de acceptorcomponent. Deze metingen toonden aan dat alle fotonvoltatische parameters ( $V_{OC}$ ,  $J_{SC}$ , FF) ongeveer hetzelfde bleven na incorporatie van de benzotrithiofeenkern, resulterend in gelijkaardige gemiddelde efficiënties van 3.92 en 4.00% voor de organische zonnecellen gebaseerd op respectievelijk het lineaire en vertakte copolymeer.

## LIST OF PUBLICATIONS

G. Pirotte, J. Kesters, P. Verstappen, S. Govaerts, J. Manca, L. Lutsen, D. Vanderzande, W. Maes, "Continuous flow polymer synthesis toward reproducible large-scale production for efficient bulk heterojunction organic solar cells", *ChemSusChem*, **2015**, *8*, 3228–3233.

- Synthesis and characterization of the conjugated polyelectrolyte material (CPE-TFSI)

J. Kesters, S. Govaerts, G. Pirotte, J. Drijkoningen, M. Chevrier, N. Van den Brande, X. Liu, M. Fahlman, B. Van Mele, L. Lutsen, D. Vanderzande, J. Manca, S. Clément, E. Von Hauff, W. Maes, "High-permittivity conjugated polyelectrolyte interlayers for high-performance bulk heterojunction organic solar cells", *ACS Appl. Mater. Interfaces*, **2016**, *8*, 6309–6314.

- Synthesis and characterization of the conjugated polyelectrolyte materials (P1 and P4)

S. Govaerts, P. Verstappen, H. Penxten, M. Defour, B. Van Mele, L. Lutsen, D. Vanderzande, W. Maes, "Synthesis of highly fluorescent all-conjugated alternating donor-acceptor (block) copolymers via GRIM polymerization", *Macromolecules*, **2016**, *49*, 6411–6419.

- Article writing
- Synthesis and characterization of the monomers and polymers

## List of publications

---

S. Govaerts, J. Kesters, M. Defour, B. Van Mele, H. Penxten, S. Neupane, F. U. Renner, L. Lutsen, D. Vanderzande, W. Maes, "Conjugated ionic (co)polythiophene-based cathode interlayers for bulk heterojunction organic solar cells", manuscript submitted.

- Article writing
- Synthesis and characterization of the monomers and polymers
- Photovoltaic part: performed and written by Dr Jurgen Kesters

## **DANKWOORD**

De afgave van dit proefschrift betekent het einde van een vier jaar durend doctoraat, een tijd die is voorbijgevlogen dankzij de vele leuke momenten met vrienden/collega's. Ik was nooit op dit punt geraakt, was het niet zonder de hulp en steun van vele mensen. Bij deze zou ik hun graag allemaal willen bedanken:

Prof. Dr Wouter Maes, mijn promotor, voor de mogelijkheid om dit doctoraat binnen zijn onderzoeksgroep uit te voeren. Ook voor de goede begeleiding, de steun wanneer het even wat minder ging en uiteraard ook voor het verbeteren van mijn artikels en thesis.

Prof. Dr Dirk Vanderzande, mijn copromotor, voor de nuttige feedback en het nalezen van de artikels. And also Dr Laurence Lutsen, my other copromoter, thank you for the daily management of our labs and for giving me the opportunity to visit some conferences.

I would also like to thank all members of the jury for taking the time to evaluate this work and to take part in the defense.

Iedereen die mij gehopen heeft met het uitvoeren van bepaalde meettechnieken: Gunter, Koen, Huguet, Pieter, Jurgen, Ruben, Joris, Gijs en Neomy.

Maxime Defour and Prof. Dr Bruno Van Mele from the VUB for performing several thermal analyses, their interpretations and feedback concerning the papers.

Natuurlijk mogen mijn goede vrienden en collega's niet ontbreken in dit lijstje. Allereerst Yasmine, Jeroen B. en Mathias: samen zijn we aan dit avontuur

begonnen en zonder jullie waren de afgelopen vier jaar niet hetzelfde geweest. Bedankt voor alle toffe momenten samen en de steun die we aan elkaar gehad hebben! Pieter en Jurgen, de twee 'anciens' van onze onderzoeksgroep, bedankt voor de leuke samenwerking, de vele raad en toffe babbels! Geert en Evelien, mijn 'verdedigingsmaatjes', bedankt voor het regelen van de administratieve zaken en het luisterende oor! De andere leden van onze groep – Ruben, Jorne, Dries, Sam, Frederik en Tom – voor de aangename werksfeer, de leuke uitjes en feestjes samen! De andere leden van de OBPC-groep mag ik zeker ook niet vergeten te bedanken voor de fijne sfeer: Veronique, Nok, Luk, Neomy, Stephan, Joris, Joachim, Martijn, Erika, Gijs, Svitlana, Kirsten, Maarten, Jeroen D.N., Lowie, Jeroen V., Roald, Wouter V.G., Tien, Brecht en Rebekka. Hopelijk ben ik nu niemand vergeten!

Last but not least, zou ik ook nog graag mijn familie en vrienden willen bedanken voor de nodige ontspanning en interesse tijdens mijn doctoraat. In het bijzonder mijn ouders en zus, dankzij hun steun en vertrouwen heb ik dit alles tot een goed einde kunnen brengen. Zij waren er altijd voor mij wanneer ik het eens wat moeilijker had!

**BEDANKT ALLEMAAL!**